IAEA RADIATION TECHNOLOGY REPORTS No. 5

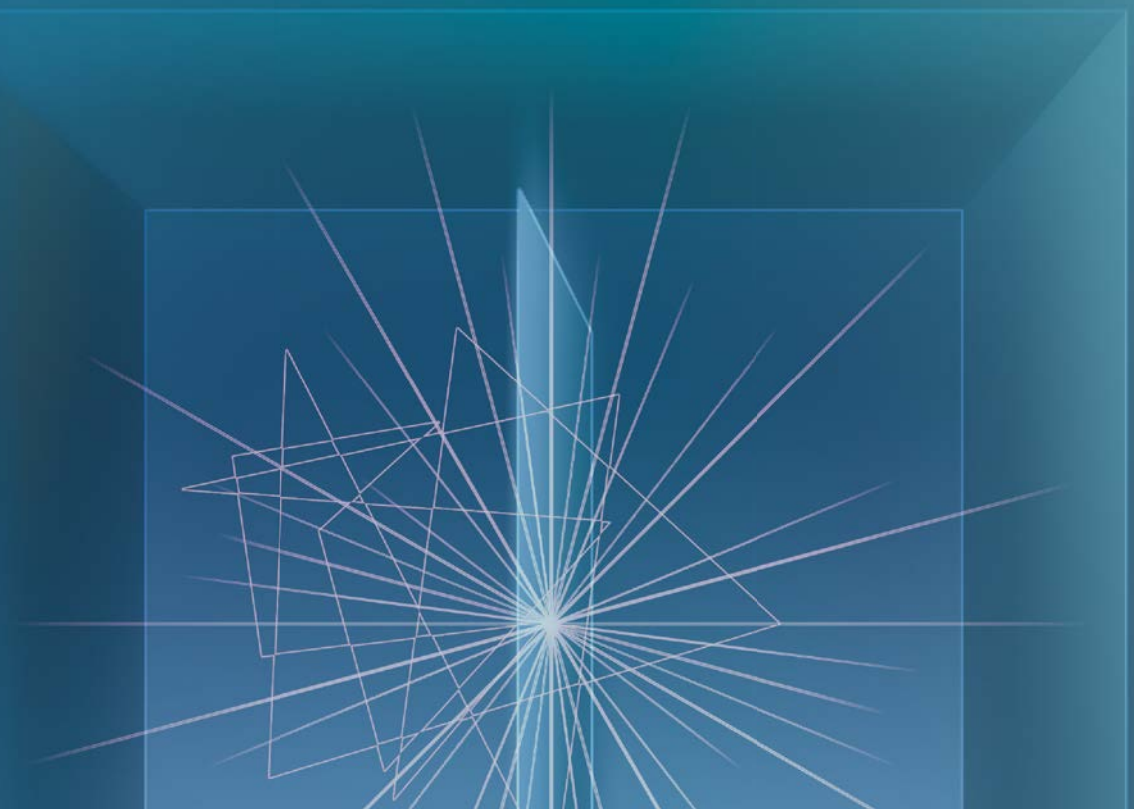

Nanoscale Radiation Engineering of Advanced Materials for Potential Biomedical Applications

IAEA
International Atomic Energy Agency

IAEA RADIATION TECHNOLOGY SERIES PUBLICATIONS

One of the main objectives of the IAEA Radioisotope Production and Radiation Technology programme is to enhance the expertise and capability of IAEA Member States in utilizing the methodologies for radiation processing, compositional analysis and industrial applications of radioisotope techniques in order to meet national needs as well as to assimilate new developments for improving industrial process efficiency and safety, development and characterization of value-added products, and treatment of pollutants/hazardous materials.

Publications in the IAEA Radiation Technology Series provide information in the areas of: radiation processing and characterization of materials using ionizing radiation, and industrial applications of radiotracers, sealed sources and non-destructive testing. The publications have a broad readership and are aimed at meeting the needs of scientists, engineers, researchers, teachers and students, laboratory professionals, and instructors. International experts assist the IAEA Secretariat in drafting and reviewing these publications. Some of the publications in this series may also be endorsed or co-sponsored by international organizations and professional societies active in the relevant fields.

There are two categories of publications: the **IAEA Radiation Technology Series and the IAEA Radiation Technology Reports**.

IAEA RADIATION TECHNOLOGY SERIES

Publications in this category present guidance information or methodologies and analyses of long term validity, for example protocols, guidelines, codes, standards, quality assurance manuals, best practices and high level technological and educational material.

IAEA RADIATION TECHNOLOGY REPORTS

In this category, publications complement information published in the IAEA Radiation Technology Series in the areas of: radiation processing of materials using ionizing radiation, and industrial applications of radiotracers, sealed sources and NDT. These publications include reports on current issues and activities such as technical meetings, the results of IAEA coordinated research projects, interim reports on IAEA projects, and educational material compiled for IAEA training courses dealing with radioisotope and radiopharmaceutical related subjects. In some cases, these reports may provide supporting material relating to publications issued in the IAEA Radiation Technology Series.

All of these publications can be downloaded cost free from the IAEA web site:

http://www.iaea.org/Publications/index.html

Further information is available from:

Marketing and Sales Unit
International Atomic Energy Agency
Vienna International Centre
PO Box 100
1400 Vienna, Austria

Readers are invited to provide feedback to the IAEA on these publications. Information may be provided through the IAEA web site, by mail at the address given above, or by email to:

Official.Mail@iaea.org

NANOSCALE RADIATION ENGINEERING OF ADVANCED MATERIALS FOR POTENTIAL BIOMEDICAL APPLICATIONS

The following States are Members of the International Atomic Energy Agency:

AFGHANISTAN
ALBANIA
ALGERIA
ANGOLA
ARGENTINA
ARMENIA
AUSTRALIA
AUSTRIA
AZERBAIJAN
BAHAMAS
BAHRAIN
BANGLADESH
BELARUS
BELGIUM
BELIZE
BENIN
BOLIVIA, PLURINATIONAL STATE OF
BOSNIA AND HERZEGOVINA
BOTSWANA
BRAZIL
BRUNEI DARUSSALAM
BULGARIA
BURKINA FASO
BURUNDI
CAMBODIA
CAMEROON
CANADA
CENTRAL AFRICAN REPUBLIC
CHAD
CHILE
CHINA
COLOMBIA
CONGO
COSTA RICA
CÔTE D'IVOIRE
CROATIA
CUBA
CYPRUS
CZECH REPUBLIC
DEMOCRATIC REPUBLIC OF THE CONGO
DENMARK
DJIBOUTI
DOMINICA
DOMINICAN REPUBLIC
ECUADOR
EGYPT
EL SALVADOR
ERITREA
ESTONIA
ETHIOPIA
FIJI
FINLAND
FRANCE
GABON
GEORGIA
GERMANY
GHANA
GREECE
GUATEMALA
GUYANA
HAITI
HOLY SEE
HONDURAS
HUNGARY
ICELAND
INDIA
INDONESIA
IRAN, ISLAMIC REPUBLIC OF
IRAQ
IRELAND
ISRAEL
ITALY
JAMAICA
JAPAN
JORDAN
KAZAKHSTAN
KENYA
KOREA, REPUBLIC OF
KUWAIT
KYRGYZSTAN
LAO PEOPLE'S DEMOCRATIC REPUBLIC
LATVIA
LEBANON
LESOTHO
LIBERIA
LIBYA
LIECHTENSTEIN
LITHUANIA
LUXEMBOURG
MADAGASCAR
MALAWI
MALAYSIA
MALI
MALTA
MARSHALL ISLANDS
MAURITANIA
MAURITIUS
MEXICO
MONACO
MONGOLIA
MONTENEGRO
MOROCCO
MOZAMBIQUE
MYANMAR
NAMIBIA
NEPAL
NETHERLANDS
NEW ZEALAND
NICARAGUA
NIGER
NIGERIA
NORWAY
OMAN
PAKISTAN
PALAU
PANAMA
PAPUA NEW GUINEA
PARAGUAY
PERU
PHILIPPINES
POLAND
PORTUGAL
QATAR
REPUBLIC OF MOLDOVA
ROMANIA
RUSSIAN FEDERATION
RWANDA
SAN MARINO
SAUDI ARABIA
SENEGAL
SERBIA
SEYCHELLES
SIERRA LEONE
SINGAPORE
SLOVAKIA
SLOVENIA
SOUTH AFRICA
SPAIN
SRI LANKA
SUDAN
SWAZILAND
SWEDEN
SWITZERLAND
SYRIAN ARAB REPUBLIC
TAJIKISTAN
THAILAND
THE FORMER YUGOSLAV REPUBLIC OF MACEDONIA
TOGO
TRINIDAD AND TOBAGO
TUNISIA
TURKEY
UGANDA
UKRAINE
UNITED ARAB EMIRATES
UNITED KINGDOM OF GREAT BRITAIN AND NORTHERN IRELAND
UNITED REPUBLIC OF TANZANIA
UNITED STATES OF AMERICA
URUGUAY
UZBEKISTAN
VANUATU
VENEZUELA, BOLIVARIAN REPUBLIC OF
VIET NAM
YEMEN
ZAMBIA
ZIMBABWE

The Agency's Statute was approved on 23 October 1956 by the Conference on the Statute of the IAEA held at United Nations Headquarters, New York; it entered into force on 29 July 1957. The Headquarters of the Agency are situated in Vienna. Its principal objective is "to accelerate and enlarge the contribution of atomic energy to peace, health and prosperity throughout the world".

IAEA RADIATION TECHNOLOGY REPORTS No. 5

NANOSCALE RADIATION ENGINEERING OF ADVANCED MATERIALS FOR POTENTIAL BIOMEDICAL APPLICATIONS

INTERNATIONAL ATOMIC ENERGY AGENCY
VIENNA, 2015

COPYRIGHT NOTICE

Marketing and Sales Unit, Publishing Section
International Atomic Energy Agency
Vienna International Centre
PO Box 100
1400 Vienna, Austria
fax: +43 1 2600 29302
tel.: +43 1 2600 22417
email: sales.publications@iaea.org
http://www.iaea.org/books

Printed by the IAEA in Austria
September 2015
STI/PUB/1684

IAEA Library Cataloguing in Publication Data

Nanoscale radiation engineering of advanced materials for potential biomedical applications. — Vienna : International Atomic Energy Agency, 2015.
p. ; 30 cm. — (IAEA radiation technology reports series, ISSN 2225–8833 ; no. 5)
STI/PUB/1684
ISBN 978–92–0–101815–1
Includes bibliographical references.

1. Radiation chemistry. 2. Nanochemistry. 3. Irradiation. 4. Nanostructured materials. I. International Atomic Energy Agency. II. Series.

IAEAL 15–00991

FOREWORD

There is a critical need for advanced materials in the area of biomaterial engineering, primarily in generating biomaterials of enhanced specific functionalities: improved biocompatibility and minimal natural rejection, but with enhanced interfacial adhesion. These qualities can be achieved by the introduction of proper functionalities at nanoscale dimensions. Radiation techniques are uniquely suited for this task, and in most cases are the only possible method of synthesis. Accordingly, many Member States have an interest in creating advanced materials for various healthcare applications using a wide array of radiation sources and their broad expertise.

The proposal for this coordinated research project (CRP), entitled Nanoscale Radiation Engineering of Advanced Materials for Biomedical Applications, was formulated based on the requests and information received from Member States and the conclusions and recommendations of the Consultants Meeting on Advanced Materials on the Nano-scale Synthesized by Radiation-induced Processes, held in Vienna from 10 to 14 December 2007. Based on these conclusions, this CRP aimed to support Member States in developing methodologies for the use of radiation in the synthesis, modification and characterization of nanomaterials — nanogels, nanoparticles, nanovehicles, nanoporous membranes and surfaces with enhanced biocompatibility for potential biomedical applications such as cell sheet engineering and artificial tissue construction, diagnostics and imaging, and drug delivery. Additionally, this CRP facilitated networking between radiation technologists and biomedical scientists for the development of such applications.

This publication presents the achievements of the CRP. It provides background information and short summaries of the achievements, followed by individual full reports. Additionally, all publications resulting from the CRP are listed for further in-depth reading.

The IAEA wishes to thank all the participants for their valuable contributions. The IAEA officer responsible for this publication was A. Safrany of the Division of Physical and Chemical Sciences.

EDITORIAL NOTE

The papers in these Proceedings (including the figures, tables and references) have undergone only the minimum copy editing considered necessary for the reader's assistance. The views expressed remain, however, the responsibility of the named authors or participants. In addition, the views are not necessarily those of the governments of the nominating Member States or of the nominating organizations.

This report does not address questions of responsibility, legal or otherwise, for acts or omissions on the part of any person.

Although great care has been taken to maintain the accuracy of information contained in this publication, neither the IAEA nor its Member States assume any responsibility for consequences which may arise from its use.

The use of particular designations of countries or territories does not imply any judgement by the publisher, the IAEA, as to the legal status of such countries or territories, of their authorities and institutions or of the delimitation of their boundaries.

The mention of names of specific companies or products (whether or not indicated as registered) does not imply any intention to infringe proprietary rights, nor should it be construed as an endorsement or recommendation on the part of the IAEA.

The authors are responsible for having obtained the necessary permission for the IAEA to reproduce, translate or use material from sources already protected by copyrights.

Material prepared by authors who are in contractual relation with governments is copyrighted by the IAEA, as publisher, only to the extent permitted by the appropriate national regulations.

This publication has been prepared from the original material as submitted by the authors. The views expressed do not necessarily reflect those of the IAEA, the governments of the nominating Member States or the nominating organizations.

The IAEA has no responsibility for the persistence or accuracy of URLs for external or third party Internet web sites referred to in this book and does not guarantee that any content on such web sites is, or will remain, accurate or appropriate.

CONTENTS

SUMMARY 1

REPORTS BY THE PARTICIPANTS OF THE COORDINATED RESEARCH PROJECT

Nanostructuring materials by ionizing radiation technology: Protein nanoparticle preparation and functionalization of track etched membranes 17
M. Grasselli, S. Soto Espinoza, L.J. Martinez, G. Casajus, M. Siri, S. Alonso, E.E. Smolko

Encapsulation and nanoencapsulation of papain active sites to enhance radiolytic stability and decrease toxicity 31
G.H.C. Varca, C.C. Ferraz, M. Beatriz Mathor, P. Santos Lopes, S. Rogero, J.R. Rogero, A.B. Lugão

Radiolytic syntheses of NPs and inorganic polymer hybrid microgels 47
Q. Chen, G. Shen, J. Shi, H. Liang, X. Shen

Radiation engineering of PVP/PAAc nanogel dispersions for ophthalmic applications 57
E.A. Hegazy, H.A. Abd El-Rehim, A.E. Swilem

Architectures based on gold NPs associated with targeting agents for tumour therapy by photothermia 75
M.-C. Clochard, G. Rizza, M. Sangermano, J. Amici, S. Deshayes, H. Cabral, K. Miasaki

Porous polymer drug eluting coatings prepared by radiation induced polymerization 81
M. Veres, B. Beiler, L. Himics, S. Tóth, M. Koós

γ radiation mediated synthesis of anisotropic MNPs for potential biomedical applications 93
S. Francis, J. Biswas, L. Varshney, S. Sabharwal

PLA nanocomposites with potential biomedical applications using γ irradiation 101
S. Dadbin, F. Naimian, V. Ahmadian

Radiation engineered nanogels as platforms for medical diagnostics and therapeutic nanodevices 113
C. Dispenza, M.A. Sabatino, N. Grimaldi, S. Alessi, G. Spadaro, S. Rigogliuso, G. Adamo, G. Ghersi

Introduction of functional structures on nanoscales into engineering polymer films using radiation techniques 125
Y. Maekawa

Radiation induced incorporation of nanocomponents into electrospun mats: Preparation of prospective functional nanobiowebs for nitrite detection 133
K.-P. Lee, A.I. Gopalan, S.-H. Lee, K.R. Ko

Radiation synthesis of PEGDA and APO nanosized gels for bioactive immobilization 143
M.Y. Hamzah, R. Tajau, M. Zah Salleh, N. Mat Isa, K. Hashim

Polymeric nanogels and nanolayers obtained by radiation techniques 153
P. Ulanski, S. Kadłubowski, A. Henke, A.K. Olejnik, B. Rokita, R. Wach, J.M. Rosiak

Radiolytically synthesized hybrid nanosystems for bionanotechnologies 167
Z. Kacarevic-Popovic, A. Radosavljevic (Krkljes), J. Krstic, J. Spasojevic

Modification of CS NPs by radiolytic methods: Approach to drug controlled release systems 179
W. Pasanphan, T. Rattanawongwiboon, S. Choofong, P. Rimdusit

Surface and bulk nanostructuring of polymers by radiation engineering for biomedical applications 189
O. Güven, M. Barsbay, M. Akbulut, S. Duygu Sütekin

PUBLICATIONS RESULTING FROM THE COORDINATED RESEARCH PROJECT 201
ABBREVIATIONS 211
LIST OF PARTICIPANTS 213

SUMMARY

1. INTRODUCTION

Nanoparticles (NPs) and nanostructures are not entirely new, but the ability of humans to work, measure and manipulate at the nanoscale is new. Radiation technologies, which are already established in materials processing, have properties that are uniquely suited for the creation and characterization of new functional materials on the nanoscale.

For example, low energy ion beams enable fabrication of three dimensional structures, and high energy ion beams are used for preparation of ion track membranes and nanowires. Membranes containing a single pore or any number of pores up to 10^9 pores/cm^2 of highly uniform pore size are already commercially available. By further modification, there are endless possibilities for creating track membranes with special properties and functions. These membranes may also be used as template materials for the synthesis of microstructures and nanostructures, in the form of wires or tubules. Magnetic, conducting and superconducting nanowires and nanotubules, single or in an array, have been manufactured in this way. These processes are well developed in France, Japan, Germany and the United States of America (USA).

Generation of NPs using radiolytic techniques has been known for several decades. Strategies to produce NPs of metallic and semiconductor materials have been developed, and production of metallic core shells or alloyed metallic NPs is possible. Radiation techniques offer unique advantages by creating a wide range of species with redox levels that are not achievable by other means. Moreover, by adjusting the dose and dose rate, better control and fine-tuning of the particle size and size distribution are possible.

The use of pulsed irradiation to synthesize polymer nanogels was initiated in Poland, and accepted and further developed in laboratories in Germany, Hungary, Kazakhstan, Malaysia and an ever increasing number of Member States. Properties of polymer nanogels, as compared to single macromolecules or non-cross-linked NPs include: stability of shape and size, ability to react to external stimuli, ability to host small molecules and release them in a controlled way, ability to form non-flat, structured surfaces and stability against degradation. These properties make them ideally suited to healthcare applications, for example, in diagnostics as carriers of contrast agents or markers and in therapy as stimuli responsive coatings for drug or gene delivery, encapsulation and wound healing. These nanogels can be additionally functionalized by coupling with suitable biomolecules for targeting and imaging, and can be used as additives to synovial fluids and intravenous drug carriers.

Nanoscale grafting of environmental sensitive hydrogel onto a surface of cell culture dishes (by γ or electron irradiation) enables harvesting of these cells by a simple change in the temperature or pH of the cell culture media. In this way, no proteolytic enzymes that often damage the cells are needed, and cells can be harvested in a continuous sheet form. Such cell sheets overcome the limitations of conventional tissue engineering methods, such as the use of single cell suspension injection, and have already shown good results in regenerative medical applications in Japan. Skin and corneal defects have been treated with transplantable cell sheets fabricated on these surfaces. Severe heart failure has also been treated with cell sheets fabricated from patients' own skeletal myoblasts. With further improvements of stimuli responsive culture, surface reconstruction of more complex tissues will be possible, leading to treatment of a wider range of diseases. This process has generated vast interest in a number of Member States (Hungary, Italy, Poland, Turkey and USA, among others), which are now exploring various routes for preparation of surfaces that are suitable for cell sheet engineering and which have requested guidance and coordination of their efforts from the IAEA.

The IAEA has recognized the challenges and opportunities of these new scientific and technological developments, has organized several technical and consultants meetings and published, in 2005, a TECDOC entitled Emerging Applications of Radiation in Nanotechnology.

This Coordinated Research Project (CRP), entitled Nanoscale Radiation Engineering of Advanced Materials for Biomedical Applications, was formulated based on the requests and information received from Member States and the conclusions and recommendations of the Consultants' Meeting on Advanced Materials on the Nano-scale Synthesized by Radiation-induced Processes, held from 10 to 14 December 2007, in Vienna. The CRP generated significant interest, but owing to funding constraints, many good proposals had to be rejected. The CRP comprised 17 participants, and was thus one of the largest projects. The first research coordination meeting (RCM) was convened in Vienna from 30 March to 3 April 2009, where the work plans for individual

participants and collaborations were discussed and accepted. The meeting report is available as working material at http://www-naweb.iaea.org/napc/iachem/working_materials/RC-1124-1_report_complete.pdf. The second RCM was held from 15 to 19 November 2010 in Paris, and was attended by 17 participants (chief scientific investigators) and 1 cost free observer from Brazil. The participants presented their research achievements since the first RCM, and the meeting report is available as working material at http://www-naweb.iaea.org/napc/iachem/meetings/RCMs/RC-1124-2_report_complete.pdf.

The final RCM was held from 8 to 12 October 2012 in Krakow, just a week preceding the International Symposium on Ionizing Radiation and Polymers, which is one of the most important conferences in the radiation technology field, devoted to basic and applied polymer radiation sciences and technologies. In this way, an opportunity was given to the participants of the RCM to meet and discuss recent achievements in research and applications, and plan future projects and collaboration at this high level event. The RCM was attended by 16 participants (chief scientific investigators) and 3 cost free observers from Brazil, Serbia and Thailand. The participants presented their research achievements under this CRP, centred on the main expected outputs.

1.1. Methodologies to prepare and characterize NPs, nanogels and nanoporous membranes, as well as to synthesize and modify NP surfaces by attaching organic ligands by radiation

A number of synthetic methodologies that use radiation to prepare nanogels and NPs were developed and described by participants from Argentina, Brazil, China, Egypt, Hungary, India, Italy, Republic of Korea, Malaysia, Poland, Serbia, Thailand and Turkey. These approaches were aimed at precise control of the structure, size, shape and functionality of the nanoscale products. In some cases, the scientists attempted to develop processes that were compatible with existing large scale irradiation facilities and procedures. The nanoscale products were based on proteins (Argentina and Brazil), natural polymers (Malaysia and Thailand), synthetic polymers (Egypt, Hungary, Italy, Republic of Korea, Malaysia, Poland and Turkey) and inorganic compounds (China, France, India, Republic of Korea and Serbia). In some cases, procedures were developed for preparing 'hybrid' products, e.g. where the surfaces of NPs and nanogels were decorated with functional polymers and biomolecules (France, Italy and Thailand).

The participants from the USA and Turkey are planning to use radiation to synthesize polymeric inclusion complex nanogels for hydrophobic anticancer drug delivery. This is a novel approach, and nanogels have great potential for cancer treatment. The collaboration would not have happened without this CRP.

It has been demonstrated that radiation can be used to reinforce weak interpolymer associations between synthetic polymers and biopolymers, by introducing covalent cross-links and thus fixing their structure and making them irreversible nanogels (Argentina, Brazil, Egypt and Poland). In this way, valuable properties of these complexes can be utilized, for instance, in pharmaceutical formulations and in drug delivery.

Nanoporous membranes were successfully fabricated by ion beam irradiation of polymeric films and functionalized by conventional and reversible addition fragmentation chain transfer (RAFT) mediated grafting (Argentina, France, Japan and Turkey). Some of these membranes were used for detection of heavy metal ions.

Nanoporous membranes prepared by γ radiation were tested for protein drug delivery (Argentina and Brazil).

Hydrogel/NP composites were developed, including a product for antileishmanial drug release (Brazil), a protective drug eluting coating for medical implants (Hungary) and coatings with antimicrobial properties (Serbia). Biodegradable polymer/inorganic nanocomposites have been developed by radiation induced modifications in the polymeric phase, as a potential material for bone fracture fixation devices (Islamic Republic of Iran).

Radiolytically synthesized $BaSO_4$ mesoporous microspheres were shown to selectively remove CrO_4^{2-} ions from neutral and alkaline aqueous solutions with high salinity. Furthermore, the morphology of the mesoporous microspheres can be effectively reconstructed via Ostwald ripening at room temperature. Prussian blue (PB) NPs were synthesized by γ radiation, where the morphology and size of the NPs can be accurately controlled (China).

1.2. Methodologies to radiation synthesize polymeric, inorganic and hybrid nanocarriers, providing controlled loading and improved release rates of drugs

Radiation synthesized nanomaterials were prepared and investigated for potential applications as drug carriers. Such materials can be loaded with hydrophobic drugs that are released in a controlled manner.

Radiation cross-linked, pH sensitive polyvinylpyrrolidone (PVP)/poly(acrylic acid) (PAAc) nanogels are efficient in the management of dry eye syndrome and in the delivery of pilocarpine in vitro and in vivo (Egypt). Amphiphilic chitosan (CS) NPs can encapsulate hydrophobic antifungal and anticancer drugs and control their release while prolonging their bioactivity (Thailand). NPs from polyethylene glycol diacrylate (PEGDA) and acrylated palm oil (APO), synthesized using a radiation technique, can improve the solubility of curcumin and thymoquinone in water and permit their sustained release (Malaysia). Effective release of an antileishmanial drug from a nanohydrogel was demonstrated (Brazil).

1.3. Novel functional surfaces for cell sheet engineering fabricated utilizing advanced radiation techniques that permitted enhanced cell surface interactions and control of cell functions

Fully functional thermoresponsive materials for cell sheet engineering were elaborated by the Polish participant and tested on fibroblast cultures. A thin layer of thermosensitive polymer was grafted onto a solid polymer substrate by a postirradiation method. The product allowed proliferation of a confluent cell monolayer at 37°C. Upon lowering the temperature to 15°C, the cell layer became detached and was ready for application or further processing. This product is designed for use in burn wound treatment.

1.4. Additional relevant developments

A multifunctional electrospun nanofibre network was produced. It comprised the polymer host, silica, gold NPs and cytochrome (Cyt) C (the nitrite selective enzyme). γ radiation has been effectively utilized for the incorporation of silica and gold NPs in a single step. It was demonstrated that the multifunctional electrospun fabric exhibits excellent bioelectrocatalytic properties towards reduction of nitrite ions. The multifunctional electrospun nanofabric was applied as a nitrite ion sensor (Republic of Korea).

It was demonstrated that γ radiation initiated polymerization can be used to prepare nanodiamond (ND)/polymer composites. This method has great potential for surface functionalization of individual NDs, which can be used for in vivo sensing of biological materials (Hungary).

A simple and efficient one step method of producing a hybrid of uniformly dispersed Ag NPs supported on carbon nanotubes (CNTs) was achieved without acid purification or without using any surfactant or polyelectrolyte to functionalize the CNTs (Serbia).

Methodologies were developed to control the in vitro degradation of polylactic acid (PLA) nanocomposites by controlling the hydroxyapatite (HAP) NP content, extent of crystallinity and irradiation dose. It was found that radiation can induce crystallinity and different crystalline structure formation in nanocomposites (Islamic Republic of Iran).

2. CRP OVERALL OBJECTIVE

The overall objective of this project was to support Member States in the use of radiation for the synthesis, modification and characterization of advanced materials by nanoscale control of their properties. This is in line with the intention of the IAEA to enhance Member State capabilities in applying radiation technology for advanced materials development and processing natural polymers into value added products.

2.1. Specific research objectives

The purpose of this project was to coordinate the research in Member States on the use of radiation in the synthesis, modification and characterization of advanced materials by nanoscale control of their properties, specifically to:

— Develop radiolytic methodologies for synthesis of NPs and nanoporous membranes, as well as to synthesize and modify NP surfaces by attaching organic ligands;

— Radiation synthesize polymeric, inorganic and hybrid nanocarriers, providing controlled loading and improved release rates of drugs;
— Fabricate new stimuli responsive surfaces by radiation induced grafting on the nanoscale for cell sheet engineering with improved cell matrix interactions and cell function control.

The participant groups addressed and contributed to one or more of the above topics.

2.2. Expected research outputs

The expected outcomes of the project are the following:

— Development of methodologies to prepare and characterize nanogels, NPs and nanoporous membranes, as well as to synthesize and modify NP surfaces by attaching organic ligands by radiation;
— Development of methodologies to radiation synthesize polymeric, inorganic and hybrid nanocarriers, providing controlled loading and improved release rates of drugs;
— Demonstration of novel functional surfaces for cell sheet engineering fabricated by utilizing advanced radiation technology, towards improved cell/matrix interactions and cell function control;
— Publication of the results in the IAEA Radiation Technology Reports Series.

3. ACHIEVEMENTS

3.1. Argentina

Irradiation of globular protein solutions has been extensively studied in the past. However, most of these studies have focused on physicochemical changes in the protein structure. In the present work, the globular protein bovine serum albumin (BSA) was used as a basic unit to build NPs by γ irradiation of protein solution with cosolvents. By changing the organic solvent amount, protein clusters could be dynamically created in solution, which could be further stabilized by radiation cross-linking. Protein NPs in the size range 10–40 nm were found after γ irradiation of a protein in an aqueous/ethanol solution. NPs were characterized by dynamic light scattering (DLS), fluorescence, ultraviolet (UV) and circular dichroism (CD) spectroscopy, which showed that protein molecules keep their overall structure.

Experimental evidence supports the hypothesis of a two step process, corresponding to an aggregation step that is followed by cross-linking initiated by the ionizing radiation. Thus, NP size could be controlled by the ethanol/water proportion in the sample. It is important to highlight the fact that this method can synthesize high concentrations of protein NPs without precipitation, and can achieve high yields without addition of any chemical cross-linker. This NP radiation synthesis method could be extended to other enzymes by coaggregation with BSA. Functional NPs should have the corresponding activity of the former enzyme.

In the track etched membrane field, the present work reported the functionalization of poly(ethylene terephthalate) (PET) track etched membranes in a tailor made manner by polymerization using the remaining radicals. It succeeded in implementing different fluorescence techniques to follow grafting polymerization inside the nanochannels. The grafted chains were found to be homogeneously distributed in the nanochannels, and the fluorescence techniques offered a powerful tool to apply the grafting process under different synthesis conditions. In future, the development of optical sensors based on these functionalized nanochannels is planned.

3.2. Brazil

Papain is a proteolytic enzyme that possesses desirable properties for wound healing purposes, such as debridement activity and the ability to reduce bacterial burden and to increase granulation during tissue formation. However, low stability restricts this biomolecule application to short shelf life formulations. In addition, recent concerns have been highlighted by the US Food and Drug Administration (FDA) considering the allergenic properties of such substances. Now, topical products containing papain must be registered prior to their commercialization. For such purposes, the goals of this research were to enhance the stability of this enzyme

and reduce the cytotoxic and allergenic profile through molecular encapsulation with cyclodextrins and radiation exposition, which is a technique applied to promote simultaneous cross-linking and sterilization of the hydrogel selected media for the delivery of such complexes. The encapsulation was performed as an attempt to reduce the degradation effects attributed to the radiation exposition. The radiation influence over the bioactivity of the enzyme at different radiation dosages was thus evaluated using a media and a compound based approach. Experiments were performed to characterize the molecular encapsulation changes in the bioactivity profile of the enzyme. The establishment of a methodology to determine the enzymatic activity was one of the expected outputs and was performed by validation studies where accuracy, detection limits, precision, linearity and precision values were determined using *N*-benzoyl-DL-arginine p-nitroanilide. In addition, the development of a nanostructured hydrogel for delivery of the prepared papain/cyclodextrin complex was achieved. Several hydrogel formulations based on different concentrations of PVP, polyethylene glycol (PEG) and agar were assayed for their swelling, gel fraction and mechanical properties. Scanning electron microscopy (SEM) analyses were performed as a complementary technique to provide more data about the structure of the developed material. Additionally, papain NPs to be applied as more stable bioactive compounds for biomedical purposes were developed using ionizing radiation, as a result of the collaboration between the participating laboratories from Brazil and Argentina.

3.3. China

In this CRP, achievements were mainly related to the radiolytic syntheses of inorganic NPs and nanostructures in aqueous solutions.

Firstly, mesoporous microspheres with a large pore size, the radial arrangement of irregular $BaSO_4$ nanorods, were successfully synthesized by the radiolysis of an aqueous solution of $K_2S_2O_8$, $Ba(NO_3)_2$ and disodium ethylenediaminetetraacetate at room temperature. It was confirmed that the mesoporous microspheres with a large pore size evolved from the mesoporous microspheres with a smaller pore size, which were generated at the early stage of the irradiation course and which were mainly constructed of quasi-spherical NPs, via Ostwald ripening at room temperature.

$BaSO_4$ is traditionally known as a kind of inert material. However, it was discovered that the radiolytically synthesized $BaSO_4$ mesoporous microspheres were able to selectively recover CrO_4^{2-}, which is a cancerogenic substance that exists in soil and water. The removal was successful, both from neutral and alkaline aqueous solutions with high salinity and containing several foreign anions. Moreover, with an increase of the dose rate in the course of irradiation, the ion exchange rate and capacity of the obtained $BaSO_4$ microspheres increased. This suggests that the ion exchange activity arises from the $BaSO_4$ NPs. In the nanometre size region, $BaSO_4$ is no longer inert.

Secondly, PB NPs were successfully synthesized by the partially radiolytic reduction of Fe^{3+} and $Fe(CN)_6^{3-}$ in the presence of PVP under N_2 atmosphere at room temperature. The controlled release of Fe^{2+} and $Fe(CN)_6^{4-}$ played an important role in resolving the solution problem of PB NPs, which exists in normal chemical preparation.

3.4. Egypt

Chemically cross-linked, pH sensitive, PVP/PAAc hydrogel NPs were successfully prepared with a high yield via γ radiation induced polymerization of acrylic acid (AAc) in an aqueous solution of PVP as a template polymer. The particle sizes of the PVP/PAAc nanogels at different pH values were evaluated using DLS, and the morphology was assessed using atomic force microscopy (AFM) and transmission electron microscopy (TEM). Smaller and more stable nanogel particles could be produced by irradiating a feed solution of 50–75 mol% AAc and using PVP of high molecular weight (MW). The particle size increased as the feed concentration increased, and suitable concentrations for nanogel production ranged from 1% to 2%. pH sensitive PVP/PAAc nanogels were used to encapsulate pilocarpine where the AAc rich nanogels exhibited the highest loading efficiency. Factors affecting size and encapsulation efficiency were optimized to obtain a nanogel that was sufficient to entrap the drug efficiently. The transmittance, mucoadhesion and rheological characteristics of nanogel particles were studied to evaluate their ocular applicability. An in vitro release study conducted in simulated tear fluid showed a relatively long sustained release of pilocarpine from the prepared PVP/PAAc nanogel particles compared with pilocarpine in solution.

In addition, it would be interesting to evaluate the use of PVP/PAAc nanoparticulate hydrogels as a new strategy to overcome problems associated with highly viscous polymeric materials like the carbomer gel used for dry eye treatment. The use of PVP/PAAc nanogels prepared at different compositions and irradiation doses was evaluated for dry eye syndrome application. Nanogel rheological properties and the nanogel interaction with mucin were investigated. Moreover, topical application of the prepared nanogel in a dry eye model in albino rabbits, induced by atropine sulphate 1% eye drops, was investigated. The use of AAc rich nanogels with a lower cross-linking degree (compared with the highly viscous carbomer 'Vidisic' gel) appears to be promising in the management of dry eye syndrome, with reduced dosing frequency. PVP/PAAc nanogel as artificial tears provides a layer that stabilizes the precorneal tear film, keeps the ocular surface wet and lubricated, helps to repair ocular surface damage and keeps the ocular surface smooth. Topical instillation of PVP/PAAc nanogel twice daily for 3 d is sufficient to improve dry eye problems, whereas other commercial products require prolonged application to achieve a similar effect. In conclusion, this study clearly demonstrated the potential of PVP/PAAc nanoparticles for dry eye curing and multiplying the therapeutic effect of pilocarpine delivery with enhanced bioavailability response.

3.5. France

In the framework of the CRP programme, France worked in collaboration with Italy and Japan on the development of new gold NP architecture for tumour ablation using photothermia. The main condition for such application is that NPs exhibit a surface plasmon resonance (SPR) in the near infrared (NIR) region. The French Atomic Energy and Alternative Energies Commission (CEA) has a γ ray irradiation facility and an electron beam (EB) accelerator for radiation grafting of polymers. In this programme, gold NPs were synthesized in plain, hollow and core shell forms. The plain gold NPs were covered with polyvinylidene fluoride (PVDF) by nanoemulsion polymerization to prepare particles for further radiografting. The cytotoxicities of the hollow gold nanoparticles (HGNPs) absorbing in the NIR region were evaluated. As these NPs were promising materials, the present work examined the photothermal effect on tumour cells.

3.6. Hungary

Many areas of modern medicine are almost unimaginable without the use of different kinds of implants. Implants are used as replacements, supports, auxiliary devices, etc., for various parts or functions of the human body. Their use has many advantages. However, during application, particular attention should be paid to avoid associated negative side effects such as rejection, inflammation, etc. Many of these drawbacks are directly related to the materials that the implant is made of. Coatings are widely used to eliminate unwanted effects related to the implant material. In addition to the protection and isolation of tissues from the implant, coatings could also contribute to better functionality and acceptance of the artificial device, as well as to faster regeneration of the tissues after intervention. Drug eluting coatings, for example, through the delivery and controlled elution of drugs, could actively suppress inflammatory reaction, allergy and rejection of the implant. Additionally, coating activity will be localized to the place where these effects could mainly occur, i.e. the region surrounding the implant.

This work was aimed at developing a drug eluting porous polymer coating by radiation induced polymerization that can be used in implants in different areas of medicine. The primary targets are stents made of metallic alloys; however, these coatings could also be used in other types of medical devices. The main objectives included the development and characterization of the drug eluting coating, utilizing NPs as drug containers and the elaboration of methods for application of the monomer mixture and formation of the drug eluting coating on the surface of implants that are made of medical grade metallic alloys.

The obtained results can be utilized in other areas of nanotechnology, for example, in fabrication of ND/polymer composites using γ radiation induced polymerization techniques. Functionalized NDs with specific colour centres can be used in biomedical applications such as in drug delivery or as in vivo biomarkers. The light emission peak from NDs with silicon vacancy centres, for example, falls into the region of highest optical penetration depth of tissues, so it can be even used for biosensing a few millimetres below the skin surface. The main aim in this field was to demonstrate the usability of radiation induced polymerization techniques to prepare ND/polymer composites of different morphologies: particulate, porous and bulk materials.

Within the framework of this project, a composite drug eluting coating that can be used in stents and other types of medical implants was developed. The coating consisted of an amorphous carbon interlayer, a drug container of diethylene glycol dimethacrylate (DEGDMA) particles and a hydroxyethylmethacrylate (HEMA) based hydrogel matrix. The latter can be used to control the drug eluting characteristics of the coating. The steps for the preparation of the coating included the following:

— Cleaning of the substrate surface;
— Deposition of the amorphous carbon layer on top of the surface;
— Preparation of DEGDMA particles using radiation induced polymerization;
— Filling the particles with the drug (optional);
— Adding the particles to the monomer mixture of the hydrogel;
— Coating of the implant surface with the mixture;
— Formation of the coating by radiation induced polymerization.

The thickness of the amorphous carbon interlayer has been optimized to be 30 nm. It was found that by changing the composition of the monomer mixture, the size of the DEGDMA particles can be controlled in the 400–1300 nm region.

It was demonstrated that γ radiation initiated polymerization can be used to prepare ND/polymer composites. By mixing and irradiating NDs with DEGDMA monomer in different solvents, composites of different morphologies, including particulate, porous and bulk materials, were obtained. This method has great potential for surface functionalization of individual NDs that can be used for in vivo sensing of biological materials.

3.7. India

In recent years, there has been vast interest in the synthesis of anisotropic metal nanoparticles (MNPs) owing to their shape dependent unique properties and important applications in newer fields such as photonics, sensing, imaging and medicine. The synthesis of NPs by γ irradiation is a non-polluting process that occurs at room temperature through the mediation of transient species that are generated from the radiolysis of water. The size and shape of the NPs is greatly affected by the reduction rate of metal ions, which can be controlled by proper selection of the dose rate employed in the γ radiolytic method. However, most of the time, the NPs produced are spherical or irregular in shape, and it is still a challenge to produce anisotropic shapes. As part of the efforts towards a ‘green chemistry’ (environmental friendly chemistry) process, the γ irradiation method was successfully explored as an alternative strategy for the synthesis of anisotropic NPs by tuning the experimental conditions.

3.7.1. Size tuneable synthesis of gold nanoplates by γ irradiation

A simple γ irradiation strategy was developed for the synthesis of gold nanoplates by employing a polyelectrolyte as the capping agent. The nanoplates had hexagonal, triangular and truncated triangular shapes, and the size of the nanoplates could be controlled from 500 nm to 5 μm by adjusting the concentration of Au^{3+} ions and the capping agent in the solution. X ray diffraction (XRD) investigations proved that the nanoplates were single crystals bound by the {111} planes on the top and bottom surfaces. The dose rate of γ radiation was also found to profoundly affect the morphology of the gold NPs.

3.7.2. Seeded radiolytic synthesis of anisotropic gold NPs in cetyltrimethyl ammonium bromide using γ radiation

Anisotropic gold nanorods were synthesized in the presence of the shape directing agent cetyltrimethyl ammonium bromide (CTAB) and Au seeds by controlling the dose rate of γ irradiation. At the relatively low dose rate of 0.8 kGy/h, the adsorption of Au^{3+} and its subsequent reduction on the growing NPs became slower, resulting in formation of gold nanorods with short aspect ratios. The Au nanorods were characterized by ultraviolet/visible (UV/VIS) spectroscopy and TEM.

3.7.3. Seedless synthesis of gold nanorods using the γ radiolysis technique

In this method, seeds were avoided, and the solution containing Au^{3+}, CTAB, isopropanol and acetone was irradiated at a relatively high dose rate of 3.4 kGy/h. Isopropanol and acetone were added to scavenge $H^{\bullet}$, $OH^{\bullet}$ and e^{-}_{aq}, and the isopropyl radical was generated in the solution. Isopropyl radical is a mild reducing agent that reduces Au^{+} to Au^{0} in a slow reaction. The slower reduction kinetics favour the formation of Au nanorods with an aspect ratio of 2.5.

3.7.4. Synthesis of rectangular plate like gold NPs by combining radiation and chemical methods

By combining chemical reduction with radiolytic reduction, a method was developed for the synthesis of plate like gold NPs. Initially, excess ascorbic acid was used to reduce Au^{3+} to Au^{+} in the presence of CTAB. The Au^{+} solution containing CTAB and ascorbic acid was γ irradiated for a short time to generate seeds in the solution. After irradiation, the ascorbic acid present in the solution reduced Au^{+} on the surface of the seeds, resulting in the formation of plate like gold NPs.

3.8. Islamic Republic of Iran

PLA is one of the most popular biodegradable polymers, and is the polymer matrix of choice for many researchers. It is an aliphatic thermoplastic polyester produced from renewable natural resources. The high melting temperature, good processability and mechanical properties of PLA, along with its biodegradability and biocompatibility, make it a preferred candidate for biomedical and pharmaceutical applications such as prosthetic implants, controlled release systems and three dimensional scaffolds for tissue engineering. However, its properties can be further enhanced by incorporating inorganic additives such as layered silicate, HAP and MNPs in a polymeric matrix to form a hybrid material. The goal of this research work was to improve the performance of PLA films by the incorporation of NPs. In phase I of this CRP, PLA/organically modified silicate layers were synthesized by the solution casting method and characterized by Fourier transform infrared (FTIR) spectroscopy, differential scanning calorimetry (DSC), XRD, stress-strain and TEM tests. In phase II, PLA/HAP nanocomposites were investigated. Incorporation of nanoclay and HAP particles in the PLA matrix stimulated crystal growth, as demonstrated by DSC, by higher melting. The morphology of the nanocomposites characterized by TEM and XRD revealed an exfoliated morphology in the PLA/organoclay nanocomposite films containing 4 pph of nanoclay. TEM of PLA/HAP nanocomposites demonstrated spherical HAP particles in the size range of ten to a few tens of nanometres, dispersed as single or agglomerated particles within the polymeric matrix. Subjecting the PLA nanocomposites to γ irradiation split the melting peak in both series of samples, indicating formation of crystallites with different crystalline structures. The PLA nanocomposites exposed to γ radiation exhibited higher crystallinity. The results obtained from an enzymatic degradation test showed that weight loss of the pristine PLA and PLA/organoclay nanocomposites depended on the crystallinity and morphology of the samples. However, enzymatic degradation of PLA/HAP nanocomposites in proteinase K solution showed that for a given exposure time, the rate of degradation of the PLA/HAP nanocomposites was faster than the pure and PLA/organoclay samples. In addition, the weight loss per unit of the surface increased with increasing HAP content and exposure time. It was found that, at low crystalline content, the degradation rate did not depend on the degree of crystallinity of the nanocomposites.

The results of stress-strain tests of the PLA/HAP nanocomposites showed that the mechanical properties were dependent on the composition, crystallinity and morphology of the prepared samples. Introducing NPs at low content improved the elongation at break of the nanocomposites by up to three times that of pure PLA. γ irradiation at a dose of 30 kGy increased the tensile strength in almost all of the prepared nanocomposites because of the higher crystalline content in those samples. Introducing a multifunctional monomer (triallyl isocyanurate (TAIC)) at a level of 1–2 pph increased slightly the tensile strength and decreased the elongation at break in 10 pph nanocomposites compared to neat nanocomposites.

3.9. Italy

A scalable, single step, synthetic approach to the manufacture of biocompatible, functionalized microgels and nanogels was developed: pulsed EB irradiation of PVP aqueous solutions. Relatively low energies per pulse and doses within the sterilization dose range led to a variety of 'as-born' sterile, functional nanostructures that exhibited a combination of favourable properties which made them suitable as biomedical nanocarriers. In particular, particles with different hydrodynamic diameters and surface charge densities were obtained by varying irradiation conditions, i.e. pulse frequency, dose per pulse, polymer concentration and pH. Reactive functional groups were either generated by radiation induced modification of PVP or by graft copolymerization of functional acrylic monomers. These groups can be used to attach fluorescent probes to the NPs, to bioconjugate the ligands of specific cell receptors and to incorporate therapeutics. To support the applicability of these nanogels and for their preparation procedure for biomedical use, several different biocompatibility tests were carried out. As a result, it can be concluded that these nanogels are non-cytotoxic and non-immunogenic at the cellular level. Their affinity towards the cells in vitro is manifested by a rapid uptake followed by a progressive release of the nanogels from the cells. Colocalization experiments carried out on cell cultures with fluorescent nanogels conjugated with a fluorescent antibody support the stability of this binding. The described approach, based on the use of industrial type linear accelerators (LAEs), provides strong evidence that this technology can be electively used to fabricate biohybrid nanogel based devices with a very promising future in nanomedicine.

3.10. Japan

Introduction of functional regions at a nanometre scale in polymeric films using γ rays, EBs and ion beams was proposed. Two approaches for building up nanoscale functional domains in polymer substrates were used: (i) radiation induced grafting to transfer nanoscale polymer crystalline structures (morphology), acting as a nanotemplate, to nanoscale graft polymer regions (the nanostructural polymers obtained can be applied to high performance polymer electrolyte membranes (PEMs) for fuel cells) and (ii) fabrication of nanopores and functional domains in thermally stable fluorinated plastic films using ion beams, which deposit the energy in a very narrow region of polymer films. The following are the outcomes of the research project performed over the last 2 years:

— Hydrophilic grafting polymers were introduced into hydrophobic fluorinated polymers, cross-linked polytetrafluoroethylene (cPTFE) and partially fluorinated copoly(ethylene tetrafluoroethylene (ETFE)) films, which are known to have lamellae and crystallites in the polymer films. Then, the hierarchical structures of hydrophilic graft domains were analysed by small angle X ray scattering (SAXS) and small angle neutron scattering (SANS) experiments as a function of grafting degree (GD). For the cPTFE substrate, graft polymers of 40 nm were introduced between the lamellar crystals at low GDs (<5%). The delocalized grafted domain around the lamellar crystals provided conducting paths, resulting in relatively high conductivity of the cPTFE PEM with low GDs, namely, low ion exchange capacity. At GDs above 15%, the grafting layers were totally connected to each other, but kept the lamellar crystal structures, resulting in higher conductivity with moderate mechanical strength. In the case of ETFE substrates, similar grafting domains with a 25 nm scale were generated from the lamellar templates of ETFE films at lower GDs. These results of cPTFE and ETFE clearly showed that the size of grafting domains can be controlled by the lamellar crystal size.
— For nanofabrication of polymer films using heavy ion beams, this work investigated the energy distribution in the radial direction, which was perpendicular to the ion trajectory. The effective radius of the penumbra in which radiation induced grafting took place was re-estimated for several different ion beams. Observations were made of different diameters of nanopores in PVDF based ion track membranes prepared by heavy ion beam irradiation followed by etching in 9M KOH at 80°C. The pore diameters were determined by linear energy transfer (LET) of the ion beams, which changed the threshold of the soluble part in the penumbra. Based on this phenomenon, the irradiation conditions were selected to have a gradient LET along the film thickness and after etching with KOH to result in anisotropic shapes of ion track pores in PVDF.

3.11. Republic of Korea

Recently, there has been increasing interest about ‘catalysis and environment’ in many scientific scenarios. Scientists have expressed serious reservations about the long term health problems traditionally associated with chemical catalytic processes. Biocatalysis, using either enzymes or whole cell microorganisms (now called white biotechnology), is used in many human activities. This use has been recently extended for the remediation of many compounds that are toxic to the environment. In this context, biocatalysis can be seen as an example of green chemistry to resolve many problems in the chemical catalysis. Redox proteins and enzymes immobilized on solid electrodes are recognized as important constituents of biocatalytic interfaces for molecular recognition to be applied in nanostructured biosensors.

Nitrite is a typical inorganic pollutant in environmental, food, industrial and physiological systems. Therefore, various methods for its detection and determination have been developed. The numerous analytical assays proposed for nitrite quantification encompass sophisticated and centralized techniques such as UV/VIS spectrophotometry (Griess reaction), ion chromatography, polarography, capillary electrophoresis, and gas chromatography coupled to mass spectrometry or fluorescence spectrophotometry. However, most of these analytical methods have shown important limitations such as sample pretreatment, susceptibility to matrix interferences, insufficient detection limits, long analysis time and lack of portability. This situation has challenged analytical sciences to develop innovative and improved tools, leading to the emerging field of enzyme based nitrite biosensors. Consequently, major progress has been made in nitrite analysis through the employment of highly selective, active and stable nitrite reducing enzymes.

The participating laboratory from the Republic of Korea is involved in research activities to develop highly selective and sensitive nitrite biosensors. A layer by layer technique and surface modification of carbon nanostructures were employed to fabricate biosensors for biomedical applications. Recently, a multifunctional electrospun nanobioweb using γ radiation has been developed. The multifunctional electrospun nanobioweb comprises the polymer host, silica, gold NPs and Cyt C (the nitrite selective enzyme). γ radiation was effectively utilized for the incorporation of silica and gold NPs in a single step. It was demonstrated that the multifunctional electrospun nanobioweb exhibited excellent bioelectrocatalytic properties for reduction of nitrite ions. These research studies demonstrated that γ radiation can be effectively used to incorporate the required functional components through a one step process, in an easier way compared to conventional multistep processes. Electrospinning is a simple, versatile and cost effective method, and γ irradiation can be judiciously used for the postmodification of electrospun fibre mats in biomedical applications.

3.12. Malaysia

The use of a microemulsion in the development of nanosized gel based on PEGDA and APO was demonstrated. PEGDA was solubilized in n-heptane with the use of dioctyl sodium sulphosuccinate (AOT) at 0.15M concentration to form reverse micelles, while APO was solubilized with sodium dodecyl sulphate (SDS) in water to form direct micelles. These micelles were then irradiated at 1–30 kGy using γ irradiation or EB radiation to cross-link the entrapped polymer in the micelles. Ionizing radiation was imparted to the emulsions to generate cross-linking reactions in the micelles formed. The nanosized gel was evaluated in terms of particle diameter using DLS, and the images of the nanosized gel were studied using TEM. Results showed that the size, MW and shape of the particles were influenced by the concentration of surfactants and irradiation dose. Curcumin was loaded into PEGDA nanogel, but 80% of the drug was released within 1 h. Thymoquinone can be absorbed and released by APO nanogels: smaller nanogels gave a sustained release, while the larger ones demonstrated a burst effect, releasing most of the loaded drug in the early phase.

3.13. Poland

Research activities within the project concentrated on two main areas: application of radiation techniques in the synthesis of polymer nanogels and radiation grafted thermocontrolled surfaces for cell layer technology. Within the first area, studies were performed on further development of polymer nanogel synthesis based on radiation induced intramolecular cross-linking of polymers, reinforcing labile H bonded interpolymer complexes (IPCs) using radiation and synthesizing nanogels by irradiation of substrates in ‘nanoreactors’, i.e. in inverse micelles.

Two new synthetic approaches were elaborated, allowing control of the physicochemical properties of the products — nanogels. One of them was based on two step irradiation, where, in the first step, the target weight was reached by mostly intermolecular cross-linking, while subsequently, mostly intramolecular cross-linking led to reducing the nanogel dimensions to the desired value. These approaches allowed the synthesis of nanogels of predetermined, independently chosen diameter and weight. In this way, the internal segment density of nanogels could be controlled. It was demonstrated that radiation could be used as a tool to reinforce labile IPCs by introducing covalent bonds and thus fixing their structure and making them irreversible. Application of classical grafting tools of radiation chemistry allowed the synthesis of new, thermocontrolled thin surfaces. Varying the temperature between 37°C and 15°C led to pronounced changes in the surface properties (from hydrophobic to hydrophilic). Fibroblast cells could be cultivated on such surface at 37°C to form a monolayer within 24 h. Lowering the temperature to 15°C led to detachment of the cell layer. These properties were confirmed in biological tests with human fibroblast cells. Such materials may be utilized to cultivate and detach fibroblast layers used in curing large surface burn wounds.

3.14. Serbia

The studies carried out under the scope of the project Radiolytically Synthesized Hybrid Nanosystems for Bionanotechnologies were related to:

— Radiation synthesis of Ag NPs in previously radiolytically polymerized and/or cross-linked hydrogels chosen for potential biomedical applications and antibacterial purposes;
— Investigation of the ability of γ irradiation to decorate CNTs with Ag nanoclusters, to obtain a potential optical teranostic probe;
— Study of the influence of the structure of capping agents on the optical properties of resulting Ag NPs during synthesis by γ irradiation.

Obtained results indicated that γ irradiation was suitable for in situ generation of Ag NPs in the investigated hydrogel matrix by using radiolytic products of water. NanoAg was successfully incorporated into a hydrogel matrix such as polyvinyl alcohol (PVA), PVP, poly(HEMA-co-IA) copolymer hydrogel, poly(*N*-isopropylacrylamide) (PNIPA) and poly(NIPA-co-IA) (IA = itaconic acid). These systems were suitable for various applications in reconstructive surgery. Ag/hydrogel nanocomposite systems had higher equilibrium swelling compared with neat hydrogel in simulated body fluid (SBF) solution. The release of Ag^+ from nanocomposite systems was continuous over long periods of time, which meant that the investigated hydrogel nanosystems met the criterion of a sustained, steady supply of active silver. The elements of the drug delivery paradigm were applied to Ag/hydrogel nanocomposites for the study of Ag release kinetics. The model that best fit the release data was selected based on the correlation coefficient. In the case of *Staphylococcus aureus* (Gram positive), the Ag NPs were more effective as antibacterial agents compared to *Escherichia coli* (Gram negative). Results clearly indicated that the smaller sized NPs were more potent, probably because of their greater solubility.

A simple and efficient one step method of producing a hybrid of uniformly dispersed Ag NPs supported on CNTs without acid purification or using any surfactant or polyelectrolyte to functionalize CNTs was achieved. The functionalization of CNTs with Ag NPs was achieved by anchoring the polymer to the surface of CNTs and simultaneous reduction of Ag^+ ions by the radiolytically produced polymer radicals. In addition, the structure and stability in the gas phase of Ag_n clusters formed by γ irradiation using the matrix assisted laser desorption/ionization, time of flight (MALDI TOF) technique, the matrix assisted laser desorption/ionization, time of flight/time of flight (MALDI TOFTOF) technique and theoretical ab initio calculations were investigated. Both the theoretical and the experimental results showed that the most stable clusters were small clusters with an odd number of atoms.

Results have shown that rod shaped Ag NP agglomerates were obtained from the solution of lower PVP concentration and lower MW, while spherical Ag NPs with a narrow size distribution and a diameter of 6 nm were obtained from the solution of higher PVP concentration and higher MW, as well as in hydrogel networks. On C coated Cu grids, some Ag NPs stabilized by higher concentrations of longer chains formed the dendritic Ag nanostructures after deposition. The optical properties of the investigated Ag/PVP nanosystems, as measured by the values of optical band gap energy (E_g), obtained by employing Tauc's expression, were the result of the simultaneous effects of several parameters: interparticle distance, concentration, structure of surrounding PVP macromolecules and, finally, the surface effect on the Ag NP lattice.

3.15. Thailand

Investigation of the radiolytic protocol for preparation of non-modified CS NPs and hydrophobic/hydrophilic modified CS NPs was proposed. The CS NPs were aimed at drug controlled release systems. γ radiation from a ^{60}Co source was used for nanomaterialization by controlling the MW, molecular structure, morphology and particle size of CS NPs. In this work, the roles of ionizing radiation were induced chain scission and grafting. Radiolysis served as a green method and a simple procedure for preparation of CS NPs of nanoscale sizes. Amphiphilic core shell CS NPs of 80 nm in size were obtained, and the shell thickness could be controlled by varying the irradiation dose. Water insoluble drug encapsulation efficiency and in vitro release behaviour confirmed the efficacy of CS NPs in drug controlled release systems. A bioactivity study via a paper disc diffusion method revealed the inherent antibiotic properties of the drug, as well as its controlled release from CS NPs. Cytotoxicity tests confirmed that the synthesized CS NPs obtained by radiolysis tended to reduce the toxicity of the drug.

3.16. Turkey

The scope of this research on radiation formation of nanostructures for potential biomedical applications comprised three main areas:

— Radiation formation of nanogels with controlled sizes;
— Preparation of molecularly imprinted matrices for recognition of glucose;
— Control of radiation induced polymerization via the RAFT process for the preparation of polymer drug conjugates.

The first two parts were the subject of research in the first 2 years of the project, and the final part was initiated after the second RCM held in Paris, following discussions with A. Hoffman from the USA, which led to collaboration between the two participating laboratories of Turkey and the USA on polymer drug conjugation.

For biomedical applications, controlling the size of nanogels is very important because it strongly affects the circulation time in blood and the bioavailability of the particles (at the nanoscale). It is known that particles in the 10–70 nm size range are the most effective for distribution in certain tissues, whereas those in the 70–200 nm range have the longest circulation times. The aim therefore was to prepare nanogels within these size ranges, with narrow distributions and great reproducibility. This work showed that PVP nanogels of these sizes can be prepared by controlling the initial MW, the concentration of PVP solutions, the total absorbed dose and the dose rate. Additionally, by controlling the coil size of the precursor polymer by solution thermodynamics by approaching theta conditions, it was possible to fine-tune the sizes of the resulting 10 kGy or 20 kGy irradiated nanogels. The PVP nanogels thus synthesized were later complexed with a KI/I_2 system to impart antimicrobial properties to the NPs. Thus, non-metallic nanoscale antimicrobial agents were prepared.

In the final phase of this CRP, nanogels of one of the most frequently studied thermoresponsive polymers, PNIPA, were prepared. It was demonstrated that this polymer shows a significant amount of aggregation in aqueous solutions and that to prepare well defined narrow distributed nanogels, these aggregations should first be dissolved. This was achieved using acetone, as proved by DLS studies. When aqueous solutions of PNIPA with individual, monomodal, narrowly distributed coils were irradiated, nanogels with a size range of 20–100 nm were obtained. To avoid any disturbance that might arise from using wide MW distribution polymers, PNIPA was synthesized using the RAFT process.

In collaboration with A. Hoffman, a new line of study was initiated, namely preparation of polymer drug conjugates. Styrene and maleic anhydride were copolymerized by irradiating equimolar solutions with γ rays in the presence of a RAFT agent. Styrene maleic anhydride (SMA) alternating copolymers with low MW and narrow distributions were obtained and characterized. Acetaminophen was conjugated to maleic acid moieties to prepare the polymer drug conjugate, and its drug release behaviour at different pH values was later investigated.

3.17. United States of America

In this study, new drug delivery nanogels have been synthesized by forming polymeric inclusion complexes. These complexes were formed by mixing polymer drug molecules (e.g. poly-paclitaxel) with polymer cyclodextrin

molecules. The maleic anhydride copolymers that were used to synthesize these polymer conjugates were commercially available; however, in the future, they will be synthesized by radiation initiated RAFT polymerization. These RAFT copolymers will have controlled MWs with narrow MW distributions, as indicated by a polydispersity index (PDI) close to 1.0.

The rationale for selecting this copolymer system comes from the previous clinical use of SMA copolymers with conjugated drug, neocarzinostatin, forming drug polymer amide bonded conjugates known as the 'SMANCS' drug delivery system. In these studies, the maleic anhydride group should be readily opened by hydroxyl groups on the cyclodextrin or paclitaxel molecules, forming ester groups that should be hydrolysable, releasing the drug. It is important to note that when the drug and the cyclodextrin are each conjugated to the different maleic anhydride copolymer backbones, carboxyl groups are simultaneously formed, enhancing the water solubility of the conjugated drug as well as the solubility of the nanogel NPs. Thus, the final nanogel particles will be negatively charged, and will grow to a limiting size, perhaps because of charge repulsion. It is intended to form an injectable formulation from the drug loaded nanogel. The nanogel particles should accumulate in a solid tumour owing to the enhanced permeability and retention effect.

Future work will use radiation to synthesize the maleic acid copolymers. Animal studies will also be carried out, and the nanogel will be targeted to cancer cells by using, as a targeting ligand, the peptide that is recognized by, and binds to interleukin 4 receptor, which is expressed by many cancer cells.

4. CONCLUSIONS

All participants concluded that the CRP was very successful. All the objectives were met and expected goals and products were delivered. Radiation technologies were once again shown to be an excellent tool for the synthesis and modification of nanomaterials for biomedical applications.

Some results have already been published in peer reviewed international journals and reported at international and national conferences. A list of publications is given at the end of this report.

These 'proof of concept' papers have been used to obtain additional resources to support further radiation nanotechnology applications.

Some of the products are already considered for transfer of technology to industry (Argentina, Brazil, Hungary, Malaysia and Poland).

The high level of achievements was possible as a result of establishing many collaborative links and exchanges of information between participating members and their institutions. For these collaborations, IAEA Technical Cooperation support, European Union seventh framework and national resources were mobilized.

It was agreed by the participants that the results should be published as this IAEA Radiation Technology Report.

5. RECOMMENDATIONS

Because, during the course of the CRP, the radiation technique was shown to be an excellent tool for synthesis and modification of nanomaterials for biomedical applications, the next step should focus on optimization of the process methods with regard to product properties. This should then be followed by scale-up of production from the laboratory to the manufacturing environment. The IAEA's Technical Cooperation Programme may offer opportunities for supporting this endeavour.

One important subject for further study is the investigation of long term stability, toxicity and biocompatibility of the synthesized nanomaterials.

Establishment of a strong collaboration between radiation chemists, engineers, biologists and medical scientists is needed for expanding future practical applications in nanobiotechnology.

REPORTS BY THE PARTICIPANTS OF THE COORDINATED RESEARCH PROJECT

NANOSTRUCTURING MATERIALS BY IONIZING RADIATION TECHNOLOGY: PROTEIN NANOPARTICLE PREPARATION AND FUNCTIONALIZATION OF TRACK ETCHED MEMBRANES

M. GRASSELLI[1], S. SOTO ESPINOZA[1], L.J. MARTINEZ[1], G. CASAJUS[1], M. SIRI[2], S. ALONSO[2], E.E. SMOLKO[3]

[1] Laboratorio de Materiales Biotecnologicos (LaMaBio)
Dpto. de Ciencia y Tecnología
Universidad Nacional de Quilmes
Bernal, Buenos Aires
[2] Laboratorio de BioMembranas (LBM)
Dpto. de Ciencia y Tecnología
Universidad Nacional de Quilmes
Bernal, Buenos Aires
[3] Comisión Nacional de Energía Atómica
Buenos Aires

Argentina

Abstract

Radiation technology is an industrially available technology with a potential application in the field of material nanostructuring. More than 20 years ago, it was demonstrated that it could be used for preparation of polymer microparticles with a very narrow particle size distribution. The report shows how smaller particles, in the nanoscale range, can be prepared by γ ray irradiation of an albumin solution containing a certain amount of ethanol. Particle sizes, between 10 nm and 20 nm can be tuned by changing the solvent conditions and independent of the irradiation dose. Near CD, UV/VIS and fluorescence spectroscopies were used for protein characterization in the nanoparticulate material. A scheme for a plausible mechanism of nanoparticle formation is also shown. Light scattering data, under protein denaturing conditions, show the cross-linking effect by measuring a low increment in the hydrodynamic radii of protein nanoparticles compared to the albumin under the same conditions. Track etched membranes are also nanostructured materials developed from swift heavy ion bombardment. The report also demonstrates membrane functionalization by grafting techniques. Two techniques for grafting polymerization — by a simultaneous radiation induced technique and by a novel technique using residual radicals — have been compared. Fluorescence techniques were implemented in order to follow the grafting process onto the tracks. The latter approach yields a modification that is homogeneously distributed in the nanochannels.

1. RADIOSYNTHESIS OF PROTEIN NPs

1.1. Introduction

More than 20 years ago, it was demonstrated that radiation technology could be used to generate polymer microparticles by precipitation polymerization with a very narrow particle size distribution [1]. In this way, methacrylate based microspheres could be prepared by radiation induced polymerization of DEGDMA and other cross-linked monomers in organic solvents. Particle diameters in the range 0.8–8 μm could be achieved by selection of the appropriate organic solvent [1, 2]. Tailor made microspheres were further developed by copolymerization of DEGDMA with reactive monomers, such as glycidyl methacrylate (GMA), or a special type of monomers to reach functional microspheres [3, 4]. However, smaller diameter particles (<0.8 μm) have not yet been achieved using this technique.

Another strategy was to obtain nanosized polymeric particles using ionizing radiation technology. Soluble synthetic polymers could be intramolecularly cross-linked in diluted solutions by quantum ray creating nanogels [5, 6]. By changing irradiation conditions, it was possible to generate intermolecular or intramolecular cross-linking of soluble polymer molecules in random coil conformations. Considering their aqueous environment and their rheological properties, they were called nanogels.

Proteins are also soluble macromolecules. However, most proteins have a very compact and defined three dimensional structure instead of a random coil, and are known as globular proteins. The impact of γ ray irradiation on globular protein solutions has been studied for many years, mainly regarding the biological effect of protein degradation or agglomeration, especially using human related proteins such as albumin [7, 8]. All these studies were conducted in physiological solutions.

Albumin is the most abundant protein in the mammalian plasma, and it serves as a carrier of hydrophobic biological and synthetic molecules such as anticancer drugs. Thus, preparation of albumin NPs should improve the drug delivery properties of this natural carrier.

Globular proteins are very sensitive to their microenvironment, thus the effects of the solvent during the irradiation process can be considerable. Noting that organic polar solvents induce protein aggregation without protein denaturation, they have been used for preparation of protein NPs by radiosynthesis. Ethanol is the preferred solvent because it has been used for protein precipitation for more than 60 years in plasma fractionation via the Cohn process [9].

In the present work, protein based NPs prepared by γ irradiation of globular protein solutions are described, with albumin as the basic building block, keeping its original conformational shape.

1.2. Materials and methods

BSA, fraction V, was obtained from Sigma-Aldrich. All other reagents were of analytical grade and used as received.

BSA was dissolved in 30mM, pH7 buffer phosphate. Different amounts of ethanol were added dropwise to the protein solution, keeping the temperature at 0°C under constant stirring. BSA solutions were irradiated with γ rays from a ^{60}Co source (Semi-industrial Irradiation Facility, National Atomic Energy Comission) at a dose rate lower than 1 kGy/h, and the sample temperature was maintained in the range 5°C–10°C during the irradiation. Protein solutions were diluted to a suitable concentration with phosphate buffered saline (PBS) for different experiments.

Particle size was determined by DLS at 25°C using a 90Plus/Bi-MAS particle size analyser with a light source of wavelength 632.8 nm and a 10 mW laser. Each result was the average of three measurements. Samples were kept at 4°C until analysed, and measurements were carried out on days 1 and 30 after sample preparation.

CD spectroscopy measurements were carried out at 20°C on an 810 spectropolarimeter equipped with a Peltier effect device for temperature control (Jasco Corporation, Japan). Six or ten spectra were recorded and averaged.

1.3. Results and discussion

Engineered NPs are attracting great interest for application in different medical fields. These nanosized materials have a high absorption efficiency in biological tissues. This constitutes one of the relevant characteristics for cosmetic and medical applications [10, 11].

For a long time, albumin has attracted the attention of the pharmaceutical industry, because it is the most abundant serum protein and because it has the ability to bind a wide variety of drug molecules and alter their pharmacokinetic parameters. Albumin NPs can be prepared by emulsification, but this method requires an organic solvent for removal of oil and surfactant. The desolvation process with organic solvents is another commonly used method for protein NP preparation [12, 13]. Chemical cross-linking with glutaraldehyde or heat denaturation are standard stabilization steps that are carried out to avoid particle dissolution. It is also known that albumin oligomerization by a thermal process involves protein denaturation [14].

Globular proteins are macromolecules that are very sensitive to the microenvironment, and their two most common protein precipitants — ethanol and ammonium sulphate — were considered as modifiers in irradiated protein solutions. Both additives alter solubility by a dewatering effect on the solvated protein. In the particular case of BSA, more than 60% ethanol is required to induce precipitation.

Samples were analysed by DLS to determine the population of particle sizes in the solution. Figure 1 shows NP formation from irradiated protein solution under subprecipitant concentrations of ethanol and ammonium sulphate. The addition of increasing quantities of ammonium sulphate to the protein solution did not change the average size of the particles after irradiation. However, in buffer/ethanol mixtures, NPs can be found with sizes that increased in the same proportion that the solvent increased in the irradiated mixture.

To analyse other protein compatible polar solvents, acetonitrile and isopropanol were used as additives to the protein solution in an equivalent molar concentration of ethanol (40% volume per volume (v/v)). Both solvents, which are compatible with globular proteins, can also induce NP formation; acetonitrile reaches an NP size of 14 ± 1 nm and isopropanol a size of 35 ± 4 nm under the same irradiation conditions.

The effect of γ irradiation dose on a BSA solution in buffer and buffer/ethanol 40% v/v was studied. A dose rate lower than 1 kGy/h and different irradiation times were used for each condition. Figure 2 shows the DLS measurements after sample dilution in PBS, corresponding to BSA solutions irradiated at different radiation doses in the range 1–20 kGy. Irradiations higher than 5 kGy were necessary to obtain NPs. The protein sizes of samples irradiated in the buffer remained approximately at their original size when they were irradiated within this dose range. These results are in agreement with data reported for MW determination by DLS of an irradiated BSA solution in an oxygen atmosphere [8].

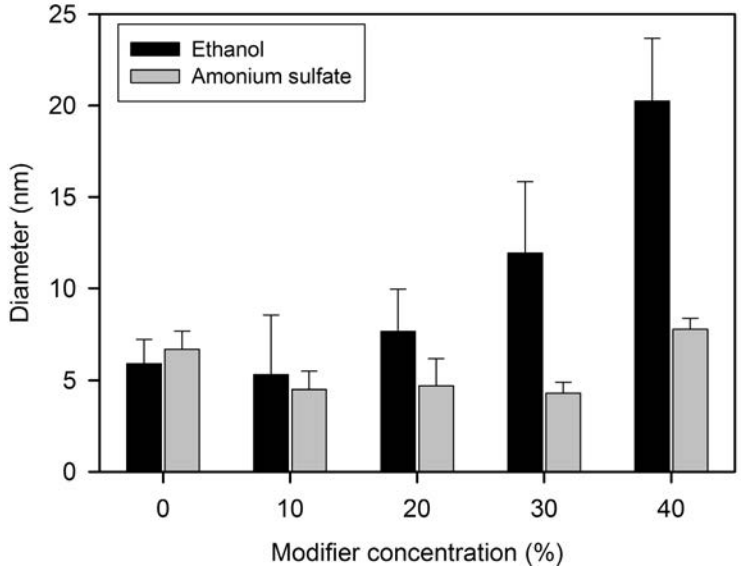

FIG. 1. Particle size for BSA irradiated samples (dose = 10 kGy; dose rate = 1 kGy/h) with two different additives: ethanol and ammonium sulphate. Standard deviations correspond to three independent samples.

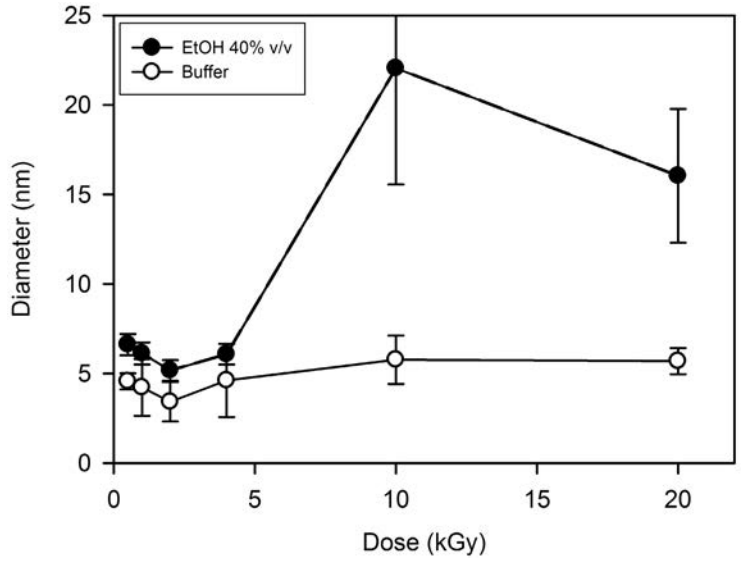

FIG. 2. Particle sizes for irradiated BSA samples in buffer and buffer/ethanol mixtures at different doses. Samples were diluted in buffer for DLS determination. EtOH: ethanol.

To study the occurrence of NPs by a more sensitive technique, a small amount of BSA molecules (<5%) was labelled with fluorescein isothiocyanate (FITC), prior to NP radiosynthesis. Fluorescence emission of irradiated and non-irradiated protein samples was measured after 10 kGy irradiation for different buffer/ethanol ratios from 0% to 40% v/v. In Fig. 3, the relative fluorescence unit (RFU) of irradiated BSA versus non-irradiated BSA shows a decrease that is proportional to the amount of ethanol in the solution. Fluorescence of irradiated BSA sample in ethanol 40% v/v has only 25% of the initial RFU, which can be explained as a quenching process for the aggregation of BSA molecules in the NP. Irradiated samples without ethanol do not show any evident change in fluorescence emission. This graph shows a progressive effect of the solvent concentration on protein aggregation.

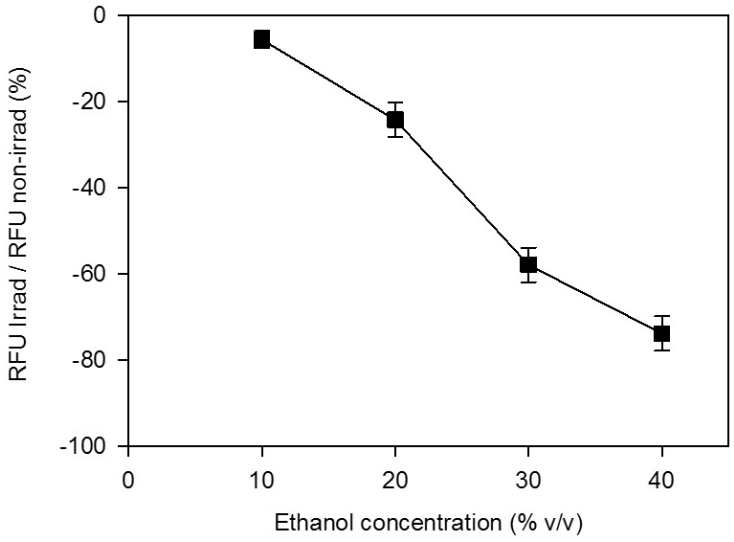

FIG. 3. Fluorescence ratio at 518 nm of irradiated and non-irradiated BSA samples in buffer/ethanol mixtures.

The three dimensional structure of BSA included in the NPs was studied using fourth derivative UV/VIS spectroscopy and near CD spectroscopy. It was established that both techniques are sensitive in detecting instantaneous protein conformational changes. Alteration of the microenvironment (polarity, hydration, hydrophobic interactions and packing density) of tyrosine and tryptophan amino acids can be followed using these spectroscopic techniques.

The fourth derivative UV/VIS spectra of the irradiated BSA samples have the same spectrum shapes, and no absorbance peaks shifts were noticed, indicating that the microenvironments of aromatic amino acids have the same conformational features as the protein [15].

Near CD spectroscopy gives information about the ternary protein structure and the symmetry around aromatic amino acids where only folded proteins have CD spectral information. Figure 4 shows the CD characterization of BSA samples. CD spectra of the irradiated samples show no changes in the general spectral shape. However, ethanol concentrations from 20% to 40% show an increase in the CD signal. This effect could be attributed to a more rigid conformational structure of the protein.

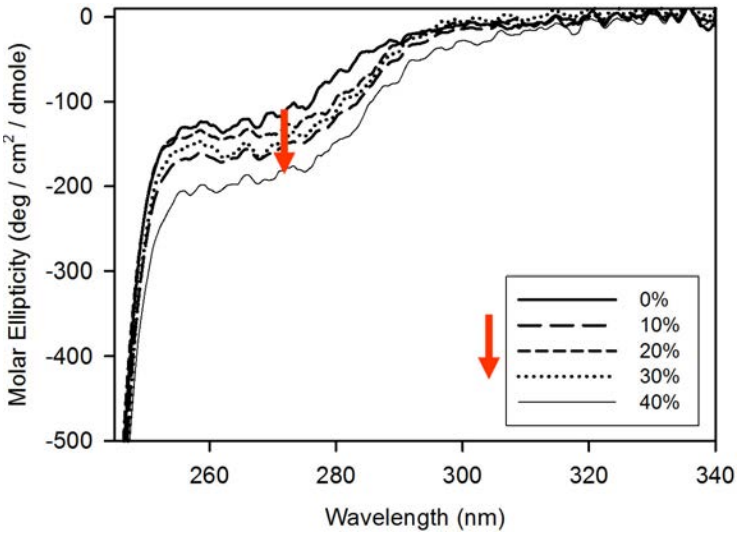

FIG. 4. CD spectroscopy of the irradiated BSA samples with different ethanol proportions.

The CD and UV/VIS data show that most BSA proteins in the samples keep their native structure. Thus, NPs should be formed by an aggregation of protein molecules in their native conformation.

To study the nature of the linkage between protein molecules, irradiated samples were analysed using DLS under chaotropic conditions to unfold proteins. DLS measurements in 6M guanidinium chloride (GdmCl) medium are shown in Table 1. All recorded data reached much larger diameters than the ones plotted in Fig. 1, as can be expected for unfolded and open protein structures. Data of higher dispersion can be attributed to the random coil unstructured particles in the present solvent conditions. Additionally, an inverse correlation between the initial ethanol concentration and particle diameter in the unfolded condition is shown in Table 1. Thus, it seems that higher amounts of ethanol induce more protein aggregation; thus, there is a higher probability that the particles are covalently intercatenary cross-linked.

TABLE 1. AVERAGE PARTICLE DIAMETERS OF BSA SOLUTIONS IRRADIATED AT 10 kGy WITH THE ADDITION OF ETHANOL*

Ethanol (%)	Particle diameter ± standard deviation (nm)
0	630 ± 500
10	650 ± 200
20	440 ± 400
30	190 ± 140
40	100 ± 80

* Samples were diluted in 6M GdmCl, 20 h prior to DLS measurement.

NP yield is also an important parameter to be determined. Size exclusion chromatography (SEC) analysis to study the abundance of the different molecules of the sample shows that more than 95% of the protein is in the high MW fraction (see Fig. 5(a)).

One of the possibilities of BSA covalent aggregation could be by a dithiol bridge through cysteine amino acids. By treatment of BSA NP with dithiotreitol solution, a strong reducing reagent can reduce dithiol bridges to release BSA. According to Fig. 5(b), BSA NP does not show monomeric BSA leaching or reduction in BSA NP molecular size when analysed by SEC.

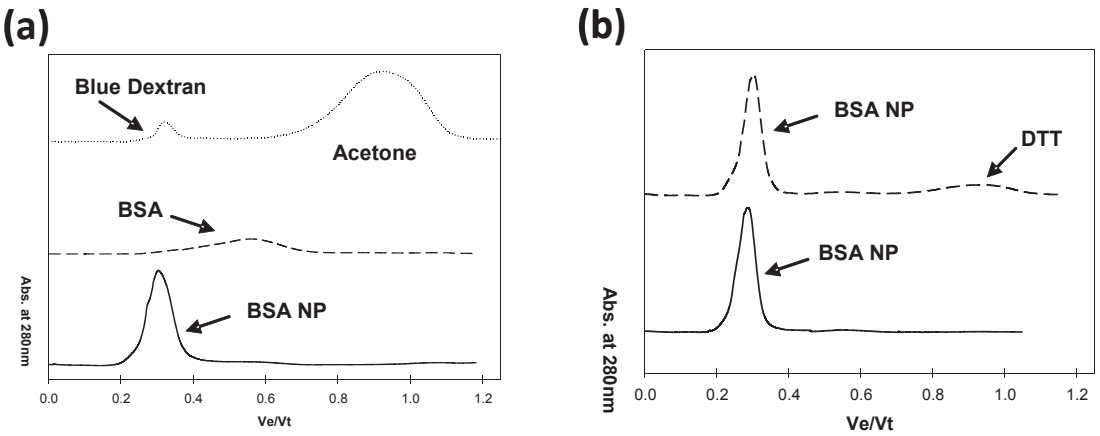

FIG. 5. SEC (a) MW analysis: MW markers, BSA and BSA NP and (b) MW analysis of BSA NP (___) and BSA NP treated with dithiotreitol (_ _ _). Abs.: absorbance; DTT: dithiothreitol.

As is shown in Table 2, BSA dissolved in the buffer/ethanol mixture gives particles of similar sizes to those using glutaraldehyde or γ irradiated treatment. This observation suggests that aggregation and cross-linking are sequential independent steps.

TABLE 2. AVERAGE PARTICLE DIAMETERS OF BSA IN PB WITH ETHANOL 40% v/v AFTER PARTICLE SYNTHESIS*

Condition	Particle diameter ± standard deviation (nm)
Irradiated 10 kGy	20.5 ± 3.5
Glutaraldehyde 2.5%	17.5 ± 3

* Samples were diluted in PB prior to DLS measurement.

To elucidate the mechanism of NP formation, further studies using DLS were performed (Fig. 6). BSA and BSA NP prepared in buffer/ethanol were diluted with the corresponding solvent or with buffer. Under these conditions, DLS measurements showed quite different results. Diameter distribution profiles of BSA in the presence of ethanol showed protein aggregation, irrespective of irradiation condition. Non-irradiated samples prepared with buffer/ethanol and further buffer diluted did not show aggregation. Thus, it can be concluded that the protein aggregation step is a fast reversible process that varies dynamically according to the ethanol concentration in the media.

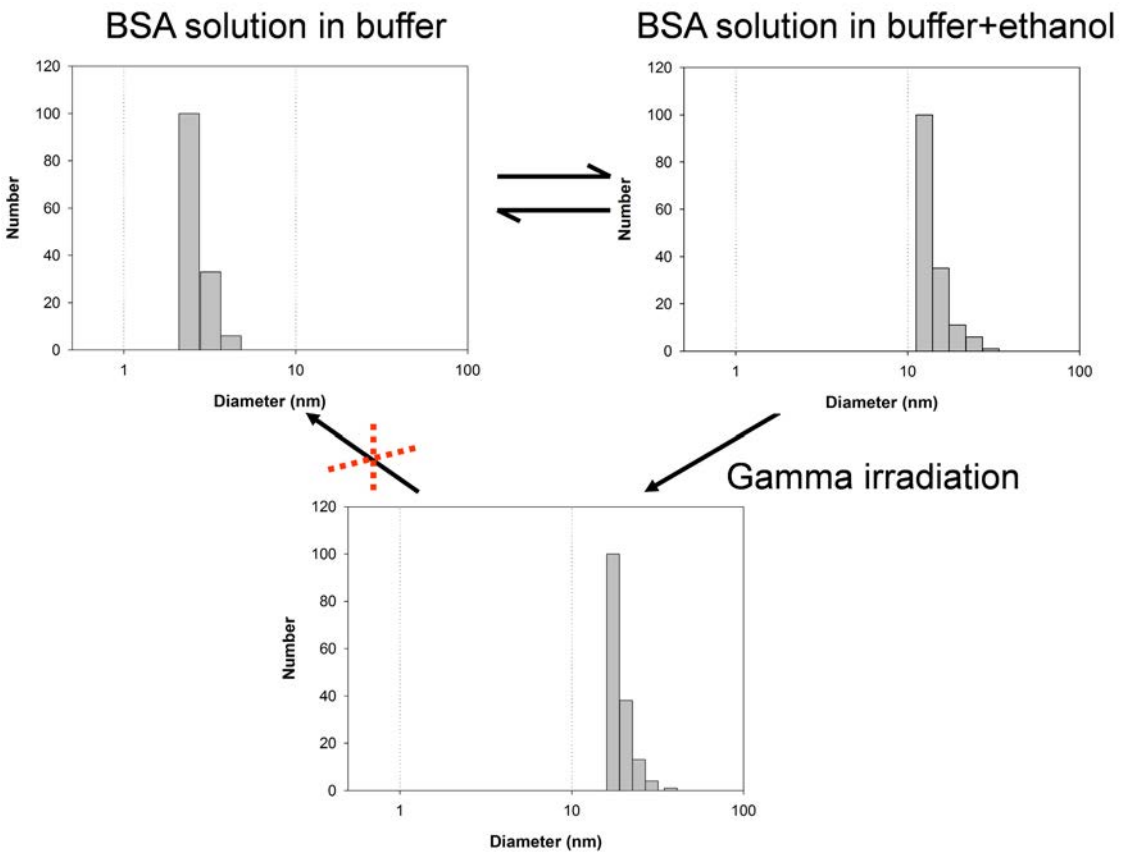

FIG. 6. Schematic of BSA NP formation according to DLS data from different steps.

TEM pictures are shown in Fig. 7, depicting in Fig. 7(a) that BSA NP has a spherical shape with a slight elliptical deformation. According to the literature, this is an advantage because the ratio between volume and surface will be optimized and the surface tension reduced. This structure also allows better circulation and less adhesion to the surface of blood vessels, and better encapsulation and slower extravasation.

It is envisioned that BSA NP can be used as a drug carrier. Discovery of new drug delivery systems and more efficient carriers have been important issues to address. An efficient carrier is one that is biodegradable, has a favourable shape and improves its circulation, biodistribution and uptake, as well as drug release. In this work, an albumin/emodin complex was prepared as a model of a drug delivery carrier. Emodin is an antitumoural, anti-inflammatory drug obtained from plants. Figure 7 shows TEM pictures corresponding to BSA emodin complexes. In Figs 7(b) and 7(c), BSA NP/emodin and BSA/emodin can be compared. It can be inferred that the NPs have a better molecular encapsulation and a more homogeneous drug distribution.

This report covers the study of other protein NP synthesis. Lysozyme (Lys), which is a commercial bacteriolytic enzyme, was used as a second protein model. Lys has an antimicrobial activity against Gram positive bacteria, thus Lys NPs should have a similar enzymatic activity.

Lys NPs were prepared by mixing different ratios of BSA and Lys. BSA and Lys (10/1 molar ratio) were irradiated in 35% ethanol in water. To demonstrate the presence of Lys in the NPs, bacteriolytic activity against *Micrococcus lysodeikticus* was tested. NPs were purified by successive centrifugation steps. Figure 8 shows that the enzymatic activity of BSA Lys NPs has a similar trend to free Lys NPs.

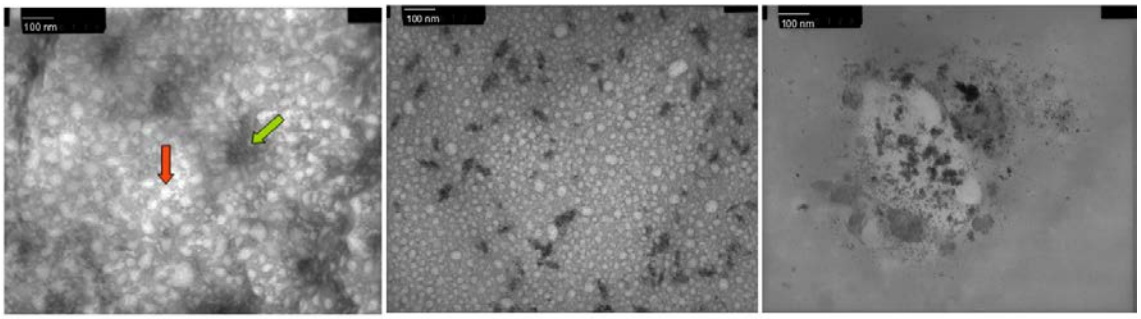

(a) (b) (c)

FIG. 7. TEM pictures of (a) BSA NP, (b) BSA NP/emodin (1/1), (c) BSA/emodin (1/1). The red arrow points to the BSA NP and the green arrow points to the BSA free molecule.

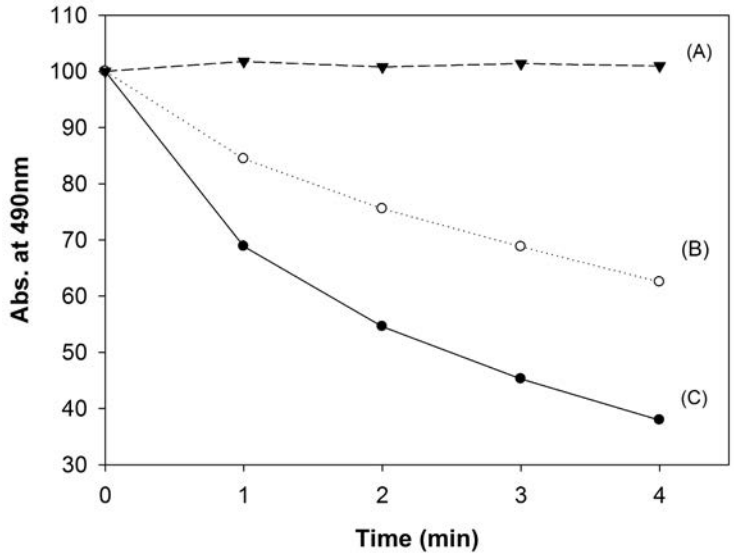

FIG. 8. Enzyme activity measured as the reduction of light dispersion by the lytic effect of Lys (absorbance measurement at 490 nm of bacteria suspension). ▼: Control; ●: addition of Lys solution (0.5 mg/mL); ○: addition of Lys BSA NP. Abs.: absorbance.

The effect of atmosphere during the irradiation process was studied by saturation of the BSA solution with gaseous nitrogen, air or acetylene previous to the γ irradiation. Samples were analysed by DLS after dilution in PBS. In Table 3, the results corresponding to triplicate samples that were irradiated with 10 kGy are summarized.

TABLE 3. AVERAGE PARTICLE DIAMETERS OF BSA NP IN PB WITH ETHANOL 35% v/v AFTER PARTICLE SYNTHESIS UNDER DIFFERENT ATMOSPHERES

Condition	Particle diameter ± standard deviation (nm)
Nitrogen atmosphere	28 ± 15
Air atmosphere	37 ± 10
Acetylene atmosphere	22 ± 3

BSA NP prepared under different gaseous atmospheres gives different NP sizes. Air and acetylene conditions give significantly different NP sizes.

2. NANOCHANNEL FUNCTIONALIZATION

2.1. Introduction

Nanotechnology has been growing faster than other technologies in the past decade. In particular, swift heavy ion bombardment is a well established technique to generate membranes with micropores and nanopores. An important feature of this approach is the ability to control properties such as the size and shape of these nanostructures.

Membrane technology has had a very high impact on chemical and biotechnology industries in the last 30 years. Sustainable processes and low energy consumption are the main features and advantages. Today, the most important industrial market segments are medical devices and water treatment. However, novel applications involve adsorptive membranes, catalysis or sensor systems, in addition to their separation properties by MW discrimination [16, 17].

Track etched membranes are a special kind of membrane where pores are built, one by one, using swift heavy ion bombardment of polymeric films. Latent tracks made by particle bombardment are subsequently etched with specific chemical reagents according to the chemical structure of the trunk polymer. The unique properties of these membranes — very narrow pore size distribution and controlled pore number per area — have specific applications in biology. Track etched membranes are currently commercial products that are useful for cell separation and air monitoring, cell biology and liposome preparation by lipid extrusion.

Novel applications of nanotechnology, such as preparation of nanowires, nanofilters and sensors for special usage, have been reviewed [18]. In addition, single ion nanochannels and nanowire fabrication are currently possible [19].

Wet chemical protocols have been applied to achieve functionalization of track etched membranes [20–22] for different applications. However, special reagents and protocols are required.

During ion bombardment, a high energy deposition along the ion path through the polymer produces a cylindrical damage region in the material. The core of the trace has a significantly reduced diameter. However, there is a large amount of energy dissipated by emitting a huge number of electrons (delta rays) perpendicular to the ion trace, which extends the damage zone to a radius of a few tens of nanometres around the trace core [23].

The chemical etching process can dissolve the polymer's damaged region by hydrolysing the polymer chains, reaching pore diameters in the nanometre to micrometre range on the material. After the etching procedure on the irradiated polymer, there are enough active sites left that can be used to initiate a polymerization process. In this way, grafting can be performed selectively in the etched pores. AAc has been polymerized on track etched pore walls of polypropylene (PP) and PVDF [24, 25].

Another unique property of track etched membranes is their transparency, as suggested by Apel [26]. Taking this into account, fluorescence derivatization of PET track etched membranes was studied in the present work. In addition, the high sensitivity of the fluorescence technique will be a useful tool for studying the grafting process in these nanostructures.

2.2. Materials and methods

GMA and cysteamine for synthesis were from Sigma Chemical Co. and FITC was from Merck. All reagents were used without further purification. Analytical grade solvents (ethanol) were all from Bioanalitica. All other reagents were of analytical grade.

Nuclear track PET foils were irradiated with 250 MeV ions of ^{84}Kr or 125 MeV ions of ^{129}Xe, with fluences of 3×10^7 cm^{-2} and 7×10^7 cm^{-2}, respectively, kindly donated by M.-C. Clochard from CEA (France).

The etching procedure was performed on 5 cm × 5 cm foils. Samples were previously washed with distilled water and ethanol and dried at 40°C. UV sensitization pretreatment with a UV light was carried out by irradiating, for 1 h, each side of the foils, using a UV lamp. The etching step was run in NaOH solution at 50°C. The grafting procedure was run immediately after etching by soaking in 10% GMA monomer solution (ethanol/water, 1/1 ratio)

under nitrogen atmosphere at 62°C for different periods of time. Then, grafting samples were washed in water and ethanol in alternate cycles and dried in an oven at 40°C overnight. Chemical modifications of grafted samples were carried out to epoxide pendant groups of polyGMA by soaking them in 50mM, pH7.5, buffer Tris containing 10 mg/mL cysteamine. Fluorescent labelled samples were labelled with a 0.25 mg/mL solution of FITC in 0.1M, pH9.0, buffer carbonate.

Fluorescence measurements were performed in a Nanodrop 3300 microvolume full spectrum fluorospectrometer (Thermo Scientific). RFUs for fluorescence were acquired at 508 nm during sample excitation with a blue light emitting diode. RFU measurements correspond to a cylindrical section of area 0.1256 mm^2.

Field emission scanning electron microscopy (FESEM) was carried out using a Zeiss Supra 40 (Carl Zeiss NTS, LLC). Fluorescence and confocal images were recorded using an Eclipse TE2000 (Nikon) fluorescence microscope.

2.3. Results and discussion

To achieve nanopore functionalization of track etched membranes, two different approaches using radiation technology were studied: simultaneous radiation induced grafting polymerization and grafting from residual radicals from the etching process.

2.3.1. Simultaneous radiation induced grafting

In this strategy, track etched PET membranes were soaked in a monomer solution and irradiated with a ^{60}Co γ source according to the methodology developed in our laboratory (Laboratory for Biotechnological Materials) [27]. Monomer solutions of GMA were prepared at very low concentrations (0.3%–0.6%) in ethanol/water (1/1 v/v) mixtures and degassed by bubbling nitrogen. A dose of 10 kGy and a dose rate of 1 kGy/h were the standard irradiation conditions.

Weight differences of the grafted membrane were below the detection limits of an analytical microbalance, and so microscopy techniques were used instead. In Fig. 9, FESEM pictures of PET membranes are shown. A grafted layer of polyGMA can be seen on the polymer surface, in addition to pore diameter reduction (490–180 nm pore diameter reduction).

Grafted layer thickness was not easily controlled by the monomer concentration because of the high error in volume handling. In addition, the skinned layer was very sensitive to peeling from the surface. Thus, this approach was discarded for future work.

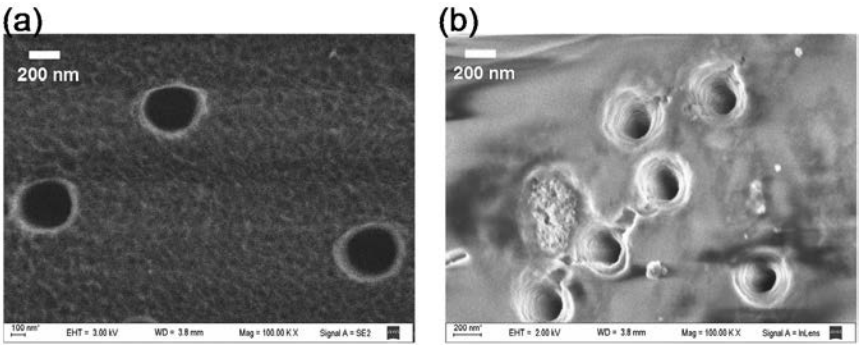

FIG. 9. FESEM pictures of (a) a PET track etched membrane and (b) a grafted membrane using 0.3% GMA and a 10 kGy dose.

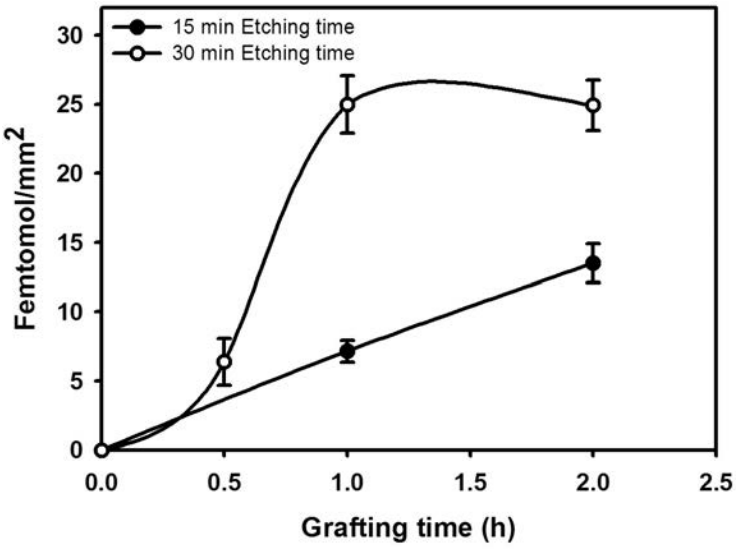

FIG. 10. Grafting amount for two different PET track etched membranes versus grafting time at 62°C and 10% GMA.

2.3.2. Grafting from residual radicals

Grafting onto the walls of the submicroscopic pores of the track-eched membranes was performed by utilizing the residual radicals [24]. Briefly, immediately after etching, membranes were grafted by soaking in a methacrylate monomer solution of GMA under nitrogen atmosphere at 62°C.

To visualize the grafting yield, two methods were used: FESEM and fluorescence detection of the cysteamine and fluorescein labelled epoxy groups of the grafted chains. Labelled membranes were measured directly using a spectrofluorometer to quantify the grafting. Figure 10 shows the evolution of the grafting process on two PET track etched membranes previously etched with 2N NaOH.

To confirm that the grafting localization is in the nanochannel region, labelled membranes were visualized using fluorescence microscopy. In Fig. 11, an etched grafted membrane and an etched membrane as control are compared. Additionally, image analysis determined that experimental fluence of the grafted and etched membranes reached $7.3 \pm 0.5 \times 10^7$ cm^{-2} and $7.6 \pm 0.3 \times 10^7$ cm^{-2}, respectively. Thus, the modification process involves all the nanochannels.

Several etched membranes with different pore diameters were grafted with GMA over 4 h and fluorescein tagged as previously described. A linear correlation between fluorescent labelled grafting and pore diameter was found for a broad range of track etched membranes of the same fluence prepared at different etching temperatures (see Fig. 12). This result agrees with homogeneous internal pore surface modification.

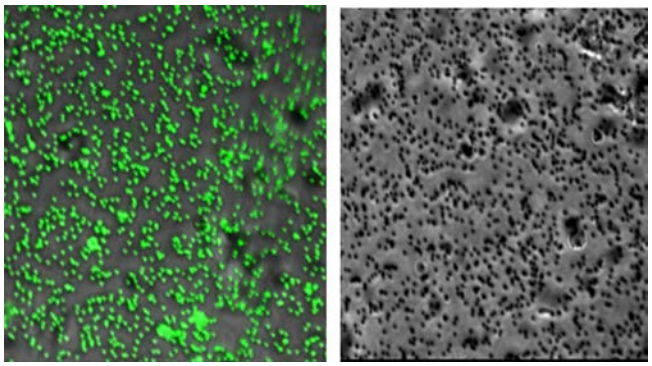

FIG. 11. Fluorescence microscopy images corresponding to a labelled grafted etched membrane (left) and an etched membrane (right).

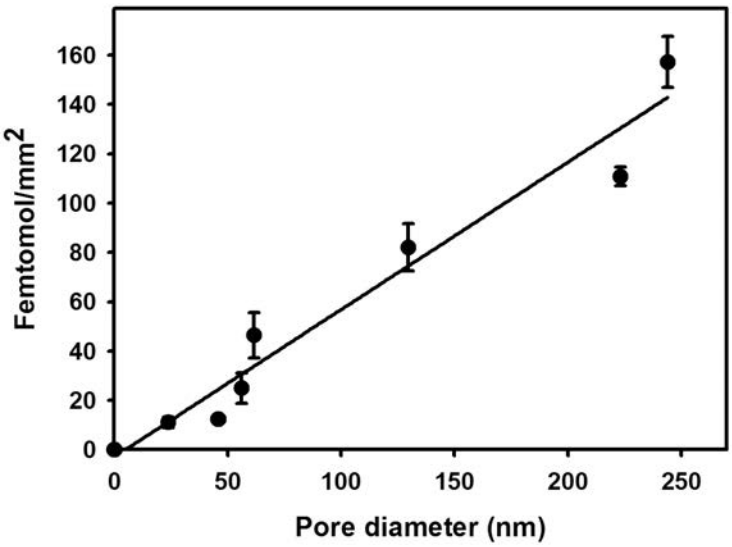

FIG. 12. Grafting amounts for different PET track etched membranes of different pore diameters and the same fluence.

3. CONCLUSION

Irradiation of globular protein solutions has been extensively studied in the past. Most of these studies have focused on the physicochemical changes in the protein structure.

In this report, globular protein BSA was used as a basic unit to build NPs by γ irradiation of protein solutions with cosolvents. By changing the organic solvent amount, protein clusters could be dynamically created in solution, which were further stabilized by radiation cross-linking. Protein NPs in the range 20–40 nm were found after γ irradiation of a protein in an aqueous/ethanol solution. NPs were characterized by DLS, fluorescence, UV and CD spectroscopy, which showed that protein molecules keep their overall structure.

Another important achievement of this report is the potential for size tailoring the BSA NPs. Correlation between cosolvent concentration and NP size was demonstrated by different techniques. This report has also contributed to a deeper understanding of the mechanism of protein NP synthesis. Experimental evidence supports the hypothesis of a two step process, corresponding to an aggregation step and further cross-linking performed by ionizing radiation. Thus, NP size could be controlled by the ethanol/water proportion in the sample. It is important to highlight that this method can synthesize high concentrations of protein NPs without precipitation and can achieve high yields without use of any additional chemical cross-linkers.

NP radiosynthesis could also be extended to other enzymes by coaggregation with BSA. Functional NPs should have the corresponding activity of the former enzyme. Further studies to develop drug delivery based on this technology will be carried out in the near future.

In track etched membranes, the functionalization of PET track etched membranes in a tailor made manner by polymerization on the remaining radicals has been reported. Different fluorescence techniques to follow the grafting process onto the nanochannels have been implemented. The grafting process was revealed, and was homogeneously distributed in all the nanochannels. Fluorescence techniques give us a powerful tool to follow grafting processes under different synthesis conditions. The development of optical sensors based on these functional nanochannels is also envisioned.

ACKNOWLEDGEMENTS

S.L. Soto Espinoza and L.J. Martinez thank the National Agency for the Promotion of Science and Technology, Argentina, for fellowships. S. Alonso and M. Grasselli are researchers from the National Scientific and Technical

Research Council, Argentina. This work was partially supported by grants from the National University of Quilmes and the Ministry of Science, Technology and Productive Innovation, Argentina.

REFERENCES

[1] YOSHIDA, M., ASANO, M., KAETSU, I., MORITA, Y., Characteristics of polymer microspheres prepared by radiation-induced polymerization in the presence of organic solvents, Radiat. Phys. Chem. **30** (1987) 39–45.
[2] NAKA, Y., KAETSU, I., YAMAMOTO, Y., HAYASHI, K., Preparation of microspheres by radiation-induced polymerization. I. Mechanism for the formation of monodisperse poly(diethylene glycol dimethacrylate) microspheres, J. Polym. Sci. A: Polym. Chem. **29** (1991) 1197–1202.
[3] CHEN, C.-H., LEE, W.-C., Preparation of methyl methacrylate and glycidyl methacrylate copolymerized nonporous particles, J. Polym. Sci. A: Polym. Chem. **37** (1999) 1457–1463.
[4] SAFRANY, A., et al., Functional polymeric microspheres synthesized by radiation polymerization, Radiat. Phys. Chem. **46** (1995) 203–206.
[5] KADLUBOWSKI, S., GROBELNY, J., OLEJNICZAK, W., CICHOMSKI, M., ULANSKI, P., Pulses of fast electrons as a tool to synthesize poly(acrylic acid) nanogels. Intramolecular cross-linking of linear polymer chains in additive-free aqueous solution, Macromol. **36** (2003) 2484–2492.
[6] ULANSKI, P., JANIK, I., ROSIAK, J.M., Radiation formation of polymeric nanogels, Radiat. Phys. Chem. **52** (1998) 289–294.
[7] DAVIES, K.J.A., Protein damage and degradation by oxygen radicals. I. General aspects, J. Biol. Chem. **262** (1987) 9895–9901.
[8] KUME, T., MATSUDA, T., Changes in structural and antigenic properties of proteins by radiation, Radiat Phys. Chem. **46** (1995) 225–231.
[9] COHN, E.J., HUGHES, W.L., Jr., WEARE, J.H., Preparation and properties of serum and plasma proteins, XIII. Crystallization of serum albumins from ethanol-water mixtures, J. Am. Chem. Soc. **69** (1947) 1753–1761.
[10] PARDEIKE, J., HOMMOSS, A., MULLER, R.H., Lipid nanoparticles (SLN, NLC) in cosmetic and pharmaceutical dermal products, Int. J. Pharm. **366** (2009) 170–184.
[11] FORTINA, P., et al., Applications of nanoparticles to diagnostics and therapeutics in colorectal cancer, Trends Biotechnol. **25** (2007) 145–152.
[12] MARTY, J.J., OPPENHEIMER, R.C., SPEISER, P., Nanoparticles—a new colloidal drug delivery system, Pharm. Acta Helv. **53** (1978) 17–23.
[13] WEBER, C., COESTER, C., KREUTER, J., LANGER, K., Desolvation process and surface characterisation of protein nanoparticles, Int. J. Pharm. **194** (2000) 91–102.
[14] VAIANA, S.M., EMANUELE, A., PALMA-VITTORELLI, M.B., PALMA, M.U., Irreversible formation of intermediate BSA oligomers requires and induces conformational changes, Proteins **55** (2004) 1053–1062.
[15] SOTO ESPINOZA, S.L., SÁNCHEZ, M.L., RISSO, V., SMOLKO, E.E., GRASSELLI, M., Radiation synthesis of seroalbumin nanoparticles, Radiat. Phys. Chem. **81** (2012) 1417–1421.
[16] ULBRICHT, M., Advanced functional polymer membranes, Polymer **47** (2006) 4217–4262.
[17] VENTURA, M., FERNANDEZ LAHORE, M., SMOLKO, E.E., GRASSELLI, M., High-speed protein purification by adsorptive cation-exchange hollow-fiber cartridges, J. Membr. Sci. **321** (2008) 350–355.
[18] WAHEED, A., et al., The track nanotechnology, Radiat. Measure. **44** (2008) 1109–1113.
[19] SPOHR, R., et al., Controlled fabrication of ion track nanowires and channels, Nucl. Instr. Meth. B **268** (2010) 676–686.
[20] RERAT, V., POURCELLE, V., DEVOUGE, S., NYSTEN, B., MARCHAND-BRYNAERT, J., Surface grafting on poly(ethylene terephthalate) track-etched microporous membrane by activation with trifluorotriazine: application to the biofunctionalization with GRGDS peptide, J. Polym. Sci. A: Polym. Chem. **48** (2010) 195–208.
[21] FRIEBE, A., ULBRICHT, M., Controlled pore functionalization of poly(ethylene terephthalate) track-etched membranes via surface-initiated atom transfer radical polymerization, Langmuir **23** (2007) 10 316–10 322.
[22] SMULEAC, V., BUTTERFIELD, D.A., BHATTACHARYYA, D., Permeability and separation characteristics of polypeptide-functionalized polycarbonate track-etched membranes, Chem. Mater. **16** (2004) 2762–2771.
[23] CHAPIRO, A., Chemical modifications in irradiated polymers, Nucl. Instr. Meth. B **32** (1988) 111–114.
[24] MAZZEI, R., GARCÍA BERMÚDEZ, G., CHAPPA, V.C., DEL GROSSO, M.F., FERNANDEZ, A., Grafting on nuclear tracks using the active sites that remain after the etching process, Nucl. Instr. Meth. B **251** (2006) 99–103.
[25] CUSCITO, O., CLOCHARD, M.-C., ESNOUF, S., BETZ, N., LAIREZ, D., Nanoporous b-PVDF membranes with selectively functionalized pores, Nucl. Instr. Meth. B **265** (2007) 309–313.
[26] APEL, P., Swift ion effects in polymers: industrial applications, Nucl. Instr. Meth. B **208** (2003) 11–20.
[27] GRASSELLI, M., et al., Immobilized metal ion affinity hollow-fibre membranes obtained by the direct grafting technique, Radiat. Phys. Chem. **55** (1999) 203–208.

ENCAPSULATION AND NANOENCAPSULATION OF PAPAIN ACTIVE SITES TO ENHANCE RADIOLYTIC STABILITY AND DECREASE TOXICITY

G.H.C. VARCA, C.C. FERRAZ, M. BEATRIZ MATHOR, P. SANTOS LOPES,
S. ROGERO, J.R. ROGERO, A.B. LUGÃO
Instituto de Pesquisas Energéticas e Nucleares — IPEN-CNEN/SP
Av. Prof. Lineu Prestes, 2242 Cidade Universitária
05508-000 São Paulo-SP
Brazil

Abstract

Papain is used as an ingredient in various enzymatic debridement preparations. These pharmaceutics are based on water solutions and are usually sterilized by radiation. As a consequence, there is a major decrease in papain activity. Papain containing preparations are used in chronic wound treatment, to clean and remove necrotic tissue. However, the US Food and Drug Administration is taking action against such products because of severe adverse events reported in patients submitted to papain treatments. Thus, the main goal of the present work is to develop encapsulated papain containing membranes based on hydrogels in an attempt to achieve a controllable distribution of size and delivery profile, a toxicity reduction and provide stability towards radiation processing through molecular encapsulation with β-cyclodextrin, which may also provide protection to the enzyme against radiation induced degradation.

1. INTRODUCTION

This report addresses the research project entitled Encapsulation and Nano-encapsulation of Papain Active Sites to Enhance Radiolytic Stability and Decrease of Toxicity, Research Contract No. 15459, and contains information related to research progress, mainly describing the activities and goals achieved.

Papain is a proteolytic enzyme obtained from *Carica papaya* L., and its mechanism of action occurs through protein molecule dissociation resulting in chemical debridement. Its catalytic centre is formed by a triad of amino acid residues known as Cis 25, His 159 and Asn 175. The interactions between these compounds are responsible for a catalytic mechanism over the substrate [1].

The use of papain for wound healing purposes has a long history. Its enzyme therapeutic value is recognized in difficult recovery wound treatments, where a large area has been affected and quick debridement is required [2]. It is relevant to note that the application of products on wounds requires effective sterilizing methods.

The safe use of this enzyme was confirmed by human keratinocytes and in vitro stratum corneum. Its effectiveness was proven by the analysis of human stratum corneum component disarray through biophysical methods [3].

Recently, the Department of Health and Human Services of the US Food and Drug Administration imposed restrictions on papain applications after several adverse effects related to topical papain products were reported, raising serious doubts regarding these products. Cases of anaphylaxis, anaphylactic shock and hypersensitivity were reported, and these products now require FDA approval prior to their commercialization [4].

Such restrictions have highlighted the importance of finding new alternatives to solve these issues in order to obtain an adequate product or reduce undesirable reactions to commercially available papain containing formulations. Among other biophysical methods, radiation may not only represent an effective sterilization method, but also an alternative to enhance the intrinsic characteristics of biomolecules and reduce their toxicity. Previous studies have already pointed out the ability of irradiation technology for reducing the allergenicity of certain foods [5].

Ionizing radiation is known as the best method for destructing pathogens and deteriorating microorganisms [6], and its usage is increasing worldwide. γ radiation is capable of sterilizing a product. γ rays induce covalent bond cleavage owing to a direct impact over the molecules, and after reaching the water molecules, it is also capable of disrupting them, leading to a release of free radicals that may be harmful to other molecules [7]. Ionizing radiation has also been proposed to control cluster size, which may reduce aggregate formation, leading to an enhanced enzymatic activity and also conferring a longer stability. In such a way, the complex formation between

cyclodextrins and papain may be explored at a nanolevel, where more activity and less toxicity could be promoted at low concentrations.

However, a radiation technique may not only lead to benefits to the exposed molecules, because bond cleavages and conformational changes are frequently observed. In addition it could also decrease the bioactivity of enzymes and lead to inactivation [8].

2. MAIN ACHIEVEMENTS/PROGRESS

2.1. Papain γ radiation

To clarify and understand the influence of radiation over papain activity in typical cosmetic and medicinal formulations, papain was exposed to γ radiation in different media, such as powder, aqueous and buffer solutions and gel like formulations in an enzyme stability based approach.

Protein formulation requires careful planning. These bioactive molecules undergo different degradation processes, which may take place with ease under unusual conditions. Not only do the media and excipients play important roles in such processes, but so do all the stages involved, from production to final product storage, as they are able to cease or induce degradation [9]. For wound care purposes, the medium must not only facilitate the maintenance of biological activity, which is essential to final product efficacy, but it must also provide adequate applicability for and acceptance by consumers.

Powder samples present an extra advantage (Table 1) against undesirable effects of irradiation exposition compared to other pharmaceutical forms tested, mainly because of their low water content, which decreases the free radicals generated by water radiolysis, which are known to cause a significant impact on enzyme stability [10]. Thus, no changes in the activity profile were observed under the tested conditions. Such information is important considering that some formulations may not tolerate radiation exposition. Under such circumstances the preformulations may be manufactured aseptically, and then papain could be irradiated prior to its addition to the formula without affecting the final product integrity.

TABLE 1. RELATIVE ENZYMATIC ACTIVITY VALUES (UNITED STATES PHARMACOPEIA UNITS (USP-U)/mL) OF EACH MEDIUM DURING THE ASSAYED CONDITIONS

Sample	0 kGy	5 kGy	15 kGy	25 kGy
Powder	240	240	240	240
Aqueous solution	216.5	169.2	57.24	42.76
Phosphate buffer	283.1	258	243.5	233.8
Gel	255.12	241.5	226.1	201

The previous information not only corroborates the results obtained, but also clarifies why activity loss is dose dependent. As the radiation dose increases, a longer exposition period is required to reach such a dosage, increasing the formation of reactive species and contact time, leading to a more pronounced activity loss.

As observed in Fig. 1, the medium with a high water content presented a decrease in enzymatic activity compared to the powder sample. The main reason is that proteins in aqueous media are more likely to undergo degradation pathways because radiation on water molecules often produces compounds, such as oxygen radicals, which, in solution, interact with these biomolecules and lead to oxidation [10].

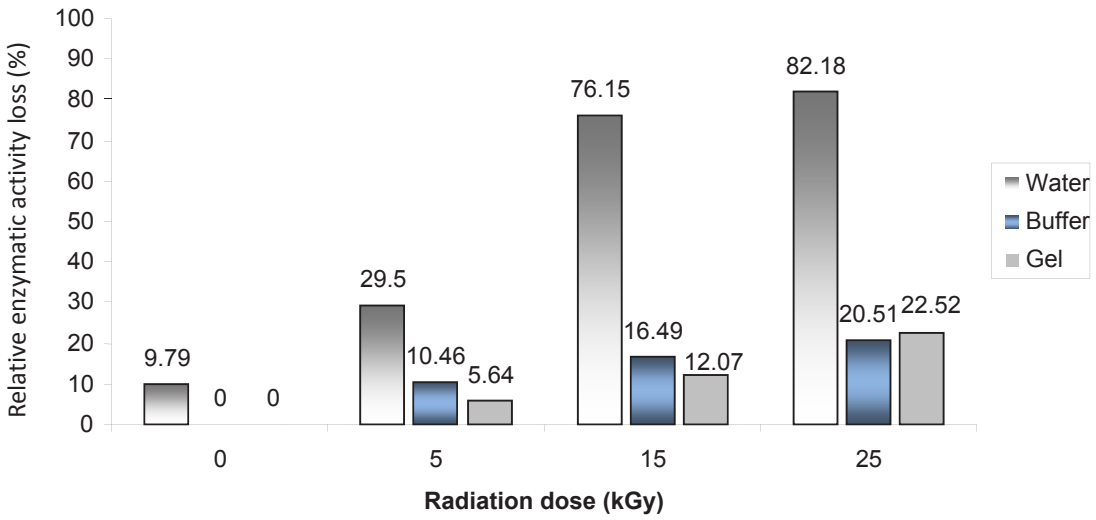

FIG. 1. Percentage of relative enzymatic activity loss of each medium after exposure to selected radiation doses.

Gel like and phosphate buffer formulations were found to be more effective in terms of preserving the enzymatic activity even when exposed to higher radiation dosages. For the gel, this phenomenon may be attributed to the fact that the generated radicals are in reduced contact with the enzyme, and also to the entrapment of the substance in the medium, which decreases the mobility of the involved compound, making it more difficult for the unfolding mechanism to take place as well. The phosphate buffer, on the other hand, may provide a more adequate microenvironment for the protein, and also diminish the sensitivity to pH changes that frequently leads to protein denaturation and activity loss.

The papain aqueous solution offered the lowest protection of the tested media owing to several limitations. The pH, which is essential to enzyme activity, is not stable, and a natural unfolding mechanism present in the enzyme that exposes its active sites and leads to inactivation is favoured in this specific medium [11]. Therefore, this particular medium does not support the use of sterilizing radiation.

Under the assayed conditions and concentrations, the viability of the γ radiation process was directly related to the medium. Therefore, adequate medium selection seems to be essential for such process applications.

2.2. Establishment of methodology for papain activity/stability determination

Another part of this research involved the establishment of a general protocol for assessing papain enzymatic activity, considering the importance of such analysis for the work. Through literature analysis, a colorimetric method to quantify papain activity was selected, and validation studies to ensure the efficacy and applicability of the method were performed.

The assessment of enzymatic activity is fundamental to any study, research or industrial process involving this particular group of protein macromolecules [12] because it provides data about the bioactivity and stability of these molecules in presence of a particular process or reagent.

Current techniques available in the literature regarding papain activity quantification are low in number, are often linked to intensive laboratory work and require long periods for analysis, as well as involving expensive equipment, reagents and substrates [13]. Previous research has evaluated the kinetics of papain catalysed hydrolysis over *N*-benzoyl-DL-arginine p-nitroanilide and highlighted the potential application of such a substrate in papain activity assays [14]. This particular compound is a low MW substrate that releases p-nitroaniline as a product after contact with active papain. This substrate is cheap, and product formation is evaluated using UV techniques.

However, validation studies must be performed to ensure the ability of any analytical method to generate reliable and interpretable information, as well as to confirm that the features implemented in the method meet the standards for the analytic applications applied [15], through consistently documented evidence, established by laboratory studies.

Thus, validation of the technique to assay papain activity using *N*-benzoyl-DL-arginine p-nitroanilide as a substrate was carried out to guarantee its accordance with technical specifications, as well as to ensure applicability of the selected methodology and validity of the results.

The enzyme activity was measured based on the enzyme ability to cleave an amide bond in a low MW substrate, *N*-benzoyl-DL-arginine p-nitroanilide. The p-nitroaniline formed during the reaction of hydrolysis of the product substrate can be followed colorimetrically using an enzyme linked immunosorbent assay reader. Thus, the amount of substrate hydrolysed can be calculated according to the absorbance of p-nitroaniline at 405 nm, depending on the reaction time [16].

From the results obtained by the reaction of the enzyme with the substrate as a function of time, a calibration curve was constructed (Fig. 2).

A linear relationship between papain concentration and increased rate of formation of the compound was observed. The linear correlation coefficient was 0.9978, which is consistent with the limit values specified in distinct standards [16, 17] ($R^2 = 0.99$), demonstrating the linearity of the analytical method. The precision value was equal to 1.77%. The results of the recovery test revealed an accuracy of 94.15%, while the limits of detection and quantification corresponded to 123.9825 United States Pharmacopeia Units (USP-U)/mL and 413.2785 USP-U/mL, respectively. The results achieved were in accordance with standards and specifications [17, 18].

The methodology validated for enzyme activity quantification was suitable for purpose. The linearity of absorbance versus reaction time was satisfactory, and the ratio of hydrolysis was proportional to concentration of enzyme, 40–480 mg/mL. The chromogenic substrate used to measure the papain activity was sensitive to the method. More detailed information related to the technique was recently published as a result of this work [19].

2.3. Complex formation

The papain/cyclodextrin complex was synthesized and the bioactivity profile is described in Fig. 3. The specific environmental conditions for the process were also determined. This part involved the characterization of the complexes produced including a computerized analysis of a possible interaction between papain amino acids and cyclodextrin molecules.

No statistical changes were observed for the bioactivity of the complexes. On the other hand, the physicochemical parameters analysed confirmed the changes in the papain fluorescent spectra as a result of the complex formation.

The computational studies, by means of accessible surface area (ASA) of papain revealed the accessibility of each amino acid present in the structure through an evaluation of the structure of the enzyme and its interaction with solvents. The amino acid fractional accessibility is presented in Fig. 4.

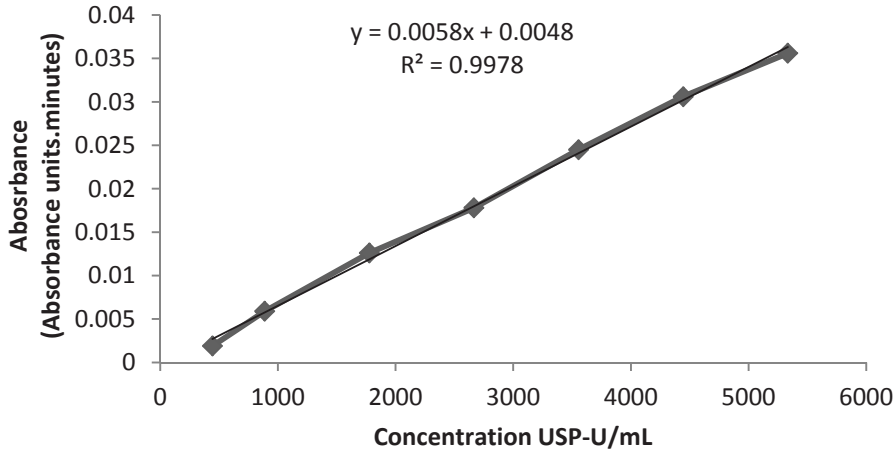

FIG. 2. Standard curve for papain as a function of time using N-benzoyl-DL-arginine p-nitroanilide as a substrate at 37°C for 45 minutes.

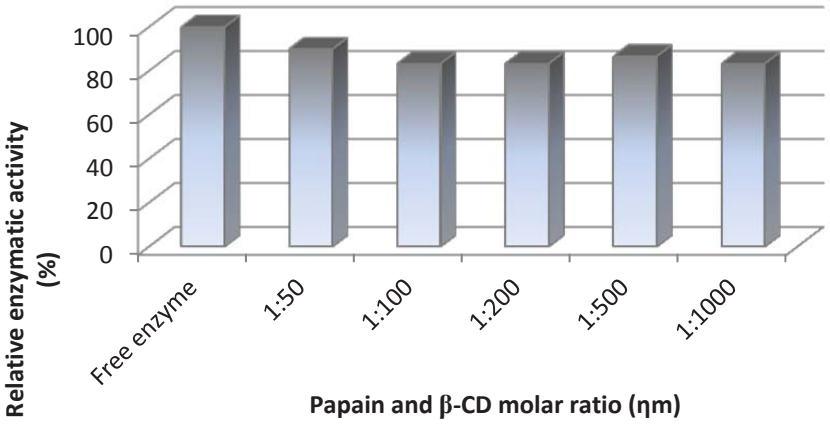

(a)

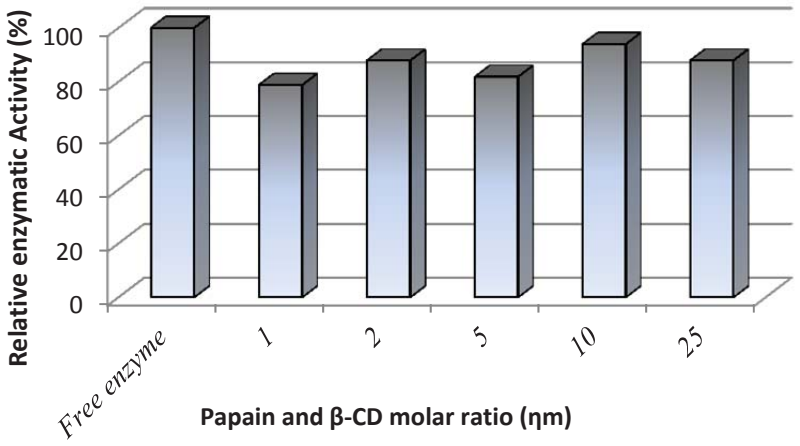

(b)

FIG. 3. Relative activity profiles at (a) distinct cyclodextrin concentrations and (b) low cyclodextrin concentrations after 6 h of incubation.

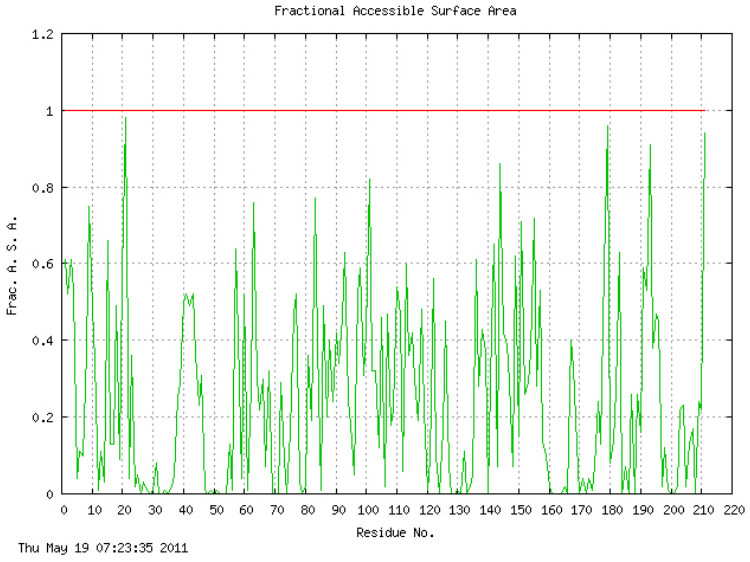

FIG. 4. Fractional accessible surface area estimated for the papain structure.

The phenylalanine residues (Phe-28, Phe-141, Phe-149 and Phe-207) present in the papain structure are presented in Table 2, where the ASA values are found to be relatively low. The displacement of the phenylalanine and its accessible surface area is described in Fig. 5.

The low accessibility of the phenylalanine indicates the presence of biochemical/sterical implications, which would restrict the complex formation; thus the phenylalanine is less likely to interact with the cyclodextrin molecules.

The tryptophan residues (Trp-7, Trp-26, Trp-69, Trp-177 and Trp-181) are presented in Table 3 and the solvent interaction is demonstrated in Fig. 6. The residues Trp-69 and Trp-177 presented higher ASA values when compared to phenylalanine.

TABLE 2. PHENYLALANINE ANALYSIS

Residue	Structure	Side surface (ASA (Å^2))	Fractional surface (ASA (Å^2))	Residual (ASA (Å^2))	Fraction (ASA (Å^2))	Residual volume (Å^3)	Residual fraction volume
28	H[a]	6.2	0.03	6.4	0.03	204.4	1.04
141	H[a]	0.0	0.00	0.0	0.00	205.1	1.05
149	B[b]	15.2	0.08	15.2	0.07	189.3	0.97
207	B[b]	29.5	0.16	29.5	0.13	188.2	0.96

[a] H = helix structure.
[b] B = sheet.

FIG. 5. Phenylalanine solvent interaction profile (9pap.pdb).

TABLE 3. TRYPTOPHAN ANALYSIS

Residue number	Structure	Side surface (ASA (Å^2))	Fractional surface (ASA (Å^2))	Residual (ASA (Å^2))	Fraction (ASA (Å^2))	Residual volume (Å^3)	Residual fraction volume
7	B[a]	27.0	0.12	27.0	0.10	246.9	1.07
26	C[b]	4.0	0.02	12.8	0.05	240.8	1.04
69	H[c]	85.7	0.38	86.3	0.32	218.5	0.95
177	C[b]	50.9	0.22	64.7	0.24	213.3	0.92
181	C[b]	21.1	0.09	21.1	0.09	216.9	0.94

[a] B = sheet
[b] C = random coil.
[c] H = helix structure.

FIG. 6. Tryptophan solvent interaction profile (9pap.pdb).

Among the hydrophobic aromatic amino acids that naturally occur in the papain structure, the tyrosine residues (Tyr-4, Tyr-61, Tyr-67, Tyr-78, Tyr-82, Tyr-94, Tyr-103, Tyr-116, Tyr-123 and Tyr-197) presented more accessibility (Table 4), when compared to tryptophan or phenylalanine, thus indicating that the complex formation is more likely to take place with these specific residues. The tyrosine interaction profile is shown in Fig. 7.

The results have demonstrated that the complexation may be applied to papain, even though some biochemical implications were identified. The biological changes, including conformational and activity variations, may occur as a result of complex formation.

The results highlight the need for techniques that are sensitive enough to measure and characterize the synthesized material, through monitoring of changes in the aromatic residues. For such a purpose, tyrosine fluorescence techniques were selected to identify possible changes/perturbations in the fluorescence of the evaluated residues. The use of cyclodextrins, at the determined molar ratio of 1/10, led to shifts in absorbance/fluorescence spectra, varying as a function of time, from a decrease to an increase in units. Different cyclodextrins conferred different responses, and the results are described in Fig. 8 (48 h of complexation).

TABLE 4. TYROSINE RESIDUE ANALYSIS

Residue number	Structure	Side surface (ASA (Å^2))	Fractional surface (ASA (Å^2))	Residual (ASA (Å^2))	Fraction (ASA (Å^2))	Residual volume (Å^3)	Residual fraction volume
4	B[a]	120.9	0.59	128.5	0.53	184.5	0.9
48	B[a]	2.4	0.02	2.4	0.01	208.5	1.09
61	C[b]	119.9	0.59	124.8	0.52	163.8	0.86
67	C[b]	72.7	0.36	72.7	0.30	181.7	0.95
78	H[c]	122.2	0.60	126.1	0.52	180.9	0.95
82	B[a]	86.1	0.42	86.1	0.36	202.7	1.06
86	C[b]	1.5	0.01	1.6	0.01	195.0	1.02
88	C[b]	26.6	0.13	49.5	0.20	184.6	0.97
94	C[b]	150.9	0.74	151.6	0.63	169.2	0.88
103	B[a]	58.1	0.29	77.8	0.32	186.6	0.98
116	C[b]	88.0	0.43	101.4	0.42	169.9	0.89
123	H[c]	136.3	0.67	136.3	0.56	183.5	0.96
144	C[b]	16.5	0.08	17.5	0.07	195.3	1.02
166	B[a]	4.0	0.02	4.8	0.02	216.3	1.13
170	B[a]	30.6	0.15	30.6	0.13	201.9	1.06
186	B[a]	16.7	0.08	16.7	0.07	199.8	1.04
197	C[b]	108.3	0.53	108.3	0.45	174.5	0.91
203	C[b]	4.9	0.02	5.7	0.02	216.8	1.13
208	B[a]	41.8	0.21	41.8	0.17	200.6	1.05

[a] B = sheet
[b] C = random coil.
[c] H = helix structure.

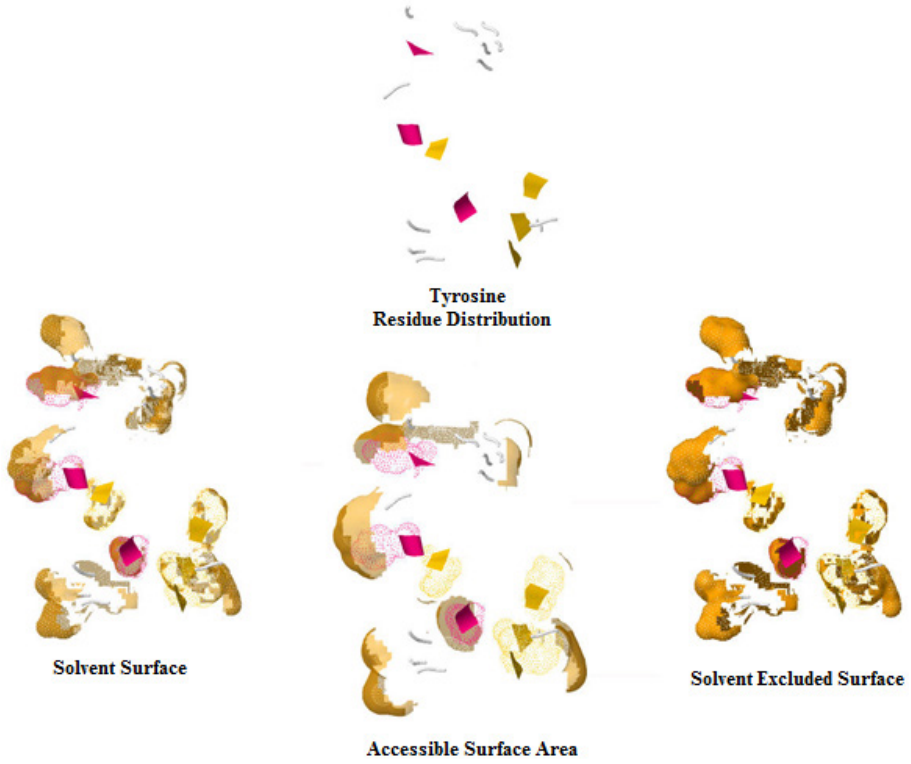

FIG. 7. Tyrosine solvent interaction profile (9pap.pdb).

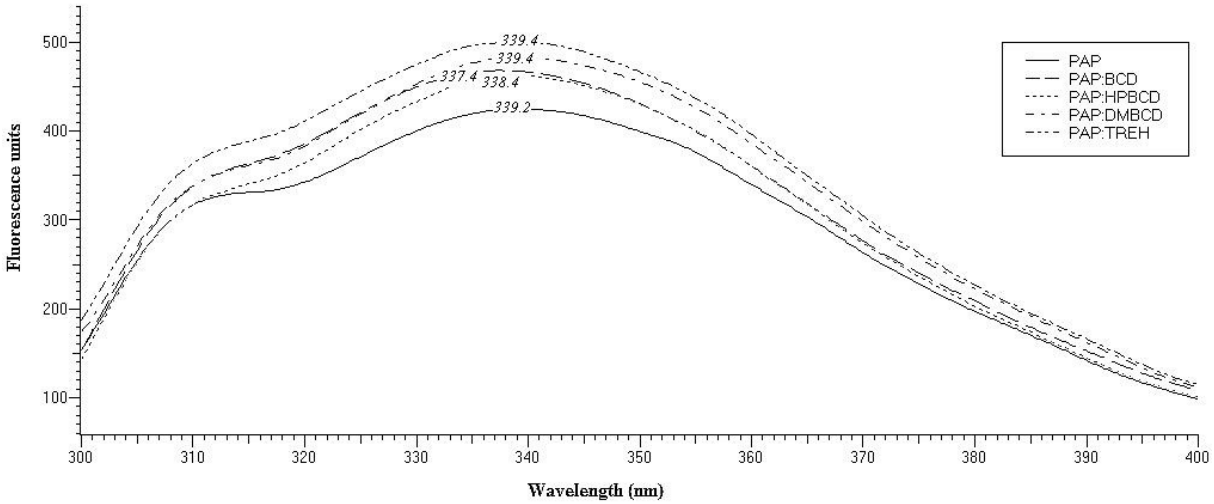

FIG. 8. Papain/cyclodextrin complexes after 48 h of complexation. PAP — Papain; PAP:BCD — papain and B-CD complex; PAP:HPBCD — papain and HP-BCD complex; PAP:DMBCD — papain and DM-BCD complex; PAP:TREH: papain and trehalose mixture.

The effects of the complexation over the cytotoxic profile of the enzyme are demonstrated in Fig. 9. Cyclodextrins were able to modify the cytotoxic properties of the enzyme. Cell viability increased by up to 20% compared to the free enzyme. However, the results were limited in terms of changing the profiles from cytotoxic to non-cytotoxic.

2.4. Hydrogel development

The development of a hydrogel matrix and its characterization, as well as methodologies to assess papain stability and characterize the complex produced by means of biological and biochemical analysis, are also presented. The screening of PVP hydrogels with different formulations for papain delivery was performed. The selection was based on swelling capacity, gel fraction and mechanical properties. The formulations and main results obtained are presented in Table 5. It is relevant to note that this part of the work was developed under collaboration with D. Rodriguez-Linares, fellowship code no. CUB/09034, from Cuba.

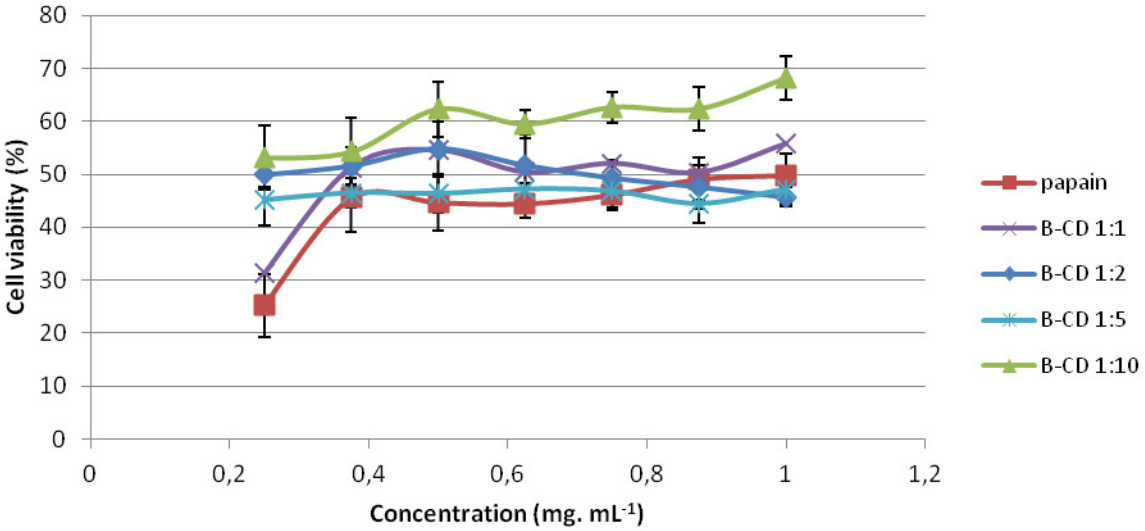

FIG. 9. Papain/β-cyclodextrin (B-CD) complex cytotoxic profiles.

TABLE 5. ASSAYED FORMULATIONS AND RESULTS FOR PVP HYDROGELS SYNTHESIZED

Formulation ID	PVP (%)	PEG (%)	Agar (%)	Swelling (%)	Gel (%)	Mechanical properties		Approved
						Traction* (MPa)	Compression F (N)	
F-1A	6	0	0	—	95.3	—	—	No
F-2A	6	1.5	0	121	76.6	—	—	No
F-3A	6	5	0	263	44.3	—	—	No
F-1B	6	0	0.5	27	90.0	0.00040	53.56	No
F-2B	6	1.5	0.5	127	64.5	0.00025	45.22	Yes

TABLE 5. ASSAYED FORMULATIONS AND RESULTS FOR PVP HYDROGELS SYNTHESIZED (cont.)

Formulation ID	PVP (%)	PEG (%)	Agar (%)	Swelling (%)	Gel (%)	Mechanical properties		Approved
						Traction* (MPa)	Compression F (N)	
F-3B	6	5	0.5	201	44.1	0.00029	27.78	No
F-1C	6	0	1.5	49	78.2	0.00082	50.57	No
F-2C	6	1.5	1.5	104	46.4	0.00080	40.87	Yes
F-3C	6	5	1.5	92	41.4	0.00087	30.41	No
F-1D	15	0	0	242	90.5	0.00017	93.33	No
F-2D	15	1.5	0	438	82.1	0.00010	55.35	Yes
F-3D	15	5	0	504	67.7	0.00004	62.40	No
F-1E	15	0	0.5	218	93.4	0.00044	110.34	No
F-2E	15	1.5	0.5	256	85.7	0.00043	41.81	Yes
F-3E	15	5	0.5	282	92.9	0.00062	73.65	No
F-1F	15	0	1.5	185	87.1	0.00119	73.93	No
F-2F	15	1.5	1.5	124	72.5	0.00141	105.58	Yes
F-3F	15	5	1.5	121	68.5	0.00168	108.13	No

* elastic module.

Figures 10–12 contain the pictures taken by SEM at different resolutions for the selected samples. The selection of the samples for this analysis is an attempt to understand the effects of PEG, agar and papain inclusion on the PVP membrane formulation and consequently on the final structure.

It is well known that agar induces more reticulation as well as a more polycrystalline structure on the PVP membranes, which is a fact that was also observed in this experiment, where F-2C formulation contained 6% PVP and 0.5% agar, while F-2D contained 15% PVP, and both membranes presented an adequate hydrogel formation (Figure 10).

The microscopy images also indicated that the effect of PEG percentage over the membrane formation was observed in terms of increasing the homogeneity of the hydrogel (Fig. 11). Moreover, comparing F-3E pictures with the pictures of the hydrogel with the same formulation including papain at 2% (F-3E-P, Fig. 12), it can be observed how the presence of papain led to a membrane with major porosity, and a wide variety of pore sizes, probably because of the agglomeration of protein molecules.

Considering all the factors previously described, five formulations were selected for the next stage (Table 6).

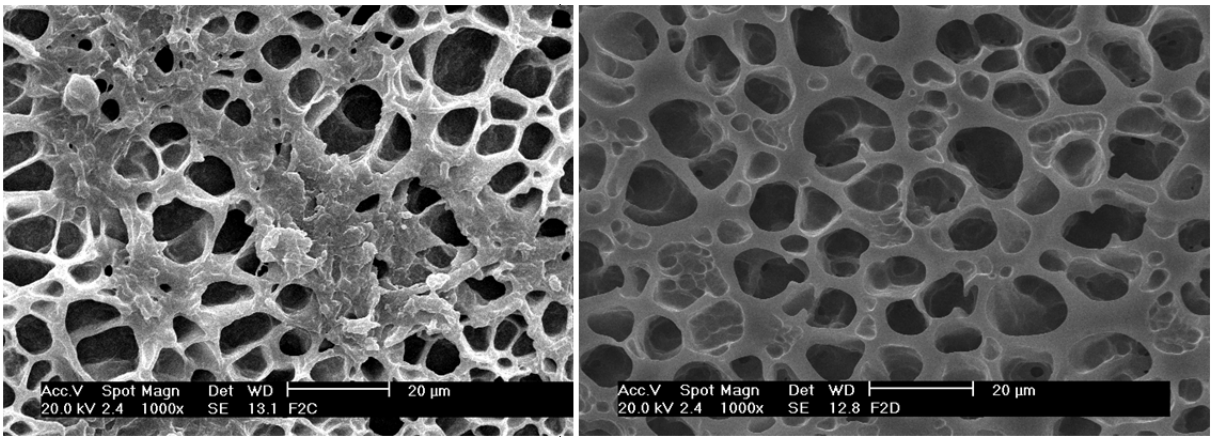

F-2C **F-2D**

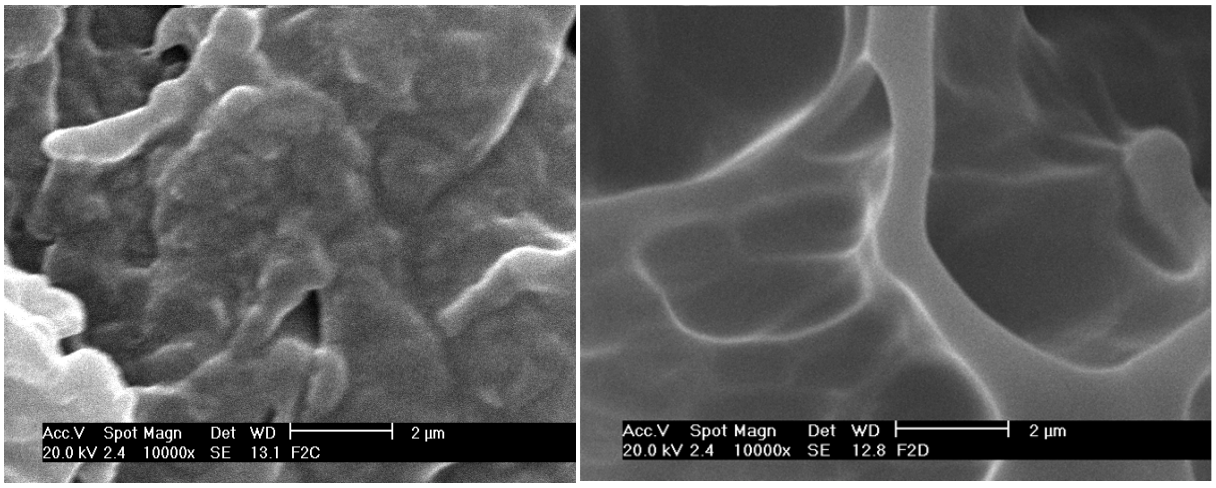

F-2C **F-2D**

FIG. 10. PVP membranes: F-2C contains agar and F-2D does not contain agar.

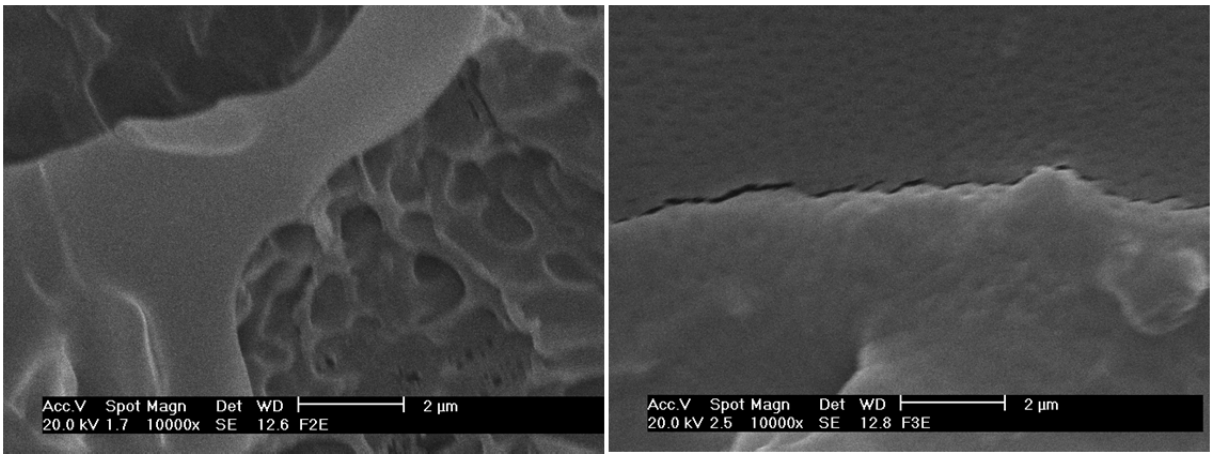

F-2E **F-3E**

FIG. 11. PVP membranes: F-2E contains 3% PEG and F-3E contains 5% PEG.

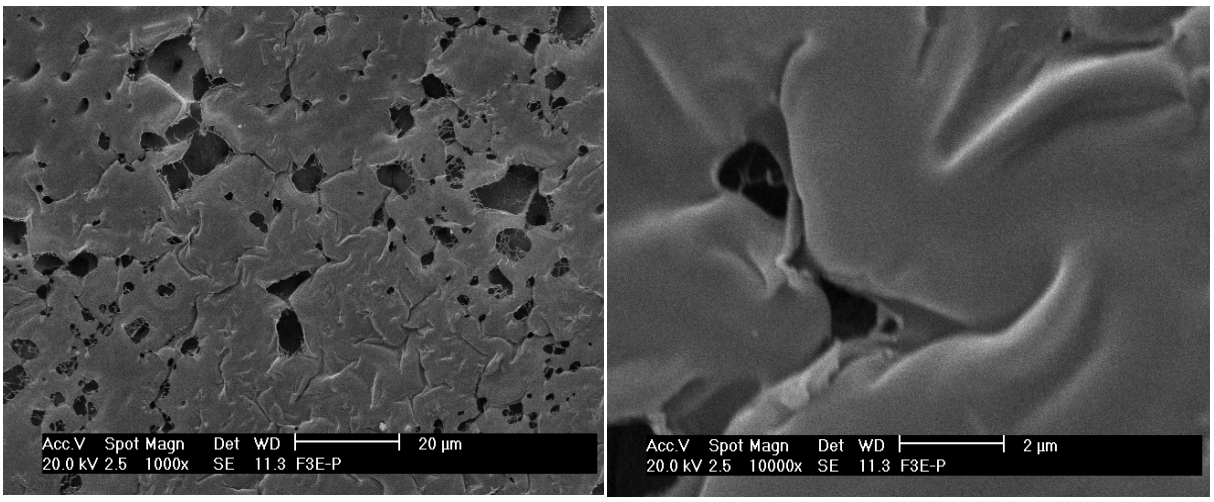

F-3E-P

FIG. 12. PVP membranes containing papain.

TABLE 6. SELECTED PVP HYDROGEL FORMULATIONS

Formulations		PVP (%)	PEG (%)	Agar (%)
1	F-2B	6	1.5	0.5
2	F-2C	6	1.5	1.5
3	F-2D	15	1.5	0
4	F-2E	15	1.5	0.5
5	F-2F	15	1.5	1.5

However, when papain was incorporated into the membranes, only formulation 2F presented the desired mechanical characteristics, and the other membranes did not present any suitable mechanical properties. Thus, the hydrogels were synthesized using polyacrylamide at distinct concentrations or using PVA in O_2 and N_2 atmospheres. In both cases the materials presented the desirable characteristics in presence of papain.

The hydrogel matrices developed (Figure 13) were able to deliver papain in a controlled way. However, owing to the intrinsic characteristics of each polymer, polyacrylamide tended to release most of its content initially (up to 6 h), while PVP membranes were able to release papain over time, and the release was more pronounced after 24 h. The increase continued for up to 48 h. Descriptions of the polyacrylamide hydrogels developed were also published [20].

2.5. Development of protein based nanocarriers

The development of protein based nanocarriers (Fig. 14) was carried out under collaboration with M. Grasselli, from the University of Quilmes, Argentina. The idea of inducing the intermolecular cross-linking using γ radiation has been proved effective, even though a relevant loss in bioactivity was observed. The route developed is represented in Fig. 15.

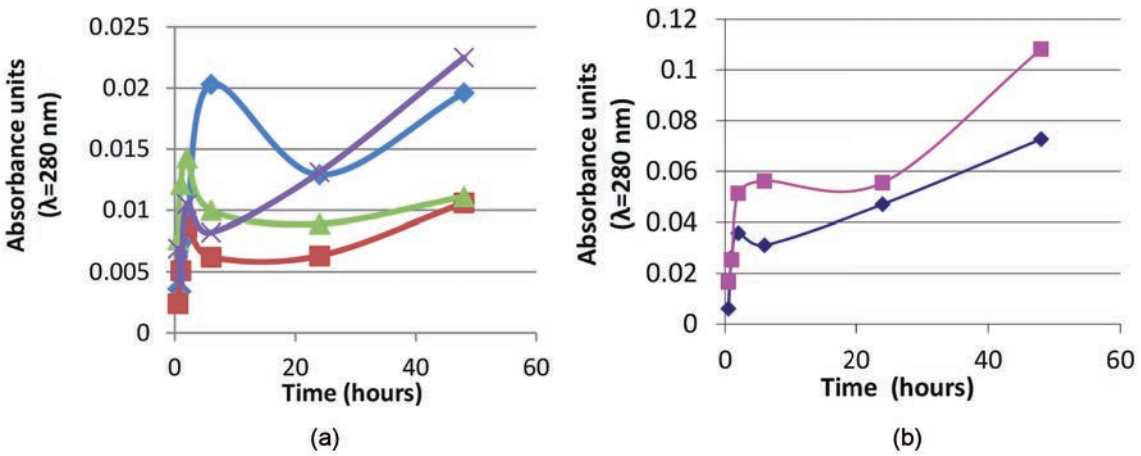

FIG. 13. (a) Polyacrylamide (PAAM) and (b) PVA membrane papain release profiles. (a) Purple: PAAM 10%; green: PAAM 6%; red: PAAM 5%; blue: PAAM 4%; (b) pink: PVA in N2 atmosphere; blue: PVA in O2 atmosphere.

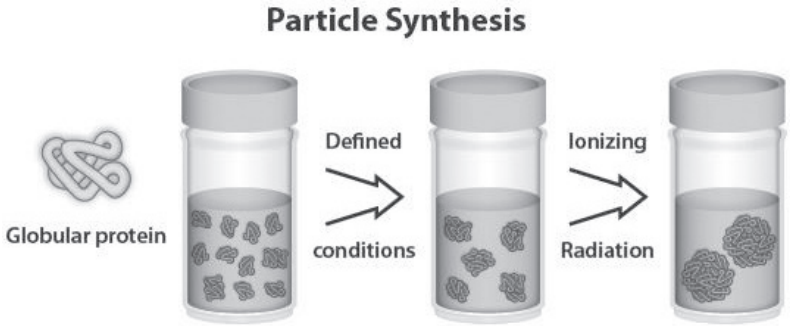

FIG. 14. Representative scheme of the radiation induced synthesis of protein nanoparticles. Adapted from Varca et al. [21].

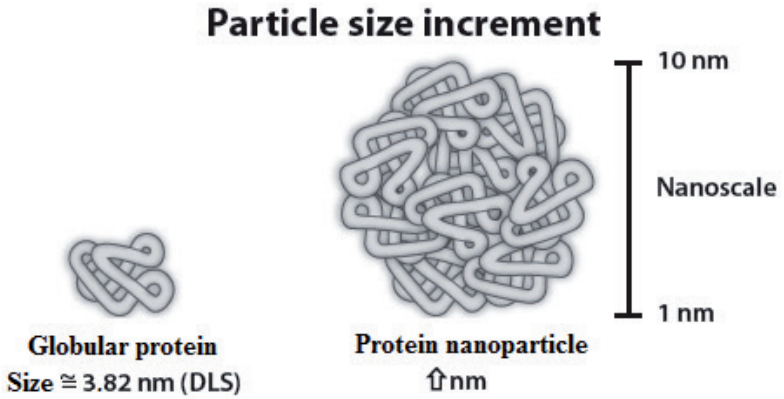

FIG. 15. Representative scheme of the radiation induced protein based drug carriers developed. Adapted from Varca et al. [22].

A detailed explanation of the technique and the particles developed was published [21, 22]. In summary, the radiation induced synthesis of papain nanoparticles led to the formation of protein based nanoparticles with sizes ranging from 5 to 13 nm and a wide range of protein concentrations. The mechanism of nanoparticle formation was attributed to the formation of bityrosine crosslinks, possibly of intermolecular nature.

The complexation with cyclodextrins of the produced system may allow solubilisation and thus ensure applications of the material as a possible natural and less toxic drug carrier.

The last part of the research concerns the loading and release of the complex by the developed matrices and its correlation with the nanostructure of the hydrogel. The results are preliminary, but indicated a suitable release as a function of time, with relative preserved enzymatic activity.

3. CONCLUSION

This technical report has summarized the results of the initial project. Its main goals have been achieved and are described in the following paragraphs.

To promote molecular encapsulation of the papain amino acid residues using β-cyclodextrin: The complex was synthesized and characterized. Structural background was provided by computational studies, while analytical experiments covered the stability of such complexes, as well as the influence of radiation over complex stability and the radioprotective effect conferred. As planned, the overall effects of complex formation over the allergenic and cytotoxic properties of the enzyme were also discussed.

To develop a nanostructured hydrogel for papain/cyclodextrin complex delivery: Development of the hydrogel matrix was carried out. Papain release was achieved; however, only one formulation was found suitable, after incorporation of papain in the system. The protein released was also active, although some activity loss as a function of exposition to ionizing radiation was observed.

To develop a route for the synthesis of protein based nanoparticles for biomedical purposes: The technique developed — radiation synthesis of protein based nanoparticles — was effective in terms of controlling protein particle size and size distribution. The technique also led to the formation of stable nanoparticles with preserved biological activity.

REFERENCES

[1] SANGEETHA, K., ABRAHAM, E.T., Chemical modification of papain for use in alkaline medium, J. Mol. Catal. B: Enzymol. **38** (2006) 171–177.

[2] ALVAREZ, O.M., et al., A prospective, randomized, comparative study of collagenase and papain-urea for pressure ulcer debridement, Wounds **14** (2002) 293–301.

[3] LOPES, P.S., Avaliação da eficácia e segurança da papaína como promotor de absorção cutâneo utilizando técnicas biofísicas e cultura celular de queratinócitos humanos, PhD Thesis, University of São Paulo (2003).

[4] FOOD AND DRUG ADMINISTRATION, Topical Drug Products Containing Papain; Enforcement Action Dates, Department of Health and Human Services, Docket No. FDA2008N0481 (2008).

[5] BYUN, M., LEE, U., YOOK, O., JO, H., KIM, H., Application of gamma irradiation for inhibition of food allergy, Radiat. Phys. Chem. **63** (2002) 360–370.

[6] WORLD HEALTH ORGANIZATION, High Dose Irradiation: Wholesomeness of Food Irradiated with Doses Above 10 kGy, WHO Technical Report Series 890, Geneva (1999) 9–37.

[7] EAGLE, M.J., ROONEY, P., LOMAS, R., KEARNEY, J.N., Validation of radiation dose received by frozen unprocessed and processed bone during terminal sterilization, Cell Tissue Bank **6** (2005) 221–230.

[8] SAHA, A., MANDAL, P.C., BHATTACHARYYA, S.N., Radiation-induced inactivation of enzymes – A review, Radiat. Phys. Chem. **46** (1995) 123–145.

[9] POLLIZI, K.M., BOMMARIUS, A.S., BROERING, J.M., CHAPARRO-RIGGERS, J.F., Stability of biocatalysts, Curr. Opin. Chem. Biol. **11** (2007) 220–225.

[10] DAVIES, K.J.A., DELSIGNORE, M.E., LIN, S.W., Protein damage and degradation by oxygen radicals. II. Modification of amino acids, J. Biol. Chem. **262** (1987) 9902–9907.

[11] ZHUANG, P., BUTTERFIELD, D.A., Denaturation studies of active-site labeled papain using electron paramagnetic resonance and fluorescence spectroscopy, Biophys. **60** (1991) 623–628.

[12] LAD, R. (Ed.), Biotechnology in Personal Care, Cosmetic Science and Technology Series, Vol. 29, Taylor & Francis, New York (2006).

[13] PINTO, C.A.S.O., et al., Determination of papain activity in topical dosage forms: single laboratory validation assay, Lat. Am. J. Pharm. **26** (2007) 771–775.

[14] MOLE, J.E., HORTON, H.R., Kinetics of papain-catalyzed hydrolysis of α-N-benzoyl-L-arginine-p-nitroanilide, Biochem. **12** (1973) 816–822.
[15] GÜNZLER, H., Accreditation and Quality Assurance in Analytical Chemistry, Springer-Verlag (1996).
[16] ERLANGER, B.F., KOKOWSKY, N., COHEN, W., The preparation and properties of two new chromogenic substrates of trypsin, Arch. Biochem. Biophys. **95** (1961) 271–278.
[17] NATIONAL AGENCY FOR SANITARY SURVEILLANCE, Guidelines for Validation of Analytical and Bioanalytical Methods, Resolution no. 899, Brazil (29 May 2003).
[18] UNITED STATES PHARMACOPEIAL CONVENTION, United States Pharmacopeia and National Formulary (USP 30-NF 25), Rockville, MD (2007).
[19] FERRAZ, C.C., VARCA, G.H.C., VILA, M.M.D.C., LOPES, S.S., Validation of in vitro analytical method to measure papain activity in pharmaceutical formulations, Int. J. Pharm. Pharm. Sci., **6** (2014) 658–661.
[20] FERRAZ, C.C., VARCA, G.H.C., LOPES, P.S., MATHOR, M.B., LUGÃO, A.B., Radio-synthesized polyacrylamide hydrogels for proteins release, Rad. Phys. Chem. **94** (2014) 186–189.
[21] VARCA, G.H.C, FERRAZ, C.C., LOPES, P.S., MATHOR, M.B., GRASSELLI, M., LUGÃO, A.B., Radio-synthesized protein-based nanoparticles for biomedical purposes, Rad. Phys. Chem. **94** (2014) 181–185.
[22] VARCA, G.H.C., PEROSSI, G.G., GRASSELLI, M., LUGÃO, A.B., Radiation synthesized protein-based nanoparticles: a technique overview, Rad. Phys. Chem. **105** (2014) 48–52.

RADIOLYTIC SYNTHESES OF NPs AND INORGANIC POLYMER HYBRID MICROGELS

Q. CHEN, G. SHEN, J. SHI, H. LIANG, X. SHEN
Department of Applied Chemistry
College of Chemistry and Molecular Engineering
Peking University
Beijing, China

Abstract

The radiolytic syntheses and application of inorganic nanoparticles and nanostructures in aqueous solutions was explored. Firstly, mesoporous microspheres with a large pore size and radial arrangement of irregular $BaSO_4$ nanorods were successfully synthesized by the radiolysis of an aqueous solution of $K_2S_2O_8$, $Ba(NO_3)_2$, and disodium ethylenediaminetetraacetate at room temperature. It was confirmed that the mesoporous microspheres with a large pore size evolved from the mesoporous microspheres with a smaller pore size that were generated at the early stage of the irradiation course and were mainly constructed by quasi-spherical NPs via Ostwald ripening at room temperature. $BaSO_4$ is traditionally known as a kind of inert material. However, for the first time, it was found that the radiolytically synthesized $BaSO_4$ mesoporous microspheres were able to selectively recover CrO_4^{2-}, which is a cancerogenic substance that is mobile in soil and water, from neutral and alkaline aqueous solutions with high salinity and which contain many foreign anions. Moreover, with the increase of the dose rate in the course of irradiation, the ion exchange rate and capacity of the obtained $BaSO_4$ microspheres increased. This suggests that the ion exchange activity arises from the $BaSO_4$ NPs. In the nanometre size region, $BaSO_4$ is no longer inert. Secondly, PB NPs were successfully synthesized by the partially radiolytic reduction of Fe^{3+} and $Fe(CN)_6^{3-}$ in the presence of PVP under N_2 atmosphere at room temperature. The controlled release of Fe^{2+} and $Fe(CN)_6^{4-}$ played an important role in resolving the solution problem of PB NPs, which exists in normal chemical preparation.

1. RADIOLYTIC SYNTHESES OF INORGANIC NPs AND NANOSTRUCTURES IN AQUEOUS SOLUTIONS

1.1. Introduction

In the realm of nanoscience and nanotechnology, most activity has been focused on the synthesis and application of new NPs with different sizes and shapes [1–5]. Recently, the synthesis of NPs for ion exchange has begun to attract much attention [6–9]. Similar to other properties, the ion exchange performance of NPs is also affected by their morphology. So far, the present results have indicated that only a few special morphologies of some NPs (e.g. nanofibres (NFs) and nanosheets) have high exchange capacities with some heavy metal (Hg^{2+} and Pb^{2+}) ions and alkali metal and alkaline earth metal (Cs^+, Sr^{2+} and Ba^{2+}) ions. It is believed that nanometre sized ion exchangers will be widely used in the future. Obviously, syntheses and systematic exploration of new ion exchangers within nanometre regions are important and necessary, which will benefit their application.

Among the numerous methods of preparing NPs, ionizing radiation (e.g. γ irradiation, EB irradiation, etc.) is powerful because it can conveniently produce a series of species with tuneable redox potentials that are not achievable by other means, over a wide range of temperatures [10–13]. In addition to a few reports about metal halide and non-metal NPs [14–17], most efforts have focused on the syntheses of metal, core shell metal or alloy, and metal chalcogenide NPs in aqueous solutions and organic solvents [10–13, 18, 19]. In the past few years, extension of the application areas of ionizing radiation in the preparation of NPs has been attempted, as has exploration of possible uses.

1.2. Radiolytic syntheses of mesoporous $BaSO_4$ microspheres for selective recovery of CrO_4^{2-}

Barium sulphate ($BaSO_4$), commonly known as barite, is a kind of inert material that has been widely used in many areas as a catalyst carrier [20–22], as a contrast agent in the field of radiology [23], as a filler and additive in polymers, etc. [24–27]. In addition, $BaSO_4$ has been used to adsorb radioactive Ra^{2+} [28], a method that is not widely used because of its limited adsorption capacity, which is only 5×10^{-5} mg/g [28]. Recently, it has been

reported that porous $BaSO_4$, on which Neopelex was loaded, has been used to remove cationic dyes and persistent organic pollutants [29]. Therein, $BaSO_4$ is still used as a carrier because of its inert nature.

It is well known that the properties of nanomaterials are very different from those of bulk materials [1]. Thus, it is reasonable to suggest that nanometre sized $BaSO_4$ particles may be active. However, with respect to the nanometre sized $BaSO_4$, most efforts have been focused on the research of crystal growth (e.g. morphology control, crystallization and formation of mesocrystals) [30]. There has been little reported on the reactivity of nanometre sized $BaSO_4$.

Chromium is a toxic contaminant found in electroplating, leather tanning, pulp production, metal finishing, paint and petroleum refining wastes. Contamination of the environment with Cr is a potential concern owing to the cancerogenic dangers of Cr and the mobility of the Cr in soil, subsurface groundwater and landfill environments [31]. Chromium exists in both the Cr(III) and Cr(VI) oxidation states in the environment. The Cr(III) species is not highly mobile in soil owing to precipitation of insoluble $Cr(OH)_3$ and CrOOH solid phases and adsorption on soil mineral surfaces. In contrast, the Cr(VI) species is a soluble anion ($Cr_2O_7^{2-}$ or CrO_4^{2-}) with a relatively poor affinity for mineral surfaces. In addition, the oxidizability of CrO_4^{2-} is very poor in neutral and basic circumstances. Therefore, the removal of CrO_4^{2-} is not easy [31]. Up until now, many technologies (e.g. ion exchange, precipitation, reverse osmosis, etc.) have been used to remove CrO_4^{2-}. At the same time, the application of ion exchange technology is more economic, convenient and free from secondary pollution. However, the exchange capacity of the most used anion exchange resins is always restrained by salinity and foreign anions because of their poor selectivity [32]. Therefore, it is necessary to explore new kinds of ion exchangers.

In previous work, 'solid' $BaSO_4$ microspheres, mainly consisting of quasi-spherical NPs, have been synthesized by precipitating Ba^{2+} ions with SO_4^{2-} ions, which were generated from the reduction of $K_2S_2O_8$ in the presence of ethylenediaminetetraacetic acid at an absorbed dose of 6 kGy under N_2 atmosphere by γ irradiation [33]. According to the results of N_2 adsorption–desorption isotherm experiments, the solid $BaSO_4$ microspheres synthesized at an absorbed dose of 5 kGy under N_2 atmosphere were mesoporous and the diameter of the pores was about 4 nm, which is not easy to measure using SEM (Figs 1(A) and 1(B)). When the absorbed dose increased to 20 kGy, most of the synthesized $BaSO_4$ microspheres had an obvious mesoporous structure (Fig. 1(C)) and the pore size was in the range 20–60 nm (Fig. 1(D)). The results of fragment analysis show that the microspheres synthesized at 5 kGy were constructed of quasi-spherical NPs and a few irregular nanorods (Fig. 2(D)), while the icrospheres synthesized at 20 kGy mainly consisted of irregular nanorods, and there was a small angle between the building blocks, leading to a radial arrangement of the nanorods (Figs 2(A)–(C)). The generation of $BaSO_4$ has been confirmed by XRD, X ray photoelectron spectroscopy (XPS) and selected area electron diffraction analysis.

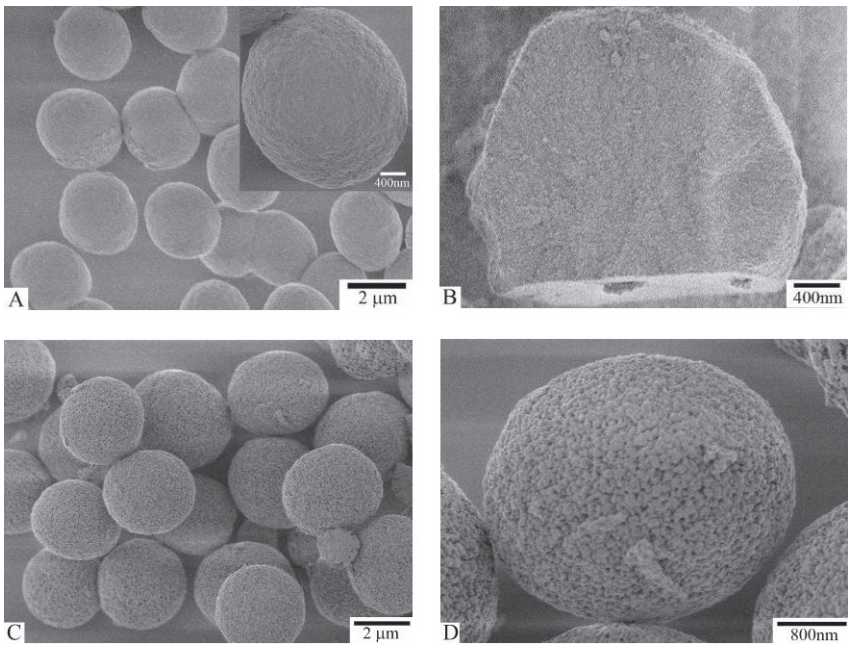

FIG. 1. SEM images of the samples synthesized with different absorbed doses: (A, B) 5 kGy and (C, D) 20 kGy.

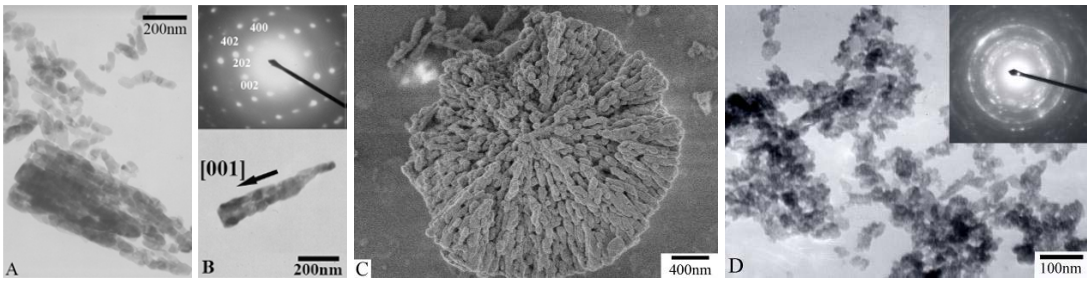

FIG. 2. (A, B, D) TEM and (C) SEM images of the fragments in the samples synthesized with different absorbed doses: (A–C) 20 kGy and (D) 5 kGy. The insets show the selected area electron diffraction patterns of the corresponding product.

It is confirmed that the mesoporous microspheres with a large pore size evolved from the mesoporous microspheres with a smaller pore size, which are generated at the early stage of the irradiation course and which are mainly constructed of quasi-spherical NPs, through Ostwald ripening (Fig. 3). In the process, some species may preferentially adsorb on the surfaces parallel to the [001] axes of $BaSO_4$ NPs, resulting in the formation of nanorods. It is the radial arrangement and the irregular shape that cause the generation of the mesoporous structures with a larger pore size.

It was found that the radiolytically synthesized $BaSO_4$ mesoporous microspheres were able to effectively remove CrO_4^{2-} from neutral and alkaline aqueous solutions, in accordance with the model of pseudo-second-order reaction (Table 1), but the trade $BaSO_4$ sample (>100 μm) could not (Fig. 4). Based on the results of ion chromatograph analysis, there is an ion exchange process between the CrO_4^{2-} and SO_4^{2-} of the $BaSO_4$ microspheres. According to the results of dynamic analysis, this process could arrive at a balanced state after 24 h (Fig. 4 and Table 1). Moreover, with an increase of dose rate in the course of irradiation, the ion exchange rate and capacity (q) of the obtained $BaSO_4$ microspheres increased (Fig. 4 and Table 1). These were ascribed to the smaller size of $BaSO_4$ NPs and the resulting larger Brunauer–Emmett–Teller surface area (S_{BET}) (Table 1). When the sample prepared at a dose rate of 20 Gy/min ripened in the mother solution for 24 h, the exchange rate increased for the bigger pore size, but the exchange capacity decreased for the larger size of $BaSO_4$ NPs and the resulting smaller S_{BET} (Table 1). These results indicated that the ion exchange activity arises from the $BaSO_4$ NPs. In the nanometre region, $BaSO_4$ is not inert any more. The results of XRD analyses further suggested that the (210), (212), (400), (113) and (150) crystal surfaces of $BaSO_4$ NPs may play an important role in the ion exchange process.

Furthermore, the ion exchange between CrO_4^{2-} and $BaSO_4$ microspheres is in accordance with the isothermal equation of Langmuir, and the maximum exchange capacity (q_{max}) of the sample synthesized at a dose rate of 200 Gy/min is determined to be 66.7 mg/g, which reaches the normal level of anion exchange resins. However, the exchange capacity of $BaSO_4$ microspheres increased slightly when the concentration of NaCl increased (Fig. 5), which is very different from the nature of normal anion exchange resin. In addition, in the mixture solutions of CrO_4^{2-} and one of the other anions with an identical concentration, the recovery of CrO_4^{2-} by $BaSO_4$ microspheres is obviously higher than that of other anions, and is seldom affected (Fig. 6). In other words, the ion exchange between CrO_4^{2-} and $BaSO_4$ microspheres is selective. Because of their novel properties, the radiolytically synthesized $BaSO_4$ microspheres could be suitable to recover CrO_4^{2-} from neutral and alkaline aqueous solutions with high salinity and which contain plenty of foreign anions.

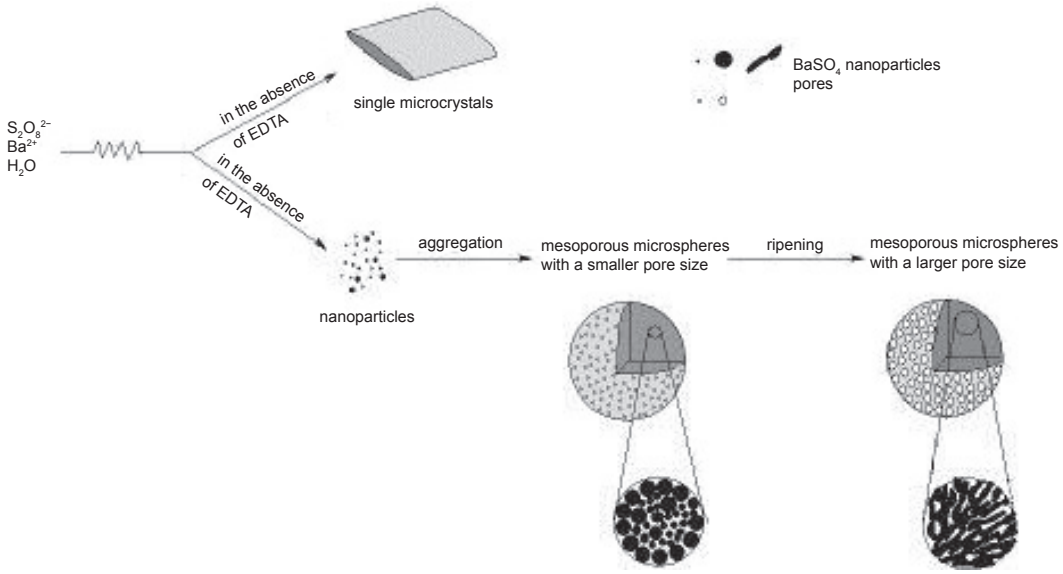

FIG. 3. Growth mechanism of mesoporous $BaSO_4$ microspheres with larger pore sizes. EDTA: ethylenediaminetetraacetic acid.

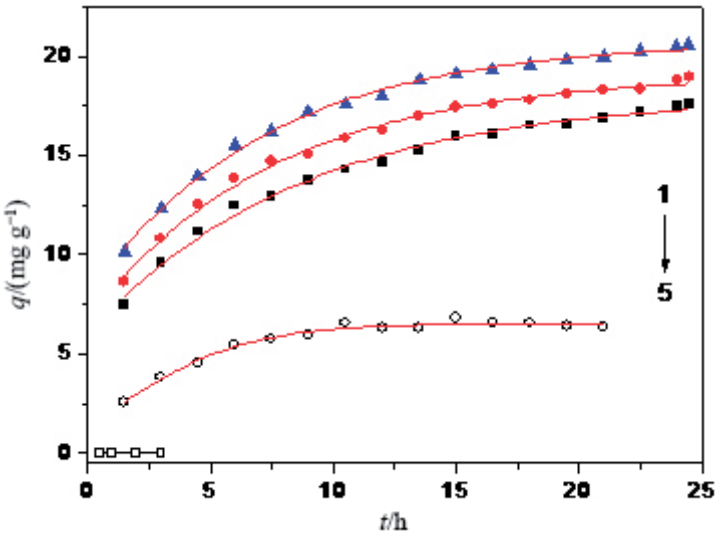

FIG. 4. Adsorption time curve of different $BaSO_4$ samples. All of the initial CrO_4^{2-} concentrations are identical. 1: 200 Gy/min; 2: 100 Gy/min; 3: 20 Gy/min, without ripening; 4: 20 Gy/min, ripening in the mother solution for 24 h; 5: trade $BaSO_4$. (For the radiolytic synthesized samples, the absorbed dose is 6 kGy.)

TABLE 1. BRUNAUER–EMMETT–TELLER ANALYSIS AND PSEUDO-SECOND-ORDER REACTION SIMULATION RESULTS OF DIFFERENT $BaSO_4$ SAMPLES

Condition	S_{BET} (m^2/g)	Φ_{hole} (nm)	k_2 (mg/(g·h))	q_{max} (mg/g)	R^2
200 Gy/min	59.2	4	1.97×10^{-2}	21.99	0.99
100 Gy/min	55.6	4	1.82×10^{-2}	20.30	0.99
20 Gy/min unripened	50.6	4	1.67×10^{-2}	19.18	0.99
20 Gy/min ripened	25.6	35	4.69×10^{-2}	7.68	0.98

Note: S_{BET}: surface area; Φ_{hole}: hole diameter; k_2: kinetic constant for adsorption; q_{max}: maximum exchange capacity; R^2: rate of adsorption.

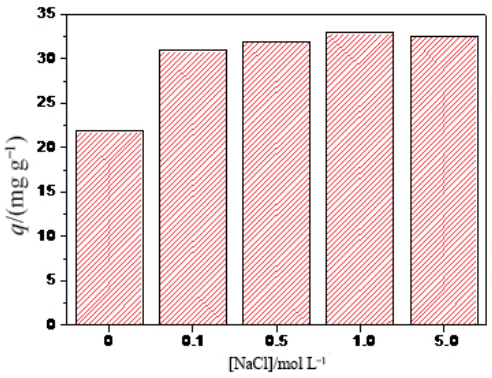

FIG. 5. Effect of concentration of NaCl on the exchange capacity of $BaSO_4$ microspheres (dose rate = 200 Gy/min, absorbed dose = 6 kGy).

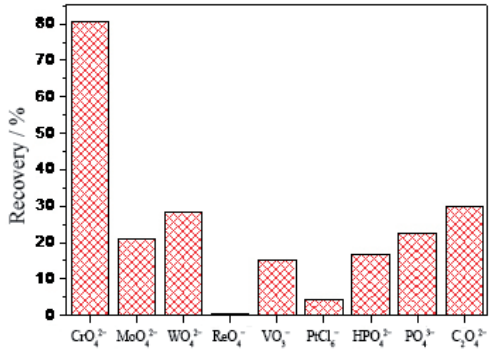

FIG. 6. Effect of other anions with identical concentrations (dose rate = 200 Gy/min, absorbed dose = 6 kGy).

1.3. Syntheses of PB NPs

Ferric ferrocyanide, i.e. PB, is not only an old blue dye, but it is also an efficient toxicide for thallotoxicosis and ion exchange for the recovery of Cs^+. Many methods have been used to synthesize PB NPs. However, the normal chemical method has always led to the formation of PB colloidal sols, which makes the collection of PB more difficulty and lowers the productivity. In this CRP, the synthesis of PB NPs by γ irradiation, which may be applied to resolve the solation problem of PB NPs, has been achieved.

Under N_2 atmosphere, parts of the Fe^{3+} and $Fe(CN)_6^{3-}$ ions in the aqueous solution were simultaneously reduced to Fe^{2+} and $Fe(CN)_6^{4-}$ ions by the radiolytically generated hydrated electrons (e_{aq}^-) and H atoms, respectively:

$$H_2O \xrightarrow{\text{irradiated}} e_{aq}^-, H, \bullet OH, H_3O^+, ... \quad (1)$$

$$H_3O^+ e_{aq}^- \rightarrow H, k = 6\times10^{10}\ L\cdot mol^{-1}\cdot s^{-1} \quad (2)$$

$$Fe^{3+} + e_{aq}^- \rightarrow Fe^{2+}, k = 6\times10^{10}\ L\cdot mol^{-1}\cdot s^{-1} \quad (3)$$

$$Fe(CN)_6^{3-} + e_{aq}^- \rightarrow Fe(CN)_6^{4-}, k = 3.1\times10^{9}\ L\cdot mol^{-1}\cdot s^{-1} \quad (4)$$

$$Fe^{3+} + H \rightarrow Fe^{2+} + H_3O^+, k = 5\times10^{7}\ L\cdot mol^{-1}\cdot s^{-1} \quad (5)$$

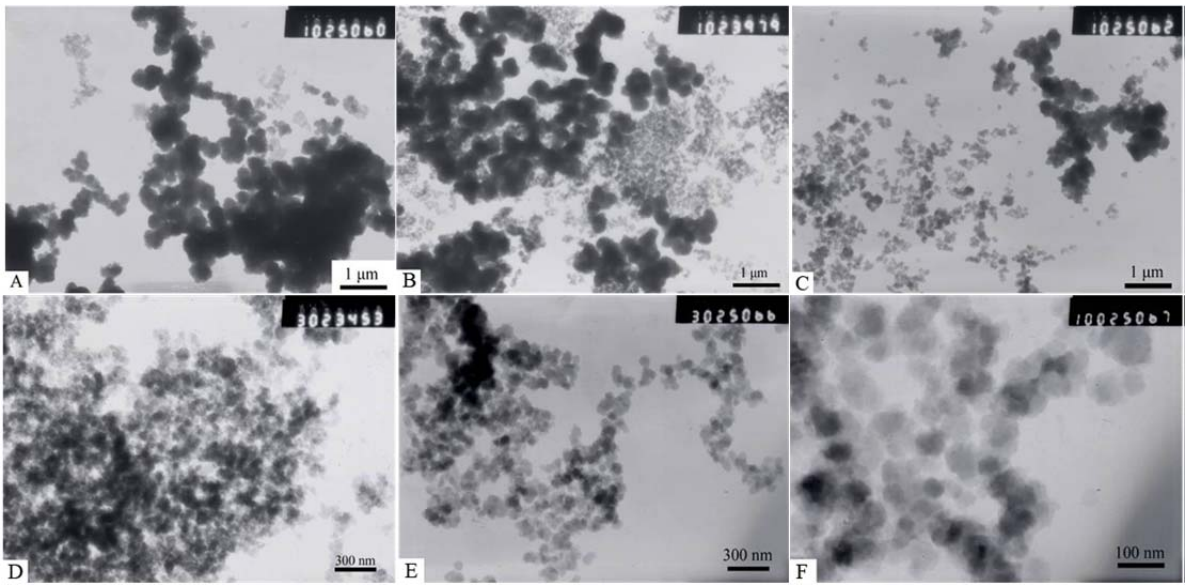

FIG. 7. TEM images of the samples synthesized at different concentrations of PVP: (A–F) [PVP] = 11.1 mg/L, 22.2 mg/L, 33.3 mg/L, 55.6 mg/L, 66.7 mg/L and 77.8 mg/L.

$$Fe(CN)_6^{3-} + H \rightarrow Fe(CN)_6^{4-} + H_3O,\ k = 3.9\times10^9\ L\cdot mol^{-1}\cdot s^{-1} \quad (6)$$

Thus, the controlled release of Fe^{2+} and $Fe(CN)_6^{4-}$ was obtained. Then, PB NPs were generated by precipitating the obtained $Fe(CN)_6^{4-}$ ions with the residual Fe^{3+} ions. The Fe^{2+} ions were precipitated by the residual $Fe(CN)_6^{3-}$ ions, leading to the formation of Thénard's blue NPs. Because PB and Thénard's blue have the same structure, pure PB NPs were successfully obtained, which was confirmed by their XRD patterns and X ray photoelectron spectra.

To obtain monodispersed PB NPs, several kinds of protective agents were tested, and PVP was the most effective. The added PVP can eliminate the radiolytically generated oxidative·OH• radicals and produce a reductive circumstance, favouring the generation of PB NPs. In addition, PVP can effectively protect the generated PB NPs from aggregation and growth. When the concentration of PVP was 11.1 mg/L, an interconnected microstructure of NPs was obtained (Fig. 7(A)). With an increase of concentration of PVP, the aggregation degree of the NPs decreased obviously (Fig. 7). At the same time, the peak position of the characteristic absorption in the UV/VIS spectra, corresponding to the electron transfer between Fe(II) and Fe(III) in PB (i.e. $Fe^{III}(t_{2g}^3e_g^2)$–CN–$Fe^{II}(t_{2g}^6)$ and $Fe^{II}(t_{2g}^4e_g^2)$–CN–$Fe^{III}(t_{2g}^5)$), has a hypsochromic shift from larger than 900 nm to 735 nm, which presents an obvious particle size effect.

When the concentration of PVP was 77.8 mg/L, PB NPs were collected with a satisfactory productivity of 70%. However, in spite of the identical final concentrations of Fe^{3+} and $Fe(CN)_6^{4-}$, no PB could be collected by slow addition of $Fe(CN)_6^{4-}$ solution into Fe^{3+} solution or the inverse, when the concentration of PVP was 77.8 mg/L. Controlled release of Fe^{2+} and $Fe(CN)_6^{4-}$ played an important role in resolving the solation problem of PB NPs. In other words, the radiolytic method is efficient in the preparation of PB products.

2. PREPARATION OF INORGANIC POLYMER HYBRID MICROGELS BY γ IRRADIATION AND SURFACTANT FREE EMULSION POLYMERIZATION

2.1. Introduction

As inorganic/polymer nanocomposite microspheres, hybrid microgels have been used extensively in the fields of coatings, colloid crystals, catalysis, diagnostics, etc. [34–37]. To synthesize the nanocomposite microspheres, a variety of methods have been employed, such as ion exchange [36, 38], photothermal patterning [39], block polymer micelles [40] and surface graft processing [41]. In these methods, the synthesis of the polymer and

the preparation of inorganic NPs are operated individually. Thus, inorganic NPs are difficult to disperse well in polymer microspheres. Microemulsions [42–44] and micelles [45] are also often used to prepare nanocomposite microspheres. Because the surfactants are difficult to completely remove, the application of the products is limited, especially in biomedical applications [46, 47]. The combination of γ irradiation and surfactant free emulsion polymerization can simultaneously achieve the formation of microgels, reduction of inorganic ions and sterilization in the absence of surfactants, which are able to overcome the above problems and meet the requirements of biomedical applications. Nevertheless, because the choice of monomers is limited, the development of this method is slow.

In previous work, 4-vinylpyridine, with a feasible coordination with metal ions [48, 49], as well as its easy formation of microgel [50], was applied to the preparation of a hybrid microgel through the simultaneous formation of Ag NPs and poly(4-vinylpyridine) microgel by γ irradiation and surfactant free emulsion polymerization in a single step [51, 52]. It was found that the Ag NPs were well dispersed within the polymer microspheres [51, 52]. However, poly(4-vinylpyridine) is not a biocompatible polymer. Moreover, the only commercial monomer that can be used as the succedaneum of 4-vinylpyridine is scarce. To overcome this difficulty and obtain microgels that are suitable for biomedicine, it has been attempted to use several kinds of monomers to substitute 4-vinylpyridine. In addition, cadmium sulphides are a series of promising candidates for biomedical examination. However, cadmium is toxic, which makes its usage in biomedicine ambiguous. It has been considered that the toxicity of these NPs could be reduced if the stabilizer is suitable. In this CRP, CdS polymer hybrid microgels are prepared, and possible uses in biomedical examinations explored.

2.2. Research results

CdS/poly(methacrylic acid-*co*-methyl methacrylate) hybrid microgel has been designed, where $CdCl_2$ and $Na_2S_2O_3$ were used as the cadmium and sulphur sources, respectively. Because the coordination ability of $S_2O_3^{2-}$ to Cd^{2+} is much stronger than that of the methacrylate anion, there were two kinds of CdS NPs (microsphere diameter (Φ) ~ 2 nm): one existed in the poly(methacrylic acid-*co*-methyl methacrylate) microgel (Φ = 100–130 nm) and the other was distributed outside (Fig. 8). Therefore, the selection of a suitable sulphur source and a monomer with a stronger coordination ability to Cd^{2+} is most important.

It is known that thiourea can coordinate with many metal ions (e.g. Cd^{2+} and Zn^{2+}) and can generate S^{2-} by γ radiolysis, which leads to the formation of metal sulphide NPs [53]. Therefore, it has been attempted to modify thiourea by a methacryloyl group (Fig. 9). Unfortunately, the goal product could be transformed to a six membered ring by a side reaction in its resting period (Fig. 9). In other words, the purification of the product is very difficult. Thus, three new monomers have been synthesized (Fig. 10).

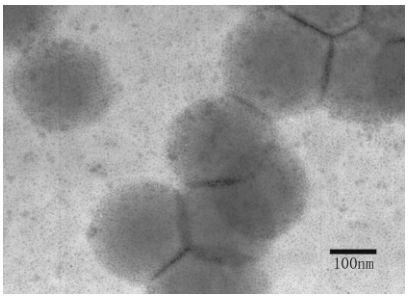

FIG. 8. TEM image of CdS NPs and CdS/poly(methacrylic acid-co-methyl methacrylate) hybrid microgel prepared by γ radiation and surfactant free emulsion polymerization in a single step.

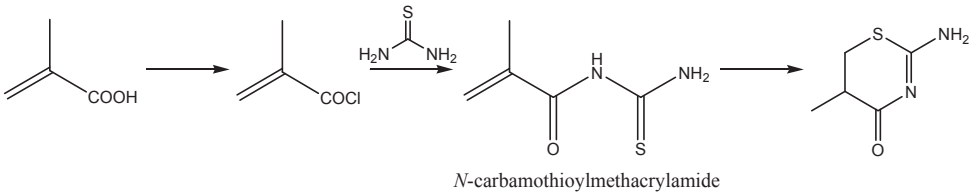

FIG. 9. N-carbamothioylmethacrylamide.

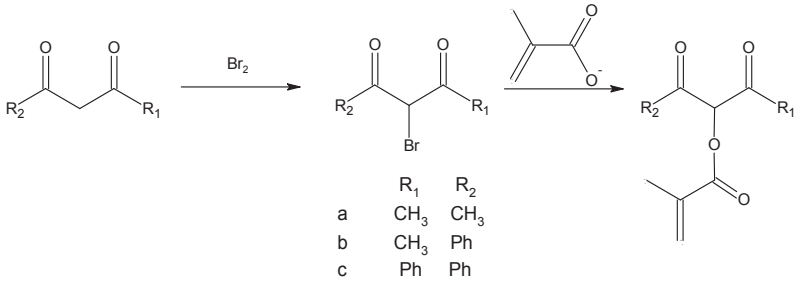

FIG. 10. Monomers.

The morphology of polymer particles was not satisfactory (Fig. 11(A)), and this will be improved in future work. When monomer (a) and methacrylate were used to prepare hybrid microgels, CdS NPs could be well distributed in the polymer particles (Fig. 11(B)), which had an obvious photoluminescence phenomenon.

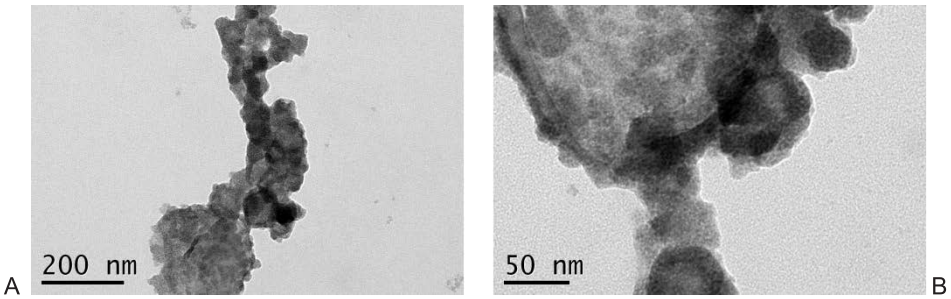

FIG. 11. TEM images of the synthesized CdS/polymer hybrid microgels.

REFERENCES

[1] BURDA, C., CHEN, X.B., NARAYANAN, R., EL-SAYED, M.A., Chemistry and properties of nanocrystals of different shapes, Chem. Rev. **105** (2005) 1025.

[2] ROUCOUX, A., SCHULZ, J., PATIN, H., Reduced transition metal colloids: a novel family of reusable catalysts? Chem. Rev. **102** (2002) 3757.

[3] SUN, Y.G., XIA, Y.N., Shape-controlled synthesis of gold and silver nanoparticles, Science **298** (2002) 2176.

[4] TIAN, N., ZHOU, Z.Y., SUN, S.G., DING, Y., WANG, Z.L., Synthesis of tetrahexahedral platinum nanocrystals with high-index facets and high electro-oxidation activity, Science **316** (2007) 732.

[5] LIU, L.P., et al., Shape control of CdSe nanocrystals with zinc blende structure, J. Am. Chem. Soc. **131** (2009) 16 423.

[6] MANOS, M.J., DING, N., KANATZIDIS, M.G., Layered metal sulfides: Exceptionally selective agents for radioactive strontium removal, Proc. Natl. Acad. Sci. USA **105** (2008) 3696.

[7] YANG, D.J., ZHENG, Z.F., ZHU, H.Y., LIU, H.W., GAO, X.P., Titanate nanofibers as intelligent absorbents for the removal of radioactive ions from water, Adv. Mater. **20** (2008) 2777.

[8] MANOS, M.J., KANATZIDIS, M.G., Highly efficient and rapid Cs^+ uptake by the layered metal sulfide $K_{2x}Mn_xSn_{3-x}S_6$ (KMS-1), J. Am. Chem. Soc. **131** (2009) 6599.
[9] DING, N., KANATZIDIS, M.G., Permeable layers with large windows in $[(CH_3CH_2CH_2)_2NH_2]_5In_5Sb_6S_{19}\cdot 1.45\ H_2O$: high ion-exchange capacity, size discrimination, and selectivity for Cs^+, Chem. Mater. **19** (2007) 3867.
[10] HENGLEIN, A., Physicochemical properties of small metal particles in solution: "Microelectrode" reactions, chemisorption, composite metal particles, and the atom-to-metal transition, J. Phys. Chem. **97** (1993) 5457.
[11] HODAK, J.H., HENGLEIN, A., HARTLAND, G.V., Photophysics of nanometer sized metal particles: Electron-phonon coupling and coherent excitation of breathing vibrational modes, J. Phys. Chem. B **104** (2000) 9954.
[12] BELLONI, J., MOSTAFAVI, M., REMITA, H., MARIGNIER, J.L., DELCOURT, M.O., Radiation-induced synthesis of mono- and multi-metallic clusters and nanocolloids, New J. Chem. **22** (1998) 1239.
[13] BELLONI, J., Nucleation, growth and properties of nanoclusters studied by radiation chemistry: Application to catalysis, Catal. Today **113** (2006) 141.
[14] ZHU, Y.J., QIAN, Y.T., CAO, Y.F., Gamma-radiation synthesis of nanocrystalline powders of copper(I)halides, Mater. Sci. Eng. B: Solid-State Mater. Adv. Technol. **57** (1999) 247.
[15] ZHU, Y.J., QIAN, Y.T., HAI, H., ZHANG, M.W., Preparation of ultrafine tellurium powders by the gamma-radiation method at room temperature, J. Mater. Sci. Lett. **15** (1996) 1700.
[16] ZHU, Y.J., QIAN, Y.T., HAI, H.A., ZHANG, M.W., Preparation of nanometer-size selenium powders of uniform particle size by gamma-irradiation, Mater. Lett. **28** (1996) 119.
[17] ZHU, Y.J., QIAN, Y., Preparation of nanometer-size amorphous powders of arsenic by gamma-irradiation at room temperature, Mater. Sci. Eng. B: Solid-State Mater. Adv. Technol. **47** (1997) 184.
[18] HULLAVARAD, N.V., HULLAVARAD, S.S., KARULKAR, P.C., Cadmium sulphide (CdS) nanotechnology: Synthesis and applications, J. Nanosci. Nanotechnol. **8** (2008) 3272.
[19] NI, Y.H., GE, X.W., XU, X.L., CHEN, J.F., ZHANG, Z.C., Developments in preparation of nano-scale materials, J. Inorg. Mater. **15** (2000) 9.
[20] LI, F.B., YUAN, G.Q., Low temperature catalytic conversion of methane to methanol by barium sulfate nanotubes supporting sulfates: $Pt(SO_4)_2$, $HgSO_4$, $Ce(SO_4)_2$ and $Pb(SO_4)_2$, Chem. Commun. **17** (2005) 2238.
[21] LI, F.B., YUAN, G.Q., Preparation of mesostructured barium sulfate and its application in methane activation, J. Catal. **239** (2006) 282.
[22] NIKAM, S.S., KORNBERG, B.E., JOHNSON, D.R., DOHERTY, A.M., Synthesis of hydroxamic acids: Pd/$BaSO_4$ as a new catalyst for the deprotection of O-benzyl hydroxamates, Tetrahedron Lett. **36** (1995) 197.
[23] O'CONNOR, S.D., SUMMERS, R.M., Revisiting oral barium sulfate contrast agents, Acad. Radiol. **14** (2007) 72.
[24] LI, Z., GUO, S.Y., SONG, W.T., YAN, Y., Effect of the interfacial interaction on the phase structure and rheological behavior of polypropylene/ethylene-octene copolymer/$BaSO_4$ ternary composites, J. Polym. Sci. B **40** (2002) 1804.
[25] LEE, S.S., KIM, J., PARK, M., LIM, S., CHOE, C.R.M., Transesterification reaction of the $BaSO_4$-filled PBT/poly(ethylene terephthalate) blend, J. Polym. Sci. B **39** (2001) 2589.
[26] QU, M.H., et al., Flammability and thermal degradation behaviors of phosphorus-containing copolyester/$BaSO_4$ nanocomposites, J. Appl. Polym. Sci. **102** (2006) 564.
[27] HEINRICHS, U., et al., Statistical studies on the light output and energy resolution of small LSO single crystals with different surface treatments combined with various reflector materials, Nucl. Instrum. Methods Phys. Res. Sect. A **486** (2002) 60.
[28] GERMANN, F.E.E., Adsorption of radium by barium sulfate, J. Am. Chem. Soc. **43** (1921) 1615.
[29] LIN, J., GAO, H.W., SDBS@BaSO4: An efficient wastewater-sorbing material, J. Mater. Chem. **19** (2009) 3598.
[30] COLFEN, H., ANTONIETTI, M., Mesocrystals: Inorganic superstructures made by highly parallel crystallization and controlled alignment, Angew. Chem. Int. Ed. **44** (2005) 5576.
[31] VENDITTI, F., CUOMO, F., CEGLIE, A., AMBROSONE, L., LOPEZ, F., Effects of sulfate ions and slightly acidic pH conditions on Cr(VI) adsorption onto silica gelatin composite, J. Hazard. Mater. **173** (2010) 552.
[32] ZHANG, Y.W., et al., Radiation synthesis and Cr(VI) removal of cellulose microsphere adsorbent, Carbohydr. Polym. **88** (2012) 931.
[33] CHEN, Q.D., BAO, H.Y., SHEN, X.H., Radiolytic synthesis of $BaSO_4$ microspheres, Radiat. Phys. Chem. **77** (2008) 974.
[34] SCHARTL, W., Crosslinked spherical nanoparticles with core-shell topology, Adv. Mater. **12** (2000) 1899.
[35] CARUSO, F., Nanoengineering of particle surfaces, Adv. Mater. **13** (2001) 11.
[36] XU, S.Q., ZHANG, J.G., PAQUET, C., LIN, Y.K., KUMACHEVA, E., From hybrid microgels to photonic crystals, Adv. Funct. Mater. **13** (2003) 468.
[37] KARG, M., HELLWEG, T., Smart inorganic/organic hybrid microgels: Synthesis and characterisation, J. Mater. Chem. **19** (2009) 8714.
[38] ANTONIETTI, M., GROHN, F., HARTMANN, J., BRONSTEIN, L., Nonclassical shapes of noble-metal colloids by synthesis in microgel nanoreactors, Angew. Chem. Int. Ed. Engl. **36** (1997) 2080.
[39] JONES, C.D., LYON, L.A., Photothermal patterning of microgel/gold nanoparticle composite colloidal crystals, J. Am. Chem. Soc. **125** (2003) 460.

[40] MOFFITT, M., VALI, H., EISENBERG, A., Spherical assemblies of semiconductor nanoparticles in water-soluble block copolymer aggregates, Chem. Mater. **10** (1998) 1021.
[41] CHEN, C.W., CHEN, M.Q., SERIZAWA, T., AKASHI, M., In-situ formation of silver nanoparticles on poly(*N*-isopropylacrylamide)-coated polystyrene microspheres, Adv. Mater. **10** (1998) 1122.
[42] NI, Y.H., GE, X.W., LIU, H.R., ZHANG, Z.C., YE, Q., In situ synthesis and characterization of spherical CdS/polyacrylamide nanocomposites by gamma-irradiation in W/O microemulsions, Chem. Lett. **30** (2001) 924.
[43] WANG, W., ASHER, S.A., Photochemical incorporation of silver quantum dots in monodisperse silica colloids for photonic crystal applications, J. Am. Chem. Soc. **123** (2001) 12 528.
[44] WU, D.Z., GE, X.W., ZHANG, Z.C., WANG, M.Z., ZHANG, S.L., Novel one-step route for synthesizing CdS/polystyrene nanocomposite hollow spheres, Langmuir **20** (2004) 5192.
[45] ROOS, C., et al., Design and synthesis of molecular reactors for the preparation of topologically trapped gold clusters, Adv. Mater. **11** (1999) 761.
[46] PELTON, R., Temperature-sensitive aqueous microgels, Adv. Colloid Interface Sci. **85** (2000) 1.
[47] SAUNDERS, B.R., VINCENT, B., Microgel particles as model colloids: theory, properties and applications, Adv. Colloid Interface Sci. **80** (1999) 1.
[48] BRONSTEIN, L.H., et al., Induced micellization by interaction of poly(2-vinylpyridine)-block-poly(ethylene oxide) with metal compounds: Micelle characteristics and metal nanoparticle formation, Langmuir **15** (1999) 6256.
[49] MALYNYCH, S., LUZINOV, I., CHUMANOV, G., Poly(vinyl pyridine) as a universal surface modifier for immobilization of nanoparticles, J. Phys. Chem. B **106** (2002) 1280.
[50] CHEN, Q.D., SHEN, X.H., GAO, H.C., Synthesis of poly(*N*,*N*'-methylenebisacrylamide-*co*-4-vinylpyridine) microgels by γ-ray irradiation, Acta Polym. Sin. **1** (2005) 60.
[51] CHEN, Q.D., SHEN, X.H., GAO, H.C., One-step synthesis of silver-poly(4-vinylpyridine) hybrid microgels by γ-irradiation and surfactant-free emulsion polymerization, Acta Polym. Sin. **1** (2006) 722.
[52] CHEN, Q.D., SHEN, X.H., GAO, H.C., One-step synthesis of silver-poly(4-vinylpyridine) hybrid microgels by gamma-irradiation and surfactant-free emulsion polymerisation: The photoluminescence characteristics, Colloid Surf. A: Physicochem. Eng. Asp. **275** (2006) 45.
[53] NI, Y.H., et al., Gamma-irradiation route to prepare silver sulfide nanocrystals, Chem. J. Chin. Univ. Chin. **23** (2002) 176.

RADIATION ENGINEERING OF PVP/PAAc NANOGEL DISPERSIONS FOR OPHTHALMIC APPLICATIONS

E.A. HEGAZY, H.A. ABD EL-REHIM, A.E. SWILEM
National Center for Radiation Research and Technology
Nasr City, Cairo
Egypt

Abstract

Chemically cross-linked, pH sensitive, PVP/PAAc hydrogel NPs have been successfully prepared at high yields via γ radiation induced polymerization of AAc in an aqueous solution of PVP as a template polymer. The particle sizes of the PVP/PAAc nanogels at different pH values have been evaluated using DLS, and the morphology assessed using AFM and TEM. Smaller and more stable nanogel particles could be produced by irradiating a feed solution of 50–75 mol% AAc and using PVP with a high MW. The particle size increased as the feed concentration increased, and a suitable concentration for nanogel production ranged from 1% to 2%. PVP/PAAc nanogels that were pH sensitive were used to encapsulate pilocarpine where the AAc rich nanogels exhibited the highest loading efficiency. Factors affecting size and encapsulation efficiency were optimized to obtain nanogels that were sufficient to entrap the drug efficiently. The transmittance, mucoadhesion and rheological characteristics of nanogel particles were studied to evaluate their ocular applicability. An in vitro release study conducted in simulated tear fluid showed a relatively long sustained release of pilocarpine from the prepared PVP/PAAc nanogel particles when compared with pilocarpine in solution. In addition, it was interesting to evaluate the use of PVP/PAAc nanoparticulate hydrogels as a new strategy to overcome the problems associated with highly viscous polymeric materials, such as carbomer gel, that are used for dry eye treatment. The use of PVP/PAAc nanogels prepared at different compositions and irradiation doses was evaluated for dry eye syndrome application. The nanogel rheological properties and the nanogel interaction with mucin were investigated. Moreover, topical application of the prepared nanogel in a dry eye model in albino rabbits, induced by atropine sulphate 1% eye drops, was investigated. The use of AAc rich nanogels with a lower cross-linking degree (compared with the highly viscous carbomer Vidisic gel) is promising in the management of dry eye syndrome, with a reduced dosing frequency. The PVP/PAAc nanogel as artificial tears provides a layer that stabilizes and thickens the precorneal tear film, prolongs tear break-up time (TBUT), keeps the ocular surface wet and lubricated, helps to repair ocular surface damage and keeps the ocular surface smooth. Topical instillation of PVP/PAAc nanogel twice daily for 3 d is sufficient to improve dry eye problems, whereas other commercial products (e.g. Vidisic gel) require a longer time (>3 d) for dry eye curing. In conclusion, this study clearly demonstrated the potential of PVP/PAAc NPs for dry eye curing, multiplying the therapeutic effect of pilocarpine delivery with enhanced bioavailability response.

1. INTRODUCTION

Nanotechnology is an emerging technology with enormous potential in biotechnology and medicine applications and promises great benefits for society in the future. Novel nanobiomaterials and nanodevices are fabricated and controlled at sizes below 100 nm, where matter functions differently from both the individual atomic scales and the macroscopic scales. Among the different application areas of nanotechnology, hydrogel NPs have gained considerable attention in recent years as one of the most promising soft NPs for drug delivery [1–6]. A fast response to environmental factors, a large surface area and a stable network structure are the main characteristic properties that make nanohydrogels suitable for this purpose.

In recent years, significant efforts have been devoted to use the potentials of NPs in ocular drug delivery [7–9]. Most ocular diseases are treated with drug solutions that are administered as eye drops. These solutions are usually highly concentrated and require frequent application because of rapid precorneal loss caused by the movement of mucus during blinking. NPs have provided an effective means to overcome these drawbacks. The primary motivation for using NPs is their use in liquid form, just like eye drops; therefore, they do not produce the discomfort caused by viscous or sticky ointments [10]. NP based drug delivery systems in ophthalmic applications have the ability to prolong drug residence times, during which drugs can act, by trapping the drug in the ocular mucus layer. There are some articles in the literature that are based on nanohydrogels as a platform for new ocular drug delivery [11, 12]. Tear replacement by artificial tears is the mainstay of therapy for the treatment of dry eye syndrome, regardless of severity [13, 14]. The main active ingredients of artificial tears are water soluble polymers. The goal of using tear substitutes is to increase humidity at the ocular surface and to improve lubrication [15]. However, most artificial

tear preparations provide only short term relief and short retention times, and have to be used frequently to be effective. Moreover, long term frequent application may not only cause inconvenience, but also even disrupt the tear film, impair epithelial cell membranes and damage the ocular surface because of the preservatives contained in the products [16–18]. Therefore, it is vital for a tear substitute to provide the longest possible lasting improvement of the symptoms and signs of dry eye. The present work focused on nanogel preparation using ionizing radiation for ophthalmic applications.

2. EXPERIMENTAL DETAILS

2.1. Materials

PVP (K85–95, MW = 1 300 000 g/mol) and AAc were obtained from Acros Organics (Belgium). (+)-Pilocarpine hydrochloride (99%, Fig. 1) was purchased from Alfa Aesar (Germany). Mucin type II was obtained from porcine stomach (Sigma-Aldrich, USA). Other chemicals were of analytical grade. Deionized water was used in all the experiments.

2.1.1. Preparation of PVP/PAAc hydrogel NPs

PVP/PAAc hydrogel NPs were prepared via γ radiation induced polymerization of AAc in an aqueous solution of PVP as a template polymer. Different compositions of PVP/AAc mixtures were dissolved in deionized water at a total concentration of 1.5% weight per volume (w/v), and then subjected to γ rays generated from a ^{60}Co source with a dose rate of 3.7 kGy/h. The irradiation process was carried out at ambient temperature under air atmosphere. To calculate the yield of NPs, the colloidal nanogel suspensions were centrifuged (Sorvall Ultra 80, USA) at 20 000 rev./min for 30 min at 4°C. Supernatants and aggregated nanogels were collected and freeze-dried to determine the weight of the polymers that formed nanogels. The production yields were calculated from the mass ratio of the polymers forming the nanogel and the polymer and monomer initially introduced in the preparation procedure.

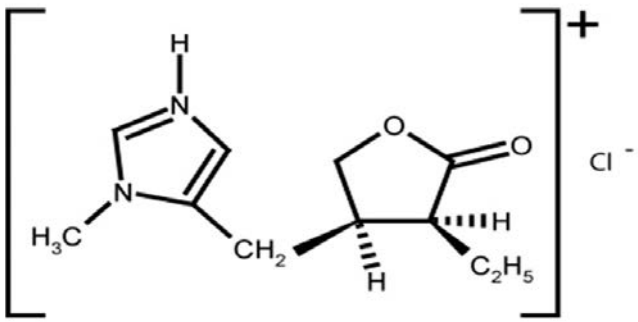

FIG. 1. Chemical structure of pilocarpine HCl.

2.1.2. Loading of pilocarpine

The prepared PVP/PAAc hydrogel NPs were neutralized by $NaHCO_3$ solution, ultracentrifuged at 40 000 rev./min and 4°C for 45 min, and finally freeze-dried to obtain pure and easily dispersible dry nanogels. The freeze-dried nanogel particles were dispersed in deionized water by sonication at a concentration of 0.5% w/v. Pilocarpine hydrochloride powder was then added to the nanogel dispersion at a 1/5 weight ratio of drug to nanogel, followed by incubation for 48 h with continuous magnetic stirring at room temperature. The drug polymer solutions were then ultracentrifuged to separate the drug loaded nanogel particles. The concentration of free pilocarpine in the supernatant was measured spectrophotometrically at 215 nm after appropriate dilution with deionized water. The loading efficiency of pilocarpine loaded nanogel particles was calculated using the following equation:

Loading efficiency (%) = (total amount of drug feed initially – amount of drug in supernatant) × 100 / total amount of drug feed initially.

2.1.3. Particle size and zeta potential measurements

Particle sizes and zeta potentials of the prepared nanogel particles were measured by DLS and electrophoretic light scattering techniques, respectively, using a zeta potential/particle size 380 ZLS (PSS Nicomp, USA). For DLS measurements, samples were properly diluted with freshly prepared deionized water until an intensity of 250–350 kHz was achieved. The scattered light intensity was detected at an angle of 90°, and measurements were run using two 5 min cycles. The volume weighted hydrodynamic mean diameters were reported so that the size contributing the most volume was known. The PDI (square of the coefficient of variation), which is a measure of the size distribution breadth, was also calculated. For zeta potential measurements, samples were properly diluted with freshly prepared deionized water and then measured at an applied electric field of strength 10 V/cm using three 30 s cycles for each sample on not less than three independently prepared samples, and their average value was recorded.

2.1.4. Rheological measurements

The dynamic viscosity (η', the real part of the complex viscosity) of the PVP/PAAc nanogel dispersions (at pH7) was determined using oscillatory squeeze flow via a piezo axial vibrator apparatus. The sample (~100 μL) was placed between two circular plates with a diameter of 20 mm. A gap width of 9 μm was selected because of the low viscosities of the solutions. The upper plate was constructed as a gas tight lid and was tightly screwed to the base plate. The lower plate was driven through two pairs of piezoelectric actuators. By applying a sinusoidal voltage via a lock-in amplifier, the plate was made to oscillate about a mean position. Two further piezoelectric sensor pairs delivered the response signal. A measurement with a sample was compared with a measurement of the empty cell, and the desired rheological properties calculated from the ratio of the output voltage with and without the sample, U/U_0, and the corresponding phase shift $\varphi - \varphi_0$. Measurements were carried out at frequencies ranging from 1 Hz to 1000 Hz at a temperature of 32°C ± 0.1°C.

2.1.5. Transmittance measurements

Transmittance of PVP/PAAc nanogel samples was measured at 500 nm with a UV/VIS spectrophotometer (JASCO V-560). The pH of the medium was adjusted by adding a few drops of HCl or NaOH solution.

2.1.6. TEM

The morphology of nanogel particles was observed using a transmission electron microscope (JEOL JEM-100CX, Japan). Samples were dripped onto a carbon coated copper grid without staining, followed by drying at room temperature.

2.1.7. AFM

An atomic force microscope (Agilent 5500, USA) was used to observe the morphology of the resultant nanogel particles. One drop of properly diluted nanogel dispersion was placed on the surface of freshly cleaved mica and then dried at room temperature.

2.1.8. Interaction with mucin

Two in vitro methods were used to assess the mucoadhesive interaction of the prepared PVP/PAAc nanogels with mucin.

2.1.9. In vitro release of pilocarpine

The in vitro release of pilocarpine from the nanogel particles was evaluated in simulated tear fluid at pH6 through a dialysis membrane (molecular weight cut-offs (MWCOs) of 12 000–14 000 Da). The membrane was firstly soaked in the dissolution medium for 1 h and then tied to one end of a specifically designed glass cylinder (open at both ends). A dispersion of drug loaded particles in simulated tear fluid (STF) (5 mg/mL, 2 mL) was placed into this assembly. The cylinder was attached to a stand and suspended in 50 mL of dissolution medium maintained at 32°C ± 1°C, and the membrane was approximately 1 cm below the receptor medium surface. The dissolution medium (STF) was stirred with a magnet at 50 rev./min. Released pilocarpine was sampled at selected time intervals and determined spectrophotometrically as described above. The release profile of pilocarpine was compared with a control sample in which pilocarpine was dissolved directly in STF solution, and its release profile was measured using the same procedure.

3. RESULTS AND DISCUSSIONS

3.1. Preparation of PVP/PAAc nanogel particles

The irradiation of AAc monomer in an aqueous solution of PVP as a template polymer could successfully produce nanogel particles with a stable covalently linked interior network at a relatively high concentration. The nanohydrogel formation was attributed to the interpolymer complexation via H bonding between the proton donating PAAc, and the proton accepting PVP. PVP/PAAc IPCs depend on the molar ratios and MWs of the components and can be efficiently formed only below a critical pH value (~pH4) (Fig. 2).

In this technique, the major part of the radiation was absorbed by water because dilute solutions were used, resulting in water radiolysis. Reactive products of water radiolysis, mainly hydroxyl radicals and H atoms, can, in turn, attack AAc or PVP molecules present in the feed solution, and, accordingly, macroradicals were formed (an indirect effect). At the first stage of the irradiation process, chain polymerization of the AAc monomer appeared to be predominant. When the PAAc chains, produced in situ, reach a critical length, they self-assemble and form IPCs simultaneously with the template PVP molecules. According to Rainaldi et al. [18], it has been proposed that the PAAc growing chains of critical length associate with the template PVP by hydrogen bonding and then propagate in contact with the template (pick-up mechanism). AAc may also be grafted onto the PVP molecules when the PVP radicals, formed as a result of hydrogen abstraction, recombine with PAAc radicals or initiate the polymerization of AAc monomer. The resultant hydrophobic complexes aggregate to form NPs of ‘micelle like’ structure. Because no macroscopic precipitation takes place in this process, it could be suggested that the PVP or PAAc chains with less complexed segments in the periphery of the NPs may still be kept solvated and thus stabilize the complex aggregates. After most of the monomer molecules are polymerized and NPs are formed, radiation is employed mainly in the cross-linking of the polymer chains inside the particles (intraparticle cross-linking), producing nanogels.

FTIR spectra for PVP, PAAc and PVP/PAAc nanogel particles were recorded, and it was observed that the C=O for PVP and PAAc appeared at 1661 cm^{-1} and 1720 cm^{-1}, respectively. Meanwhile, the FTIR spectrum for PVP/PAAc complex showed two separated bands in the carbonyl (C=O) region at 1636 cm^{-1} and 1730 cm^{-1}, which can be attributed to C=O from PVP and PAAc, respectively. The shifting in the carbonyl absorption bands of PVP and PAAc indicated that a complex was formed between the two components through hydrogen bonding.

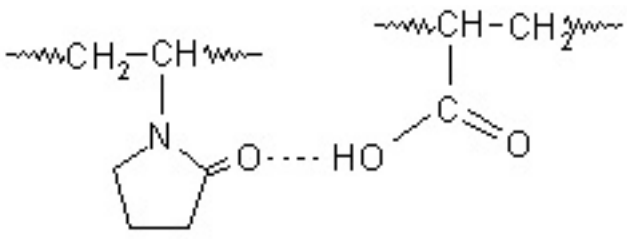

FIG. 2. Complexation between PVP and PAAc via H bonding.

3.2. Controlling the size of PVP/PAAc nanogel particles

To obtain PVP/PAAc nanogels of tuneable sizes that are capable of entrapping the drug efficiently, many factors affecting and controlling the size and cross-linking density of PVP/PAAc nanogel particles have been studied. Among the important factors that affect the size and structure of PVP/AAc NPs are the PVP/AAc composition and concentration.

The feed composition plays an important role in controlling the PVP/PAAc nanogel particle size. An apparent macroscopic PVP gel phase and PAAc soluble polymer were produced when PVP and AAc monomers were exposed individually to 20 kGy at 1.5% concentration in water. On the other hand, irradiation of a binary PVP/AAc system at different compositions leads to formation of nanogels or microgels, depending on the PVP/AAc molar ratios. Figure 3 shows the effect of feed composition on PVP/PAAc gel particle size measured at low and high pH values using the DLS technique. A synergistic effect on NP formation by combining both the reactants clearly appears. Nanogel particles of hydrodynamic mean diameters in the range 80–120 nm (measured at low pH) are formed when PVP/AAc feed compositions of molar ratios between 25/75 and 55/45 are used. At these compositions, it is proposed that the complexation between the template PVP and the growing PAAc chains leads to a contraction of the component polymer coils. Further decreases in the PVP/AAc molar ratio result in a sharp increase in the size of the nanogel particles. The higher the AAc content in the feed solution, the greater the amount of AAc diffused to participate in the polymerization at the near surface region of the particles. Subsequently, an increase in the particle size takes place.

When the DLS measurements are conducted at pH4 and pH7 (Figs 4 and 5), it can be observed that the particle size is higher at pH7 than at pH4. In addition, the mean diameter of the nanogel particles increases by increasing the AAc content in the feed solution. At high pH values, the carboxylic acid groups of PAAc chains become ionized, resulting in dissociation of the H bonds of PVP/PAAc IPCs and electrostatic repulsion between the ionized PAAc chain segments. This strengthens the water swellability of PVP/PAAc chains and, as a result, the swelling of the PVP/PAAc nanogel particles increases. Moreover, the greater the content of PAAc in the nanogel particles, the higher the amount of water molecules that penetrates the nanogel particles and, subsequently, the higher the swelling capacity of the particles. The lower values of PDI obtained in this study corroborate the observation for relatively monodisperse systems. All values of PDI are less than 0.2 (Fig. 3), which reflects the uniformity and monomodal distribution for the particles prepared at different compositions.

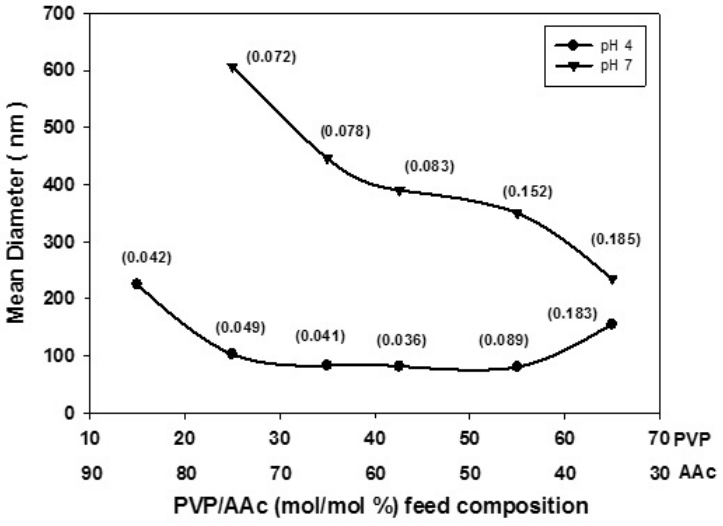

FIG. 3. Effect of feed composition on the particle size of the prepared PVP/PAAc nanogels dispersed in deionized water at pH4 and pH7. Feed concentration = 1.5% w/v, irradiation dose = 20 kGy. Numbers in parentheses represent PDI.

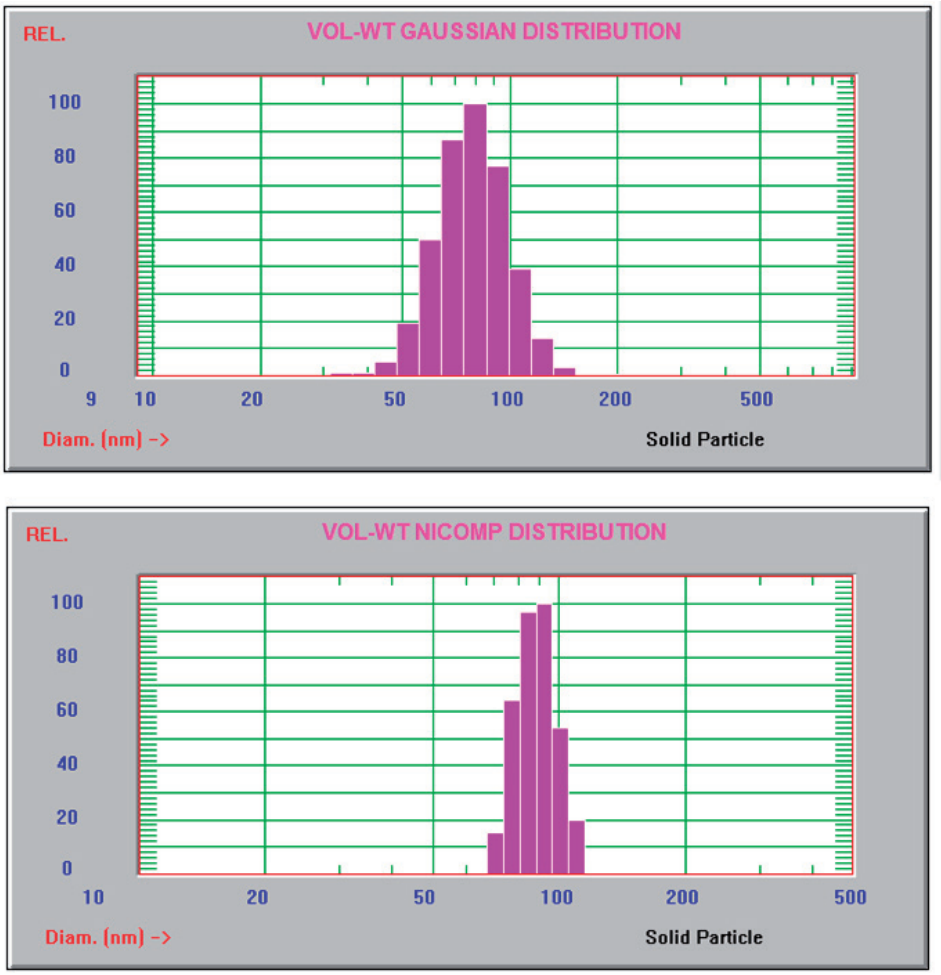

FIG. 4. DLS results for PVP/AAc in deionized water (mean diameter = 83 nm, PDI = 0.041). PVP/AAc = 35/65 mol/mol%, total concentration = 1.5%, PVP MW = 1 300 000 g/mol, irradiation dose = 20 kGy. Measurements conducted at pH4.

The average zeta potentials of the nanogel particles, prepared at different compositions and dispersed in deionized water, were determined to evaluate the surface charge and stability of the gel particles (Table 1). The results demonstrated that the particles are negatively charged, indicating the presence of carboxylic groups on their surface. As the amount of AAc increases in the feed solution, the zeta potential value slightly increases; the zeta potential value increases from −18.4 mV to −30.8 mV when the PVP/PAAc composition changes from 55/45 to 25/75 (PVP/AAc mol/mol%). The zeta potential values of the NPs prepared at different compositions reflect their surface charge and stability against aggregation.

The feed concentration is another important parameter through which the particle size of the prepared PVP/PAAc nanogels can be controlled. At low pH values, it can be seen from Fig. 6 that the particle size decreases with increasing feed concentration, until it reaches 1 wt%. Thereafter, any increases in feed solution concentration lead to a limited gradual increase in the average particle size while keeping the feed composition constant. The same behaviour is noticed when the size of prepared particles is measured at high pH values.

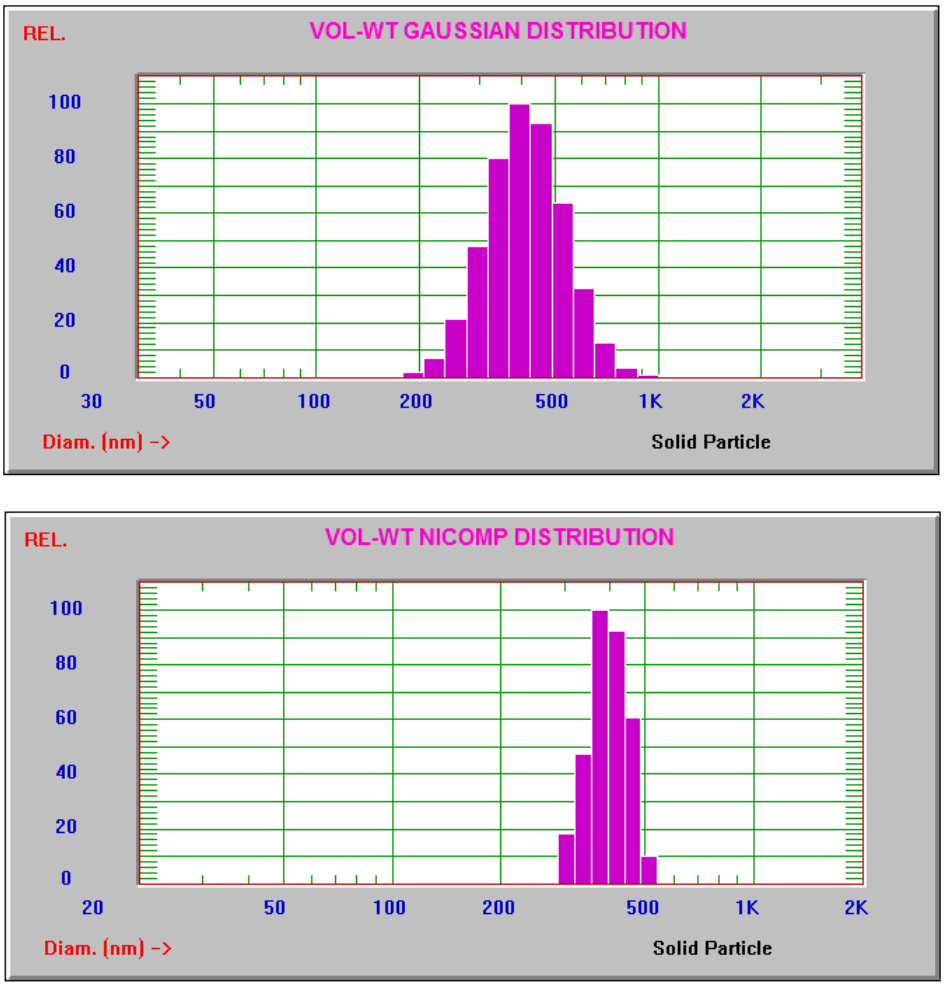

FIG. 5. DLS results for PVP/AAc in deionized water (mean diameter = 446 nm, PDI = 0.078). PVP/AAc = 35/65 mol/mol%, total concentration = 1.5%, PVP MW = 1 300 000 g/mol, irradiation dose = 20 kGy. Measurements conducted at pH7.

TABLE 1. AVERAGE ZETA POTENTIALS OF THE NANOGEL PARTICLES PREPARED AT DIFFERENT COMPOSITIONS AND DISPERSED IN DEIONIZED WATER

Feed compositions PVP/AAc (mol/mol%)	Zeta potential ± standard deviation (mV)
15/85	−30.8 ± 3.7
25/75	−24.0 ± 1.4
35/65	−22.6 ± 0.3
40/60	−17.1 ± 2.4
55/45	−18.4 ± 1.4

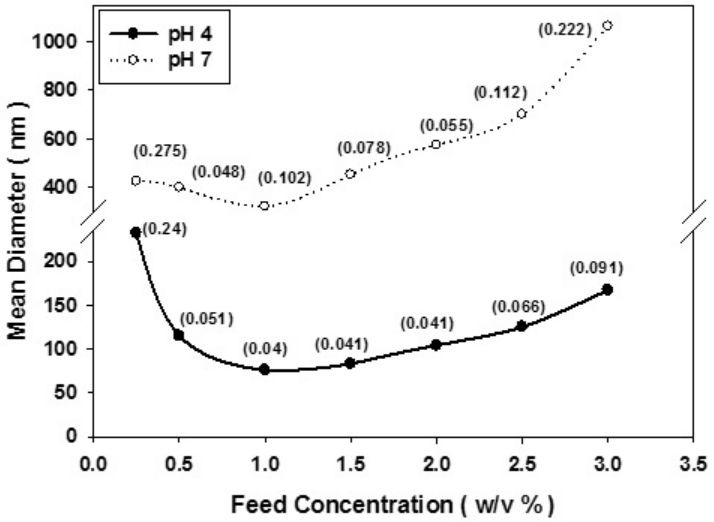

FIG. 6. Effect of feed concentration on the particle size of the prepared PVP/PAAc nanogels measured in deionized water at pH4 and pH7. Feed composition: PVP/AAc (35/65 mol/mol%), irradiation dose = 20 kGy. Numbers in parentheses represent PDI.

As mentioned above, AAc is polymerized and begins to form IPCs with PVP molecules when it reaches a critical length. Thus, at a low feed concentration, it is expected that the produced PAAc chains are not long enough to complex effectively with PVP molecules. As a result, incompact nanogel structures of relatively high average size are formed. By increasing the feed concentration, the produced PAAc chains become sufficiently long to complex effectively with PVP molecules, and small sized NPs are formed to reach a minimum mean diameter at about 1% feed concentration. Further increases in the feed concentration (>1%) lead to a significant increase in the viscosities of the prepared PVP/AAc mixtures owing to the increase in PVP concentration. This might influence chain flexibility, chain length and the dynamics of PAAc molecules. Consequently, the reorientation ability of PAAc molecules to form IPCs with PVP becomes slightly limited, and a nanogel structure of relatively large size is formed. Moreover, as the feed concentration increases, the chain intermolecular recombination, which may lead to formation of microgels or macrogels, is promoted. Thus, the particle size of the prepared PVP/PAAc gels increases. The relatively high PDI at high pH for the particles produced from the lowest and highest feed concentrations may support these suggestions.

3.3. Morphology of PVP/PAAc nanogels

Figure 7 displays the morphology, obtained by AFM, for PVP/PAAc nanogel particles prepared at irradiation doses of 20 kGy and deposited from aqueous solutions at pH4. The spherical shape and mean diameter of the nanogel particles were confirmed by AFM measurements. The AFM image shows that the particle heights (~4–6 nm) are significantly smaller than their widths (~70–150 nm), suggesting substantial flattening of the particles on the mica.

3.4. Drug loading

Pilocarpine was entrapped into the PVP/PAAc colloidal nanogels by simple mixing of this drug with the aqueous dispersion of the nanogels. Trials were carried out to load pilocarpine on PVP/PAAc colloidal nanogels at different pH values. Insignificant pilocarpine loading efficiency was recorded at pH4.5–pH5. This is evidently because of partial protonation of the carboxylic groups in the PAAc chains (acid dissociation constant (pKa) = 4.7) of the nanogels at acidic pH values. Meanwhile, it was found that pH6 is appropriate for pilocarpine loading. At this pH value, both the pilocarpine molecule (pKa = 7.2) and the carboxylic group of the PAAc (pKa = 4.7) were completely ionized, providing an opportunity to tune the electrostatic binding between the drug and PAAc chains of the nanogels. Thus, the loading of pilocarpine on PVP/PAAc colloidal nanogels prepared at different compositions and irradiation doses was carried out at pH6.

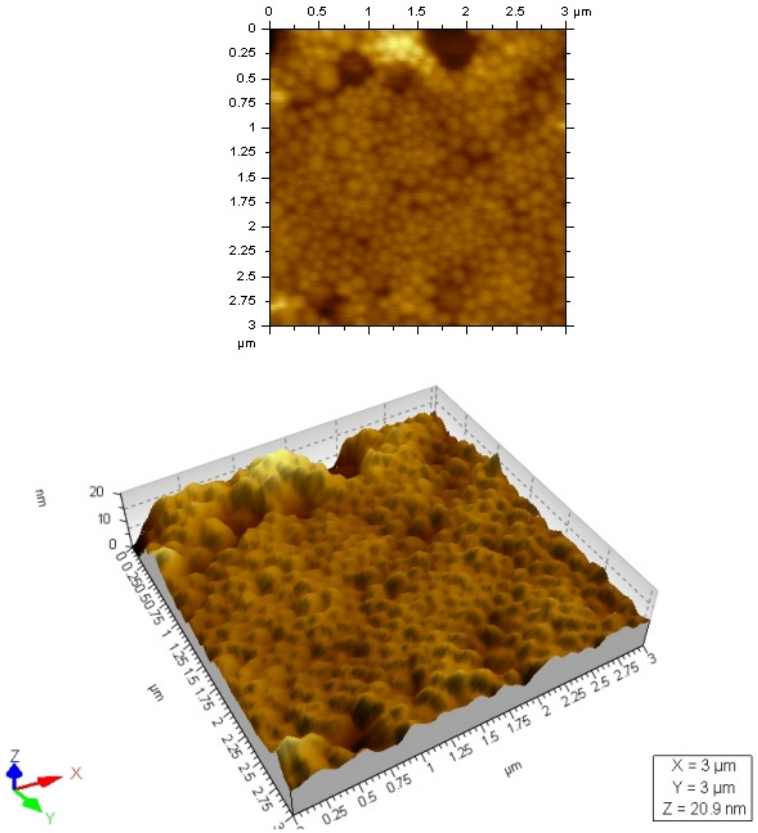

FIG. 7. AFM image (topography and three dimensional view) of PVP/PAAc nanogel particles deposited from an aqueous dispersion at pH4. Feed composition: PVP/AAc (35/65 mol/mol%), feed concentration = 1.5%, PVP (MW = 1 300 000 g/mol), irradiation dose = 20 kGy.

It can be seen from Table 2 that pilocarpine loading efficiency on PVP/PAAc colloidal nanogels depended on the feed composition and the irradiation dose at which the nanogel particles were obtained. AAc rich nanogels exhibited the highest loading efficiency. These results further reinforce the conclusion that pilocarpine binding to the ionic PVP/PAAc nanogels depended mainly on electrostatic interactions. As the amount of PAAc increased, the chance for the drug to bind electrostatically with the nanogel increased, and thus pilocarpine loading efficiency increased. On the other hand, the irradiation dose at which nanogels were formed greatly affected the drug loading efficiency; the higher the dose, the greater the pilocarpine loading efficiency on the PVP/PAAc colloid. Nanogels prepared at a low irradiation dose possess a low density network structure, resulting in easy diffusion and effusion of the drug. Moreover, during nanogel separation by an ultracentrifuge, the diffusion of incorporated pilocarpine molecules from the nanogel particles of high cross-linking density may be lower than that from nanogels of lower cross-linking density because the large centrifugal forces may expel the drug from the nanogel vehicles. The amount of pilocarpine loaded into PVP/PAAc nanogels is influenced also by the drug/nanogel weight ratio during the loading process. It was found that the pilocarpine content increased from ~9 wt% to ~25 wt% when the drug/nanogel weight ratio increased from 1/5 to 1/1, respectively, for nanogel particles prepared at 40 kGy using a PVP/AAc feed composition of 35/65 (mol/mol%).

TABLE 2. LOADING EFFICIENCY OF PILOCARPINE ONTO PVP/PAAc NANOGEL PARTICLES*

Feed composition (PVP/AAc mol%)	Irradiation dose (kGy)	Loading efficiency (%)
25/75	20	26
	40	49
35/65	20	25
	40	47
55/45	20	5
	40	12

* The concentration of the nanogels in water was 5 mg/mL and the drug concentration was 1 mg/mL.

The particle size and morphology of the nanogel particles prepared at 20 kGy using a PVP/AAc feed composition of 35/65 (mol/mol%) were investigated using DLS and TEM techniques before and after drug loading (Fig. 8). The hydrodynamic mean diameters of free nanogel and pilocarpine loaded nanogel were approximately 409 nm and 345 nm, respectively. This reduction in size was attributed to the partial charge neutralization that resulted from electrostatic interactions between the negative ionized groups of the nanogel and the positively ionized nitrogen of the pilocarpine hydrochloride. This charge neutralization is associated with a reduction in the hydrophilicity of the particles, which leads to a decrease in their swelling degree (deswelling) and average size. TEM images showed that the particles loaded with drug seem to be spherical and compact when compared with unloaded particles. This ensures that the overall effect of drug loading produced a less polar environment within the nanogel, which produced a more compact nanogel structure. Moreover, zeta potential measurements provided extra evidence of the neutralization of the PAAc segments in the nanogel particles owing to the electrostatic binding of pilocarpine. It was noticed that upon loading with pilocarpine, the net negative charge of the nanogels was decreased from −45.3 ± 1.8 mV to −37.3 ± 0.5 mV.

The FTIR spectra of pilocarpine HCl, neutralized PVP/PAAc nanogel and pilocarpine loaded nanogel are shown in Fig. 9. It can be observed that the FTIR spectrum of pilocarpine shows characteristic bands at 3082 cm^{-1}, 3028 cm^{-1}, 1766 cm^{-1} and 1612 cm^{-1} owing to absorptions of quaternary N–CH_3, aromatic CH, C=O (lactone ring) and aromatic C=C, respectively. In the PVP/PAAc nanogel spectrum, a characteristic band at 1566 cm^{-1} appears because of the carboxylate ions of the neutralized nanogel. In addition, there are two overlapping bands at about 1718 cm^{-1} and 1655 cm^{-1}, corresponding to C=O stretch of non-ionized carboxylic groups and the *N*-vinyl-pyrrolidone ring, respectively. The FTIR spectrum of pilocarpine loaded nanogel shows the carbonyl absorption band of the pilocarpine lactone ring at 1766 cm^{-1}. Moreover, it can be observed that the carbonyl band of the carboxylic groups almost disappears; conversely, the carbonyl band of carboxylate ions is enhanced and slightly shifted to a higher frequency at 1574 cm^{-1}. The C=O stretch of the *N*-vinyl-pyrrolidone ring can also be seen at 1666 cm^{-1}. These differences in the FTIR spectrum of pilocarpine loaded nanogel in comparison with that of pure nanogel might confirm the electrostatic interaction between the carboxylate ions of the nanogel and the protonated pilocarpine molecules. The mechanism of radiation synthesis of PVP/PAAc nanogels followed by loading with pilocarpine is postulated as shown in Fig. 10.

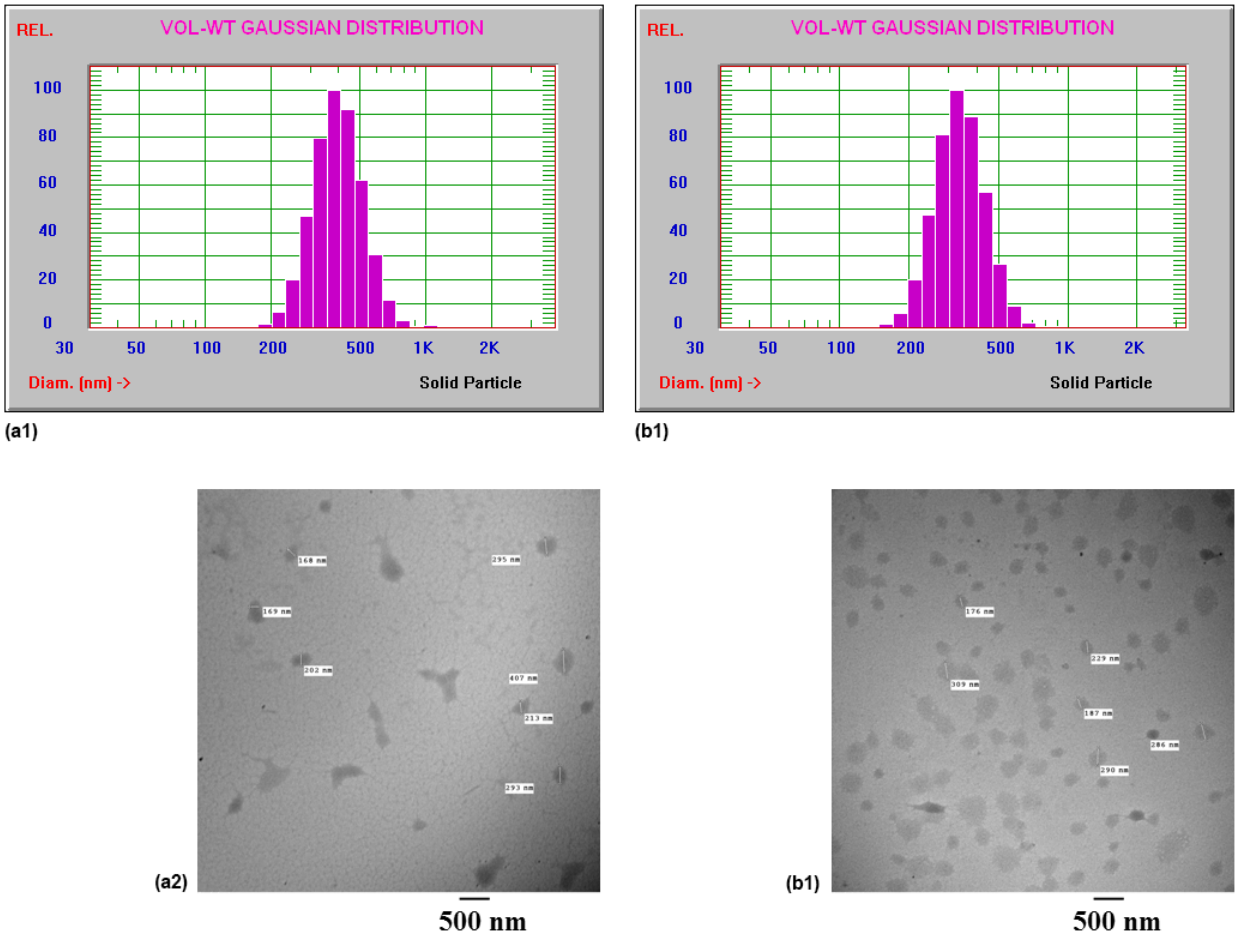

FIG. 8. DLS results for (a1) PVP/PAAc nanogels and (b1) pilocarpine loaded nanogel at pH6, and (a2, b2) their corresponding TEM images. Feed composition = PVP/AAc (35/65 mol/mol%), irradiation dose= 20 kGy.

3.5. Transparency of PVP/PAAc nanogels

To prevent blurred vision, high transparency of an ophthalmic formulation is extremely desirable. Therefore, the transmittance at different pH values of the PVP/PAAc nanogel aqueous dispersions loaded with pilocarpine was evaluated at 500 nm (Fig. 11). It can be observed that the transmittance of the PVP/PAAc nanogel dispersions increased generally with increasing pH value, to reach a maximum at ~pH5.8; thereafter, any increases in pH led to insignificant increases in transmittance. This can be attributed to the pH induced phase transition phenomenon of IPCs. At low pH values, the particles have a compact structure owing to the hydrophobic interactions resulting from the involvement of hydrophilic groups in direct hydrogen bonding. As the pH increases, the strong hydrogen bonding is weakened, and the water solubility of the chain segments within the nanogel particles is strengthened, resulting in a more transparent nanogel dispersion. Another factor affecting the percentage transparency of the nanogel dispersion at a neutral pH is the irradiation dose used for nanogel preparation. As the irradiation dose increases from 20 kGy to 40 kGy, the transparency of the nanogel decreases from ~46.5% to ~5%. At a higher irradiation dose, the produced nanogel particles have a polymer network structure of high cross-linking density (more compact); the higher the cross-linking density, the lower the transmittance of the nanogel particle.

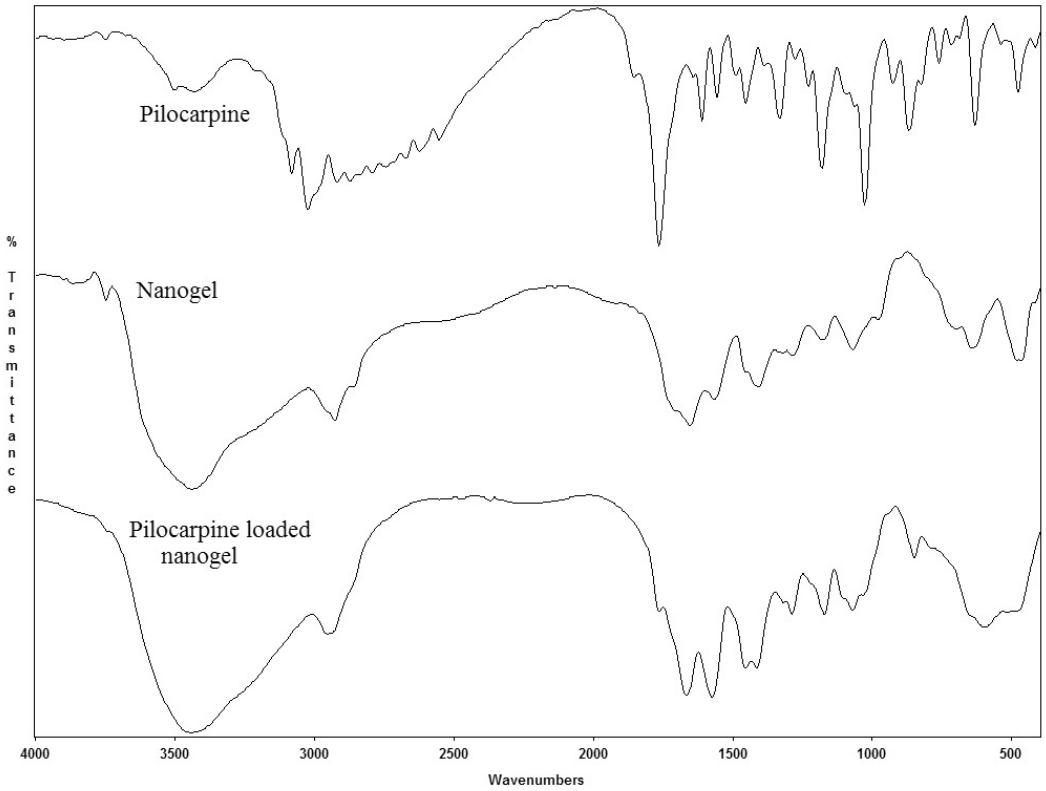

FIG. 9. FTIR spectra for pilocarpine HCl, neutralized PVP/PAAc nanogel and pilocarpine loaded nanogel.

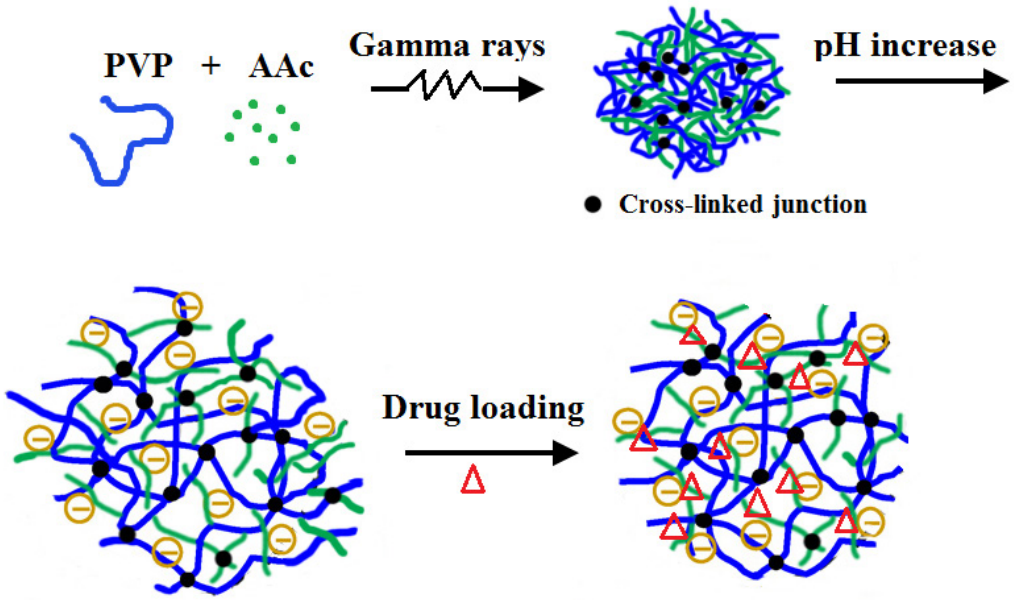

FIG. 10. Radiation synthesis of PVP/PAAc nanogels and loading with pilocarpine.

It has been reported that the ideal characteristics of ocular drug delivery systems [19–21] are good corneal penetration, prolonged contact time with corneal tissue, simplicity of installation for the patient, and non-irritative and comfortable forms (the viscous solution should not provoke lacrimation and reflex blinking). Therefore, the rheological, irritating and mucoadhesion properties of PVP/PAAc nanogels should be investigated to show how the prepared nanogel could be used as an ocular delivery matrix.

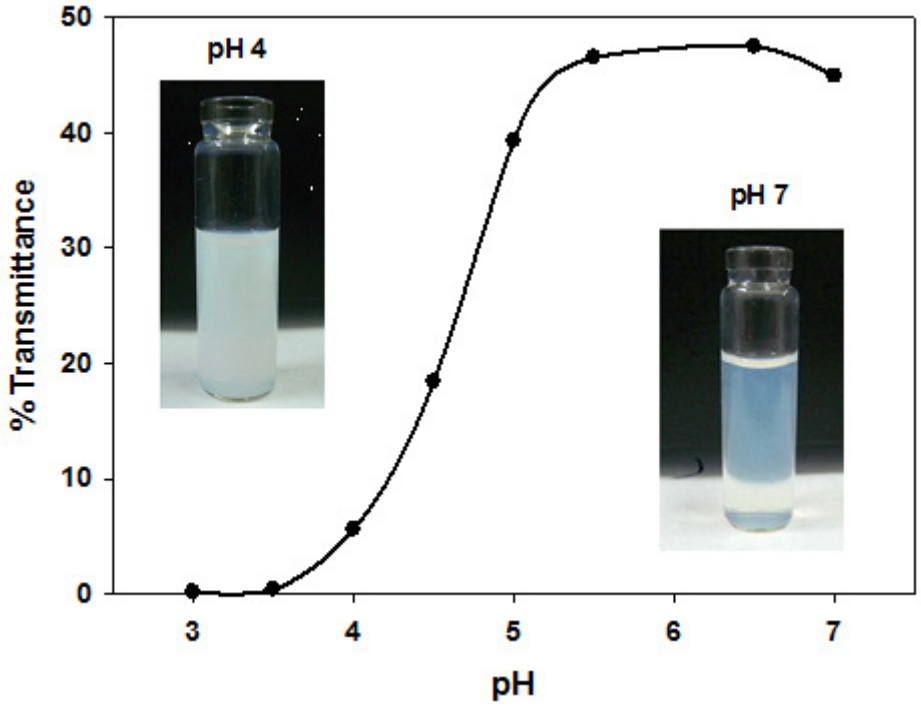

FIG. 11. Dependence of transmittance (at 500 nm) of the PVP/PAAc nanogels on the pH value (inserts are photographs of the prepared nanogels (1.5%) at pH4 and pH7). Feed composition = PVP/AAc (35/65 mol/mol%), irradiation dose = 20 kGy.

3.6. Rheological properties of PVP/PAAc nanogels

Viscosities of PVP/PAAc nanogels prepared at different compositions and irradiated with 20 kGy and 40 kGy were measured at pH9. Figure 12 shows changes of viscosity as a function of frequency for the nanogel dispersions at a concentration of 2% w/v. The viscosity of the nanogel dispersions is correlated with the content of AAc in the nanogel, as well as the cross-linking density. At the same frequency, the viscosity increases with a larger amount of AAc and a lower cross-linking density in the nanogel. At a high content of AAc, and low cross-linking density, the enhanced osmotic pressure exerted by the counter ions trapped inside the polymeric network by the large number of charged carboxylate groups causes an increase in the effective volume occupied by the particles. Such an increase in volume essentially decreases the interparticle distance, where the interaction forces between the swollen particles increase, resulting in an increase of viscosity. In addition, the nanogel dispersions display a pseudo plastic behaviour. This can be ascribed to the hysteresis of the polymer chain motion in comparison with the frequency supplied by the test machine, resulting in a decrease of the interaction of the polymer chains with the surrounding water. The lower viscosities of these PAAc based nanogels could be useful in promoting good retention and stability on the eye without significant discomfort for the patient.

3.7. Interaction with mucin (mucoadhesion)

The interaction between the drug carrier and the precorneal mucin (mucoadhesion) plays an important role in precorneal drug absorption and depends on the functionality and charges of carriers [11]. Therefore, rheological properties (viscosity) of PVP/PAAc nanogel particles prepared at different irradiation doses, and their mixtures with mucin as well as pure mucin, were investigated. In general, for all components and their mixtures investigated here, as the frequency increased, the apparent viscosity of the solution decreased. An interaction between the NPs and mucin could be seen as a synergistic effect in the rheological properties when compared with that of single component PVP/PAAc nanogel particles and mucin because of either physical entanglements or secondary bonds between them. The rheological response of the PVP/PAAc mucin mixture is larger than the sum of the rheological responses of the single components. The rheological response of the PVP/PAAc prepared at 20 kGy and mixed with mucin is higher than that of mucin PVP/PAAc prepared at 40 kGy owing to the viscosity difference. The

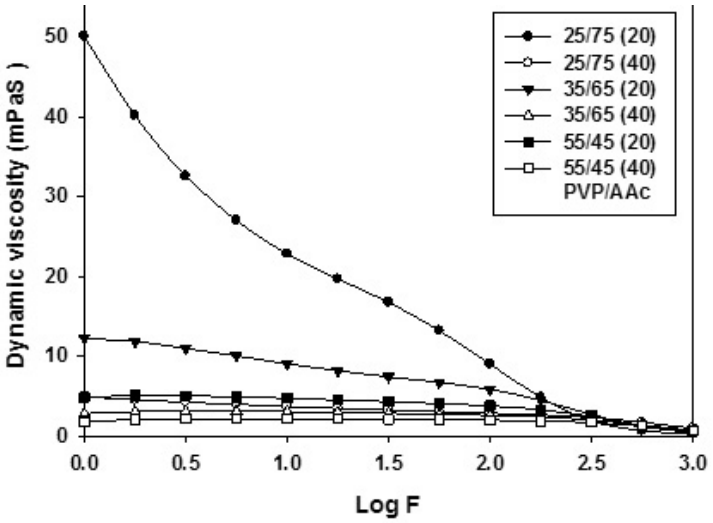

FIG. 12. Viscosity as a function of frequency for the PVP/PAAc nanogels prepared from different PVP/AAc compositions at 20 kGy and 40 kGy and dispersed in water.

improvement in viscosity of nanogel particles/mucin indicated the mucoadhesion properties of PVP/PAAc nanogel particles.

Zeta potential measurements were also used as another method to evaluate the interaction of PVP/PAAc nanogels with mucin dispersion before and after loading with pilocarpine. In the test, mucin was dispersed in water at a concentration of 1% and the pH was raised to 6 using drops of $NaHCO_3$ solution. Mucin dispersion was then mixed with an appropriate amount of the nanogel solution. It was expected that the surface charge of mucin might be changed by the adhesion of the NP polymers if they have a mucoadhesive property. The occurrence of such a change was detected by measuring the zeta potential. As can be seen from Table 3, when the mucin dispersions were mixed with the solutions of drug loaded and unloaded nanogels, the zeta potential of the mucin changed to a higher negative value owing to the negative charge of the NPs. The zeta potential value of mucin PVP/PAAc prepared at 20 kGy was slightly higher than that of mucin PVP/PAAc prepared at 40 kGy. These results suggested that NPs had a high affinity towards mucin to cover their surfaces and strongly supported the mucoadhesive properties of PVP/PAAc nanoparticulate gels.

TABLE 3. ZETA POTENTIALS ± STANDARD DEVIATIONS (MV) OF FREE NANOGEL AND PILOCARPINE LOADED NANOGEL, AND THEIR CORRESPONDING MIXTURES WITH MUCIN (MUCIN ZETA POTENTIAL = −15.5 ± 0.7 mV)

Dose	Nanogel*	Nanogel/drug	Nanogel/mucin	Nanogel/drug/mucin
20 kGy	−45.3 ± 1.9	−37.3 ± 0.5	−33.2 ± 0.15	−31.5 ± 1.5
40 kGy	−47.4 ± 1.8	−36.4 ± 0.5	−29.6 ± 1.1	−29.1 ± 3.7

* Feed composition = 35/65 mol/mol% PVP/AAc.

3.8. In vitro release of pilocarpine

Pilocarpine was loaded into PVP/PAAc nanogel, and its release was evaluated at 32°C ± 1°C in simulated tear fluid (pH8). The release profile of pilocarpine loaded nanogels (pilocarpine loading efficiency = 47%) was compared with that of a control sample in which pilocarpine was dissolved directly in STF solution. The release rate of the control sample (pilocarpine) through the dialysis membrane was relatively fast. It was found that 35% of the pilocarpine was released into the medium within 15 min, and most of the drug was released within 6 h (Fig. 13).

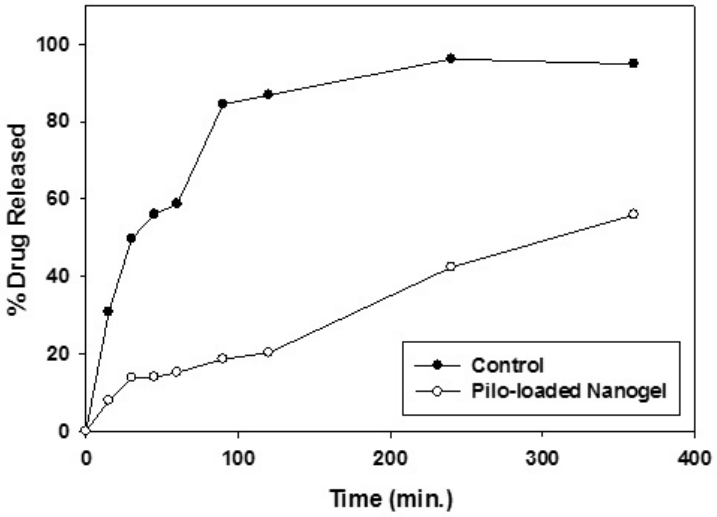

FIG. 13. In vitro release profile of pilocarpine at pH6 from PVP/PAAc nanogel particles, prepared from a feed composition of 35/65 (PVP/AAc) mol/mol% at 40 kGy.

The release profile of pilocarpine loaded nanogels showed a slow release when compared with the control sample. Only about 10% of the drug was released within the first 15 min, and then about 55% of the drug was released within 6 h.

3.9. Use of PVP/PAAc nanogels for dry eye treatment

An experimental dry eye model in albino rabbits was carried out using atropine sulphate 1% eye drops. The model produces some typical dry eye symptoms such as a significant reduction in the tear volume and TBUT, corneal staining and histopathological signs of dryness and inflammation. Therefore, it can be satisfactorily used for a preliminary assessment of the protective activity of polymeric tear substitutes. In this study, the prepared PVP/PAAc nanogels (1.5% w/v, pH7.4) were used for the treatment of the dry eye model, and the results obtained were compared with those for commercial PAAc gel Vidisic 0.2%. To follow the improvement of dry eye signs, Schirmer's test and TBUT were assessed on days 0, 2, 5 and 7 to evaluate tear volume and tear film stability, respectively. Animals were sacrificed on day 7, and histopathological examination of the cornea was performed.

Schirmer's test values and TBUT of the negative control group (only saline eye drops were applied topically for 7 d) showed the absence of any noticeable change of the tear volume and tear film stability throughout the duration of the experiment. Figure 14 shows Schirmer's test values for the untreated dry eye model group and the dry eye model groups treated with nanogel solutions (1.5% w/v) prepared at different feed compositions and irradiation doses as well as the commercial tear substitute Vidisic gel 0.2%. The mean normal tear volume in all rabbit tested groups (untreated group and treated groups before induction of dry eye model) ranged between 19.7 ± 1.6 mm and 17.2 ± 1.5 mm. Whereas, after induction of dryness for 2 d, the Schirmer's test values were reduced markedly ($p < 0.05$) to levels ranging between 6.0 ± 0.9 mm and 7.4 ± 1.2 mm in all the tested groups, denoting a marked suppression of aqueous tear production. Moreover, the untreated dry eye model group showed a mean reduction in tearing, reaching 5.1 ± 0.6 mm after 7 d, which had no significant difference from the 2 d level.

Treatment of dryness, starting from day 3, with the nanogel solutions and Vidisic gel resulted in a noticeable improvement in Schirmer's test values for all the tested groups with variable degrees. The comparison between groups, on day 7, and the untreated dry eye model group showed a significant improvement in all tested groups ($p < 0.05$). Moreover, it was noticed that the two formulations (PVP/AAc, 35/65, 20 kGy) and (PVP/AAc, 35/65, 40 kGy) had a better effect and significantly improved the dryness ($p = 0.000$) compared to the commercial gel, with Schirmer's test values of 17.7 ± 1.5 mm and 18.8 ± 1.5 mm, respectively. However, the other formulations had almost similar effects to the commercial formulation, with no significant differences.

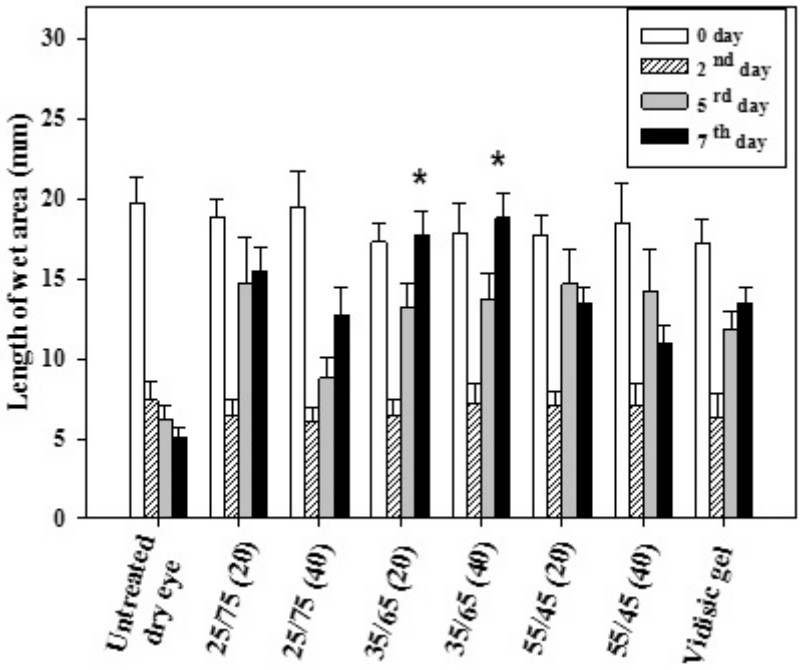

FIG. 14. Schirmer's test values for the untreated dry eye model group and dry eye model groups treated with the different nanogel solutions (1.5% w/v) and Vidisic gel. Data represent means of three rabbits with a total of six eyes ± standard deviations. Asterisks (*) denote significant difference compared with Vidisic gel.

Figure 15 shows the TBUT values for the untreated dry eye model group and treated dry eye model groups. The mean normal levels of TBUT before induction of dry eye model (on day 0) ranged between 25.0 ± 2.8 s and 22.2 ± 2.0 s in all the tested groups. Moreover, ophthalmic examination under a slit lamp and fluorescein staining revealed clear corneas with an absence of staining, indicating an intact corneal epithelium and the absence of any abrasions or ulcers.

It was noticed that the AAc rich nanogel solutions (25/75 and 35/65 PVP/AAc) subjected to 20 kGy showed a complete return of the corneal epithelium to the normal state, as indicated by the absence of corneal staining. In contrast, with the corresponding nanogels prepared at 40 kGy as well as with the commercial gel, eyes still had very minimal corneal erosions on day 7. This may be attributed to the lower flexibility and mucoadhesive properties of the nanogel particles that were prepared at high irradiation doses.

3.10. Irritant effect of PVP/PAAc nanogels

Interestingly, it was noted that the tested formulations had no irritant effect on the tested eyes. Moreover, they reversed the inflammation resulting from dryness (meiosis, photophobia and conjunctival congestion) after treatment for 7 d twice daily.

4. CONCLUSION

PVP/PAAc nanogels were prepared successfully using γ radiation. Nanogel particle sizes were controlled by adjusting radiation doses and PVP/AAc feed concentrations and ratios. Particles of hydrodynamic mean diameters in the range 80–120 nm (at low pH) were formed when PVP/AAc feed compositions of molar ratios between 25/75 and 55/45 at 1.5% w/v feed concentration were used. The nanogel particle size was significantly affected by changing the external conditions such as the pH of the medium. Rheological analysis indicated that the nanogels dispersed in tear fluid possessed low viscosities and pseudo plastic behaviour and could be used as a carrier for ocular delivery without causing blurred vision or patient compliance failure. In addition, mucoadhesive interactions between the nanogels and mucin were determined in terms of viscosity and zeta potential changes and

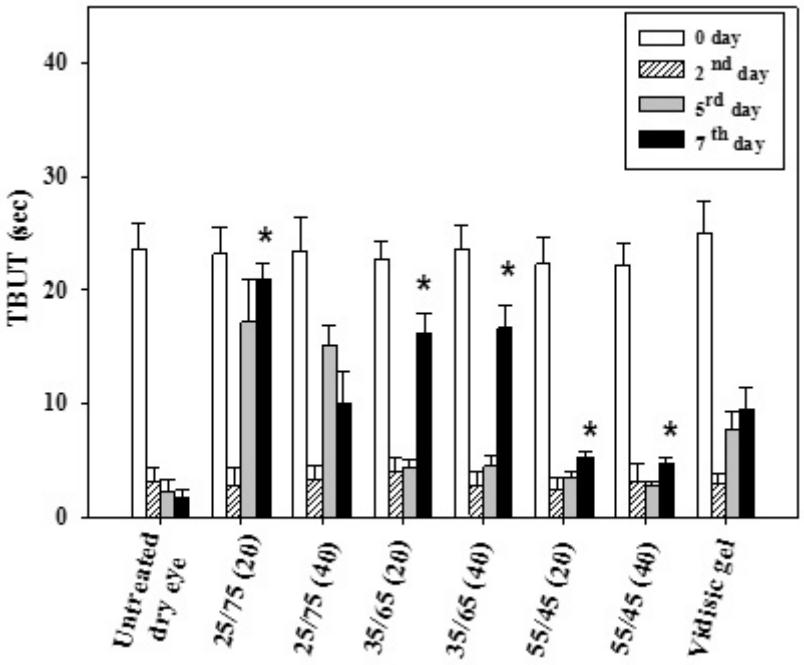

FIG. 15. TBUT values for the untreated dry eye model group and dry eye model groups treated with the different nanogel solutions (1.5% w/v) and Vidisic gel. Data represent means of three rabbits with a total of six eyes ± standard deviation. Asterisks (*) denote significant difference compared with Vidisic gel.

strongly supported mucoadhesive properties of PVP/PAAc nanoparticulate gels. It was noticed that the AAc rich nanogel solutions (25/75 and 35/65 PVP/AAc) subjected to 20 kGy could be used in dry eye treatment and showed a complete return of the corneal epithelium to the normal state, indicated by the absence of corneal staining. Furthermore, pilocarpine loaded nanogels showed a slow release compared with pilocarpine solution; only about 55% of the drug was released within 6 h. The non-irritating, mucoadhesive and rheological properties of PVP/PAAc nanogels qualify such nanomatrices for possible use in ophthalmic applications.

REFERENCES

[1] HAMIDI, M., AZADI, A., RAFIEI, P., Hydrogel nanoparticles in drug delivery, Adv. Drug Deliv. Rev. **60** (2008) 1638−1649.
[2] KABANOV, A.V., VINOGRADOV, S.V., Nanogels as pharmaceutical carriers: Finite networks of infinite capabilities, Angew. Chem. Int. Ed. **48** (2009) 5418−5429.
[3] LEE, E.S., KIM, D., YOUN, Y.S., OH, K.T., BAE, Y.H., A virus-mimetic nanogel vehicle, Angew. Chem. Int. Ed. **47** (2008) 2418−2421.
[4] OISHI, M., HAYASHI, H., IIJIMA, M., NAGASAKI, Y., Endosomal release and intracellular delivery of anticancer drugs using pH-sensitive PEGylated nanogels, J. Mater. Chem. **17** (2007) 3720−3725.
[5] RAEMDONCK, K., DEMEESTER, J., DE SMEDT, S., Advanced nanogel engineering for drug delivery, Soft Matter **5** (2009) 707−715.
[6] WU, W., ZHOU, S., Hybrid micro-/nanogels for optical sensing and intracellular imaging, Nano Rev. **1** (2010) 5730−5746.
[7] SAHOO, S.K., DILNAWAZ, F., KRISHNAKUMAR, S., Nanotechnology in ocular drug delivery, Drug Discov. Today **13** (2008) 144–151.
[8] PATHAK, M.K., SRIVASTAVA, R., CHHABRA, G., PATHAK, K., Viability of nanotechnology in ocular therapeutics, Micro Nanosyst. **4** (2012) 128–144.
[9] LIU, S., JONES, L., GU, F.X., Nanomaterials for ocular drug delivery, Macromol. Biosci. **12** (2012) 608–620.
[10] ZIMMER, A., KREUTER, J., Microspheres and nanoparticles used in ocular delivery systems, Adv. Drug Deliv. Rev. **16** (1995) 61–73.
[11] LUDWIG, A., The use of mucoadhesive polymers in ocular drug delivery, Adv. Drug Deliv. Rev. **57** (2005) 1595–1639.

[12] GUPTA, A.K., MADAN, S., MAJUMDAR, D.K., MAITRA, A., Ketorolac entrapped in polymeric micelles: Preparation, characterisation and ocular anti-inflammatory studies, Int. J. Pharm. **209** (2000) 1–14.
[13] VERSURA, P., et al., Dryness symptoms, diagnostic protocol and therapeutic management: A report on 1,200 patients, Ophthalmic Res. **33** (2001) 221–227.
[14] MACRI, A., ROLANDO, M., PFLUGFELDER, S., A standardized visual scale for evaluation of tear fluorescein clearance, Ophthalmol. **107** (2000) 1338–1343.
[15] TRIPATHI, B.J., TRIPATHI, R.C., KOLLI, S.P., Cytotoxicity of ophthalmic preservatives on human corneal epithelium, Lens Eye Toxicity Res. **9** (1992) 361–375.
[16] BECQUET, F., et al., Histopathological effects of topical ophthalmic preservatives on rat corneoconjunctival surface, Curr. Eye Res. **17** (1998) 419–425.
[17] DEBBASCH, C., et al., Mitochondrial activity and glutathione injury in apoptosis induced by unpreserved and preserved beta-blockers on Chang conjunctival cells, Invest. Ophthalmol. Vis. Sci. **42** (2001) 2525–2533.
[18] RAINALDI, I., CRISTALLINI, C., CIARDELLI, G., GIUSTI, P., Kinetics and reaction mechanism of template polymerization investigated by conductimetric measurements. Part 3. Radical polymerization of acrylic acid in the presence of poly(*N*-vinylpyrrolidone), Polym. Int. **49** (2000) 63−73.
[19] GEERLING, G., DANIELS, J.T., DART, J.K., CREE, I.A., KHAW, P.T., Toxicity of natural tear substitutes in a fully defined culture model of human corneal epithelial cells, Invest. Ophthalmol. Vis. Sci. **42** (2001) 948–956.
[20] HUTORYANSKIY, V.V., Hydrogen-bonded interpolymer complexes as materials for pharmaceutical applications, Int. J. Pharm. **334** (2007) 15−26.
[21] KEISTER, J.C., COOPER, E.R., MISSEL, P.J., LANG, J.C., HAGER, D.F., Limits on optimizing ocular drug delivery, J. Pharm. Sci. **80** (1991) 50–53.

ARCHITECTURES BASED ON GOLD NPs ASSOCIATED WITH TARGETING AGENTS FOR TUMOUR THERAPY BY PHOTOTHERMIA

M.-C. CLOCHARD[1], G. RIZZA[1], M. SANGERMANO[2], J. AMICI[2],
S. DESHAYES[3], H. CABRAL[3], K. MIASAKI[3]

[1] Laboratoire des Solides Irradiés
CEA DSM/IRAMIS
France

[2] Politecnico di Torino
Italy

[3] Department of Materials Engineering Graduate School of Engineering
University of Tokyo
Japan

Abstract

In the framework of the CRP programme, France has worked in collaboration with Italy and Japan on the development of new gold NP architecture for tumour ablation using photothermia. The main condition for such applications is that NPs exhibit an SPR in the NIR region. The CEA has a γ ray irradiation facility and EB accelerator for radiation grafting of polymers. In this programme, gold NPs were synthesized in plain, hollow and core shell forms. The plain gold NPs were covered with PVDF by nanoemulsion polymerization to prepare particles for further radiografting. The cytotoxicities of the HGNPs absorbing in the NIR region were evaluated. As these NPs were promising materials, photothermal effects on tumour cells have been examined.

1. OBJECTIVE

The objective of the project was the synthesis of nanovectors for tumour therapy by photothermia. To attain this objective, NPs exhibiting an absorption in the NIR are needed. Three classes of metallic NPs were investigated: (i) HGNPs, (ii) inorganic core shell NPs of SiO_2@Au type and (iii) composite core shell NPs of Au@fluoropolymer type. To render these NPs biocompatible, a PEG shell was added all around and functionalized with targeting agents that specifically target tumour cells. Ionizing radiation (electrons and/or γ rays) was used for the grafting process and functionalization, when possible, to limit by-products. The interest of the project is twofold: (i) testing various NP architectures with NIR absorbance properties and (ii) coupling novel promising targeting agents for tumour cells recently developed in miscellaneous vectors to NP vectors.

2. INTRODUCTION

Despite tremendous amounts of investment and research, cancer still remains responsible for 25% of all deaths in developed countries [1]. There is an extremely acute need for more sensitive, accurate and cost effective methods for detecting and treating cancer. One of the greatest problems for patients submitted to cancer therapies is the unspecificity of effects that afflict many organs and cause severe secondary side effects. In particular, traditional chemotherapy greatly damages healthy tissue in the process of killing cancer cells. Methods that offer the ability to kill only cancer cells and to affect as few healthy cells as possible are highly required. In this respect, photothermal therapy combined with a targeted vector allows drastic reduction of drug concentration and represents a new interesting perspective into the wide panorama of cancer therapy.

In particular, the present project proposed to combine the newly developed targeting agents for solid tumour cells with the synthesis of nanovectors exhibiting enhanced photothermal properties.

To reach this objective, the following steps were carried out:

— Synthesis and characterization of gold nanostructures that possess remarkable SPR optical properties and are tuneable to NIR absorption;
— Polymeric coverage of these nanostructures to: (i) functionalize them by γ or EB radiation in the case of PVDF and (ii) improve vector biocompatibility (PEG);
— Functionalization of the vector with a targeting agent towards tumour cells.

Local application of heat is a well known concept in therapeutic medicine [2, 3]. Photothermal therapy relies on heat generated from light for destroying cancer cells. This technique is based on the oscillation of gold NPs. To obtain this effect, the gold NPs are exposed to a wavelength that is larger than their size and is not absorbed by body tissue. At a specific frequency, this provokes the appearance of SPR. The specific frequency varies with the shape of the gold NPs. Under light excitation, the electrons of the conduction band swing *until the oscillation frequency matches the wavelength frequency. At that moment, the atoms are in resonance.* This resonance phenomenon provokes a vibration of the NP itself, leading to heat increases of several degrees, which is sufficient to kill tumour cells.

These effects are particularly noticeable in the visible part of NP spectra of gold, silver and copper [2]. Noble metal nanostructures are promising nano-objects in emerging medical technologies because they present a low toxicity and have no reported side effects [3]. To achieve the full therapeutic potential of photothermal therapy, it is essential to optimize its photothermal conversion efficiency, decreasing the energy dose of laser light and minimizing potential damage to surrounding normal tissue; this is why ideal material for photothermal therapy should have a strong and tuneable SPR, especially in the NIR region (700–900 nm), because body tissue is moderately transparent to NIR light, thereby providing an opportunity for therapeutic effects in deep tissues limiting the heat generated to the region of the target tissue. Of course, the efficient depth of such a treatment is relative, and it is important to note that such a therapy is generally combined with a surgical act to properly clean the area surrounding a solid tumour that has just been removed.

The plasmon resonance for ordinary gold nanospheres is at ±520 nm, while for ordinary silver nanospheres it is at ±400 nm, which is further from the NIR [2]. The shift towards the NIR region is possible only if the architecture of the NPs is modified.

Several different nanostructures have been used for photothermal therapy, including NPs, nanorods, nanoshells, nanocages and hollow nanospheres. Among these structures, hollow gold nanospheres represent one of the most promising candidates for meeting all of the requirements at the same time, because of their unique combination of small size, spherical shape and strong, narrow, tuneable SPR absorption [3–5].

These particles are generally covered by a biocompatible polymer to prevent aggregation and biodegradation for in vivo applications [6]. In addition, the coating plays an essential role for prolonged blood circulation by delaying the removal of the reticuloendothelial system [7].

PVDF is a thermoplastic polymer that is semicrystalline, biocompatible (registered in pharmacopoeia) and possesses a remarkable chemical resistance.

Numerous industrial medical applications are already commercially available in various forms: microporous membranes, vascular sutures and prostheses [8]. Despite these applications, few articles have reported on PVDF use in NP form. Partners in the present project have already reported on PVDF NPs as nanovectors for tumour therapies [8, 9]. PVDF NPs are easily functionalized in a one step reaction with AAc by γ ray irradiation.

In a continuation of this work, the present project ran a nanoemulsion polymerization of vinylidene fluoride gas in the presence of gold NPs to cover a gold NP surface with a PVDF layer. The nanoemulsion polymerization of vinylidene fluoride followed the protocol of Deshayes et al. [8]. The gold nanostructured NPs was synthesized at the Laboratory of Physics of Interfaces and Thin Films at the École Polytechnique.

The coverage by PVDF played a double role: one was to link by radiografting the molecule of interest for tumour therapy and the other one was to shift even more dramatically the SPR band towards the NIR [10]. Consequently, the polymeric coverage becomes a supplementary parameter to shift the SPR band of the nanovector in order to reach the optimal value for photothermia.

Once such a nano-object, which is hyper NIR light absorbent, is built, it is necessary to add a targeting molecule to drive it to the tumour cells [11].

The recent collaboration with the Japanese team at the University of Tokyo (K. Kataoka) makes it possible to combine partner competencies. The functionalization of the targeting agent chosen by K. Kataoka, who is an internationally recognized scientist in tumour therapies, will be carried out via the acetal function of the telechelic

poly(ethylene glycol)-acetals [12]. The targeting agent is phenylboronic acid, which targets sialic acid receptors (overexpressed sugar on the tumour cells). The antitumoural effect of phenylboronic acid shown in mice is very recent. This new molecule has a low cost and has already been accepted by the FDA.

3. NP FABRICATION

3.1. HGNPs

The synthesis of plain gold NPs is a classic synthesis that is well known to the partners of the current project. The synthesis of HGNPs, which is more original than using plain gold NPs, is achieved by reduction of cobalt salt ($CoCl_2$) with sodium borohydride in the presence of sodium citrate in water. Successively, a solution of gold salt ($HAuCl_4$) is added to the colloidal suspension, and Au ions are reduced at the Co NP surfaces to form a shell (Figs 1 and 2).

The total diameter of these NPs has been controlled in the range from 32.86 ± 7.08 nm to 65.24 ± 9.32 nm.

3.2. Gold NPs covered with PVDF by nanoemulsion radical polymerization

Adapting the protocol of large scale integration for PVDF NP synthesis (Fig. 3), the coverage of plain gold NPs by PVDF was carried out (15 nm diameter) (Figs 4 and 5).

Once covered with PVDF, core shell gold NPs were irradiated using γ ray facilities as in the protocol already used by Deshayes et al. [8] on colloidal suspension of PVDF.

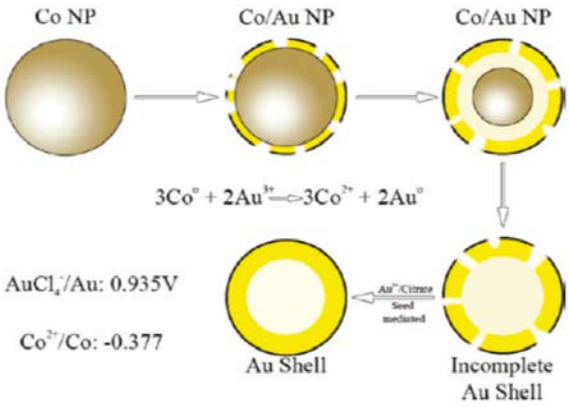

FIG. 1. Schematic representation of HGNP preparation.

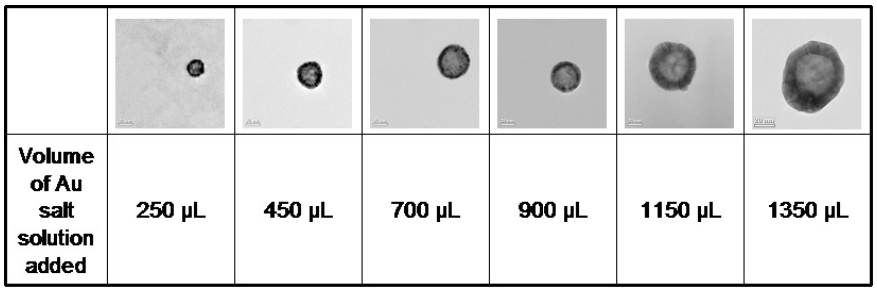

FIG. 2. TEM images of HGNPs by varying the volume of gold salts added to the colloidal suspension of cobalt NPs.

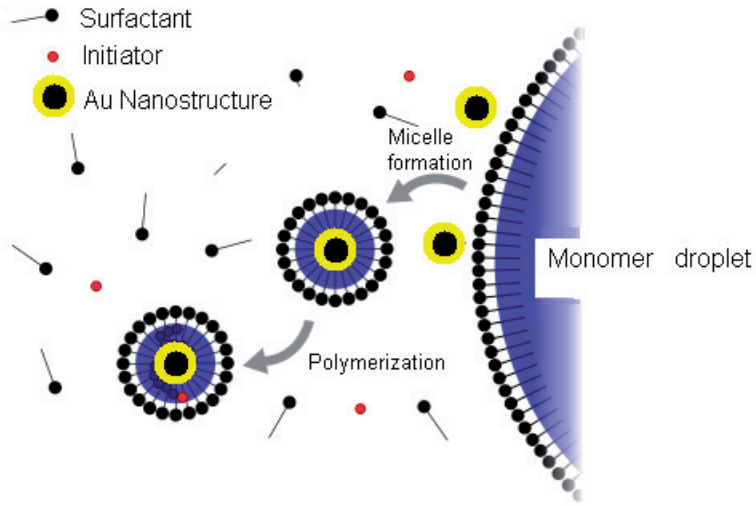

FIG. 3. Schematic diagram of nanoemulsion polymerization of a gaseous monomer around gold nanostructures.

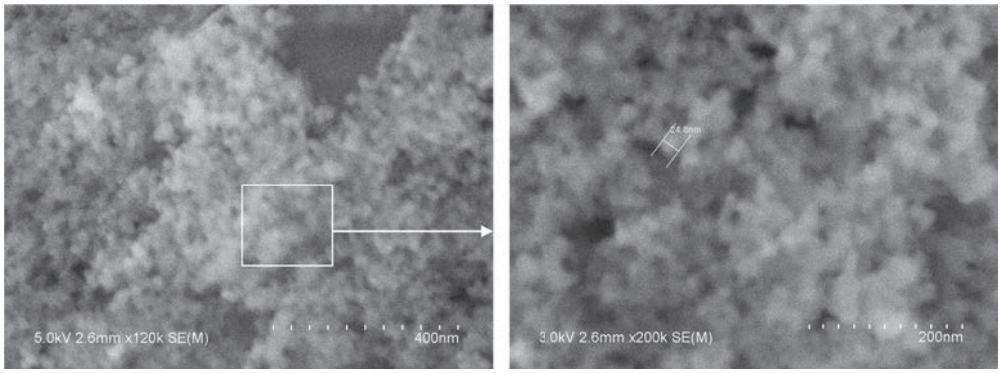

FIG. 4. FESEM images of gold NPs covered with PVDF (external diameter = 25 nm).

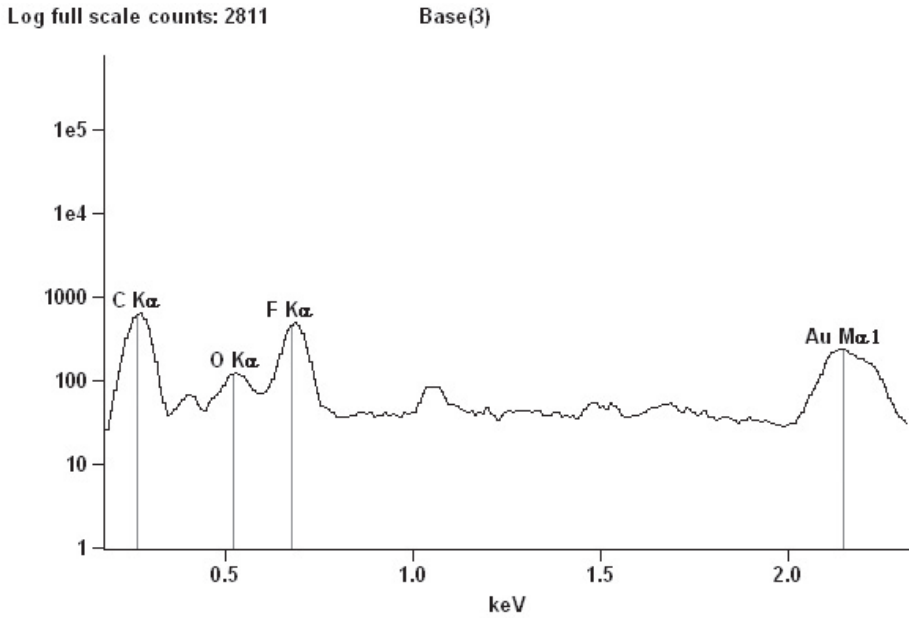

FIG. 5. Energy dispersive X ray analysis of NPs of Fig. 4.

4. RESULTS OF PHOTOTHERMIC EFFECTS

Preliminary results were obtained with monodisperse HGNPs of 60 nm diameter (zetasizer polydispersity $I_p = 0.1$) in aqueous solutions that exhibit an absorption band at 614 nm. These HGNPs were covered with thiolated PEG (79 nm in diameter after PEG modification and an unmodified $I_p = 0.1$) following a protocol on similar systems [13].

Results were obtained by K. Kataoka's team in Japan (investigators: H. Cabral and K. Miazaki). They tested non-PEGylated HGNPs and PEGylated HGNPs at a concentration of 0.2 mg/mL. The incubation time of these particles with the cancer cells was 24 h. So, both NPs are expected to be already internalized by cancer cells, as the cellular uptake of fully PEGylated nanocarriers has been seen at approximately 6 h. Although it has not yet been performed, the uptake of particles with the phenylboronic acid ligand molecule should be comparable for such a long incubation.

In Fig. 6, the term 'drug' in the bar graph refers to the HGNPs.

These first experiments showed no cytotoxicity of HGNPs in the control and after laser illumination, which is a good point for the targeted application. The coupling of HGNPs with a long laser pulse of 250 s at 0.2 mJ/cm^2 exhibited a photothermal effect. The performance was not as high as expected, and needs to be reproduced. The smallest pulse duration and highest laser intensity did not give good results. Experiments are still ongoing to search for the best protocol. Core shell NPs will also be tested.

5. CONCLUSION

One functionalized nanodevice based on HGNPs for targeting and applying the photothermal effect on cancer cells has been fabricated and evaluated. After in vitro cancer cell uptake, the first evaluation of its performance using a laser source with a wavelength of 630 nm (close to 614 nm, which is the SPR band of the studied HGNPs) displayed a photothermal effect. More experiments should be carried out to enhance the photothermal effect by adjusting the laser pulse duration and/or multiple reflection mode.

Another functionalized nanodevice alternative, based on plain gold NPs covered with a PVDF layer to radiograft specifically modified PEG NPs is still under investigation. Fabrication is not a technological problem, but the SPR, which is not yet absorbing in the NIR region (a necessary condition for photothermal therapy), is a problem.

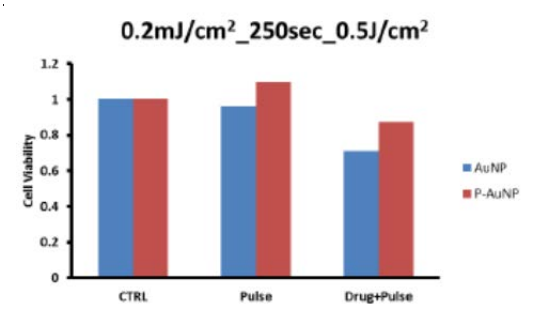

Blue: Au NP; Red: PEG Au NP

CTRL: control; Drug+Pulse: photothermal therapy

Experimental conditions
Cell: A549 cell (5000 cells/well)

Laser: Nd–YAG

Wavelength: 630 nm

Frequency: 10 Hz (10 pulse/s)

Bandwidth: 6 ns

Drug concentration: 0.2 mg/mL

Incubation time: 24 h

FIG. 6. Photothermal therapy experiments performed on non-PEGylated HGNPs (Au NP) and PEGylated HGNPs (PEG Au NP) after internalization in cancer cell (A549 cell lines).

REFERENCES

[1] JAIN, P.K., EL-SAYED, I.H., EL-SAYED, M.A., Au nanoparticles target cancer, Nanotoday **2** (2007) 18.

[2] PISSUWAN, D., VALENZUELA, S.M., CORTIE, M.B., Therapeutic possibilities of plasmonically heated gold nanoparticles, Trends Biotechnol. **24** (2006) 62.

[3] ZHANG, J.Z., Biomedical applications of shape-controlled plasmonic nanostructures: A case study of hollow gold nanospheres for photothermal ablation therapy of cancer, J. Phys. Chem. Lett. **1** (2010) 686.

[4] ZHOU, X., et al., Effects of dielectric core and embedding medium on plasmonic coupling of gold nanoshell arrays, Solid State Commun. **151** (2011) 1049.

[5] FORTINA, P., et al., Applications of nanoparticles to diagnostics and therapeutics in colorectal cancer, Trends Biotechnol. **25** (2007) 145.

[6] KAPPIYOOR, R., LIANGRUKSA, M., GANGULY, R., PURY, I.K., The effects of magnetic nanoparticle properties on magnetic fluid hyperthermia, J. Appl. Phys. **108** (2010) 094702.

[7] ARRUEBO, M., FERNANDEZ-PACHECO, R., IBARRA, M.R., SANTAMARIA, J., Magnetic nanoparticles for drug delivery, Nanotoday **2** (2007) 22.

[8] DESHAYES, S., et al., Synthesis of specific nanoparticles for targeting and imaging tumour angiogenesis using electron-beam irradiation, Rad. Phys. Chem. **79** (2010) 208.

[9] DESHAYES, S., et al., "Click" conjugation of peptide on the surface of polymeric nanoparticles for targeting tumor angiogenesis, Pharm. Res. **28** (2011) 1631.

[10] LAL, S., LINK, S., HALAS, N.J., Nano-optics from sensing to waveguiding, Nature Photonics **1** (2007) 641.

[11] LU, W., XIONG, C., ZHANG, G., Targeted photothermal ablation of murine melanomas with melanocyte-stimulating hormone analog-conjugated hollow gold nanospheres, Clin. Cancer Res. **15** (2009) 876.

[12] OISHI, M., SASAKI, S., NAGASAKI, Y., KATAOKA, K., pH-responsive oligodeoxynucleotide (ODN)-poly(ethylene glycol) conjugate through acid-labile beta-thiopropionate linkage: Preparation and polyion complex micelle formation, Biomacromol. **4** (2003) 1426.

[13] DREADEN, E.C., MWAKWARI, S.C., SODJI, Q.H., OYELERE, A.K., EL-SAYED, M.A., Tamoxifen-poly(ethylene glycol)-thiol gold nanoparticle conjugates: Enhanced potency and selective delivery for breast cancer treatment, Bioconj. Chem. **20** (2009) 2247.

POROUS POLYMER DRUG ELUTING COATINGS PREPARED BY RADIATION INDUCED POLYMERIZATION

M. VERES[1], B. BEILER[2], L. HIMICS[1], S. TÓTH[1], M. KOÓS[1]

[1] Institute for Solid State Physics and Optics
Wigner Research Centre for Physics
Hungarian Academy of Sciences

[2] Institute for Isotopes, Centre for Energy Research
Hungarian Academy of Sciences
Budapest

Hungary

Abstract

Within the framework of the CRP, a protocol for the preparation of a composite drug eluting coating for potential application in various medical implants, such as stents, was developed. It consisted of an amorphous carbon interlayer, drug containing particles, and a hydrogel matrix. The latter can be used to control the drug eluting characteristics of the coating. The steps in the preparation of the coating included deposition of the amorphous carbon layer, preparation of the radiation cross-linked polymer particles as drug carriers, coating of the implant surface with the mixture of polymer particles and monomer, and irradiation of the coating. The thickness of the amorphous carbon interlayer, the particle size and the mixture composition have all been optimized. Additionally, it was demonstrated that γ radiation initiated polymerization and cross-linking could be used to prepare ND/polymer composites. The choice of solvent determined the morphology of the composite. This method has potential for surface functionalization of individual NDs to be used for in vivo sensing of biological materials.

1. INTRODUCTION

Many areas of modern medicine are almost unimaginable without the use of different kinds of implants. They are used as replacements, supports, auxiliary devices, etc., in various parts or functions of the human body. Their use has many advantages; however, during application, particular attention should be paid to avoid associated negative side effects, which could include rejection, inflammation, etc. [1, 2].[1] Many of these drawbacks are directly related to the materials that the implants are made of. For this reason, coatings are widely used to eliminate the unwanted effects related to implant material. In addition to protection and isolation of the tissues from the implant, coatings can also contribute to better functionality and acceptance of the artificial device by the body, as well as to faster regeneration of tissues after intervention. Drug eluting coatings, for example, through the delivery and controlled elution of specific molecules, could actively suppress inflammatory reactions, allergies and rejections of the implant. Coating activity will be localized to the place where these effects could mainly occur, i.e. to the region surrounding the implant. Research and development of drug eluting coatings is a rapidly growing area nowadays, but they still have many problems that need to be resolved. Stimulated and well controlled drug release and formation of homogeneous coatings on implants with complex shapes constitute the two main directions of ongoing research.

This work is aimed at developing a drug eluting porous polymer coating by radiation induced polymerization that can be used in implants in different areas of medicine. Because it is related to previous work [3, 4], the primary targets are stents made of metallic alloys [5–7]. However, these layers could also be used in other types of medical devices. The main objectives include the development and characterization of the drug eluting coating, utilizing NPs as the drug containers, and elaboration of methods for application of the monomer mixture and formation of the drug eluting coating on the surface of the implants made of medical grade metallic alloys.

The obtained results can also be utilized in other areas of nanotechnology, for example, in fabrication of ND/polymer composites using γ radiation induced polymerization techniques. Surface functionalized NDs with

[1] For more information, see http://www.angioplasty.org.

specific colour centres can be used in biomedical applications, such as in drug delivery or as vivo biomarkers. The light emission peak from silicon vacancy centres in NDs, for example, is in the region of highest optical penetration depth of tissues, so it can be used as a biomarker, even several millimetres below the skin surface. The main aim here was to demonstrate the usability of radiation induced polymerization techniques to prepare ND/polymer composites of different morphologies: particulate, porous and bulk materials.

2. MATERIALS AND METHODS

2.1. Materials

DEGDMA and 2-HEMA (Aldrich) were used for preparation of the materials used in the coating and ND/polymer composites. Ethanol, water, acetone and ethyl propionate (Aldrich) were used as solvent materials. Amorphous carbon films were prepared from 5.0 methane and argon precursor gases (Linde). ND was obtained from Neomond (Republic of Korea). The stainless steel substrates were made of medical grade low carbon, vacuum melted 316 stainless steel (316LVM) or Inconel alloys.

2.2. Methods

The polymers, ND/polymer composites and hydrogels were prepared by γ radiation initiated polymerization. To avoid contamination from the atmosphere, the sample preparation procedures were carried out under an argon atmosphere in a UNIlab glovebox workstation (MBRAUN). Alloy substrates were used in the form of 500 μm thick plates and tubes with a 1.25 mm outer diameter and a 300 μm wall thickness. These were put into vials containing the monomer mixture. The irradiation was carried out at room temperature, the absorbed dose was 1–20 kGy and the dose rate was 6 kGy/h.

The amorphous hydrogenated carbon (a-C:H) films were deposited using radiofrequency chemical vapour deposition from methane precursor gas. The substrate was cleaned with argon plasma prior to layer growth. The film properties and thicknesses were varied by changing the deposition parameters and the deposition time, respectively.

The morphology of the obtained coatings was investigated using a DM LM optical microscope (Leica) and JSM-740 (JEOL) and S-4700 (Hitachi) scanning electron microscopes. The bonding configuration of the samples was characterized by Raman spectroscopy on a 1000 micro-Raman (Renishaw) spectrometer. A 27 mW diode laser operating at 785 nm served as the excitation source during Raman measurements. The excitation beam was focused onto a spot of diameter 1 μm. Photoluminescence spectra were recorded on a Fluorolog 3-22 fluorimeter (Jobin Yvon), using a Xe lamp as the excitation source.

3. RESULTS

First, the development was focused on forming a porous DEGDMA layer on the implant surface. However, the results showed that it was not possible to obtain perfect coverage of the surface with the porous polymer layer, so the coating lacked its protective function. Then, the concept of a composite layer was elaborated; this consisted of porous DEGDMA NPs serving as drug containers and embedded into a hydrogel matrix, thus providing the required protective properties as well as control over the release of the drug from the container particles. Problems related to wetting of the metal surface by the monomer mixtures required the introduction of an amorphous carbon interlayer into the system.

3.1. Porous polymer coatings on stainless steel surfaces

Polymerization of DEGDMA in a monomer mixture with γ radiation takes a few tens of minutes. Therefore, the main prerequisite for the formation of a porous DEGDMA layer on any surface is to keep the polymerization mixture there for the time that the reaction takes place. However, the small viscosity of the standard DEGDMA/ethanol monomer mixture [8–10] resulted in poor wetting of the stainless steel surfaces. The use of different solvents and solvent mixtures that were also suitable to form porous polymers led to similar results.

Prepolymerization of the mixture, with the aim of forming a dense gel like material, and subsequent dip coating of the substrates with this prepolymerized mixture followed by a second irradiation were also tested. However, because of the precipitation character of the polymerization process, the mixture became inhomogeneous during pretreatment and was not suitable for coating purposes.

To increase the viscosity of the initial mixture, glycerol was added to it. Preliminary experiments in bulk with 40 vol.% DEGDMA content showed separation of the polymer in the upper part of the mixture, indicating that glycerol alone cannot be used for the preparation of a porous layer. To obtain better homogeneity of the monomer solution while still keeping its viscosity high enough, ethanol was added to the DEGDMA/glycerol mixture in different concentrations. By testing several ethanol/glycerol amounts, it was found that the polymerization mixture containing 60 vol.% solvent with an ethanol/glycerol volume ratio of around 1/1 and 40 vol.% of DEGDMA had the required characteristics and that it was suitable for coating purposes. Figure 1(a) shows an optical microscope image of a stainless steel wire coated with the porous polymer formed by irradiation of the mixture of 30 vol.% ethanol, 30 vol.% glycerol and 40 vol.% DEGDMA. It can be seen that a continuous opaque layer of a few micrometres thick has formed on the surface. SEM analysis (Fig. 1(b)) showed that the coating has a fractal structure and that it comprises coalescing submicrometre sized polymer globules.

The early stage of the polymer growth and the structure of the porous material on the metal surface were also studied. Figure 2 shows SEM images of the formed polymer nuclei attached to the wire surface. It can be seen that there were aggregated polymer globules distributed non-uniformly on the surface, implying that specific active sites were required for the attachment of polymer globules on the metal surface that serve as precipitation centres. These results indicate that the surface properties of the support are critical for obtaining good adhesion.

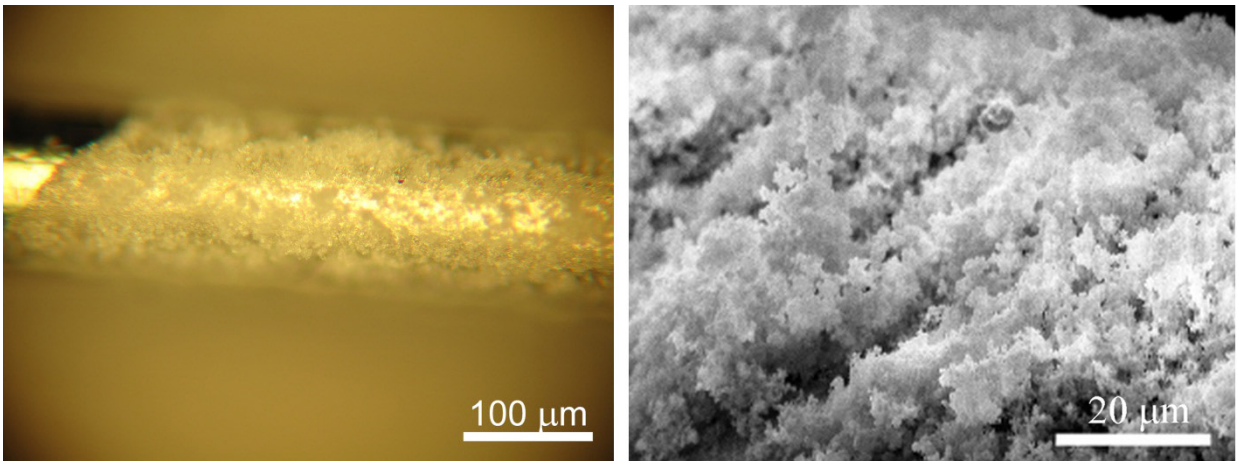

FIG. 1. (a) Optical microscope image of stainless steel wire covered with porous polymer coating. (b) Morphology of the porous polymer layer.

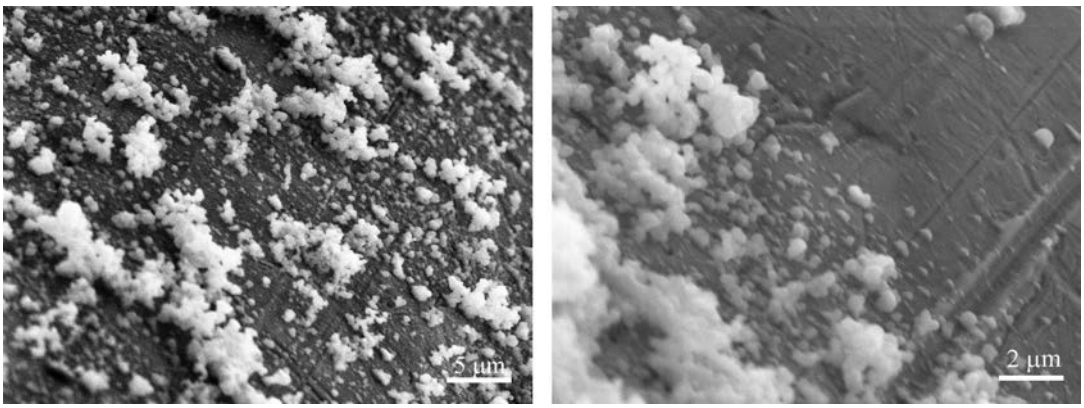

FIG. 2. Formation of porous polymer nuclei on stainless steel wire surface.

3.2. Porous coatings on amorphous carbon

Because of the porous character of the coating described above, it is desirable to use a protective bottom layer in the system that will isolate the metal from its surroundings. A passive amorphous carbon protective coating that had been developed previously for stents [4, 5] was also tested as an interlayer for the porous DEGDMA coating (Fig. 3). However, formation of a macroscopically continuous layer similar to that shown in Fig. 1 was not observed on these samples. As SEM analysis showed (Fig. 3), aggregated porous polymer structures were attached to the amorphous carbon surface in some places, and the coverage was much less than for bare metal substrates. These observations indicate that the surface characteristics of the amorphous carbon surface do not promote the formation of a continuous polyDEGDMA layer on top of it.

Simple bending tests were also performed on coated wires, and these indicated that the coating cracked and peeled off the substrate in some places around the deformation point. In spite of the large surface area and pore volume, the porous DEGDMA layer described above cannot provide the coverage required for separation of an implant from the surrounding tissues. Therefore, fabrication of a composite layer consisting of drug container particles and a host matrix has been proposed.

3.3. Composite drug eluting coating

A schematic diagram of the composite drug eluting coating is shown in Fig. 4. In this device, DEGDMA NPs serve as drug containers. They are placed in a host matrix that, in addition to being a support for the polymer particles, can also be used to control the elution of the drug from the particles [11]. These experiments showed that an interlayer is also required to provide the required adhesion of the coating to metal substrates.

3.4. Host matrix of the composite coating

The host matrix was prepared from 2-HEMA based hydrogel, a biocompatible material widely used in medical devices that can easily be produced by radiation induced polymerization and which also has the mechanical properties that a drug eluting coating requires. Based on data from the literature, the monomer mixture was composed of 60 vol.% water, 35 vol.% HEMA and 5 vol.% DEGDMA as the cross-linking agent [12].

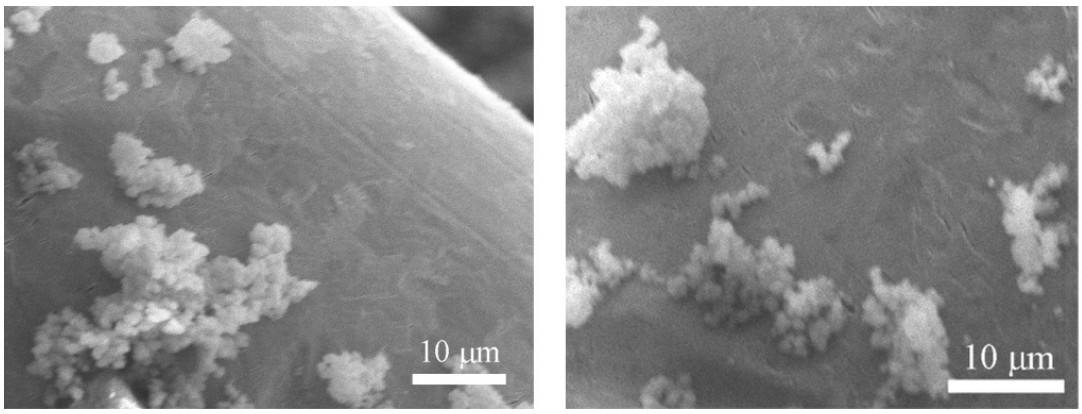

FIG. 3. Porous polymer clusters formed on stainless steel wires coated with amorphous carbon.

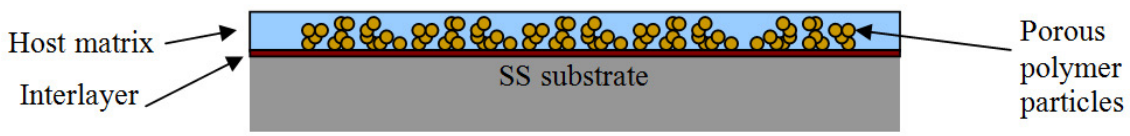

FIG. 4. Schematic diagram of the composite drug eluting coating. SS: stainless steel.

Unfortunately, the bare metal surface was found to be an unsuitable support for the preparation of a homogeneous hydrogel layer. Although it was coated by the hydrogel, a few 100 nm sized spherical particles were observed on the surface (Fig. 5(c)); these were probably related, again, to the poor wetting by the monomer mixture. This means that the metal surface has to be modified to obtain a good adhesion by the monomer mixture of the hydrogel. Different plasma treatments were applied to the substrates, including argon, nitrogen and water plasmas, but they did not change the surface properties remarkably (Fig. 6). However, the amorphous carbon layer that failed as a support for the porous DEGDMA coating earlier showed very promising results. Contact angles (CAs) close to 0° were obtained for the hydrogel monomer mixture on the a-C:H surface (Fig. 6(c)).

The hydrogel layer deposited onto this substrate was found to be homogeneous, without any aggregation of the material (Fig. 7(a)). The presence of the HEMA hydrogel on the a-C:H surface was proved also by Raman spectroscopy (Fig. 7(b)). Characteristic peaks of HEMA can clearly be seen on top of broad a-C:H bands [13]. Comparison of the spectra of bulk and deposited onto the a-C:H surface coating shows that the amorphous carbon has no effect on the structure of the hydrogel.

3.5. Amorphous carbon coating

Amorphous carbon films of 200–300 nm thickness were used during the first stage of the project, when the a-C:H interlayer was developed. These films were similar to those developed earlier for stents as a passive coating. However, in the case of some samples, peeling of the a-C:H coating was observed. Similar problems were faced earlier with amorphous carbon films deposited on Si substrates; these were caused by the thickness of the layer being too high. Experiments showed that the thickness of the a-C:H layer can be lowered to 30 nm and it will still provide the conditions required for perfect wetting by the monomer mixture of the hydrogel.

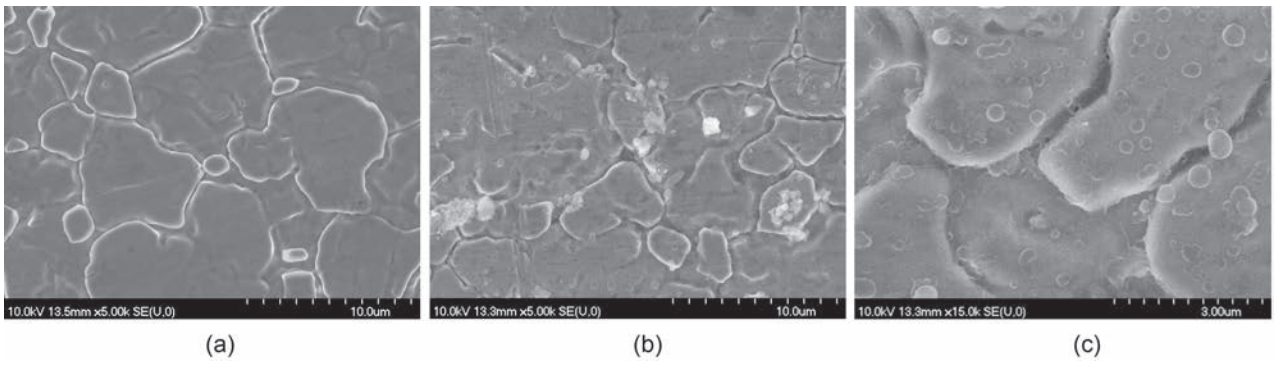

FIG. 5. SEM micrographs of (a) bare metal surface and (b), (c) HEMA hydrogel formed on this surface.

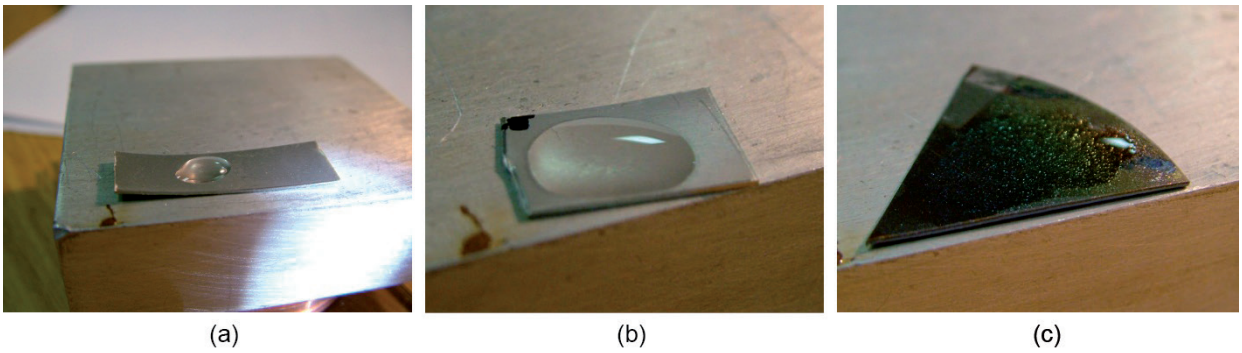

FIG. 6. Wetting of: (a) the bare metal surface, (b) the bare metal surface after Ar plasma treatment and (c) the stainless steel with the a-C:H coating by the monomer mixture.

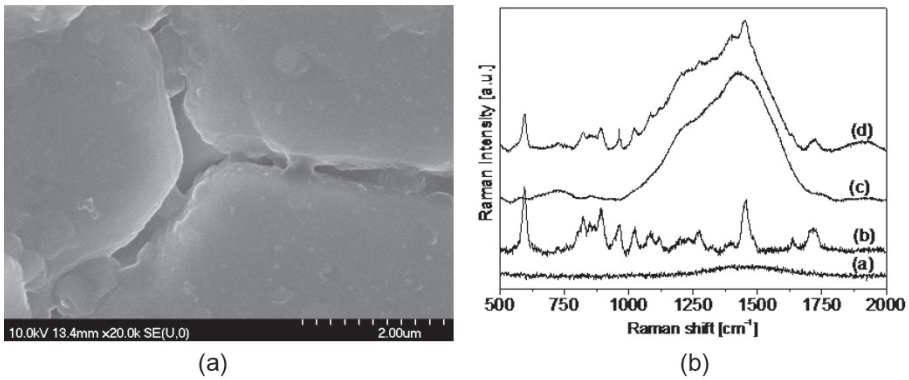

FIG. 7. (a) SEM micrograph of HEMA hydrogel on a metal substrate with an amorphous carbon coating. (b) 785 nm excited Raman spectra of: (a) the bare metal substrate, (b) the hydrogel, (c) the a-C:H layer on the metal substrate and (d) the HEMA hydrogel on top of the a-C:H coating.

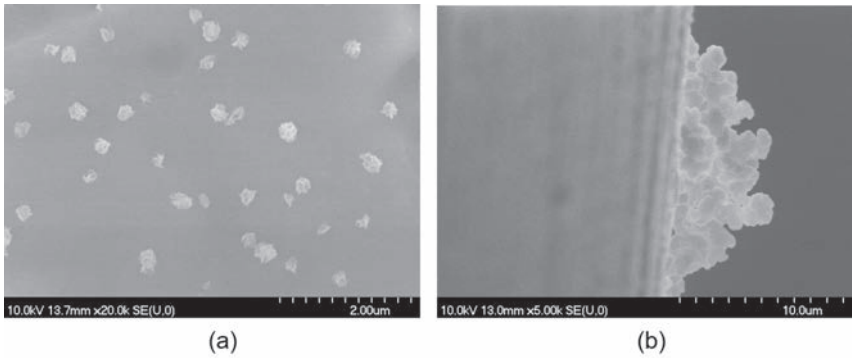

FIG. 8. (a) DEGDMA NPs embedded into the HEMA hydrogel matrix formed after irradiation of a hydrogel monomer mixture with increased DEGDMA content. (b) Porous polymeric structures formed on top of the HEMA layer.

3.6. Preparation of the composite coating

Several approaches have been tried to obtain the composite coating, consisting of the HEMA hydrogel and the DEGDMA particles. First, a one step process was used, utilizing a single monomer mixture with excess DEGDMA content (up to 15 vol.%), which resulted in formation of DEGDMA NPs (with average sizes < 100 nm) embedded into the hydrogel matrix (Fig. 8(a)). Then, a three step process was probed, where an already formed hydrogel layer was coated with a monomer mixture of the porous DEGDMA polymer and irradiated again, and a second HEMA layer was deposited on top of it during the third step. Here, aggregated porous DEGDMA structures, distributed inhomogeneously on the HEMA surface (Fig. 8(b)), were obtained.

These methods showed some promising results, but they also had several drawbacks. The use of a single step process for the preparation of the composite limits the possibilities of independent control over the characteristics of the components of the system. Variation of the composition of the monomer mixture affects the properties of both the hydrogel and the polymer particles. The irradiation is to be performed with one dose, while DEGDMA particles and the HEMA hydrogel require different doses for total conversion. On the other hand, the three step process results in inhomogeneous distribution of the porous polymer structures over the support surface, negatively affecting the uniform drug release from the coating. The above drawbacks can be eliminated, however, by separating the preparation of the porous drug container structures from that of the hydrogel and using them in the form of porous particles. In this way, the preparation parameters of the two components of the coating can be controlled independently. An additional advantage of this approach is that the particles can be filled with drug prior to adding them to the monomer mixture of the hydrogel. Therefore, further development was aimed at the preparation of DEGDMA NPs that can serve as drug containers.

3.7. Controlling the size of the DEGDMA particles

Monodisperse DEGDMA particles can be obtained using ethyl propionate as the solvent. The globules are highly uniform and have a size of 1–2 μm. Systematic investigations were performed to check how the particle size can be controlled. Monomer concentration and dose are the main parameters affecting this process. Figure 9 shows SEM pictures of DEGDMA particles prepared from monomer mixtures of 5 vol.% and 10 vol.% generally used for the preparation of these structures. It can be seen that the monomer concentration has a minor effect on the size of the polymer globules in this concentration region.

At lower concentrations, however, a remarkable decrease in the particle size was observed. As Fig. 10 shows, globules with an average diameter of below 500 nm can be obtained by decreasing the DEGDMA concentration to 1 vol.%.

Because the particle size strongly depends on the dose, the latter is also expected to be a good tool for tailoring the particle size. Monomer mixtures of the same composition (5 vol.% DEGDMA in ethylene propionate) were irradiated with different doses. It was found that particles reach a micrometre size very quickly (even at 4 kGy dose). At such small doses, however, the globules have a soft structure, which results in their aggregation after removal of the solvent (Fig. 11). To avoid this, ongoing research is focused on the use of inhibitors or chain transfer agents to control the particle size and limit it to a few tens or a few hundreds of nanometres.

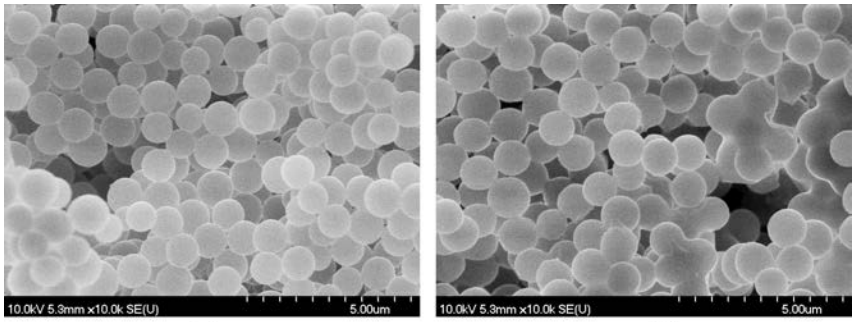

FIG. 9. Monodisperse DEGDMA particles prepared from monomer mixtures of different concentrations: (a) 5 vol.% DEGDMA and (b) 10 vol.% DEGDMA in ethylene propionate. Irradiation dose = 10 kGy.

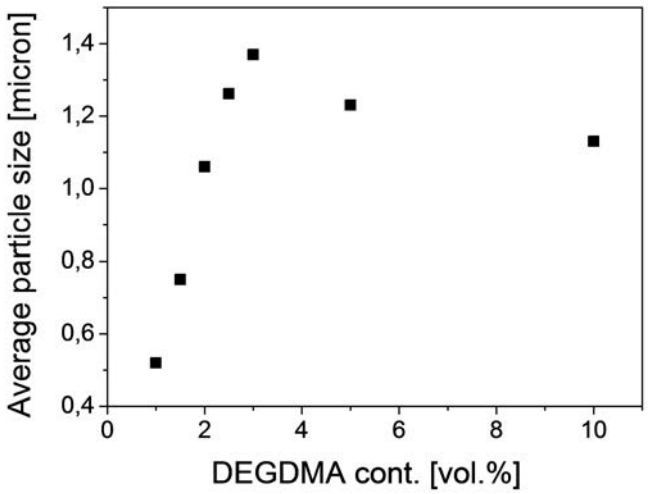

FIG. 10. Dependence of average particle size on the DEGDMA concentration in ethyl propionate. Irradiation dose = 10 kGy.

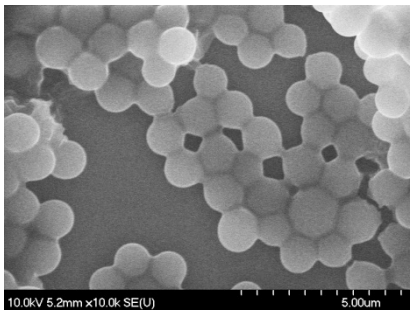

FIG. 11. Aggregated DEGDMA particles in a sample irradiated with a low dose (4 kGy). The monomer mixture was 5 vol.% DEGDMA in ethyl propionate.

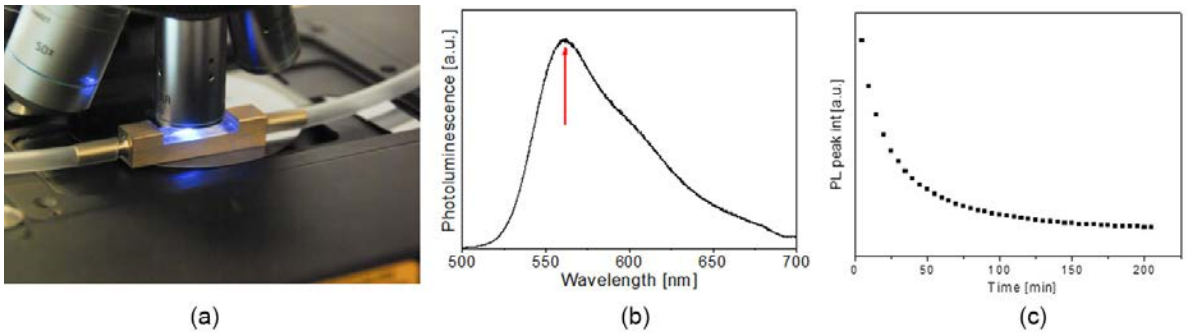

FIG. 12. (a) Measurement cell built for drug elution experiments. (b) Photoluminescence spectrum of Rhodamine 6G used for testing of the system. The arrow indicates the 562 nm wavelength used for monitoring of the drug release. (c) Evolution of the photoluminescence (PL) intensity at 562 nm with time in water used for the elution of Rhodamine 6G from DEGDMA globules.

3.8. Drug elution measurements

Recently, a measurement set-up has been built to determine the drug elution characteristics of the coatings. The system consists of a pump, a sample holder and a measurement cell (shown in Fig. 12(a)). To test the set-up, preliminary experiments were performed with DEGDMA globules soaked in Rhodamine 6G water solution. The change in the intensity of the Rhodamine 6G photoluminescence spectrum at the wavelength of highest intensity with 488 nm excitation (562 nm, Fig. 12(b)) was measured in the water solution that flowed through the DEGDMA globules with Rhodamine 6G. Figure 12(c) shows the evolution of the peak intensity with time. It can be seen that the peak intensity decreases rapidly in the first 50 min and reaches some 15% of its original value after 200 min of elution.

3.9. ND/DEGDMA composites

To test the usability of radiation induced polymerization techniques for the preparation of ND/polymer composites, a series of DEGDMA monomer mixtures with different monomer concentrations and solvent types were polymerized with and without addition of ND. Prior to their addition to the monomer mixtures, the ND particles were sonicated for 3 h, to separate them from each other, and treated with nitrogen plasma to increase the amount of sp^2 carbon atoms — and therefore the number of vinyl groups — on their surface.

Figure 13 compares SEM pictures of polymers with and without NDs obtained from the DEGDMA ethyl propionate system. It can be seen that while spherical particles were formed from pure DEGDMA in ethyl propionate, addition of NDs resulted in distorted and aggregated particles. This is caused by the incorporation of ND particles into the growing polymer globules, which stopped the polymerization in those directions. Formation of DEGDMA microspheres is a result of precipitation polymerization, and the presence of ND particles in the region of the ongoing precipitation and polymerization alters the conditions of the process.

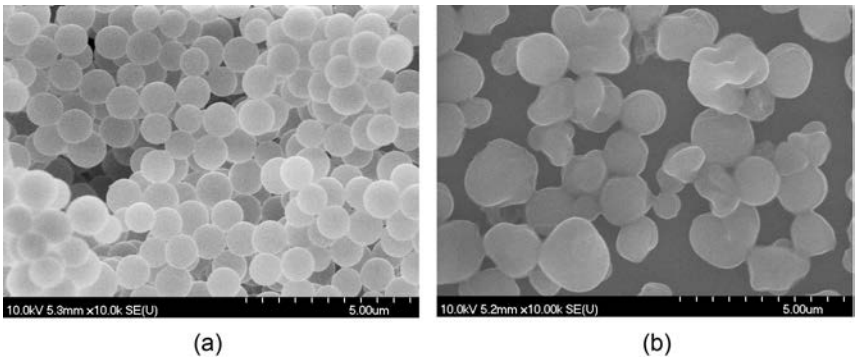

FIG. 13. Surface morphology of polymers prepared from ethylene propionate + DEGDMA: (a) without and (b) with NDs using γ radiation initiated polymerization.

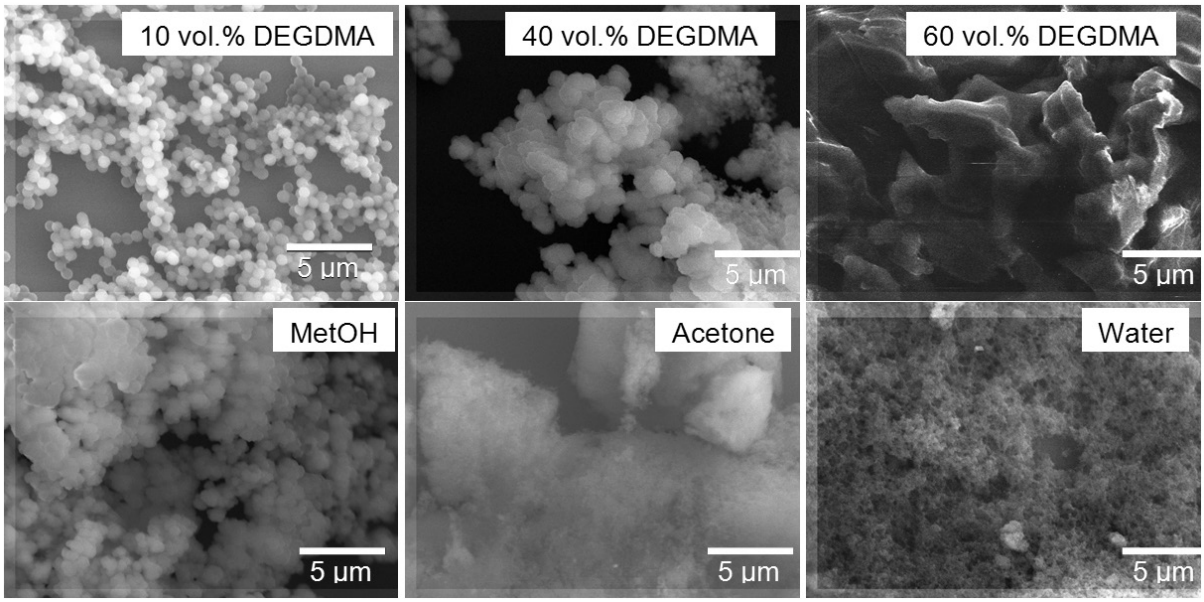

FIG. 14. ND/polymer composites prepared (upper row) from monomer mixtures of different DEGDMA contents in ethyl propionate and (lower row) using different solvents with 20 vol.% DEGDMA. Irradiation dose = 10 kGy. MetOH: methanol.

Figure 14 shows SEM pictures of ND/polymer composites obtained from monomer mixtures of different compositions. Particulate, porous and bulk materials have been prepared simply by varying the DEGDMA content in ethyl propionate. The use of different solvents resulted in porous and sponge like structures of various morphology.

Figure 15 compares the Raman spectra of the obtained ND/polymer composites. The presence of the characteristic peak around 1640 cm^{-1} in the spectrum of each sample indicates that there are still intact vinyl groups in the structure after irradiation with 10 kGy, so these are 'dangling' on trapped monomers in the polymer matrix. Comparison of conversion values obtained by fitting of the 1640 cm^{-1} peak with a Gaussian curve for samples with and without NDs (Fig. 16) shows that the addition of NDs slows down the polymerization: the conversion at 10 kGy is higher for pure polymers than for the composites. Interestingly, in the case of samples obtained from monomer mixtures of different DEGDMA contents, the highest conversion was obtained at 20 vol.% DEGDMA content. At higher concentrations, the applied dose probably was not enough to polymerize all of the monomers, while below 20 vol.%, the reaction was limited by the low monomer concentration—after the radical formation, there were no other activated monomers in the vicinity of a given monomer to react with.

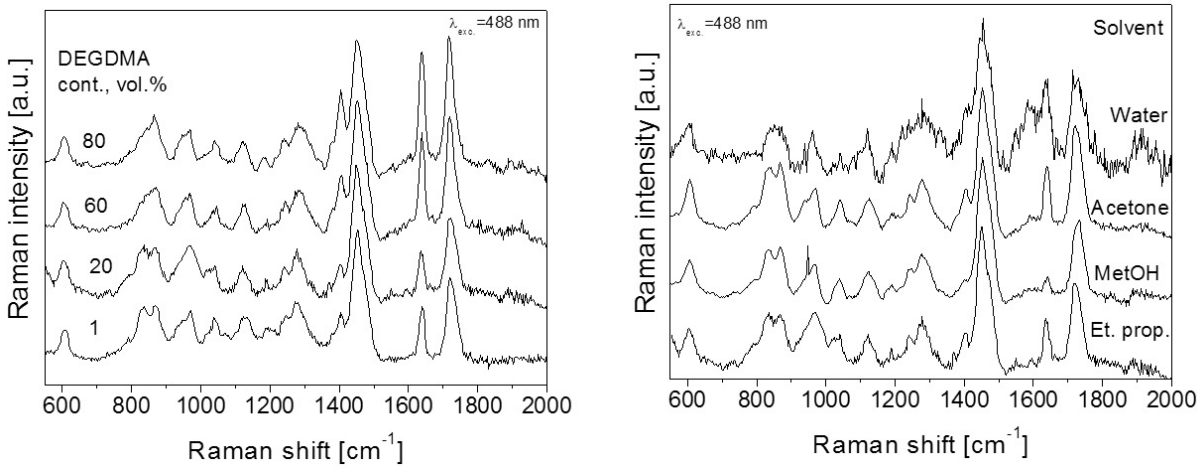

FIG. 15. Raman spectra of ND/polymer composites prepared from monomer mixtures of different DEGDMA contents in ethyl propionate and using different solvents with 20 vol.% DEGDMA. Irradiation dose = 10 kGy. Et. prop.: ethyl propionate; MetOH: methanol.

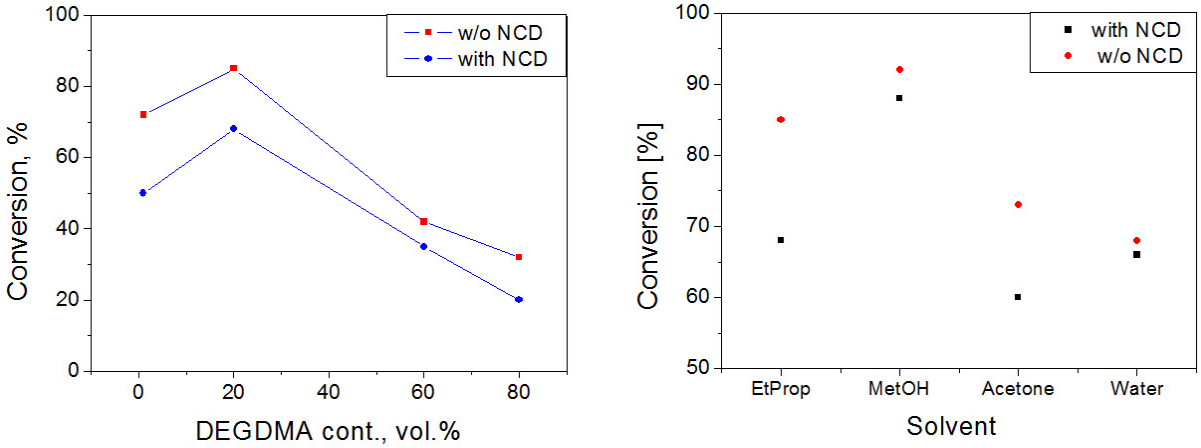

FIG. 16. Conversions determined from Raman spectra of ND/polymer composites and pure polymers prepared from monomer mixtures of different DEGDMA content in ethyl propionate and using different solvents with 20 vol.% DEGDMA. Irradiation dose = 10 kGy.

Addition of NDs also affected the light emission properties of the materials formed. Figure 17 compares the photoluminescence spectra of the ND/polymer composite samples. Characteristic peaks of ND can be seen in all of the spectra in the 350–450 nm region, except the sample prepared with water as the solvent, where only the characteristic broadband of DEGDMA was observed.

The results demonstrate the possibility of preparation of ND/polymer composites with the γ radiation initiated free radical polymerization technique. Particulate, porous and bulk materials can be obtained using this method. The ongoing work in this field is aimed at the preparation of core shell ND/polymer particles and further characterization of the composites obtained.

4. SUMMARY

A composite drug eluting coating has been developed that can be used in stents and other types of medical implants. The coating consists of an amorphous carbon interlayer, drug container DEGDMA particles and a HEMA based hydrogel matrix. The latter can be used to control the drug eluting characteristics of the coating. The steps of the preparation of the coating include: (i) cleaning of the substrate surface, (ii) deposition of the amorphous carbon layer on top of the surface, (iii) preparation of the DEGDMA particles using radiation induced

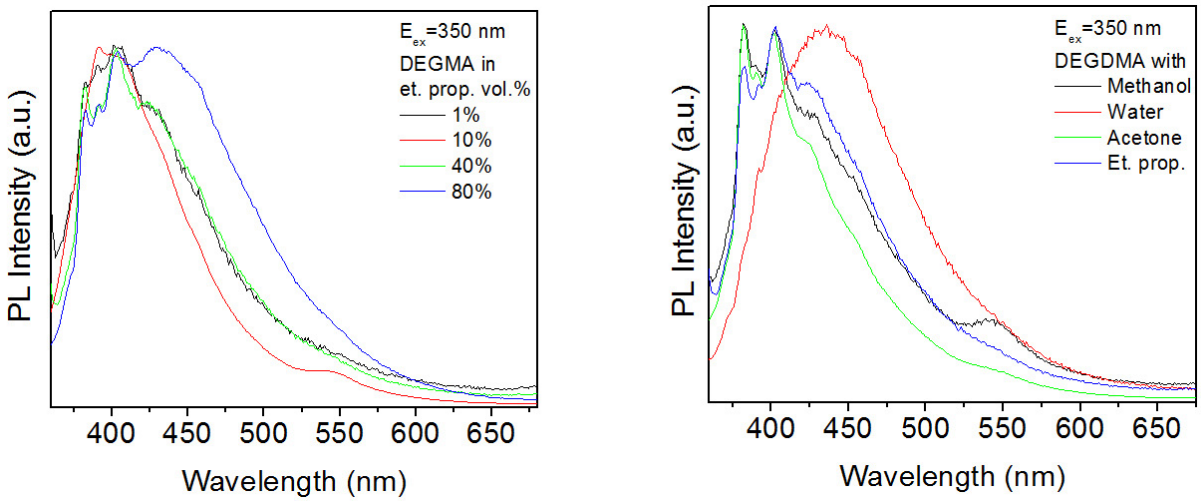

FIG. 17. Photoluminescence (PL) spectra of ND/polymer composites prepared from monomer mixtures of different DEGDMA contents in ethyl propionate (et. prop.) and using different solvents with 20 vol.% DEGDMA. Irradiation dose = 10 kGy.

polymerization, (iv) filling the particles with the drug (optional), (v) adding the particles to the monomer mixture of the hydrogel, (vi) coating the implant surface with the mixture and (vii) formation of the coating by radiation induced polymerization. The thickness of the amorphous carbon interlayer has been optimized to be 30 nm. It was found that by changing the composition of the monomer mixture, the size of the DEGDMA particles can be controlled in the 400–1300 nm region.

It has been demonstrated that γ radiation initiated polymerization can be used to prepare ND/polymer composites. By mixing and irradiating ND with DEGDMA monomer in different solvents, composites of different morphologies, including particulate, porous and bulk materials, were obtained. This method has great potential for surface functionalization of individual NDs that can be used for in vivo sensing of biological materials.

ACKNOWLEDGEMENTS

The authors of this report wish to thank Z. Papp for irradiation of the samples, and J. Dégi, L. Pogány and Á. Kukovecz for SEM measurements. Partial financial support from the IAEA is gratefully acknowledged.

REFERENCES

[1] BAIM, D.S., "Percutaneous coronary revascularization", Harrison's Principles of Internal Medicine, 16th edn (KASPER, D.L., et al., Eds), McGraw-Hill, New York (2004) 1459.
[2] SERRUYS, P.W., KUTRYK, M.J., ONG, A.T., Coronary-artery stents, New Engl. J. Med. **354** (2006) 483.
[3] VERES, M., et al., Raman analysis of diamond-like carbon films deposited onto corrosion resistant alloys used for coronary stent fabrication, Mater. Sci. Forum **277** (2007) 537–538.
[4] TÓTH, S., VERES, M., DOBRÁNSZKY, J., MAJOR, L., KOÓS, M., "Carbon-based coatings for cardiovascular stents", Proc. 5th Int. Conf. Inorganic Materials, Ljubljana, Slovenia, 23–26 September 2006, Elsevier (2006).
[5] SICK, P.B., et al., Prospective randomized comparison of early and late results of a carbonized stent versus a high-grade stainless steel stent of identical design: The PREVENT trial, Am. Heart J. **149** (2005) 681.
[6] HOLT, A.P., PATEL, M., AHMED, M.M., Palliation of patients with malignant gastroduodenal obstruction with self-expanding metallic stents: The treatment of choice? Gastrointest. Endosc. **60** (2004) 1010.
[7] BERTRAND, O.F., et al., Biocompatibility aspects of new stent technology, J. Am. Coll. Cardiol. **32** (1998) 562.
[8] SAFRANY, A., BEILER, B., LASZLO, K., SVEC, F., Control of pore formation in macroporous polymers synthesized by single-step γ-radiation-initiated polymerization and cross-linking, Polym. **46** (2005) 2862.
[9] BEILER, B., SAFRANY, A., Polymer monoliths synthesized by radiation co-polymerization in solution, Radiat. Phys. Chem. **76** (2007) 1351.

[10] BEILER, B., VINCZE, A., SVEC, F., SAFRANY, A., Poly(2-hydroxyethyl acrylate-co-ethylene dimethacrylate) monoliths synthesized by radiation polymerization in a mold, Polym. **48** (2007) 3033.
[11] WATKINS, A.W., SOUTHARD, S.L., ANSETH, K.S., Characterizing multilaminated hydrogels with spatially varying network structure and solute loading using confocal laser scanning microscopy, Acta Biomater. **3** (2007) 439.
[12] LI, L., LEE, L.J., Photopolymerization of HEMA/DEGDMA hydrogels in solution, Polym. **46** (2005) 11 540.
[13] VERES, M., TÓTH, S., KOÓS, M., New aspects of Raman scattering in carbon-based amorphous materials, Diam. Relat. Mater. **17** (2008) 1692.

γ RADIATION MEDIATED SYNTHESIS OF ANISOTROPIC MNPs FOR POTENTIAL BIOMEDICAL APPLICATIONS

S. FRANCIS, J. BISWAS, L. VARSHNEY, S. SABHARWAL
Radiation Technology Development Division
Bhabha Atomic Research Centre
Mumbai, India

Abstract

γ irradiation strategies were developed for the synthesis of gold nanoparticles of different morphologies such nanoplates, nanorods and particles with rectangular, plate like structure. The different shapes could be realized by employing a specific capping agent such as CTAB and then controlling the irradiation conditions. The nanoplates produced had hexagonal and triangular shapes, and their size could be varied from 500 nm to 5 μm by adjusting the concentration of Au^{3+} and capping agent in the solution. Gold nanorods were synthesized by both seed mediated as well as seedless procedures using CTAB. Gold nanoparticles with rectangular, plate like structure could also be produced by a variation of the procedure used for synthesizing nanorods. Gold nanorods and small nanoplates have been used for medical imaging and for therapeutic applications. Various techniques such as TEM, SEM, XRD, selected area electron diffraction, energy dispersive X ray analysis and XPS were used to characterize these nanoparticles.

1. INTRODUCTION

In recent years, there has been much interest generated by shape controlled synthesis of MNPs, because of its fundamental importance, the challenges involved and, most importantly, because of the shape dependent properties. The synthesis of various anisotropic nanostructures such as nanostars, nanobelts, nanorods, nanocubes and multipods, and their potential applications have been reported in the literature [1, 2]. The most widely used synthetic strategy for noble metal NPs is the wet chemical method wherein a reducing agent reduces the metal precursor salts in the presence of a stabilizer. NPs of desired shape, size and distribution are synthesized by tuning the experimental parameters such as concentrations of reactants, temperature, pH, seed concentration, etc.

The synthesis of NPs by γ irradiation is a simple, green process because external reducing agents are not required; instead the reduction is brought about by the transient species, e^-_{aq} and $H^\bullet$, generated from the radiolysis of water. The reduction rate of metal ions in solution is known to affect the size and morphology of the NPs produced, and, in the case of γ irradiation, this can be easily controlled by proper selection of the dose rate employed for reduction. Because of these advantages, γ radiation has been utilized for the synthesis of different types of NPs employing a variety of capping agents [3–5]; however, most of the time, the NPs produced were spherical or irregular in shape. In recent years, owing to the increasing significance and applications of anisotropic NPs, the γ irradiation method has been explored as an alternative strategy for the synthesis of shape controlled NPs, but the number of studies reported is limited compared to other established methodologies.

2. INSTRUMENTATION

UV/VIS spectra of the solution were recorded using an Evolution 300 (Thermo) spectrophotometer. TEM imaging was carried out using a Libra 120 (Zeiss) electron microscope at an accelerating voltage of 120 keV, and the selected area electron diffraction pattern was recorded using a 200 FX (JEOL) electron microscope. SEM images were recorded using an AIS2100 (Seron Technologies) scanning electron microscope operating at an accelerating voltage of 20 keV, and energy dispersive X ray analysis (EDAX) was performed with an INCA E350 (Oxford Instruments) analyser coupled to the scanning electron microscope. X ray powder diffraction studies were carried out with a PW 1729 (Philips) X ray diffractometer using Cu Kα radiation and XPS investigations were carried out with a Clam 2 (VG) spectrometer, using Mg Kα radiation.

3. RESULTS AND DISCUSSION

3.1. Size tuneable synthesis of gold nanoplates by γ irradiation

A simple γ irradiation strategy was developed for the synthesis of gold nanoplates by employing a polyelectrolyte as a capping agent. The nanoplates had hexagonal, triangular and truncated triangular shapes, and the sizes of the nanoplates could be controlled from 500 nm to 5 μm by adjusting the conditions of the experiment. The optical properties of the nanoplates were studied using UV/VIS spectroscopy (Fig. 1). The XRD pattern (Fig. 2) revealed that the nanoplates were single crystals bound by the {111} planes on the top and bottom surfaces. The dose rate of γ radiation was found to profoundly affect the morphology of the gold NPs.

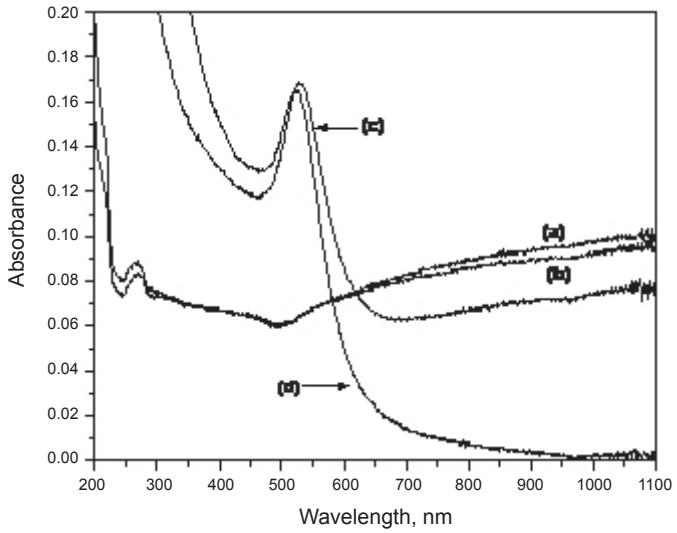

FIG. 1. UV/VIS spectra of the gold NPs synthesized at different concentrations of Au^{3+} and polyelectrolyte.

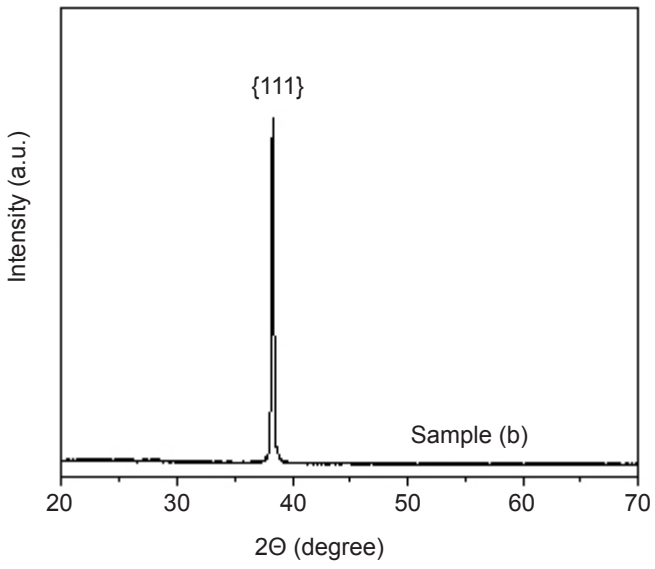

FIG. 2. XRD pattern of gold nanoplates.

3.2. Seed mediated synthesis of gold nanorods using γ radiation in the presence of CTAB as a directing agent

The chemical method for synthesis of gold nanorods involves the reduction of Au^{3+} by a weak reducing agent such as ascorbic acid in the presence of Au seeds and a shape directing surfactant such as CTAB [6]. A small amount of Ag^{+} is also used to control the anisotropy of the NPs. In the present method, reducing species were generated in situ by γ radiolysis and used for the reduction of Au^{+} to metallic Au in an aqueous medium. In a typical synthetic procedure, an aqueous solution containing 400×10^{-6} mol/L of Au^{3+}, 0.2 mol/L of isopropanol, 6×10^{-5} mol/L of $AgNO_3$, 0.1 mol/L of CTAB and 1.2×10^{-6} mol/L of seed solution was irradiated with γ rays at a dose rate of 3.4 kGy/h. Under these conditions, most of the energy was absorbed by water, resulting in the formation of highly reactive species such as e^{-}_{aq}, $H^{\bullet}$ and $OH^{\bullet}$. Among these, e^{-}_{aq} and $H^{\bullet}$ are highly reducing in nature and these radicals bring about the reduction of Au^{+} to Au^{0}. In the presence of isopropyl alcohol, the OH radical is scavenged to the isopropyl radical. The isopropyl radical thus generated is reducing in nature and is capable of reducing Au^{+} to Au^{0}. The Au atoms thus generated upon radiolysis undergo coalescence, resulting in the formation of Au NPs stabilized by CTAB. The absorption spectra of irradiated solutions at various times of irradiation are shown in Fig. 3. As can be seen from Fig. 3, only a single peak at 527 nm is observed; this is a characteristic SPR band of Au spheres.

To investigate the effect of radiation dose rate on the formation of NPs, the solution was irradiated at a dose rate of 1.7 kGy/h. At lower absorption doses, two absorption maxima at 523 nm and 610 nm were observed (Fig. 4), which disappeared with further increases in radiation dose; finally, only a single maximum at 528 nm was observed, indicating the formation of Au spheres.

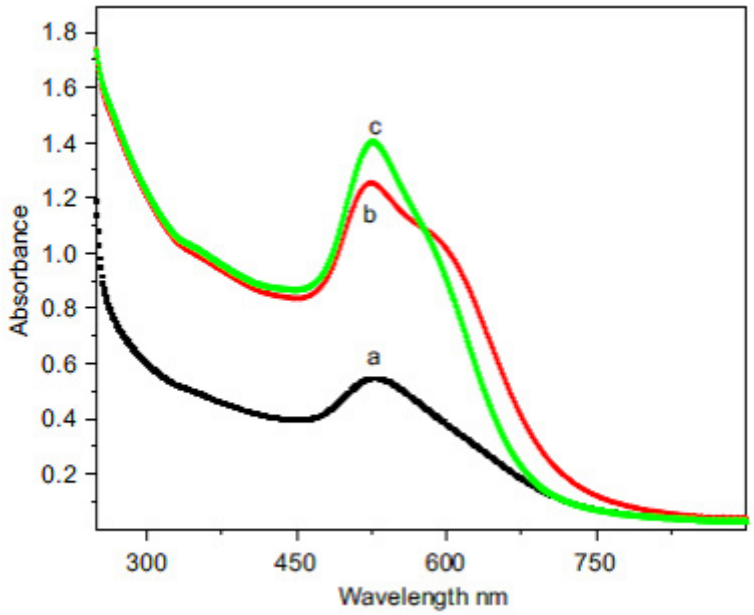

FIG. 3. Absorption spectra of irradiated solution containing 400×10^{-6} mol/L of Au^{+}, 0.2 mol/L of isopropanol, 8×10^{-5} mol/L of $AgNO_3$, 0.1 mol/L of CTAB and 1.2×10^{-6} mol/L of seed at various absorbed doses: (a) 0.85 kGy, (b) 1.7 kGy and (c) 2.6 kGy. Dose rate = 3.4 kGy/h.

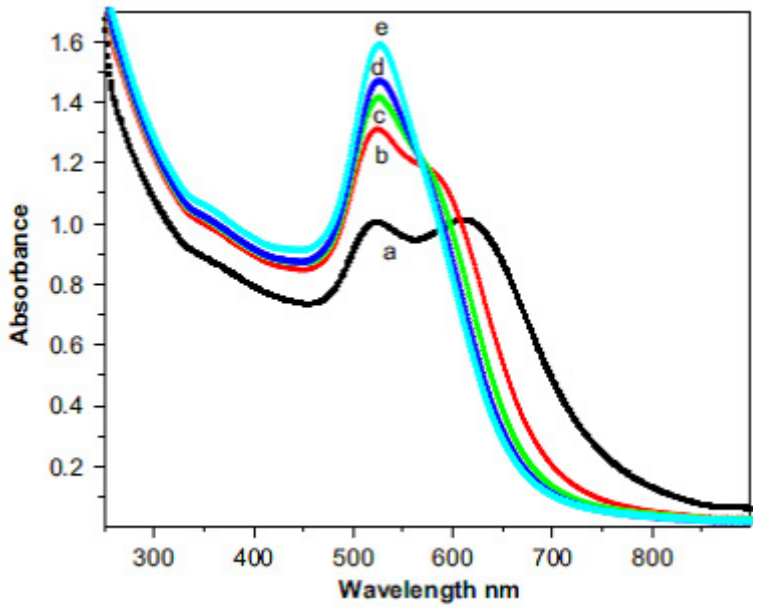

FIG. 4. Absorption spectra of irradiated solution containing 400 × 10^{-6} mol/L of Au^{+}, 0.2 mol/L of isopropanol, 8 × 10^{-5} mol/L of $AgNO_3$, 0.1 mol/L of CTAB and 1.2 × 10^{-6} mol/L of seed at various absorbed doses: (a) 0.85 kGy, (b) 1.7 kGy, (c) 2.6 kGy, (d) 3.5 kGy and (e) 4.5 kGy. Dose rate = 1.7 kGy/h.

When the above solution was irradiated to various absorbed doses at a very low dose rate of 0.8 kGy/h, the absorption spectra showed two absorption maxima (Fig. 5), indicating the formation of Au nanorods. The first absorption maximum, centred at 513 nm, did not shift with increasing radiation dose; however, the second one red shifted from 643 nm to 670 nm with an increase in radiation dose, as shown in Fig. 5. This shift of absorption maxima by 27 nm with increasing radiation dose indicated the growth of nanorods. The formation of nanorods was confirmed from TEM results. The TEM image (Fig. 6) showed uniform sized nanorods without any spherical NPs. The aspect ratio of the nanorods was estimated to be 2.4. It may be mentioned that the concentration of Ag^{+} in the solution also plays an important role in the synthesis of Au nanorods. In the absence of Ag^{+}, nanorods were not formed, and the best reproducible results were obtained at an Ag^{+} concentration of 6 × 10^{-5} mol/L.

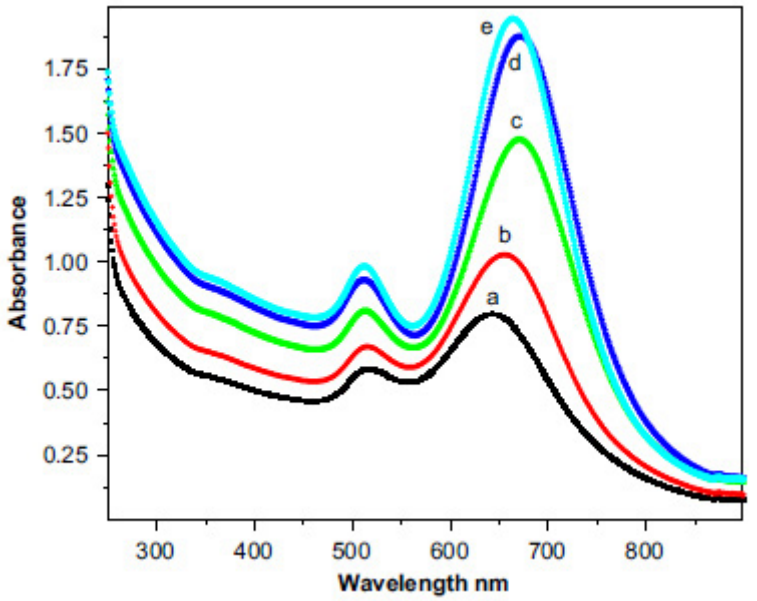

FIG. 5. Absorption spectra of irradiated solution containing 400 × 10^{-6} mol/L of Au^{+}, 0.2 mol/L of isopropanol, 8 × 10^{-5} mol/L of $AgNO_3$, 0.1 mol/L of CTAB and 1.2 × 10^{-6} mol/L of seed at various absorbed doses: (a) 0.85 kGy, (b) 1.7 kGy, (c) 2.6 kGy, (d) 3.5 kGy and (e) 4.5 kGy. Dose rate = 0.8 kGy/h.

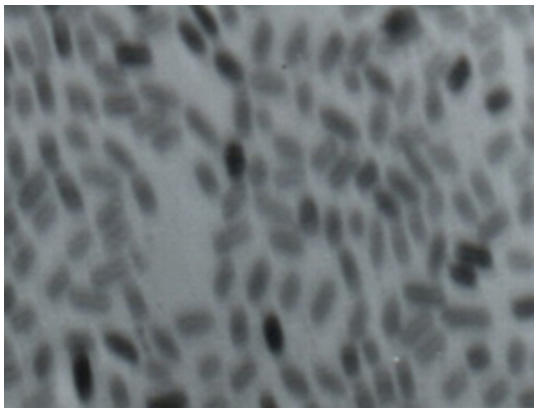

FIG. 6. TEM image of gold nanorods synthesized using the radiolytic method. Scale bar = 50 nm.

3.3. Seedless synthesis of gold nanorods employing isopropyl radicals generated using a γ radiolysis technique

In this method, seeds were avoided, and the solution containing 400×10^{-6} mol/L of Au^{+}, 2.75×10^{-2} mol/L of acetone, 0.2 mol/L of isopropanol, 6×10^{-5} mol/L of $AgNO_3$ and 0.1 mol/L of CTAB solution was irradiated with γ rays at a dose rate of 3.4 kGy/h [7]. Isopropanol and acetone were added to scavenge $H^{\bullet}$, $OH^{\bullet}$ and e^{-}_{aq}, and an isopropyl radical was generated in the solution. The isopropyl radical is a mild reducing agent that reduces Au^{+} to Au^{0} in a slow reaction. The slower reduction kinetics favour the formation of Au nanorods with an aspect ratio of 3. The UV/VIS spectra and TEM image of the nanorods are shown in Figs 7 and 8, respectively.

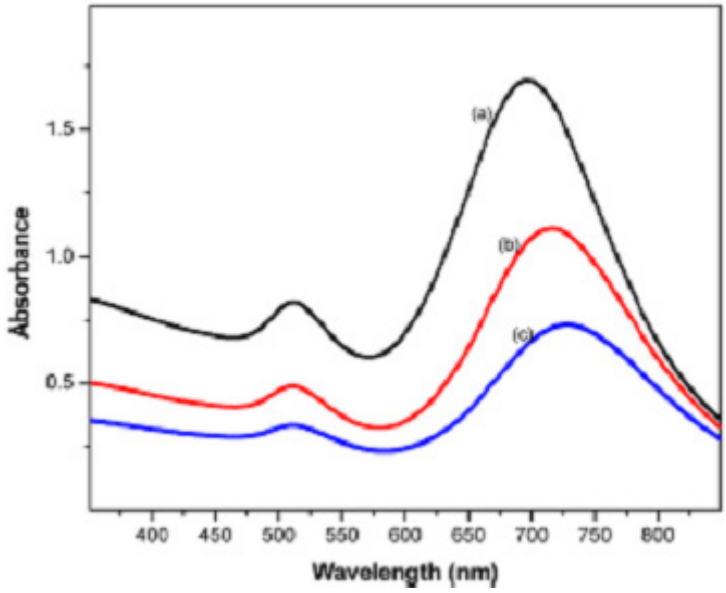

FIG. 7. Absorption spectra of irradiated solution containing 400×10^{-6} mol/L of Au^{+}, 2.75×10^{-2} mol/L of acetone, 0.2 mol/L of isopropanol, 8×10^{-5} mol/L of AgNO and 0.1 mol/L of CTAB at various absorbed doses: (a) 0.85 kGy,(b) 1.7 kGy and (c) 2.6 kGy. Dose rate = 0.8 kGy/h.

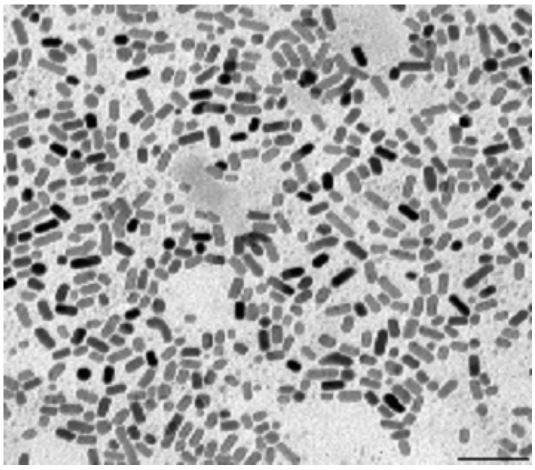

FIG. 8. TEM image of gold nanorods synthesized using the radiolytic method. Scale bar = 50 nm.

3.4. Synthesis of rectangular plate like gold NPs by a combination of radiation and chemical methods

In this method, ascorbic acid (7.2×10^{-4} mol/L) was used to reduce Au^{3+} to Au^{+} in a solution containing 400×10^{-6} mol/L of Au^{3+}, 0.2 mol/L of isopropanol, 6×10^{-5} mol/L of $AgNO_3$ and 0.1 mol/L of CTAB. Because ascorbic acid is a mild reducing agent, it cannot reduce Au^{+} to Au^{0} in the solution [8]. This solution was irradiated to a very low absorbed dose (at a dose rate of 3.4 kGy/h) for the generation of seeds. The reduction of Au^{+} to Au^{0} takes place by transient species generated from water radiolysis, and the size of the seed particle was controlled by the high concentration of the capping agent CTAB, which does not allow the seeds to grow beyond a particular size. The concentration of seeds in the system can be controlled and adjusted during irradiation. For subsequent growth of gold NPs, the irradiated solution was kept undisturbed for 2 h. In the presence of Au seed, Au^{+} gets adsorbed on the surface of the seeds and is reduced by ascorbic acid, which results in the formation of plate like gold NPs. A TEM image of the plate like gold NPs is shown in Fig. 9.

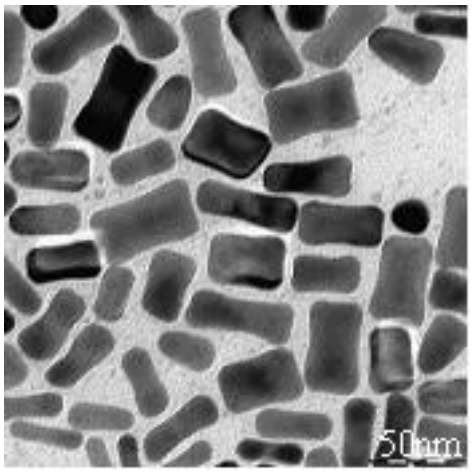

FIG. 9. TEM image of plate like gold NPs synthesized using γ irradiation. Scale bar = 50 nm.

4. SUMMARY

In summary, the efficient utilization of γ radiation for synthesis of anisotropic gold NPs has been demonstrated. In this method, γ radiation brings about the reduction of Au^{3+} through the mediation of transients species, obviating the need for any chemical reducing agent, while the shape directing agent decides the morphology of the NPs.

The size of the NPs could be controlled by varying the concentrations of the metal ions and the capping agent in the solution. In addition, the dose rate of γ irradiation exerts a strong influence on the final morphology of the gold NPs.

REFERENCES

[1] ANDREA, R.T., HABAS, S., YANG, P.D., Shape control of colloidal metal nanocrystals, Small **4** (2008) 310.

[2] MILLSTONE, J.E., HURST, S.J., METRAUX, G.S., CUTLER, J.I., MIRKIN, C.A., Colloidal gold and silver triangular nanoprisms, Small **5** (2009) 646.

[3] BELLONI, J., MOSTAFAVI, M., REMITA, H., MARIGNIER, J.L., DELCOURT, M.O., Radiation-induced synthesis of mono- and multi-metallic clusters and nanocolloids, New J. Chem. **22** (1998) 1239.

[4] BELLONI, J., Nucleation, growth and properties of nanoclusters studied by radiation chemistry: application to catalysis, Catal. Today **113** (2006) 141.

[5] HENGLEIN, A., Physicochemical properties of small metal particles in solution microelectrode reactions, chemisorption, composite metal particles, and the atom-to-metal transition, J. Phys. Chem. **97** (1993) 5457.

[6] BISWAL, J., RAMNANI, S.P., TEWARI, R., DEY, G.K., SABHARWAL, S., Short aspect ratio gold nanorods prepared using gamma radiation in the presence of cetyltrimethyl ammonium bromide (CTAB) as a directing agent, Radiat. Phys. Chem. **28** (2010) 441.

[7] BISWAL, J., RAMNANI, S.P., SHIROLIKAR, S., SABHARWAL, S., Seedless synthesis of gold nanorods employing isopropyl radical generated using gamma radiolysis technique, Int. J. Nanotechnol. **7** (2010) 907.

[8] BISWAL, J., RAMNANI, S.P., SHIROLIKAR, S., SABHARWAL, S., Synthesis of rectangular plate like gold NPs by in situ generation of seeds by combining both radiation and chemical methods, Radiat. Phys. Chem. **80** (2011) 44.

PLA NANOCOMPOSITES WITH POTENTIAL BIOMEDICAL APPLICATIONS USING γ IRRADIATION

S. DADBIN, F. NAIMIAN, V. AHMADIAN
Atomic Energy Organization of Islamic Republic of Iran
Nuclear Science and Technology Research Institute
P.O. Box 14155-1339, Tehran, North Kargar
Islamic Republic of Iran

Abstract

PLA/HAP and (PLA/organically modified nanoclay) nanocomposite films at various compositions were produced via a solution casting method. The films were irradiated with γ rays at doses of 30 kGy and 50 kGy. FTIR spectra of the nanocomposites displayed some structural changes upon irradiation, mostly because of changes that occurred in the PLA phase. The tensile strength of the nanocomposites decreased compared to that of the pure PLA, but it remained at an acceptable level. Significant ductile behaviour was observed in PLA/HAP and PLA/organoclay nanocomposites at low contents of nanofillers. Incorporation of NPs in the PLA matrix stimulated crystal growth, as deduced from DSC results. Subjecting the films to γ rays at doses of 30 kGy increased the tensile strength of the PLA/HAP nanocomposite films containing 6 pph and 10 pph HAP. This was also attributed to radiation induced crystallinity verified by DSC thermograms. Introducing a multifunctional monomer into the nanocomposites improved the tensile strength by addition of cross-links in the irradiated PLA. The morphology of the nanocomposites, characterized by TEM and XRD, revealed an exfoliated morphology in the PLA/organoclay nanocomposite films containing 4 pph of nanoclay. TEM images of PLA/HAP films displayed spherical particles in the size range of ten up to a few tens of nanometres dispersed as single or agglomerated particles within the polymeric matrix. No obvious changes in size and dispersion of HAP particles were observed in the TEM images of irradiated samples at doses of 30 kGy. The XRD patterns of irradiated PLA showed a diminishing crystalline peak at 29.6° and generation of new peaks at around 16° and 19°, which were assigned to the α crystalline form of PLA. The enzymatic degradation of PLA was accelerated in the presence of HAP particles in the PLA/HAP nanocomposites. The PLA/organoclay films with exfoliated morphology also showed higher rates of degradation.

1. INTRODUCTION

PLA is a linear aliphatic thermoplastic polyester produced either by the polycondensation of lactic acid or by ring opening polymerization of lactide cyclic dimer [1]. Lactic acid is synthesized from the fermentation of renewable sources such as corn, sugar beet and other products that are rich in starch [2–4]. Direct condensation of lactic acid leads to low MW polymers. Therefore the ring opening polymerization of lactide is more popular for producing PLA with a higher MW. The stereochemical structure of the lactide monomer (L lactide, D lactide and mesolactide) determines the stereochemical composition of the resulting polymer. Thus, PLA with different properties and degrees of crystallinity can be tailored by changing the proportions of L to D lactide and the MW of the polymer [5].

Biodegradability and bioresorbability of this plant based polymer has drawn much attention in recent years. Good mechanical properties, along with its biocompatibility, make it suitable for biomedical applications [6], such as prosthetic implants [7], three dimensional scaffolds [8], controlled release drugs [9] and resorbable sutures. PLA is a preferred choice for biomedical applications, particularly bone fracture fixation devices. In spite of the many good properties of PLA, the existence of a few weaknesses in some aspects such as thermal stability, barrier properties and toughness has led to interest in its modification. The performance of PLA can be enhanced by the incorporation of nanosized particles such as nanoclay and nanoHAP. HAP is the most biocompatible synthetic substance for use in hard tissue repair [10, 11]. Synthetic HAP not only contributes to bone bonding, but also helps with early bone formation on the implant surface [12]. Modification of the HAP phase by bioresorptive poly L lactic acid (PLLA) polymer leads to the formation of a bioresorptive composite in which the ceramic phase remains unchanged after application, while the biodegradable polymer resorbs with time, making space for new tissue generation [13].

NanoHAP/PLLA scaffolds were developed for bone tissue engineering using thermally induced phase separation techniques. The incorporation of nanoHAP improved the mechanical properties and protein adsorption of the composite scaffolds [14]. γ irradiation processing of HAP/poly L lactide composite biomaterial has been reported by Suljovrujic et al. [15]. Physiochemical changes occurred in the PLLA phase during irradiation of HAP/PLLA composites, while the HAP phase remained stable. The results obtained from wide angle X ray scattering and DSC tests showed that an irradiation dose of 0–50 kGy improved the crystallinity of the PLLA [15]. The dominant effect of ionizing radiation on the properties of PLLA is chain scission [16–18], but for doses required for sterilization, changes and damaging effects are acceptable. Improvement of heat stability of PLLA by radiation induced cross-linking has been reported previously [19]. The main objective of this CRP work is the development of PLA nanocomposites for potential biomedical applications using γ irradiation. PLA nanocomposites containing organically modified layered silicate (Nanolin) and HAP NPs with a variety of compositions, including a lower content of HAP, have been made using a solution casting method. The effects of a γ irradiation dose of 30 kGy on the chemical structure, crystalline phase, thermal behaviour, morphology and enzymatic degradation of PLA nanocomposites have been discussed in detail. The effects of TAIC and triallyl cyanurate as multifunctional monomers on mechanical properties of the nanocomposites have also been investigated. The results obtained from research work on PLA/organoclay nanocomposite have been reported previously [17–19], and investigation of PLA/HAP nanocomposites is the objective of this report.

2. EXPERIMENTAL DETAILS

2.1. Materials

High MW PLA granules were used. Nanosized organoclay with the trade name Nanolin DK4 (alkyl ammonium modified montmorillonite), with particle sizes in the range 1–100 nm, was purchased from Zhejiang Clay Chemicals (China).

HAP nanopowder with particle sizes less than 200 nm, TAIC and triallyl cyanurate were provided by Sigma-Aldrich. Proteinase K (from tritirachium album), Tris HCl and sodium azide were supplied by Merck.

2.2. Preparation of PLA/HAP nanocomposite films

Neat PLA films and films containing TAIC or triallyl cyanurate were fabricated using the solution casting method [17–19]. PLA nanocomposite films were made using the following procedure: a solution of PLA in chloroform was ultrasonically mixed with the required amounts of HAP or Nanolin nanopowder already dispersed in $CHCl_3$ solvent to make nanocomposites with different compositions, and then the films were made on a level surface inside the glass moulds by vaporizing the solvent.

2.3. Irradiation of films

The pristine PLA and nanocomposite films were irradiated with γ rays at doses of 30 kGy and 50 kGy in the presence of air. Irradiation was carried out at room temperature and a dose rate of 4.6 Gy/s using a ^{60}Co irradiator Gamma cell model 220 (Canada). The PLA/HAP nanocomposites were designated as NHx-y where x was the HAP content and y was the irradiation dose. For example, NH10-0 indicates the nanocomposite containing 10 pph of HAP before irradiation and NH10-30 denotes the same nanocomposite exposed to a radiation dose of 30 kGy.

2.4. Characterization of PLA films

2.4.1. Gel permeation chromatography

The MW of PLA granules was measured by gel permeation chromatography (GPC) on an Agilent 1100 gas permeation chromatographer at a temperature of 30°C and using chloroform as the solvent. The detector was a refractive index detector. The number averaged and weight averaged molar masses of the PLA obtained by GPC were 100 790 g/mol and 237 560 g/mol, respectively.

2.4.2. FTIR spectroscopy

Infrared spectra of the neat PLA films before and after irradiation were obtained using an IFS 45 FTIR (Bruker).

2.4.3. DSC

The thermal behaviour of the samples was investigated via DSC using a DSC-50 (Shimadzu, Japan) instrument. The tests were performed under nitrogen atmosphere between 20°C and 250°C at a heating rate of 10°C/min.

2.4.4. Mechanical properties

The mechanical properties of PLA and PLA nanocomposite films were characterized with a tensile testing machine (Zwick). The films were cut into strips with dimensions of 10 cm in length × 2 cm in width and stretched with a gauge length of 4 cm and a speed of 1 mm/min.

2.4.5. XRD

The crystalline structure of the PLA/organoclay and PLA/HAP nanocomposite films were evaluated by XRD measurements. XRD patterns were taken using an X ray diffractometer (Philips Analytical), operated at 30 kV and 20 mA, equipped with a Cu tube anode at an irradiation wavelength of 1.54056 Å. The X ray diffractograms were collected in the angle range, 2θ, of 5°–50° in a continuous scanning mode.

2.4.6. TEM

TEM was used to characterize the morphology of the PLA nanocomposite films. The TEM was performed on an EM 208 scanning electron microscope (Philips) operating at an acceleration voltage of 100 kV.

2.4.7. Enzymatic degradation

Weight loss studies of the PLA nanocomposites and neat PLA films were carried out utilizing enzymatic degradation tests. Enzymatic degradation of the nanocomposite films was performed in the presence of proteinase K in an incubator at a temperature of 37°C [19, 20]. The samples with specified dimensions were placed in vials containing 5 mL of TRIS HCl buffer (pH8.6), 1 mg of proteinase K and 1 mg of sodium azide. Then, the samples were removed after the specified incubation times, washed thoroughly and dried in a vacuum oven for 48 h. The dried samples were weighed to evaluate the weight loss values.

3. RESULTS AND DISCUSSIONS

3.1. Chemical structure

The chemical structure of the PLA/HAP nanocomposites was characterized using FTIR spectroscopy. Figure 1 displays the FTIR spectra of a PLA/HAP nanocomposite containing 10 pph of HAP. Only a small change was observed in the chemical structure of the non-irradiated nanocomposite films. The carbonyl peak at 1757 cm^{-1} in the FTIR spectra of the neat PLA [19] was shifted to a lower frequency and becomes broader, which may indicate the interaction of the carbonyl group in PLA with the OH groups in HAP. Subjecting the nanocomposite to γ irradiation led to an increase in the intensity of the peak assigned to the crystalline phase of PLA at 756 cm^{-1} [21] as compared to the peak attributed to the amorphous phase at 868 cm^{-1}.

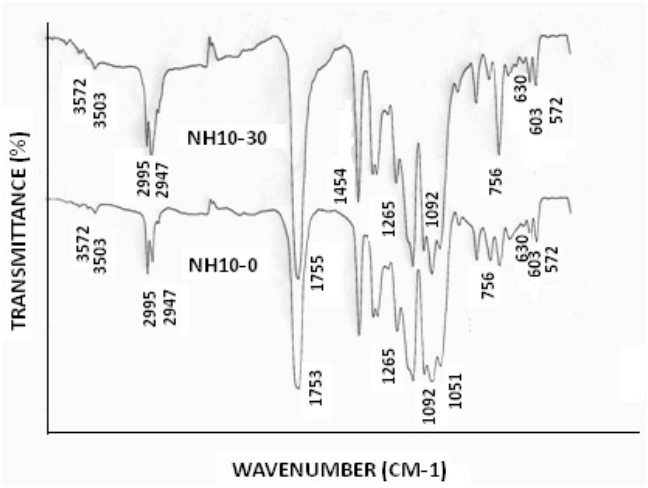

FIG. 1. FTIR spectra of PLA/HAP nanocomposite containing 10 pph of HAP at 0 kGy (NH10-0) and 30 kGy (NH10-30).

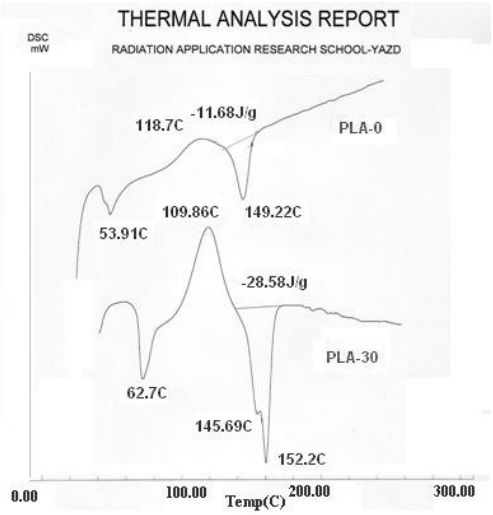

FIG. 2. Comparison of DSC thermograms of neat non-irradiated (PLA-0) and irradiated (PLA-30) PLA films.

3.2. Crystallinity

3.2.1. DSC

The crystallinities of the pure and PLA nanocomposites were investigated using DSC. A thermogram of the neat PLA film shows two endothermic peaks at 54°C and 149°C, corresponding to the glass transition and melting temperature, respectively (Fig. 2). In addition, a broad exothermic peak related to cold crystallization is observed at 118.7°C. Irradiation of the neat PLA film at a dose of 30 kGy leads to a melting peak split that is indicative of growth of different types of crystallites and/or formation of crystallites with different lamella thickness during irradiation. Furthermore, the crystallization peak becomes sharp, and the maximum crystallization temperature shifts to a lower temperature, indicating a higher crystallization rate [22] in the irradiated neat PLA film.

Figure 3 shows the DSC thermograms of the PLA/HAP samples with various compositions before irradiation. As can be seen, there is no significant change in the melting point of the non-irradiated nanocomposites, but the enthalpy of melting increases by introducing HAP NPs (compared to neat PLA), suggesting the nucleating role of HAP particles during the cold crystallization process. The enthalpy of melting (ΔH_m) and enthalpy of crystallization (ΔH_c) increase with increasing HAP content, up to 6 pph, and then they decrease with further addition of HAP particles, probably because of agglomeration and formation of larger particles that prevent crystal growth. In

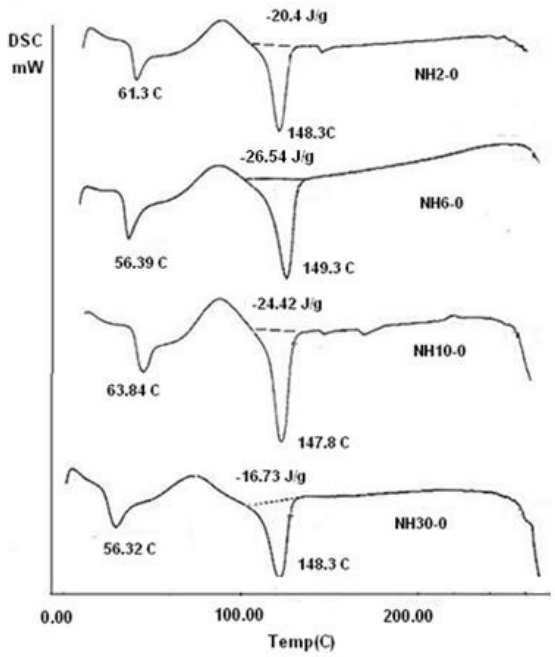

FIG. 3. DSC thermograms of non-irradiated PLA/HAP nanocomposites with various compositions.

the irradiated samples, the role of irradiation should also be taken into account. Figure 4 shows typical DSC thermograms that compare the thermal behaviour of unexposed and γ ray treated PLA nanocomposites containing 10 pph of HAP. All of the irradiated samples show a sharper cold crystallization peak at a lower temperature, indicating a higher rate of crystallization in the irradiated samples. The original degree of crystallinity X_c (Table 1) is obtained by DSC analysis using the following equation:

$$X_c(\%) = (\Delta H_m - \Delta H_c / \Delta H_f) \times 100 \quad (1)$$

where ΔH_m and ΔH_c are the enthalpies of melting and crystallization, respectively, and ΔH_f is the heat of fusion of totally crystallized PLA (93.7 J/g) [11].

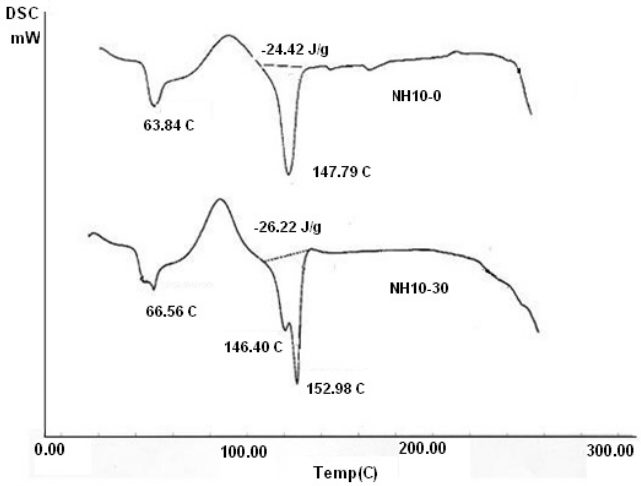

FIG. 4. DSC thermograms of the unexposed (NH10-0) and irradiated (NH10-30) PLA/HAP nanocomposites (10 pph).

TABLE 1. DATA OBTAINED FROM DSC THERMOGRAMS FOR PLA/HAP NANOCOMPOSITES AT 0 kGy AND 30 kGy

Sample code	X_c (%) 0 kGy	T_c (°C) 0 kGy[a]	X_c (%) 0 kGy	T_c (°C) 0 kGy[a]
PLA	4.28	118.71	1.37	109.86
NH2	6.27	113.41	7.8	104.97
NH6	14.32	106.05	11.98	106.05
NH10	8.40	109.91	13.05	107.33
NH30	4.7	100.59	13.57	104.38

[a] T_c = Crystallization temperature.

3.2.2. XRD

XRD patterns of HAP, neat PLA and the PLA/HAP nanocomposite at 30 pph of HAP before and after radiation treatment are displayed in Figs 5–7. The XRD pattern of HAP displays several peaks, with the most intense ones being in the ranges 30°–35° and 46°–50° (Fig. 5). XRD patterns of PLA (Fig. 6) demonstrate a broad peak assigned to the amorphous phase around 16.7° and several diffraction peaks located at 29.6°, 36.22°, 39.66° and 43.36°. As reported in the literature, PLA displays three main crystal polymorphs named α, β and γ [23, 24], depending on the preparation conditions. Moreover, a disordered modification of the α form has been proposed and named ά [25]. The wide angle XRD patterns of PLLA show two strong reflections at 16.7° and 19.2°, corresponding to 110/200 and 203 planes of the α crystal [23]. These two reflections are absent in the patterns of non-irradiated pure PLA (Fig. 6), which may be attributed to its low crystalline content, as verified by data obtained from DSC analysis (Table 1). Upon irradiation of the neat PLA, the intensity of the diffraction peak at 29.6° declines and shifts slightly to lower degrees. In addition, the broad peak around 16° starts splitting into two peaks, implying formation of new types of crystalline structures (Fig. 6).

Increasing the HAP content in the PLA/HAP nanocomposites causes the reflections from the crystalline planes of HAP to become more obvious, while the intensities of the diffraction peaks in the PLA decrease (Fig. 7).

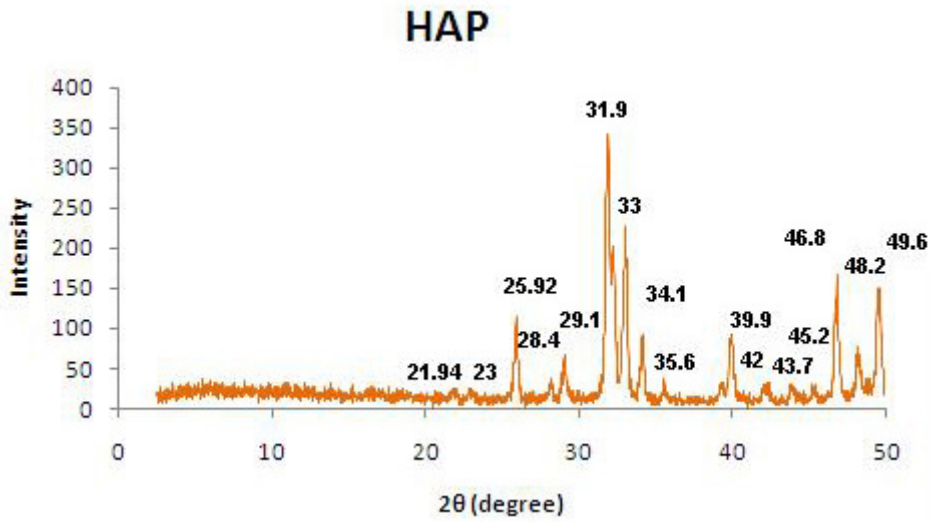

FIG. 5. XRD pattern of HAP NPs.

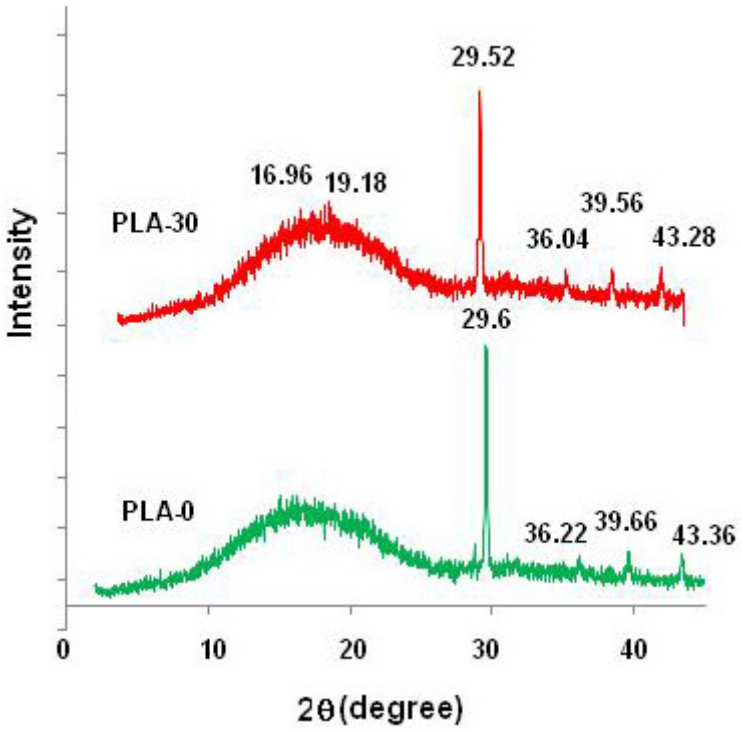

FIG. 6. XRD patterns of neat PLA before (PLA-0) and after (PLA-30) irradiation at a dose of 30 kGy.

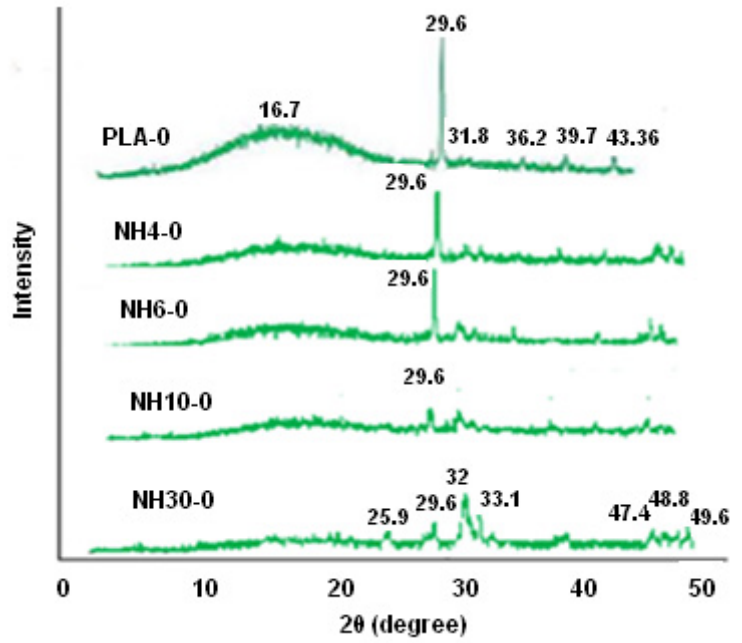

FIG. 7. XRD patterns of PLA/HAP nanocomposites at various compositions.

Subjecting the PLA/HAP nanocomposite films to irradiation promotes formation of α crystals, as the sharp reflection peaks at 16.7° and 19.2° corresponding to reflections of 200 and 203 planes of the α crystalline phase of PLA can be clearly seen in the XRD patterns of the nanocomposites containing 30 pph of HAP (Fig. 8). Analysis of diffraction data of the NH30-30 nanocomposite by PC-APD diffraction software shows characteristic peaks of poly (D lactide) and HAP powder. Formation of α type crystals with an orthorombic unit cell (a = 1.06 nm, b = 0.610 nm and c = 0.288 nm) was also suggested by this analysis. Generation of the α crystal form is in agreement

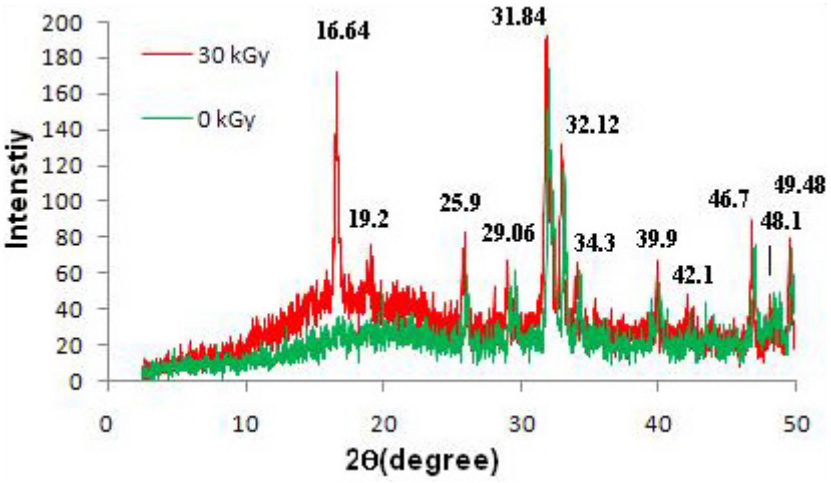

FIG. 8. XRD patterns of PLA/HAP nanocomposites at 30 pph of HAP irradiated at a dose of 30 kGy.

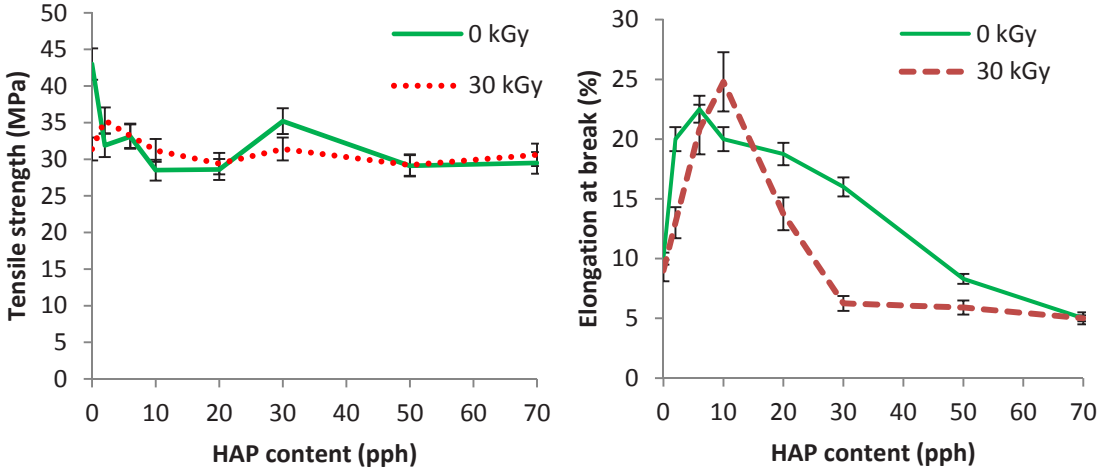

FIG. 9. Variation of tensile strength and elongation at break of the PLA/HAP nanocomposites with HAP content (before and after irradiation).

with data obtained from DSC thermograms, which show an increase in the degree of crystallinity of most of the nanocomposites upon exposure to γ irradiation (Table 1).

3.3. Mechanical properties

In spite of the increase of crystallinity in the PLA/HAP nanocomposites compared to pure PLA, the tensile strength decreased, regardless of the HAP content, but the elongation at break improved to as much as double that of pure PLA, particularly in samples containing 2–10 pph of HAP (Fig. 9).The nanocomposites containing 20 pph and 30 pph HAP still have higher elongation at break values compared to those of neat PLA. Further addition of HAP up to 70 pph decreased the elongation at break values significantly, possibly owing to inhomogeneous distribution of NPs and/or their agglomeration at high concentrations of the dispersed phase.

The neat PLA film exposed to γ radiation at a dose of 30 kGy faced some reduction in tensile strength, while the nanocomposites showed improvements upon subjecting them to high energy radiation. This enhancement in tensile strength was accompanied by significant flexibility improvements in samples with 10 pph of HAP content, which is an indication of the positive role of γ irradiation on the interaction of the polymeric matrix and the dispersed phase, possibly between a carbonyl group in the PLA component with an active group in HAP. Radiation induced changes in the contact surface between PLA and HAP particles have been also mentioned by other researchers [16].

At higher HAP contents up to 70 pph, inhomogeneous structures of these nanocomposites led to significant drops in flexibility.

Figure 10 displays the gel content of the nanocomposites treated with 30 kGy γ rays at different HAP contents and the 1 pph TAIC level. The low gel percentages in these samples should be attributed to HAP particles that inhibit cross-linking reactions in PLA. The amount of gel formation further decreases with increasing TAIC values up to 2 pph.

The tensile strength of the 10 pph and 30 pph samples improved upon addition of 1 pph TAIC as a result of the formation of a three dimensional network, even at low gel contents. Increasing the TAIC values from 1 pph to 2 pph at a dose of 30 kGy had no pronounced effect on the tensile strength of the 10 pph sample, while a significant reduction in the tensile strength of the 30 pph nanocomposite was observed (Fig. 11). The elongation at break of these samples declined with further addition of the multifunctional monomer.

In general, the PLA/HAP nanocomposites containing 1 pph of TAIC exposed to 30 kGy γ rays presented higher tensile properties compared to those of samples with 2 pph TAIC content. Irradiation of nanocomposite films at a dose of 50 kGy led to lower mechanical properties, in which the samples with 2 pph TAIC content had the lowest elongation at break and tensile strength. This indicates that the optimum TAIC value and irradiation dose for this nanocomposite system are 1 pph and 30 kGy, respectively. Raising the irradiation dose from 30 kGy to 50 kGy promotes chain scission reactions, which results in lower tensile properties.

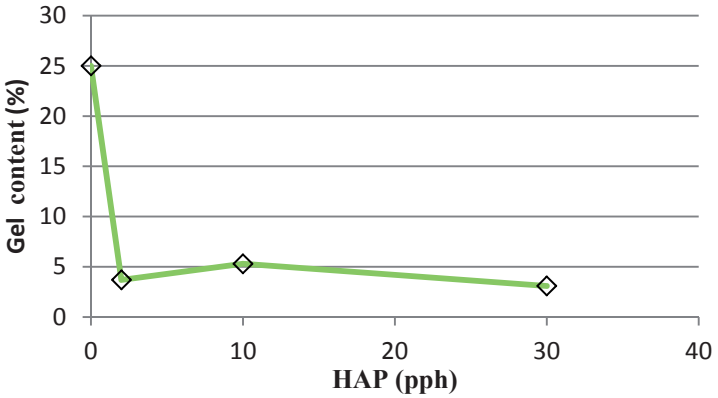

FIG. 10. Gel content of PLA/HAP nanocomposites containing 1 pph of TAIC versus HAP content.

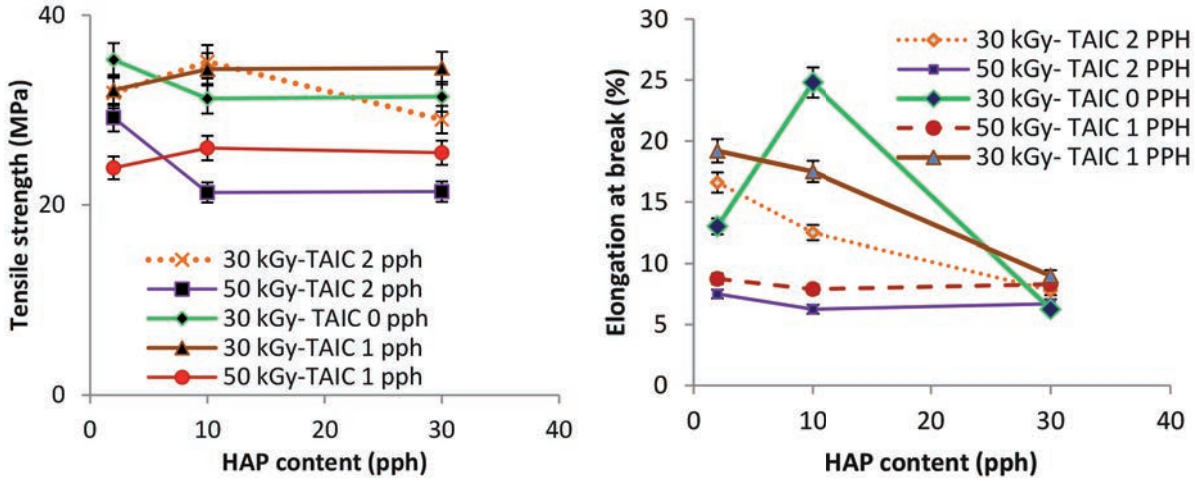

FIG. 11. Tensile strength and elongation at break of the PLA/HAP nanocomposites versus HAP content at different TAIC values and irradiation doses.

3.4. Morphology

The morphology of the nanocomposites observed by a transmission electron microscope displays spherical particles in the size range of ten to a few tens of nanometres dispersed as single or agglomerated particles within the polymeric matrix. Figure 12 depicts the PLA/HAP nanocomposite containing 10 pph of HAP before and after irradiation at a dose of 30 kGy. No remarkable influence on the size and shape of HAP particles is seen in the TEM images of the nanocomposites after irradiation at a dose of 30 kGy.

3.5. Enzymatic degradation

Figure 13 shows the weight loss of pure and PLA/HAP nanocomposite films containing 2 pph, 4 pph, 6 pph, 10 pph and 30 pph of HAP after exposure to proteinase K at different incubation times. The weight loss values versus time for 2 pph, 4 pph and 10 pph nanocomposites appear to be linear, while for the 30 pph sample, the slope of the line increases rapidly after a degradation time of 48 h. All nanocomposite films display a higher weight loss compared to the pure PLA film. The degradability also increases with inclusion of more HAP particles and longer incubation times. The imparting HAP particles provide interfacial areas between the particles and the polymeric matrix, which makes it easier for the enzymatic solution to diffuse from these areas, particularly when the interaction between the two phases is not as strong as would be expected. All the PLA/HAP nanocomposite films demonstrated higher crystallinities, as verified by the crystallinity percentages calculated by data obtained from DSC thermograms. In spite of the higher crystallinities of these samples, which should slow enzyme diffusion into the polymeric matrix and make the degradation rate slower, all of the samples showed higher degradation rates upon exposure to proteinase K. At low degrees of crystallinity, a large fraction of the specimen is amorphous, which is readily accessible for penetration of enzymatic solutions. Li and McCarthy [26] found that below a

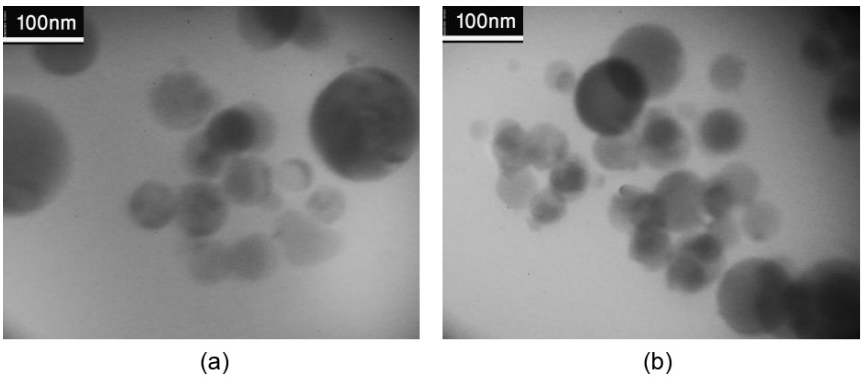

FIG. 12. TEM images of the PLA/HAP 10 nanocomposite: (a) after and (b) before irradiation.

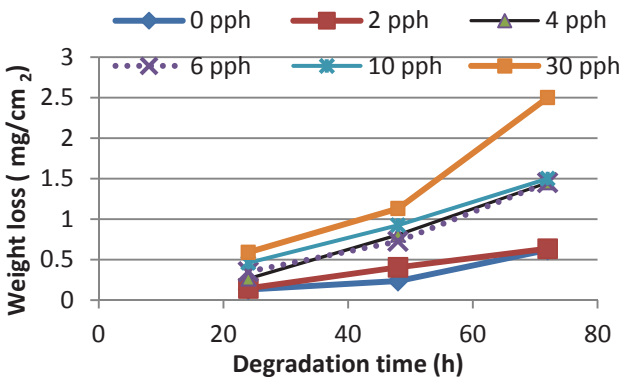

FIG. 13. Weight loss of the PLA/HAP nanocomposites versus degradation time in the presence of the enzymatic solution.

certain crystallinity (~26%), the enzymatic degradability was the same for different PLA samples, regardless of the crystalline content. The results obtained from enzymatic degradation of the PLA/HAP nanocomposites also showed that at low crystalline contents below 15%, the degradation rate was more dependent on HAP content than the crystallinity. This is evident from the degradation rate of the 30 pph nanocomposites, which is markedly higher than pure PLA, while both have nearly the same degree of crystallinity. At a given exposure time, the rate of degradation of the PLA/HAP nanocomposites is faster than the pure and PLA/organoclay samples [18].

4. CONCLUSIONS

Nanocomposite films of the PLA/HAP and PLA/layered silicate were successfully synthesized using a solution casting method. Incorporation of HAP NPs and modified clay enhanced crystallite growth in the PLA matrix. All the PLA nanocomposites showed a more intense cold crystallization peak compared to the neat PLA in the DSC thermograms, indicating a nucleating role of the nanosized particles. The cold crystallization temperature in the nanocomposites shifted to lower values, and became sharper, indicating a higher rate of crystallization. The chemical structure of the PLA phase was slightly changed under the influence of high energy γ radiation, as verified by FTIR spectra of the nanocomposite films. Subjecting the PLA/HAP nanocomposites to γ irradiation at a dose of 30 kGy promoted α crystal formation, which was investigated by wide angle XRD analysis. Irradiation of the nanocomposites also increased the enthalpy of melting ($\Delta H_m - \Delta H_c$) of the PLA component, suggesting growth of the crystalline phase in PLA. Irradiated PLA nanocomposites presented two melting points, which was indicative of the formation of different crystalline structures. Introducing nanosized particles at low contents improved the elongation at break values of the nanocomposites by up to threefold of those of pure PLA. γ irradiation at a dose of 30 kGy increased the tensile strength in almost all of the nanocomposites owing to higher crystalline contents in those samples. Addition of a multifunctional monomer at a level of 1 pph (at a dose of 30 kGy) slightly increased the tensile strength and decreased the elongation at break, suggesting three dimensional network formations upon exposure to high energy radiation at 30 kGy. No obvious changes were observed in the size and shape of NPs in the TEM images upon γ irradiation at a dose of 30 kGy. Results obtained from enzymatic degradation of PLA nanocomposites in proteinase K solution showed that at a given exposure time, the rate of degradation of the PLA/HAP nanocomposites was faster than the pure and the PLA/organoclay samples. In addition, the weight loss per unit of the surface increased with increasing HAP content and exposure time.

ACKNOWLEDGEMENTS

This project has been supported, in part, by the IAEA and the Nuclear Science and Research Institute of the Atomic Energy Organization of the Islamic Republic of Iran. The assistance of A. Akhavan and S. Hasanpour, from the Radiation Applications Research School, in performing enzymatic degradation and FTIR tests, is greatly appreciated. S. Dadbin would like to express appreciation to M. Asadi and S. Mirzanejad from the Material Research School, for performing the TEM and XRD tests, respectively.

REFERENCES

[1] MARRAS, S.I., ZUBURTIKUDIS, O., PANAYIOTOU, C., Nanostructure vs. microstructure: morphological and thermomechanical characterization of poly (L-lactic acid)/layered silicate hybrids, Euro. Polym. J. **43** (2007) 2191.

[2] PEREGO, G., CELLA, G.D., BASTIOLI, C., Effect of molecular weight and crystallinity on poly (lactic acid) mechanical properties, J. Appl. Polym. Sci. **59** (1996) 37.

[3] TSUJI, H., IKADA, Y., Blends of aliphatic polyesters, J. Appl. Polym. Sci. **67** (1998) 405.

[4] MARTIN, K., AVEROUS, Z.L., Poly (lactic acid): plasticization and properties of biodegradable multiphase systems, Polym. **42** (2001) 6209.

[5] DRUMRIGHT, R.E., GRUBER, P.R., HENTON, D.E., Poly (lactic acid) technology, Adv. Mater. **12** (2000) 1841.

[6] TSUJI, H., "Polylactides", Biopolymers for Medical and Pharmaceutical Applications (STEINBUCHEL, A., MACHESSAULT, R.H., Eds), John Wiley & Sons, Weinheim (2005) 183.

[7] BLEACH, N.C., NAZHAT, S.N., TANNER, K.E., KELLOMAKI, M., TORMALA, P., Effect of filler content on mechanical and dynamic mechanical properties of particulate biphasic calcium phosphate-polylactide composites, Biomater. **23** (2002) 1579.
[8] BURDICK, J.A., FRANKEL, D., DEMELL, W.S., ANSETH, K.S., An initial investigation of photocurable three-dimensional lactic acid based scaffolds in a critical-sized cranial defect, Biomater. **24** (2003) 1613.
[9] CHEN, C., et al., Poly (lactic acid) based nanocomposites: a novel way of drug-release, Biomed. Mater. **2** (2007) L1.
[10] IGNJATOVIC, N., SAVIC, V., NAJMAN, S., PLAVSIC, M., USKOKOVIC, D., A study of HAp/PLLA composite as a substitute for bone powder, using FT-IR spectroscopy, Biomater. **22** (2001) 571.
[11] SHIKINAMI, Y., OKUNO, M., Bioresorbable devices made of forged composites of hydroxyapatite (Hap) particles and poly L-lactide (PLLA), Biomater. **19** (1999) 247.
[12] ZHOU, S., et al., Hydrogen bonding interaction of poly (D, L-lactide)/hydroxyapatite nanocomposites, Chem. Mater. **19** (2007) 247.
[13] SHIKINAMI, Y., MATSUSUE, Y., NAKAMURA, T., The complete process of bioresorption and bone replacement using devices made of forged composites of raw hydroxyapatite particles/poly L-lactide, Biomater. **26** (2005) 5542.
[14] WEI, G., MA, X.P., Structures and properties of nano-hydroxyapatite/polymer composite scaffolds for bone tissue engineering, Biomater. **25** (2004) 4749.
[15] SULJOVRUJIC, E., IGNJATOVIC, N., USKOKOVIC, D., Gamma irradiation processing of hydroxyapatite/poly L-lactide composite biomaterial, Radiat. Phys. Chem. **67** (2003) 375.
[16] DADBIN, S. AHMADIAN, V., "Crystallinity of PLA/HAP nanocomposites: effect of gamma irradiation", Proc. Iranian Sem. Polymer Science and Technology (ISPST2012), Tehran, Islamic Republic of Iran, 21–25 October 2012.
[17] DADBIN, S., NAIMIAN, F., AKHAVAN, A., Poly(lactic acid)layered silicate nanocomposite films: Morphology, mechanical properties and effects of γ-radiation, J. Appl. Polym. Sci. **122** (2011) 142.
[18] DADBIN, S., NAIMIAN, F., KHEIRKHAH, Y., "PLA/clay nanocomposites: effects of preparation method on morphology and mechanical properties", Proc. Iranian Sem. Polymer Science and Technology (ISPST2012), Tehran, Islamic Republic of Iran, 21–25 October 2012.
[19] REEVE, M.S., McCARTHY, S.P., Polylactide stereochemistry: Effect of enzymatic degradability, Macromol. **27** (1994) 825.
[20] DADBIN, S., AKHAVAN, A., "In vitro enzymatic degradation of PLA/layered silicate nanocomposites", Proc. Iranian Sem. Polymer Science and Technology (ISPST2012), Tehran, Islamic Republic of Iran, 21–25 October 2012.
[21] PARK, J.W., et al., Biodegradable polymer blends of poly (lactic acid) and starch, Korean Polym. J. **7** (1999) 93.
[22] DI LORENZO, M.L., COCCA, M., MALINCONICO, M., Crystal polymorphism of poly (L-lactic acid) and influence on thermal properties, Thermochim. Acta **522** (2011) 110.
[23] HOOGSTEEN, W., POSTEMA, A.R., PENNINGS, A.J., TEN BRINKEG, G., ZUGENMAIER, P., Crystal structure, conformation, and morphology of solution-spun poly(L-lactide) fibres, Macromol. **23** (1990) 634.
[24] BRIZZOLARA, D., CANTOW, H.J., DIEDRICHS, K., KELLER, E., DOMB, A.J., Mechanism of the stereocomplex formation between enantiomeric poly(lactide)s, Macromol. **29** (1996) 191.
[25] ZHANG, J., et al., Crystal modifications and thermal behaviour of poly (L-lactic acid) revealed by infrared spectroscopy, Macromol. **38** (2005) 8012.
[26] LI, S., McCARTHY, S., Influence of crystallinity and stereochemistry on the enzymatic degradation of poly (lactide)s, Macromol. **32** (1999) 4454.

RADIATION ENGINEERED NANOGELS AS PLATFORMS FOR MEDICAL DIAGNOSTICS AND THERAPEUTIC NANODEVICES

C. DISPENZA[1,2], M.A. SABATINO[1], N. GRIMALDI[1], S. ALESSI[1],
G. SPADARO[1], S. RIGOGLIUSO[3], G. ADAMO[3], G. GHERSI[3]

[1] Dipartimento di Ingegneria Chimica, Gestionale Informatica, Meccanica
Università degli Studi di Palermo
Viale delle Scienze, Ed. 6,90128 Palermo

[2] CNR — Istituto di Biofisica (IBF) UOS Palermo
via Ugo La Malfa 153, 90146 Palermo

[3] Dipartimento di Scienze e Tecnologie Molecolari e Biomolecolari
Università degli Studi di Palermo
Viale delle Scienze, Ed. 16, 90128 Palermo

Italy

Abstract

A scalable, single step, synthetic approach for the manufacture of biocompatible, functionalized microgels and nanogels has been developed. Pulsed EB irradiation of PVP aqueous solutions, at relatively low energies per pulse and doses within the sterilization dose range, has led to a variety of 'as-born' sterile, functional nanostructures that exhibit a combination of favourable properties which make them suitable as biomedical nanocarriers. Reactive functional groups have been generated by graft copolymerization of functional acrylic monomers. These groups can be used to attach fluorescent probes to the NPs, to bioconjugate ligands of specific cell receptors and to incorporate therapeutics. To support the applicability of these nanogels, as well as their preparation procedure, for biomedical use, several different biocompatibility tests have been carried out.

1. OBJECTIVE

The main objective of the research was to develop a synthetic methodology to generate multifunctional nanogels using industrial type linear EB accelerators. In particular, it focused on using PVP as a model polymer, to identify irradiation conditions that would enable nanogel particle size control, colloidal stability, redispersibility from the dry form and functional reactive groups that are amenable for subsequent bioconjugation.

2. INTRODUCTION

Nanoscalar particles formed by chemical networks of cross-linked PVP and comonomers carrying reactive functional groups are promising candidates for the purpose of generating multifunctional 'smart' nanocarriers in drug delivery and diagnostics. PVP is a polymer that is widely used in pharmaceutical formulations. Both linear and cross-linked PVP show in vivo biocompatibility and escape ability from the body by natural pathways and processes, depending on MW or particle size [1]. PVP is also characterized by excellent complexing properties for ionic or π-electron systems containing substances, such as multivalent cations, acids or aromatic compounds. For this reason, PVP is often used as a polymeric stabilizer of quantum dots; or noble- and superparamagnetic metallic; or polymeric NPs in water [2–4]. PVP can be converted into a biocompatible macrogel by γ, EB or UV irradiation [5–13].

Nanoscalar PVP networks, or nanogels, couple the advantages of the PVP structure with the opportunities arising from the controlled size at the nanoscale. Cross-linked PVP NPs have already been proposed for gene delivery [14]. They have been used to encapsulate and protect DNA from intracellular degradation, facilitating internalization into vesicular structures. It has been shown that these particles can be administered intravenously and remain in circulation for a considerable period of time, evading the immune system [15].

If other functional groups are required in the PVP network, this can be pursued by heterogeneous free radical polymerization and cross-linking of vinylpyrrolidone with functional vinyl or acrylic monomers. This approach requires accurate purification procedures after synthesis for the removal of organic solvents and surfactants, which may induce cytotoxicity. Alternatively, the same result can be possibly achieved by high energy radiation induced cross-linking of PVP and simultaneous grafting of the functional monomer, when both the polymer and monomer are dissolved in an aqueous medium (water or buffer).

To develop a robust and economically viable process, 10 MeV linear EB accelerators have been utilized with the set-ups typically used for sterilization purposes in industry. In the chosen irradiation conditions, the dose per pulse is lower than that generally used for obtaining intramolecularly cross-linked nanogel particles, for example, with preparative pulse radiolysis set-ups [16]. When high doses per pulse are imparted, many radicals per chain are simultaneously formed, a significant proportion of which recombine intramolecularly, leading to polymer coil contraction. The nanoscalar networks obtained are fairly dense, with all the polymer mass concentrated in a small volume. Conversely, if only a very few radicals per chain are formed upon each pulse, the probability of their intramolecular recombination is not very high. Therefore, the polymer chains retain the ability to overlap, and other possible termination events can occur, depending on the initial system composition and its gradual modification during the irradiation process. When the polymer is irradiated in the presence of an unsaturated monomer, grafting of the monomer and/or its higher oligomers may also occur. Here, the results obtained by EB irradiation of PVP/(*N*-3-aminopropyl) methacrylamide hydrochloride (APMAM) solutions are presented. The monomer has been chosen to graft primary amino groups to the PVP network. These groups have been conjugated with either fluorescent molecules to perform localization studies in cell cultures, or with proteins, antibodies or both, as proof of a concept. The conjugation of critical markers associated with certain disease states can be particularly interesting for the development of new diagnostic tools and for active targeting purposes in drug delivery.

3. EXPERIMENTAL METHODS

3.1. Chemicals

PVP K60 (Aldrich, MW = 1.60×10^5 g/mol), APMAM (Polysciences) and FITC (Research Organics) were used without further purification. The PVP MW (4.1×10^5 g/mol) and radius of gyration (R_g = 27 nm) were estimated from Zimm plot analysis of static light scattering measurements, carried out at 25°C. Dialysis tubes of 12 kDa and 100 kDa MWCOs (Membrane Spectra/Por Biotech RC and CE, respectively, Spectrum Labs), 0.22 μm pore size syringe filters (Millipore) and a centrifuge filter device with a 10 kDa MWCO (Centricon 10, Millipore) were used.

3.2. Synthesis of PVP and PVP grafted (aminopropyl) methacrylamide microgels/nanogels

PVP aqueous solutions at different concentrations of 0.5–0.05 wt% were prepared by overnight stirring, filtered with 0.22 μm pore size syringe filters, carefully deoxygenated with gaseous nitrogen and bottled in glass vials sealed with rubber septa and aluminium caps in a glovebox under N_2 atmosphere. The oxygen content was measured to be lower than 4 ppm. Samples were individually saturated with N_2O ($N_2O \geq 99.99\%$) prior to irradiation to increase the concentration of hydroxyl radicals formed by water radiolysis upon irradiation [17]. When the acrylic monomer was present, it was added to the polymer aqueous solution at two concentrations (0.09mM and 0.18mM, corresponding to 100 and 50 PVP repeating unit to APMAM molar ratios, respectively).

EB irradiation was performed using two 10 MeV LAEs at the Institute of Nuclear Chemistry and Technology, Poland (LAE 13/9 and Elektronika 10/10), and the temperature was maintained at 0°C–4°C. A detailed description of the irradiation set-ups and dosimetry is reported in Refs [7, 18], and is summarized in Table 1. In particular, E or L refer to the accelerator used (LAE 13/9 or Elektronika, respectively), L100 and L500 refer to the two set-ups for LAE 13/9 as detailed in Table 1, and 40 or 80 refer to the total imparted doses to the samples in the irradiation runs.

TABLE 1. EB IRRADIATION CONDITIONS

Condition	Accelerator			
	Elektronika 10/10		LAE 13/9	
Average beam current (mA)	0.45	0.45	0.08	0.4
Frequency (Hz)	300	300	37.5	75
Pulse length (ms)	4.5	4.5	10–12	10–12
Dose (kGy)	40	80	40	80
Dose (Gy) per pulse	13	13	0.74	1.8
Code	E40	E80	L100-40	L500-80

Base PVP nanogels are named P*X, where X is a number indicating the weight percentage of the polymer in water. Amino graft variants are named P*-g-A(Y), where Y is a number indicating the PVP repeating unit/APMAM molar ratio.

After irradiation, samples were dialysed against distilled water for 48 h with12 kDa MWCO and 100 kDa MWCO. The pH values of the systems were measured before and after irradiation and after dialysis at the controlled temperature of 25°C ± 1°C with a GLP 22 pH and ion meter (CRISON).

3.3. Product yield determination

The yield of the microgel/nanogel production process was determined gravimetrically as the weight ratio of recovered product after irradiation, dialysis (MWCOs of 12 kDa or 100 kDa) and freeze-drying, and the corresponding initial weight of the polymer and the monomer loaded to the vial. Measurements were always carried out in triplicate from independent irradiation runs.

3.4. Preparation and characterization of fluorescent microgel/nanogel variants

Conjugation of the amino graft PVP variants with FITC was carried out at pH9.3 (Borax) and 37°C for 2 h, following an already reported protocol [18]. UV/VIS absorption and fluorescence spectroscopy were carried out on (i) the conjugated amino functionalized microgel or nanogel dispersions (P*-g-A^{FITC}), (ii) the not conjugated analogues as negative controls (P*-g-A), (iii) free probe solutions as positive controls or solutions separated from nanogels after detachment (FITC solution) and (iv) base PVP systems subjected to the same protocols applied for reacting FITC with P*-g-A variants (P*^{FITC}).

3.5. Preparation of antibody conjugated P*-g-APMAM^{FITC} variants

Conjugation of P*-g-APMAM(100) was carried out according to the protocol described above, progressively reducing the amount of FITC charged to the reactor to determine a sufficient amount of FITC attached to the nanogels for visualization purposes and leaving some unreacted primary amino groups on the nanogels for subsequent conjugation with the antibody. The rat monoclonal antihuman CD44 antibody C37 labelled with tetramethyl rhodamine isothiocyanate (TRITC) [19] was selected as the model antibody. The conjugation was performed according to a standard 1-ethyl-3-(3′-dimethylaminopropyl) carbodiimide (EDC)/sulpho-*N*-hydroxysuccinimide protocol in 2-(*N*-morpholino)ethanesulphonic acid at 25°*C* [20]. After reaction, nanogels were repeatedly washed with PBS at pH7.4 and centrifuged using centrifuge filter devices (MWCO at 300 kDa) at 500 rev./min for 10 min.

FTIR analysis was carried out using a Spectrum 400 (Perkin Elmer) apparatus by dispersing the dry product in potassium bromide and compressing it into pellets. Spectra were recorded at 30 scans per spectrum and 1 cm^{-1} resolution in the 4000–400 cm^{-1} range.

3.6. Light scattering measurements

The hydrodynamic radius (R_h) of the particle dispersion was measured by DLS using a BI200-SM goniometer (Brookhaven Instruments). Samples, placed in the quartz cell after dilution (0.025 mg/mL) with bidistilled water, were put in the thermostated cell compartment of the instrument at 20°C ± 0.1°C. The intensity autocorrelation function at different angles and the time autocorrelation function were measured using a BI-9000 correlator (Brookhaven) and a 50 mW He–Ne laser (Melles Griot) tuned at a wavelength of $\lambda = 632.8$ nm. The correlator was operated in the multi-τ mode; the experimental duration was set to have a count of at least 2000 on the last channel of the correlation function. Because the samples showed a monomodal distribution, DLS data were analysed using the method of cumulants [21]. Measurements were carried out on a minimum of two samples from three independent runs. The weight averaged MW and R_g of PVP in aqueous solution at 25°C were estimated from the Zimm plot of static light scattering measurements at different scattering angles and polymer concentrations. The refractive index increment (dn/dc) of PVP in aqueous solution, measured using a differential refractometer (Brookhaven Instruments) at $\lambda = 620$ nm, was 0.18 ± 0.004 mL/g.

3.7. Zeta potential measurements

The surface charge of the nanogels in water was measured according to the principles of laser Doppler velocitometry and phase analysis light scattering (M3-PALS technique) and expressed as the zeta potential. It was measured on diluted dispersions (0.025 mg/mL) at 25°C using a ZetaSizerNano ZS (Malvern Instruments Ltd) equipped with a He–Ne laser at a power of 4.0 mW. Similar to particle size distribution, zeta potential measurements were also carried out on a minimum of two samples from three independent runs. Error bars reported in the zeta potential plot in Fig. 4(b) refer to the width of the zeta potential distribution for each sample.

3.8. Localization studies of P*-g-A^{FITC} nanogels

Both fluorescence and confocal microscopies were used to study the uptake of P*-g-A^{FITC} nanogels (FITC excitation at 485 nm and emission at 538 nm) and (P*-g-A^{FITC})$^{Ab\text{-}TRITC}$ (TRITC) excitation at 547 nm and emission at 572 nm). MC3T3-E1 cells or ECV304 endothelial cells were grown on cover slips into 12 well plates with a seeding density of 5×10^3 cells/well in complete Dulbecco's modified Eagle's medium (DMEM) for 24 h. Next, the cells were incubated with either P*-g-A(100)^{FITC} nanogels or with (P*-g-A^{FITC})$^{Ab\text{-}TRITC}$ at 20 μg/well and processed as per the method reported in Ref. [18].

3.9. Spectrofluorimetric analysis of P*-g-A^{FITC} nanogel uptake by cells

The MC3T3-E1 cells were seeded in a 96 well tissue plate at a density of 7×10^3 cells/well, grown for 24 h in complete DMEM and incubated in the presence of P*-g-A(100)^{FITC} (4 μg/well) nanogels for different times (0 min, 30 min, 1 h, 3 h, 6 h, 24 h and 48 h). For each incubation time, three wells were subjected to spectrofluorimetric readings to measure the total fluorescence on the well, then the cells were separated from the medium and washed twice with PBS. Fluorescence from the NPs present inside the cells, in the separated medium and in the PBS used to wash the cells were evaluated one time each using a Spectra Max Gemini EM-500 instrument (Molecular Devices, using Soft Max Pro 5.2 software).

4. RESULTS AND DISCUSSIONS

4.1. Base PVP hydrogels: From macrogels to nanogels

Hydrogels have been produced by EB irradiation from aqueous solutions of a commercial grade PVP at controlled low temperatures (0°C–4°C) and relatively low doses per pulse. Different polymer concentrations, from above to below the critical chain overlap concentration for the chosen polymer (~1 wt%, as measured from DLS and intrinsic viscosity), have been investigated yielding macroscopic 'wall-to-wall' gels and micro/nanogel particles, respectively [7]. In particular, for the irradiation dose of 40 kGy, solutions at 10 wt%, 8 wt% and 6 wt% appear

completely macroscopically gelled, while at 4 wt%, 2 wt% and 0.5 wt%, they present macrogel islands and a separated aqueous phase. At lower concentrations, all irradiated systems appear to be optically transparent liquids and would be 'traditionally' classified as 'sols'. The gel fractions for the macroscopic gels as well as the mass recovery after dialysis and freeze-drying of systems with PVP concentrations below 0.5 wt% was always higher than 90%. The soluble parts of the 0.5 wt% system and all the other systems produced at lower polymer concentrations have been investigated using DLS. In Table 2, the calculated average R_h values and relative standard deviation values for a scattering angle $\theta = 90°$ before and after irradiation are reported. Reported values refer to systems that were subjected to filtration with 0.22 μm pore size filters and diluted with distilled water to the same concentration. Preliminary measurements were also carried out before and after successive filtration with filters of 5 μm, 1.2 μm, 0.8 μm and 0.45 μm pore size. It was observed that neither the dilution nor the filtrations affected the shape of the decay curves. Filtration with 0.22 μm caused a slight reduction in the scattering light intensity for the 0.1 wt% and 0.05 wt% systems only, when compared with the non-filtered systems. Finally, measurements carried out by varying the scattering angle, in the range 30°–150°, always led to similar R_h values, with standard deviations higher for the lower angles. The 0.5 wt% and 0.25 wt% systems presented NPs with average R_h values of 36 nm and 60 nm, respectively, which were higher than those of the non-irradiated PVP coils (~20 nm). On the other hand, nanogels obtained from 0.1 wt% and 0.05 wt% solutions had R_h values that were lower than those of the corresponding non-irradiated systems. The obtained results indicate that EB irradiation at relatively low doses per pulse and low frequencies leads to stable dispersions of spherical nanogels from their parent semidilute PVP aqueous solutions at doses that are within the sterilization dose ranges. The concentration has a major impact on the hydrodynamic size of the NPs obtained; at a moderate dilution (0.25 wt%), intermolecular cross-linking is a concurrent reaction with intramolecular cross-linking, leading to the formation of bigger NPs. This is confirmed by an increase of average MW, as reported in Fig. 1(a). On the other hand, at low concentrations (0.05 wt% and 0.1 wt%), mainly intramolecular cross-linking occurs, and nanogels have smaller particle sizes than the linear polymer coil and almost invariant MWs (see Fig. 1(a)).

TABLE 2. MEAN HYDRODYNAMIC RADII (R_H) AND STANDARD DEVIATIONS OF NANOGELS OBTAINED AT DIFFERENT POLYMER CONCENTRATIONS WITH LAE-100

PVP concentration (wt%)	Average R_h ± standard deviation (nm)	
	Non-irradiated	Irradiated
0.5	22 ± 3	36 ± 8
0.25	22 ± 8	60 ± 14
0.1	20 ± 10	15 ± 4
0.05	20 ± 9	13 ± 4

In Fig. 1(b), the hydrodynamic size for nanogels obtained at higher (Elektronika) and lower (LAE-100) dose rates for the three concentrations of 0.05 wt%, 0.1 wt% and 0.25 wt% and an integrated dose of 40 kGy are reported.

It is interesting to observe that, while at the low concentration, no influence of dose rate is observed, there is a dramatic effect on particle size when nanogels are generated at 0.25 wt%.

Surface charge density was also measured for all the nanogels produced. In Fig. 2, the zeta potential distribution curves for the non-irradiated PVP and two representative nanogel systems, P*(0.1)-E40 and P*(0.25)-E40, are reported. Non-irradiated PVP has an inherent slightly anionic character owing to the keto enol tautomerism of the pyrrolidone group, but it becomes more anionic upon irradiation, presumably because of the pyrrolidone ring opening reactions leading to the formation of carboxylated groups. Nanogels obtained at low concentrations also show higher heterogeneities in surface charge distribution.

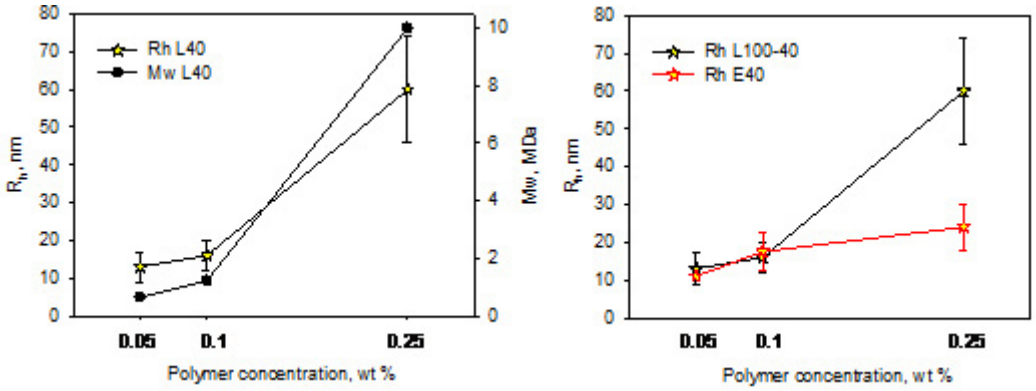

FIG. 1. (a) Rh and average MW of nanogels obtained with LAE at the lowest dose per pulse and pulse frequency from PVP solutions at three different concentrations. (b) Comparison of the Rh of nanogels obtained at two different doses per pulse and frequencies.

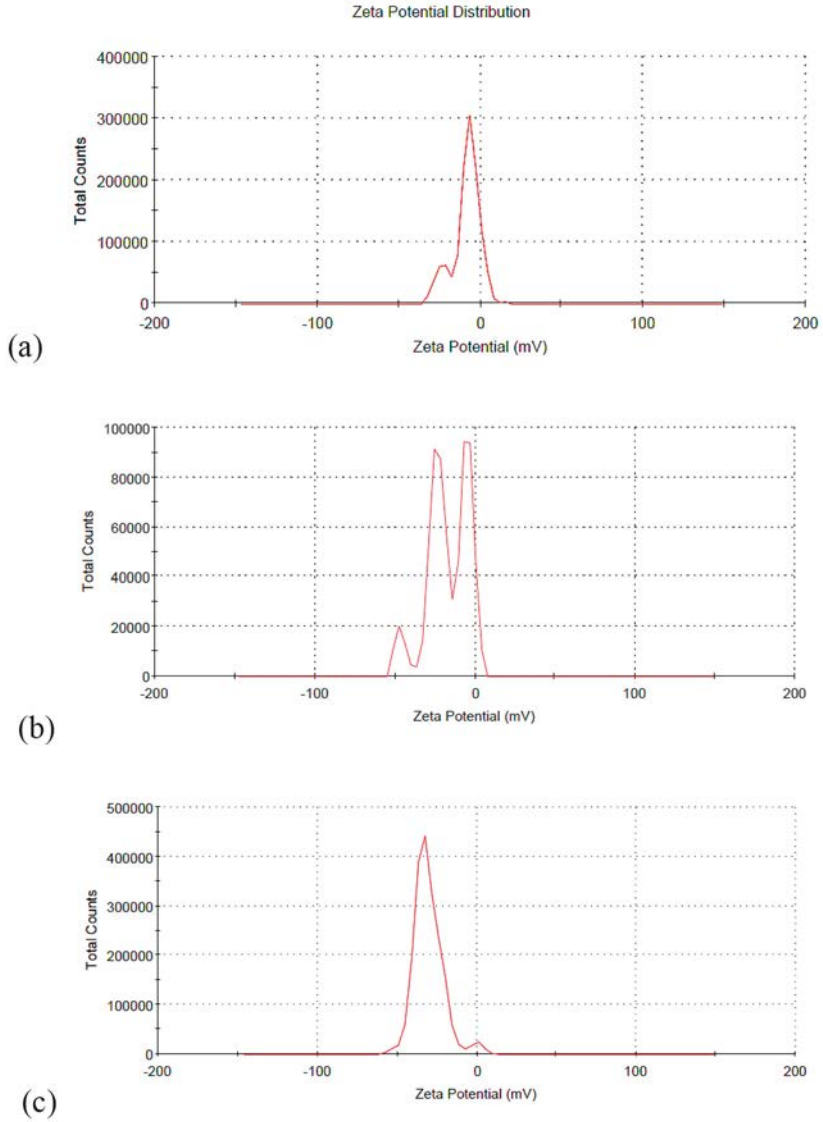

FIG. 2. Zeta potential curves for (a) non-irradiated PVP, (b) P(0.1)-E40 and (c) P*(0.25)-E40 nanogels in water.*

A structural characterization of the formed nanogels has been attempted by applying complementary spectroscopic techniques [22]. FTIR spectra for non-irradiated PVP, P*(0.1)-E40 and P*(0.25)-E40 nanogel systems are reported in Fig. 3. Enhanced absorptions from OH and NH groups at 3700–3000 cm^{-1} are evident. The characteristic carbonyl peak of PVP becomes a multiband envelope that stretches both towards the higher and lower wavenumbers. Two new peaks appear, at 1769 cm^{-1} and 1698 cm^{-1}, near the amide I band of the pyrrolidone ring, which refer to C=O symmetric and asymmetric stretching vibrations, respectively, of five member cyclic imides. New bands at 1397 cm^{-1} and 1384 cm^{-1} can be associated with the presence of carboxylate anions, which may be also responsible for the enlargement of the carbonyl band towards 1600 cm^{-1}. Bands at 1058 cm^{-1} and 986 cm^{-1} suggest the formation of oxygen atom mediated cross-links, which results from PVP hydroxylation. These results are corroborated by Raman and solid state ^{13}C nuclear magnetic resonance (NMR) spectroscopies (not reported here).

4.2. Amino graft PVP nanogels

When APMAM has been added at different concentrations to the semidiluted PVP aqueous solutions and subjected to EB irradiation, significant modification of hydrodynamic size and surface charge density is observed. In particular, Fig. 4 shows nanogels obtained at 0.1 wt% PVP and two PVP repeating unit to APMAM molar ratios.

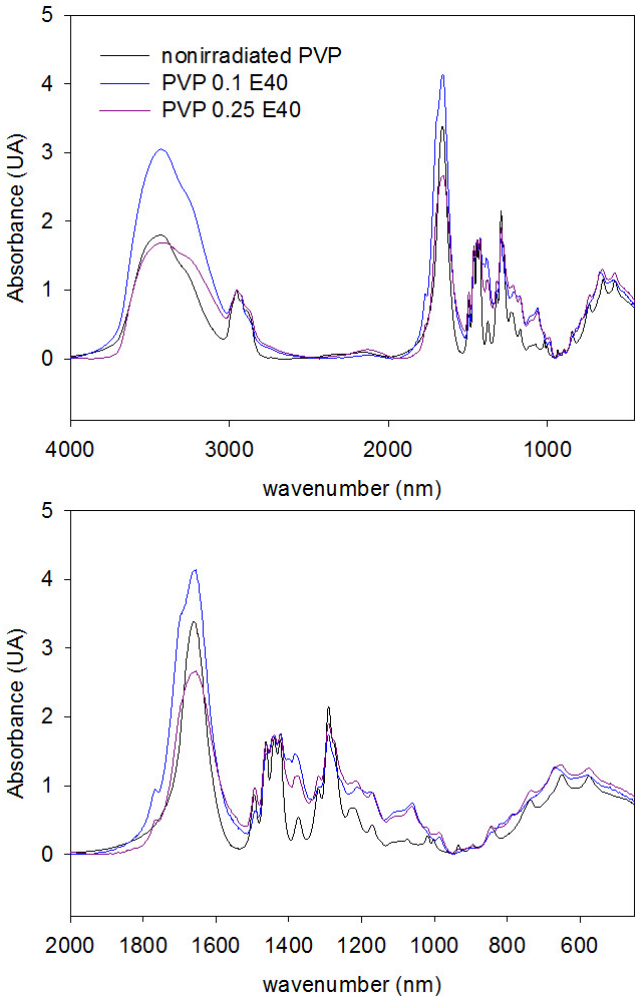

FIG. 3. FTIR spectra of non-irradiated PVP and P(0.1)-E40 and P*(0.25)-E40 nanogels.*

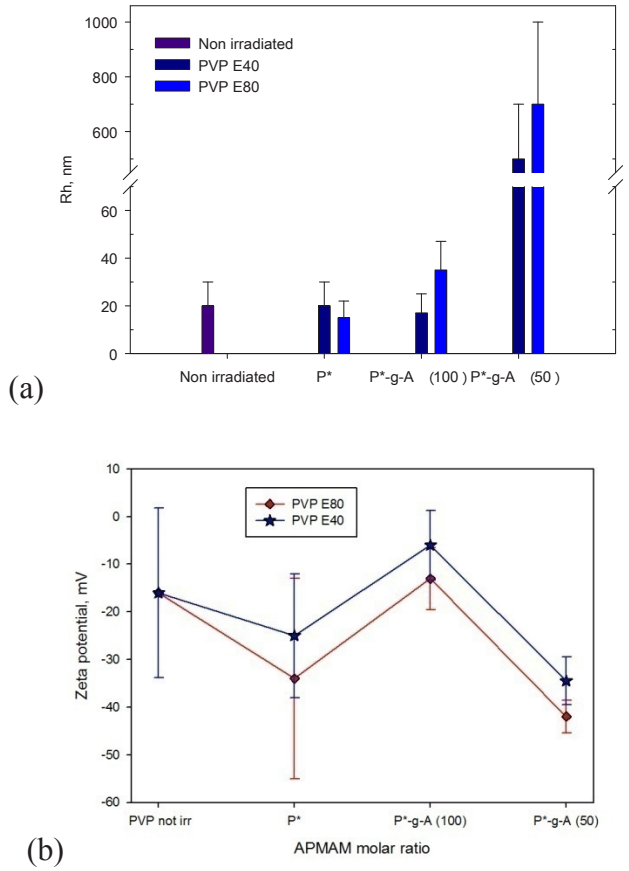

FIG. 4. (a) Hydrodynamic radius and (b) surface charge density of PVP grafted APMAM nanogels. Non-irradiated PVP and irradiated PVP solutions at 0.1 wt% are also reported as references.

In the presence of APMAM, the hydrodynamic size increases slightly for the 1/100 and significantly for the 1/50 ratios. This sudden increase of R_h is likely to be associated with a step change in the main type of cross-linking reactions upon irradiation. When EB irradiation of the aqueous solutions of PVP with APMAM is carried out with both components present at low concentration, it induces grafting of APMAM to the individual PVP NPs, while when the concentration of APMAM is increased, interparticle bridging may concur. It must be emphasized that APMAM homopolymerization is not favoured at the irradiation pH (~6) owing to the electrostatic repulsion among the positively charged monomer molecules. The effect of increasing the dose, from 40 kGy to 80 kGy, for the base PVP and for the amino graft systems, reduces the nanogel particle size and narrows the particle size distribution. Prolonged irradiation acts both as an axe and as a cement for the already formed nanogels, thus suggesting chain scission of less densely cross-linked portions, macromolecular segment grafting and intramolecular cross-linking as concurrent phenomena, all of which contribute to the formation of a more uniform distribution of microparticles/NPs. In Fig. 4(b), zeta potentials of E40 and E80 systems are shown. It has been pointed out that the non-irradiated PVP at the same concentration (0.1 wt%) shows a slightly anionic character, while the irradiated base systems present a marked anionic behaviour, which is more pronounced at the higher dose. Nanogels obtained from PVP in the presence of increasing amounts of APMAM show a progressively reduced anionic character, which is likely to be because of a screening effect of the negative charges of PVP by the protonated amino groups of APMAM. At the highest concentration of APMAM, when microgels are formed from aggregation of several PVP chains, it is expected that this monomer and/or its oligomers are no longer preferentially located at the particle surfaces, but are in their interiors; therefore, zeta potential values become comparable to those of the base PVP systems. Amino graft PVP nanogels were tested for their redispersability in PBS from the freeze-dried form and for their colloidal stability as aqueous dispersions upon storage for 1 year at room temperature. In all cases, dispersions

were tested for particle size distribution by DLS and surface charge density. No significant differences were observed with respect to the original dispersions.

Preliminary to any further development of these nanogels as biomedical nanocarriers, in vitro toxicity was evaluated via 3-(4,5-dimethylthiazol-2-yl)-2,5diphenyltetrazolium bromide (MTT) assay and caspase 3 enzymatic assay. All the gathered evidence indicates the absence of cytotoxicity in vitro [18]. Genotoxic effects induced by the nanogels are also under investigation using comet assay [23]. Results from this analysis (data not reported) demonstrate the absence of genotoxicity.

Different conjugation reactions were carried out to attach the relevant molecules to the nanogels by converting the primary amino groups of the PVP graft APMAM nanogels. In particular, the amino groups were made to completely or only partially react with the isothiocyanate group of FITC, to generate fluorescein labelled nanogels. Details of the efficiency of this reaction and attempts to use it to quantify the available amino groups present in the different nanogel variants are reported elsewhere [18]. The green emission from the P*(0.1)-g-A(100)^{FITC} nanogels is evident from the confocal microscopy image of Fig. 5(a) (left), where the NPs have been observed after incubation with cells. The combination of confocal microscopy observations and spectrofluorimetric readings of the cells, after extraction and purification from the culture medium (Fig. 5(b)), provide interesting information on the preferential uptake of these NPs by the cells from the culture medium, their accumulation during the first few hours and their progressive release in the following hours. It is also evident that the NPs that cross the cellular membrane accumulate preferentially near the nucleus. In Fig. 5(c), the image from florescence microscopy carried out on a nanogel system, namely P*-g-A(100)^{FITC}, conjugated with a TRITC labelled antibody is shown. The antibody/nanogel hybrids, visible thanks to the characteristic red emission of TRITC, seem to localize in the same compartment of the cells as the P*-g-A(100)^{FITC} bare nanogels.

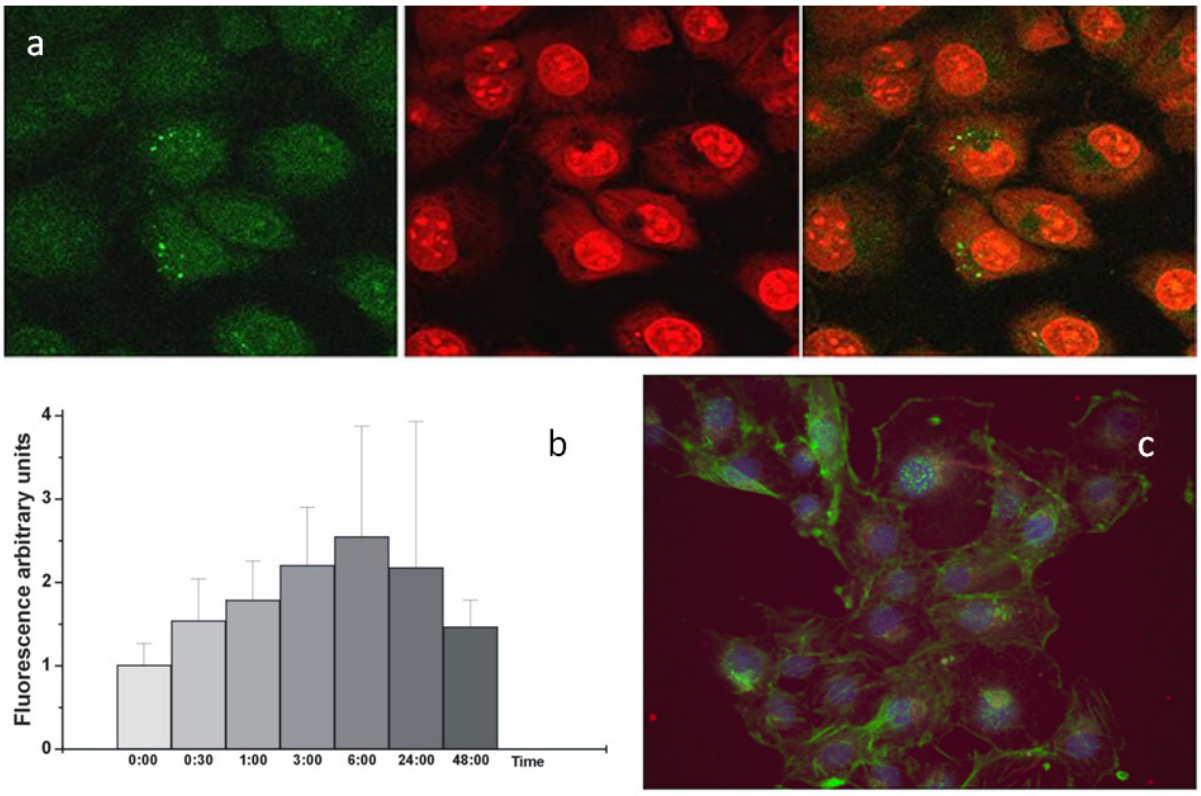

FIG. 5. (a) Confocal microscopy of MC3T3-E1 cells incubated with PVP grafted APMAM nanogels after 3 h. Merger of all confocal sections in an overall thickness of about 20 μm: (a, left) green fluorescein labelled NPs; (a, middle) cells stained using ethidium bromide to visualize nuclei; (a, right) merger of (a, left) and (a, middle) images. (b) Localization of P-g-A (100)FITC nanogels in MC3T3-E1 cells. The histogram represents the amount of fluorescent NPs present inside the MC3T3-E1 cells at different times (from 0 h to 48 h). (c) Image of ECV304 endothelial cells incubated with red fluorescent (P*-g-AFITC)Ab-TRITC nanogels. F-actin marked with green fluorescent phalloidin, nuclei with 4',6-diamidino-2-phenylindole.*

5. CONCLUSIONS

The work presented here shows that EB radiation processing is a viable and effective synthetic methodology for manufacturing PVP based functional nanocarriers, in a single step and with high yields. After irradiation, no expensive or time consuming purification procedures are required, as no recourse to catalysts, initiators or surfactants is made. Simultaneous sterilization can also be achieved by proper selection of the irradiation doses. In particular, cross-linked PVP grafted with APMAM, a monomer that bears primary amino groups, has been chosen to demonstrate the potential of the approach. Amino graft PVP nanogels are redispersible from the dry form and are stable upon storage at room temperature for 1 year. The analysed P*-g-A (100) nanogels are non-cytotoxic, non-immunogenic and able to stably bind biological molecules. Their affinity towards the cells was studied in vitro. While the final fate of these NPs will be the subject of future investigations through animal in vivo and ex vivo tests, different strategies to bind molecular drugs to the nanogels using cleavable linkers are being tested. The described approach, based on the use of industrial type LAEs, provides strong evidence that this technology can be effectively used to fabricate biohybrid nanogel based devices with a very promising future in nanomedicine.

ACKNOWLEDGEMENTS

The assistance of the Centre for Radiation Research and Technology, Institute of Nuclear Chemistry and Technology, Poland, is acknowledged for EB irradiation. In particular, we are grateful to A. Chmielewski, G. Przybytniak and I. Kaluska for support and advice. We are also grateful for the support and advice of D. Bulone of Institute of Biophysics UOS Palermo, Italy CNR, for the laser scattering measurements and M.L. Bondì of Institute for Nanostructured Materials UOS Palermo, Italy CNR, for zeta potential measurements.

REFERENCES

[1] LOGIN, R.B., SHIL, J.S., CHUANG, J.C., Method of Crosslinking PVP, Patent US005219950A (1993).
[2] DISPENZA, C., SABATINO, M.A., CHMIELEWSKA, D., LOPRESTI, C., BATTAGLIA, G., Inherently fluorescent polyaniline nanoparticles in a dynamic landscape, React. Funct. Polym. **72** (2012) 185–197.
[3] BIJU, V., et al., Photoinduced photoluminescence variations of CdSe quantum dots in polymer solutions, J. Phys. Chem. C **111** (2007) 7924–7932.
[4] ZHANG, Y., et al., Synthesis of PVP-coated ultra-small Fe_3O_4 nanoparticles as a MRI contrast agent, J. Mater. Sci.: Mater. Med. **21** (2010) 1205–1210.
[5] AJJI, Z., OTHMAN, I., ROSIAK, J.M., Production of hydrogel wound dressings using gamma radiation, Nucl. Instrum. Methods Phys. Res., Sect. B **229** (2005) 375–380.
[6] DISPENZA, C., et al., E-beam irradiation and UV photocrosslinking of microemulsion-laden poly(*N*-vinyl-2-pyrrolidone) hydrogels for "*in situ*" encapsulation of volatile hydrophobic compounds, Polym. Chem. **2** (2011) 192–202.
[7] DISPENZA, C., et al., Studies of network organization and dynamics of e-beam crosslinked PVP: From macro to nano, Radiat. Phys. Chem. **81** (2012) 1349–1353.
[8] RICCA, M., et al., Probing the internal environment of PVP networks generated by irradiation with different sources, Colloid. Polym. Sci. **288** (2010) 969–980.
[9] DISPENZA, C., LOPRESTI, C., BELFIORE, C., SPADARO, G., PIAZZA, S., Electrically conductive hydrogel composites made of polyaniline nanoparticles and poly(*N*-vinyl-2-pyrrolidone), Polym. **47** (2006) 961–971.
[10] DISPENZA, C., SABATINO, M.A., NICONOV, A., CHMIELEWSKA, D., SPADARO, G., E-beam crosslinked, biocompatible functional hydrogels incorporating polyaniline nanoparticles, Radiat. Phys. Chem. **81** (2012) 1456–1459.
[11] ZHU, X., LU, P., CHEN, W., DONG, J., Studies of UV crosslinked poly(*N*-vinylpyrrolidone) hydrogels by FTIR, Raman and solid-state NMR spectroscopies, Polym. **51** (2010) 3054−3063.
[12] LOPERGOLO, L.C., LUGAO, A.B., CATALANI, L.H., Direct UV photocrosslinking of poly(*N*-vinyl-2-pyrrolidone) (PVP) to produce hydrogel, Polym. **44** (2003) 6217–6222.
[13] DISPENZA, C., et al., Large-scale radiation manufacturing of hierarchically assembled nanogels, Chem. Eng. Trans. **27** (2012) 229–234.
[14] SAXENA, S.M., JOHRI, A.K., Ultra-low sized cross-linked polyvinylpyrrolidone nanoparticles as non-viral vectors in vivo for gene delivery, Biomater. **27** (2006) 5596–5602.

[15] BHARALI, D.J., SAHOO, S.K., MOZUMDAR, S., MAITRA, A., Cross-linked polyvinylpyrrolidone nanoparticles: A potential carrier for hydrophilic drugs, J. Colloid Interface Sci. **258** (2003) 415–423.
[16] ULANSKI, P., ROSIAK, J.M., The use of radiation technique in the synthesis of polymeric nanogels, Nucl. Instr. Methods Phys. Res. B **151** (1999) 356–360.
[17] WOODS, R.J., PIKAEV, A.K., "Applied radiation chemistry", Radiation Processing, John Wiley & Sons, Canada (1994) Ch. 6.
[18] DISPENZA, C., et al., Minimalism in radiation synthesis of biomedical functional nanogels, Biomacromol. **13** (2012) 1805–1817.
[19] GHERSI, G., et al., Regulation of fibroblast migration on collagenous matrix by a cell surface peptidase complex, J. Biol. Chem. **277** (2002) 29 231–29 241.
[20] HERMANSON, G.T., Bioconjugate Techniques, 2nd edn, Academic Press (2008) 219 pp.
[21] STEPANEK, P., "Data analysis in dynamic light scattering", Dynamic Light Scattering: The Method and Some Applications (BROWN, W., Ed.), Oxford University Press, Oxford (1993) 177−240.
[22] SABATINO, M.A., et al., Structure of e-beam sculptured poly(N-vinylpyrrolidone) networks across different length-scales, from macro to nano, Polym. **54** (2013) 54–64.
[23] ROJAS, E., LOPEZ, M.C., VALVERDE, M., Single cell gel electrophoresis assay: Methodology and applications, J. Chromatogr. B **722** (1999) 225–254.

INTRODUCTION OF FUNCTIONAL STRUCTURES ON NANOSCALES INTO ENGINEERING POLYMER FILMS USING RADIATION TECHNIQUES

Y. MAEKAWA
Quantum Beam Science Directorate
Japan Atomic Energy Agency
1233 Watanuki, Takasaki, Gunma 370-1292
Japan

Abstract

The introduction of functional regions, on a nanometre scale, into polymeric films using γ rays, EBs and ion beams is proposed. Two approaches for building nanoscale functional domains in polymer substrates have been attempted: (i) radiation induced grafting to transfer nanoscale polymer crystalline structures (morphology), acting as nanotemplates, to nanoscale graft polymer regions and (ii) fabrication of nanopores and functional domains in thermally stable fluorinated plastic films using ion beams, which deposit the energy in very narrow regions of the polymer films. Hydrophilic grafting polymers are introduced into hydrophobic fluorinated polymers, cPTFE and partially fluorinated copoly(ETFE) films, which are known to have lamellae and crystallites in the polymer films. Then, the hierarchical structures of hydrophilic graft domains are analysed by SAXS and SANS experiments as a function of GD. For the cPTFE substrate, the graft polymers with about a 45 nm scale are introduced between the lamellar crystals at low GDs (<5%). The grafted domain delocalized around the lamellar crystals is a good conducting path, resulting in relatively high conductivity of the cPTFE PEM with low GD, namely, low ion exchange capacity. At GDs above 15%, the grafting layers are totally connected to each other, but retain the lamellar crystal structures, resulting in higher conductivity with moderate mechanical strength. In the case of ETFE substrates, similar grafting domains with a 26 nm scale are generated from the lamellar templates of ETFE films at lower GDs. These cPTFE and ETFE results clearly show that the size of the grafting domains can be controlled by the lamellar crystal size. For nanofabrication of polymer films using heavy ion beams, the energy distribution in the radial direction, which is perpendicular to the ion trajectory, is studied. The effective radius of the penumbra, in which radiation induced grafting takes place, for several different ion beams is re-estimated. The different diameters of nanopores in PVDF based ion track membranes prepared by heavy ion beam irradiation followed by etching in 9M KOH at 80°C are observed. These are the first examples of pore diameter being determined by the LET of the ion beams, which change the threshold of the soluble part in the penumbra. By taking account of these phenomena, the irradiation condition is made to have a gradient LET along the film thickness and etched in KOH to create an anisotropic shape in the ion track pores in PVDF.

1. INTRODUCTION

Two approaches have been attempted to introduce functional regions on a nanometre scale into polymeric films using γ rays, EBs and ion beams. The first approach is radiation induced grafting to transfer nanoscale polymer crystalline structures (morphology), acting as nanotemplates, to nanoscale graft polymer regions. The obtained nanostructural polymers can be applied to high performance polymer membranes. The second approach is fabrication of nanopores and functional domains in engineering plastic films using ion beams, which deposit the energy in very narrow regions of the polymer films.

As shown in Fig. 1(a), one of the advantages of EBs and γ rays should be the high transmittance properties. Thus, polymer films can receive energy homogeneously along the film thickness direction. However, most polymer films have crystallites at the nanoscale. Because active species (radicals) generate only in a crystalline region, the functional domains are propagated from the nanoscale crystalline templates when functional monomers are added [1–3]. The hybrid polymer films can also be utilized; namely, inorganic crystals should act as a template for the new functional regions. In this case, the sizes and shapes of the crystallites can be changed. This technique has been recently applied to the development of PEMs for fuel cells. Fuel cells show high power generation efficiency, so they are expected to help solve energy resource depletion. Hydrogen type fuel cells, such as residential cogeneration systems and fuel cell hybrid vehicles, should reduce CO_2 emissions, which are thought to be the main reason for climate change. Hydrogen or methanol can be used as fuels, and direct methanol and hydrogen fuel types have been developed. Direct methanol fuel cells (DMFCs) have been developed for very compact mobile type devices such as mobile phones and notebooks. The main goals of hydrogen fuel cells are residential cogeneration systems and fuel cell vehicles. Natural gas is converted to H_2, and fuel cell electricity is generated. At the same

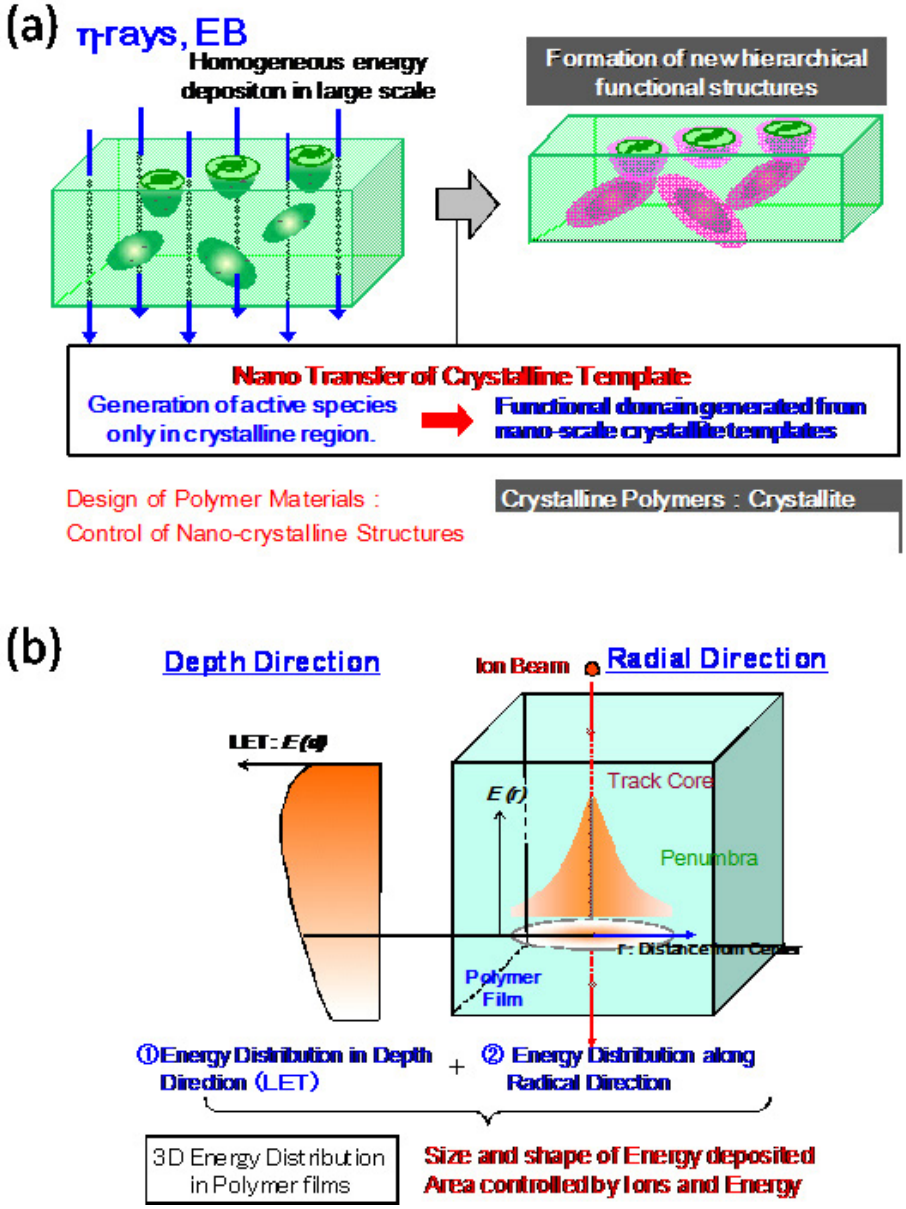

FIG. 1. Two approaches to building nanoscale functional domains in polymer substrates. (a) Radiation induced grafting to transfer nanoscale polymer crystalline structures acting as a nanotemplate to nanoscale graft polymer regions. (b) Fabrication of nanopores and functional domains in engineering plastic films using ion beams, which deposit the energy in very narrow regions of polymer films.

time, the fuel cell generates heat, which can be used to raise the temperature of water at greater than 70% energy efficiency. In fuel cell vehicles, the energy efficiency is greater than 50%, and is much higher than in engine type automobiles. In addition, only water is emitted, and it is good for the environment because of the reduction in CO_2 emissions. Fuel cell hybrid vehicles are expected to have a very large market.

When polymeric films are irradiated, radicals are generated in the films. Then, if two generated radicals react with each other, cross-linking occurs, which can enhance the mechanical strength of the films. On the other hand, if functional monomers exist in the system, graft polymerization introduces functional graft polymers into the films. Another advantage of the radiation technique is to achieve the required properties of PEM by introducing functional polymer grafts and selected polymer film substrates. By choosing these two components, or a combination of them, the required properties of PEM have been improved [4, 5].

The second approach is the nanofabrication of engineering plastic films using ion beams [6, 7]. An ion deposits its energy, on nanometre to micrometre scales, into the polymer film. Then, nanopores can be generated by resolving the damaged area, or functional regions can be introduced by grafting functional monomers into the area.

Compared with other energetic particles, heavy ion beams give a very narrow nanoscale energy deposition through their straight trajectory. The trajectory of the heavy ion beam, Xe ions with 450 MeV incident energy, is amazingly narrow, with very little broadening — no more than a few nanometres in more than 40 μm depth of polymer film. In other words, a high energy heavy ion beam is an interesting tool for developing nanostructures with very high aspect ratios in polymer films tens of micrometres to several hundred micrometres thick.

When one ion particle penetrates into the polymer films or any material, the energy is deposited into the film with a distribution in the film thickness direction. Furthermore, the position of the ion trajectory in the film has another energy distribution along the radial direction, namely, perpendicular to the direction of the penetrating ion beam. Thus, one can obtain a three dimensional energy distribution in a polymer film, and this distribution can be controlled by changing the mass and acceleration energy of the ion beam.

2. RADIATION INDUCED TRANSFER OF NANOSTRUCTURES

First, fluorinated polymers, cPTFE and copoly(ETFE) were irradiated with γ rays. Then, the films were immersed in styrene solutions to introduce polystyrene grafting chains. Subsequently, the obtained grafting chains were sulphonated with chlorosulphonic acid in dichloroethane to give grafted type fluorinated PEMs (see Fig. 2). At the first stage of the current research, a direct methanol type PEM using a technique that suited the above fluorinated polymers [8, 9] was developed.

The cPTFE membranes showed several excellent polymer properties such as mechanical strength, radiation resistance, heat deflection temperature and wear resistance. Thus, cPTFE films kept their mechanical strength after irradiation for grafting, even with quite high doses, resulting in cPTFE based PEM with higher GDs, namely, higher conductivity (σ = 2.5 S/cm) and ion exchange capacity (3.0 mmol/g). The cPTFE based PEM is dimensionally quite stable in bulk methanol and aqueous methanol solutions owing to the cross-linking structure. Furthermore, the PEM has recently been revealed to have quite low permeability of methanol and water with superior proton conductivity compared with Nafion. Thus, the cPTFE based PEM should be promising, especially for DMFC applications [8, 9]. The polymer electrolyte fuel cell performance of the cPTFE based PEM has been examined. The membrane electrode assembly of the cPTFE based PEM with higher GDs (higher ion exchange capacity) showed almost the same fuel cell performance as that of Nafion based membrane electrode assembly [8].

Recently, Chen et al. precisely evaluated the effects of graft monomers and cross-linking procedures on PEM properties [9]. They clearly showed that graft monomer structures, cross-linker structures and radiation induced cross-linking procedures were important parameters for oxidative stability of the PEM (3% H_2O_2 at 60°C), which was one of the most distinct characteristics to evaluate PEM stability in fuel cell operation. Compared with poly(styrenesulphonic acid) grafts, the ETFE based PEM with cograft polymers, poly(methyl styrene co-t-butylstyrene sulphonic acid), showed four times longer durability periods. They introduced 1,2-distyrylethane as a flexible cross-linker and the small amount of 1,2-distyrylethane with divinylbenzene enhanced the durability of the PEM in the oxidative condition. Furthermore, the postradiation cross-linking after grafting of styrene monomers, which induced multiple cross-links of substrate/substrate, graft/grafts and substrate/graft, possessed

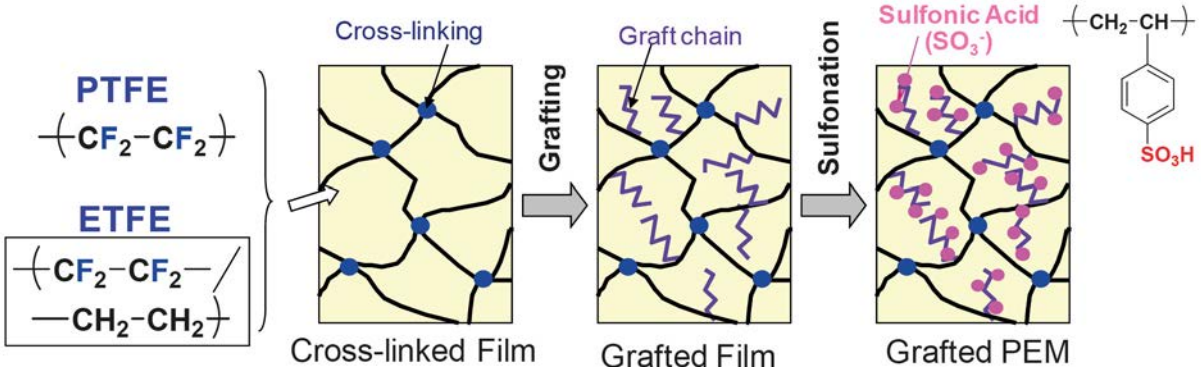

FIG. 2. Preparation procedure of graft type PEM consisting of fluorinated polymers using the radiation technique.

durability three times longer than the PEM without post-cross-linking. Accordingly, it was concluded that the ETFE based PEM with hydrophobic styrene monomers and a small amount of cross-linker with a post-cross-linking process exhibited quite high power generation in a DMFC operation with high oxidative stability.

The structures of the graft type PEM consisting of fluoro and hydrocarbon polymer substrates were characterized on nanoscales to mesoscales using SANS and SAXS [10]. Figure 3 shows the SANS profile of cPTFE, grafted cPTFE and cPTFE based PEM and proposed structures of the PEM on nanoscales to mesoscales. A clear peak at the position of the correlation length of 45 nm was observed in the profile of the cPTFE substrate, which should correspond to the correlation distances between crystallites. The SANS profile of the grafted cPTFE has a similar profile to the cPTFE substrate, in which the peak for the correlation length of 47 nm appeared with relatively higher intensities in the modulus of the scattering vector Q region, compared with those of the cPTFE substrate. Namely, the grafting layers should propagate under the influence of crystallites. A slight increase of the correlation distance from 45 nm to 47 nm should correspond to an expansion of the films owing to the introduced graft polymer layers on the crystallites. Because the profile of cPTFE based PEM is almost the same as that of the precursor grafted cPTFE, the sulphonation reaction of polystyrene grafts did not affect the size and shape of the grafted cPTFE film. The grafted cPTFE and cPTFE based PEM exhibited Q^{-2} power law behaviour, which is explained well by Porod's law as being because of the sharp interface between the graft domains and the tetrafluoroethylene-hexafluoropropylene copolymer substrates. This is because polystyrene and poly(styrenesulphonic acid) grafts were not miscible to the fully fluorinated cPTFE substrate.

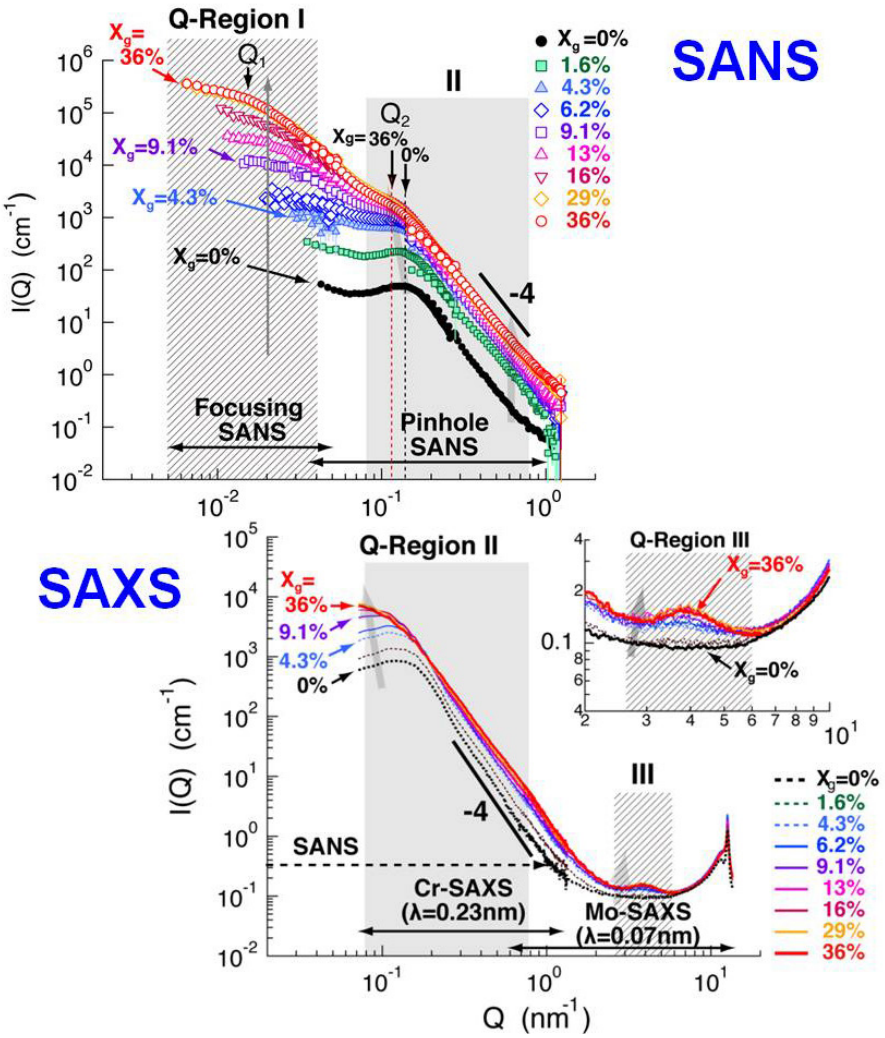

FIG. 3. Variation of SANS and SAXS profiles for cPTFE PEM under dry states depending on the degree of grafting (Xg) from 0% to 36%. The same cPTFE PEM used for the SANS and SAXS was used concurrently. Inset shows the expanded SAXS profiles around Q region III (Q = 0.2–1 nm−1).

Small angle scattering in a wide Q range (0.004–1.5 nm^{-1}) of polymer electrolyte membranes consisting of poly(styrenesulphonic acid) and cPTFE (cPTFE PEM) with various GDs up to 36% was observed by using focusing SANS, SANS and SAXS techniques (Fig. 3).

The hierarchical structure of the PEM was characterized as being composed of conducting layers (graft domains) in lamellar stacks with 48–57 nm spacing on the surfaces of 480 nm diameter crystallites and ultrasmall structures with a 1.7 nm correlation distance of the sulphonic acid groups in the conducting layers. The PEMs with GDs less than 15% possessed only grafting domains in the amorphous layers of the lamellar stacks of cPTFE. An increase in the GD of up to 5% led to an increase in the lamellar spacing of 20%, while the lamellar spacing remained constant with GDs above 5% because of crystalline restriction. Moreover, with GDs of greater than 15%, grafting domains were phase separated from the cPTFE substrate and covered the crystallites with a diameter of 480 nm (the length of a crystallite is above the observed Q region (>1.6 μm). The graft domains around the crystallites were connected to adjoining domains; accordingly, the PEMs with a higher degree of grafting had a conductivity higher than that of Nafion. Furthermore, in the SAXS measurements, the nano-order internal structure (1.7 nm) corresponded to the distance between the sulphonic acid groups of the graft polymers in the conducting layers of the cPTFE PEM. The nano-order correlation distances of the sulpho groups, which cannot be observed in Nafion, should result in methanol and water cross-over levels that are lower than those in Nafion (Fig. 4).

3. NANOFABRICATION OF POLYMER FILMS USING ION BEAMS

For nanofabrication of polymer films using heavy ion beams, the energy distribution in the radial direction, which is perpendicular to the ion trajectory, was studied. The high energy was deposited at the centre where the beam just passed through, called the track core, and the deposited energy gradually decreased with increases of radial distance from the centre at the penumbra area. The track core is defined by physical parameters; most ions with a wide range of energy possess a track core radius of about 1 nm. The penumbra is defined as the distance that the knock-on electrons from the core reach; in general, the penumbra is several micrometres.

Nanoporous ion track membranes of PVDF have been investigated because they are interesting for application to fuel cells, as well as to functional filtration membranes [4, 5]. A 25 μm thick PVDF film was bombarded by heavy ions with high total energies (^{58}Ni, ^{84}Kr, ^{129}Xe and ^{208}Pb at energies of 6.71 MeV/atomic mass unit (u), 6.21 MeV/u, 3.51 MeV/u and 11.1 MeV/u, respectively) from the Takasaki Ion Accelerators for Advanced Radiation Application (TIARA) cyclotron of the Japan Atomic Energy Agency and the Universal LAE (UNILAC) of the GSI Helmholtz

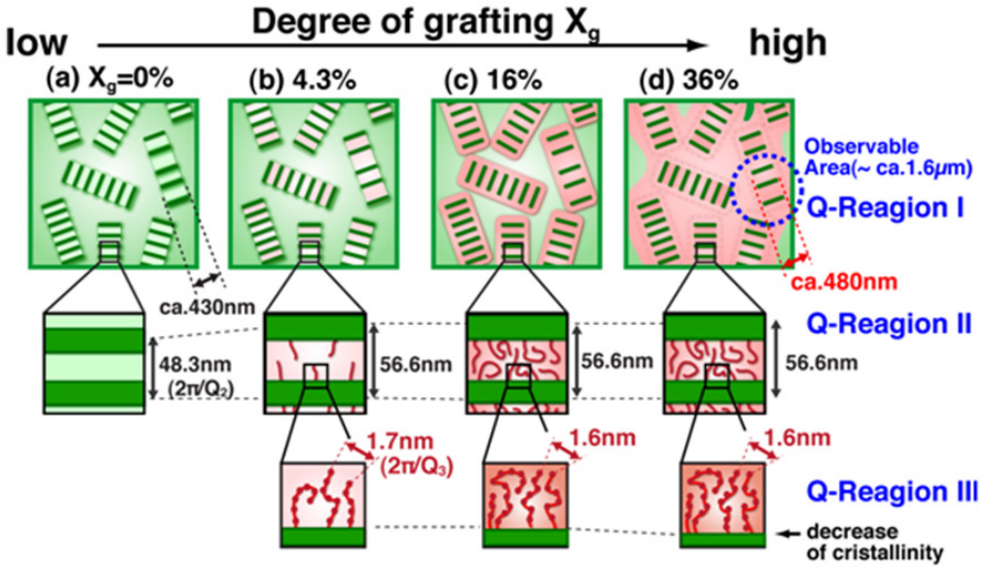

FIG. 4. Schematic illustrations of the morphology change in the hierarchical structure for cPTFE PEM under dry states with increasing degree of grafting, which are drawn from analysis of a wide Q range of SAXS. Xg = (a) 0% (before grafting), (b) 4.3%, (c) 29% and (d) 36%. The illustrations show the mechanism of the graft polymerization of cPTFE PEM.

Centre for Heavy Ion Research, Germany (Table 1). Ion irradiation with high LET was considered to enhance the etching sensitivity (defined as the ratio of the track to bulk etch rates), even under milder conditions. When the LET increased from 5.4 eV/nm to 19.0 eV/nm, the track etch rate, V_t increased by four times, and the pore size also increased from less than 100 nm to 300 nm [11]. In this case, the bulk etch rate, V_b was very small, so even for long etching of a few days, the pore sizes were not changed much. Therefore, this fourfold difference resulted from the increase of the effective penumbra radius, which had an energy higher than that required for etching in this condition. It should be noted again that pore sizes are controlled only by LET and not by etching time, as in the case of other ion track membranes.

TABLE 1. PARAMETERS OF ION BEAM EXPERIMENTS ESTIMATED BY TRIM (TRANSPORT OF IONS IN MATTER) SIMULATION CODE AND ETCHING RESULTS OF THE IRRADIATED PVDF FILMS AT 80°C IN 9M KOH

Ion	Energy (MeV)	LET (eV/nm)	V_t (μm/h)	Q value (V_t/V_b)*	Pore size ± standard deviation (nm)
Pb-208	2300	19.0	2.3	5000	305 ± 31
Xe-129	450	13.0	1.6	3500	118 ± 11
Kr-84	520	8.0	1.4	3000	109 ± 14
Ni-58	388	5.4	0.82	1800	93 ± 8

* $V_b = 4.6 \times 10^{-4}$ (μm/h).

In ion beam irradiation of PVDF films, higher LET made the chemical etching faster, thereby increasing the etching sensitivity and the resulting pore diameter [12]. Thus, the above LET sensitive etching has been used for making the LET gradient along the ion path to develop asymmetric pores in PVDF films (Fig. 5). A stack of two layers of PVDF with 100 μm and 25 μm thicknesses was irradiated at room temperature with 11.1 MeV/u ^{197}Au (fluence = 3×10^7 ions/cm^2). The Au ions were sufficiently energetic (17.7 MeV/μm at the beam entry surface) to pass through the first layer of film with 100 μm thickness with deposition of their energy rather uniformly along the full path. The Au ions also passed through the second layer of 25 μm thickness; however, the LET value was only 5.2 MeV/μm at the back face compared with 19.6 MeV/μm at the front face. Subsequent track etching was performed for 48 h in a 9M aqueous KOH solution at 80°C. SEM observations of the second layer demonstrated that, in agreement with expectation, the entry face contained pore apertures with diameters of 232 ± 14 nm, while the exit face had 50% smaller pore orifices with diameters of 117 ± 14 nm (Fig. 6). Compared with widely employed asymmetric etching methods involving chemical etching of only one side of the film, this new approach is based solely on the LET significantly varying in the thickness direction [6, 7].

In the future, the polymer properties of the functional polymer films in the nanostructural transformation of original polymer films, such as lamellae and crystallites, to the newly introduced functional polymer domains will be studied. Furthermore, control of the shapes and sizes of crystallites in polymer substrates for changing shapes and sizes of graft polymer domains will be attempted. For ion beam nanofabrication, it is planned to apply the new nanopore formation method of PVDF by changing the LET of the incident ion beams to other fluorinated polymers such as ETFE. These films should be applied for selective separation membranes.

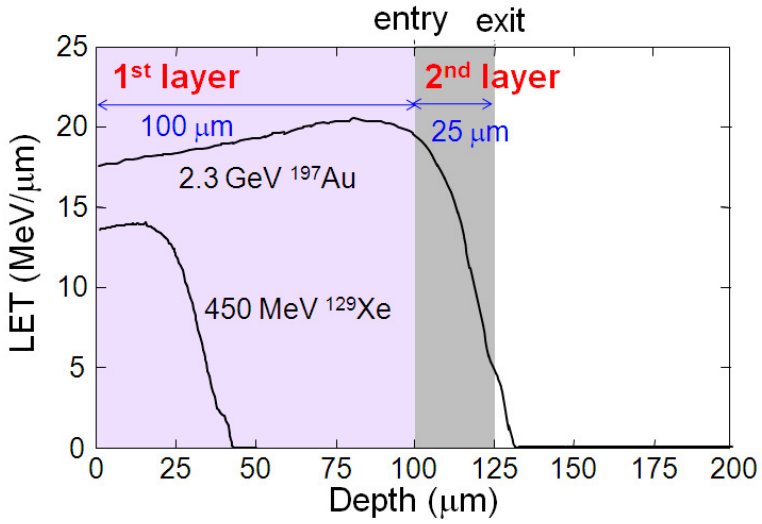

FIG. 5. Depth profiles of the LET of (a) ^{197}Au and (b) ^{129}Xe ions in PVDF, which were calculated by TRIM simulation. This figure also depicts the combination of stacked PVDF films consisting of the first 100 μm thick layer and the second 25 μm thick layer.

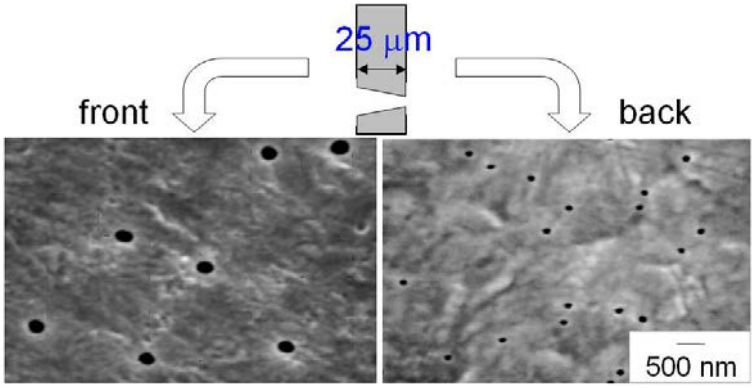

FIG. 6. SEM images of the front (left) and back (right) surfaces of the second layer of the irradiated and etched PVDF film.

4. CONCLUSION

For introducing functional regions, on a nanometre scale, into polymeric films using γ rays, EBs and ion beams, two approaches have been attempted for building nanoscale functional domains in polymer substrates: (i) radiation induced grafting to transfer nanoscale polymer crystalline structures (morphology), acting as nanotemplates, to nanoscale graft polymer regions and (ii) fabrication of nanopores and functional domains in thermally stable fluorinated plastic films using ion beams, which deposit the energy in very narrow regions of the polymer films. By SAXS and SANS experiments, for the cPTFE substrate, the graft polymers with about a 45 nm scale are introduced between the lamellar crystals at low GDs (<5%). The grafted domain delocalized around the lamellar crystals is a good conducting path, resulting in relatively high conductivity of the cPTFE PEM with low GD, namely, low ion exchange capacity. At GDs above 15%, the grafting layers are totally connected to each other, but retain the lamellar crystal structures, resulting in higher conductivity with moderate mechanical strength. In the case of ETFE substrates, similar grafting domains with a 26 nm scale are generated from the lamellar templates of ETFE films at lower GDs. These cPTFE and ETFE results clearly show that the size of the grafting domains can be controlled by the lamellar crystal size. For nanofabrication of polymer films using heavy ion beams, by using several different ion beams, different diameters of nanopores in PVDF based ion track membranes could be prepared by heavy ion beam irradiation followed by etching in 9M KOH at 80°C. This is the first example of pore diameter being determined by the LET of the ion beams, which changes the threshold of the soluble part in the

penumbra. By taking account of these phenomena, the irradiation condition (a kind of ion and energy) for gradient LET along the film thickness led to an anisotropic shape in the ion track pores in PVDF by the alkaline etching.

REFERENCES

[1] CHAPIRO, A. (Ed.), Radiation Chemistry of Polymeric Systems, Interscience Publishers, John Wiley & Sons, New York (1962) Ch. XII.

[2] SMIT, I., BEZJAK, A., Structural changes in the grafted copolymer polyethylene-styrene, Polym. **22** (1981) 590–596.

[3] SEGUCHI, T., TAMURA, N., Mechanism of decay of alkyl radicals in irradiated polyethylene on exposure to air as studied by electron spin resonance, J. Phys. Chem. **77** (1973) 40–44.

[4] DARGAVILLE, T.R., GEORGE, G.A., HILL, D.J.T., WHITTAKER, A.K., High energy radiation grafting of fluoropolymers, Prog. Polym. Sci. **28** (2003) 1355–1376.

[5] TAMADA, M., MAEKAWA, Y., "Radiation processing of polymers and its applications", Charged Particles and Photon Interactions with Matter (HATANO, Y., KATSUMURA, Y., MOZUMDER, A., Eds), CRC Press, Boca Raton (2011) 737–759.

[6] SPOHR, R., Ion Tracks and Microtechnology, Principles and Applications, Vieweg & Sohn Verlagsgesellschaft mbH, Braunschweig (1990).

[7] APEL, P., SCHULZ, A., SPOHR, R., TRAUTMANN, C., VUTSADAKIS, V., Track size and track structure in polymer irradiated by heavy ions, Nucl. Instrum. Methods B, **146** (1998) 468–474.

[8] YAMAKI, T., et al., Radiation grafting of styrene into crosslinked PTEE films and subsequent sulfonation for fuel cell applications, Radiat. Phys. Chem. **67** (2003) 403–407.

[9] CHEN, J., ASANO, M., YAMAKI, T., YOSHIDA, M., Chemical and radiation crosslinked polymer electrolyte membranes prepared from radiation-grafted ETFE films for DMFC applications, J. Power Sources **158** (2006) 69–77.

[10] IWASE, H., et al., Hierarchical structure analysis of graft-type polymer electrolyte membranes consisting of crosslinked polytetrafluoroethylene by small-angle scattering in a wide-*Q* range, Macromol. **45** (2012) 9121–9127.

[11] YAMAKI, T., et al., Conductometric analysis for the formation of poly(vinylidene fluoride)-based ion track membranes, ECS Trans. **35** (2011) 1–12.

[12] NUNUNG, N., et al., Poly(vinylidene fluoride)-based ion track membranes with different pore diameters and shapes: SEM observations and conductometric analysis, Electrochem. **78** (2010) 146–149.

RADIATION INDUCED INCORPORATION OF NANOCOMPONENTS INTO ELECTROSPUN MATS: PREPARATION OF PROSPECTIVE FUNCTIONAL NANOBIOWEBS FOR NITRITE DETECTION

K.-P. LEE, A.I. GOPALAN, S.-H. LEE, K.R. KO
Advanced Analytical Science & Nanomaterials Laboratory
Kyungpook National University
1370 Sankyuk-dong, Puk-gu, Daegu 702-701
Republic of Korea

Abstract

A novel PVDF based multifunctional conductive nanoweb (NW) was prepared and used for bioelectrocatalytic detection of nitrite ions. Firstly, PVDF NFs comprising a silica source were produced by electrospinning a mixture solution of PVDF and a silica source. Subsequently, γ irradiation was used to obtain the multifunctional NW through simultaneous incorporation of gold particles and silica into PVDF NFs. γ irradiation was effectively used to distribute Au NPs into the NW. Thus, the new PVDF silica Au NP NW (PVDF@silica/Au NP NW) was prepared by γ irradiation though successive incorporation of components into an electrospun mat. The morphology of PVDF@silica/Au NP NW was examined by FESEM. The presence of Au particles was confirmed by EDAX. The crystal structure of Au particles and the formation of silica were confirmed by XRD analysis. To convert the PVDF@silica/Au NP conductive web into a biocatalytic NW, the enzyme Cyt C was immobilized onto the surface of PVDF@silica/Au NP. A modified electrode was fabricated for bioelectrocatalytic detection of nitrite ions. The PVDF@silica/Au NP/Cyt C NW modified electrode exhibited high electroactivity and direct electron transfer took place between Cyt C and the electrode. Amperometric responses of nitrite ions were recorded at the PVDF@silica/Au NP/Cyt C NW modified electrodes. The modified electrode exhibited electrochemical detection of nitrite ions in the concentration range 2–300μM with a sensitivity of 0.0175 μA. It is anticipated that PVDF@silica/Au NP/Cyt C NW could be used for analysis of nitrites in food, soils, vegetables and fertilizers.

1. INTRODUCTION

PVDF is a semicrystalline polymer with a few special features, such as piezoelectric and pyroelectric characteristics, good chemical resistance and high mechanical properties [1, 2], and it has various applications. Incorporation of MNPs into a PVDF matrix imparts electromagnetic shielding and antistatic discharge properties. PVDF has been effectively used as a host matrix for importing multifunctional properties to composites.

Electrospinning has been proved to be a useful method for generating nanofibrous materials with high surface to volume ratios. Electrospinning is a simple and effective method to obtain ultrafine fibres with diameters ranging from tens of nanometres to micrometres. Electrospinning involves drawing of fibres from polymer solutions. In the electrospinning process, an electric field is applied to surpass the surface tension of the polymer and to generate fine jets of the polymer solution through the capillary tip. As a result, ultrathin fibres are formed. The electrospinning technique has been effectively used for the preparation of nanoscale fibres from a variety of materials, such as polymers, inorganic materials and organic/inorganic hybrids. The main features of electrospun fibres include large surface area, reusability and retention of catalytic activities. The incorporation of MNPs into polymer NFs can also be achieved by electrospinning. In a typical approach, a solution mixture of a polymer and a palladium salt was electrospun and subsequently subjected to a reduction process [3]. The polymer/MNP composite NF has been used as a catalyst. The interesting feature of this preparation method is the incorporation of MNPs within the fibres. To the best of our knowledge, preparation of a multifunctional electrospun NW composed of MNPs and an enzyme and studies on the utilization for biocatalytic application have not yet been attempted in great detail.

In the present work, new PVDF based multifunctional conductive NWs were prepared and used for bioelectrocatalytic application. The methodology adopted in this work was as follows. A mixture solution of PVDF and the silica source was electrospun to obtain a silica source loaded PVDF fibre. Silica and gold NPs were

then loaded into the PVDF@silica NW by γ radiation. Cyt C was subsequently immobilized onto the surface of PVDF-Si@Au NP NW by physisorption to obtain the PVDF@silica/Au NP/Cyt C biocatalytic NW. To demonstrate the efficiency of PVDF@silica/Au NP/Cyt C towards bioelectrocatalysis, electrocatalytic detection of nitrite ions was investigated.

2. EXPERIMENTAL METHODS

2.1. Chemicals

Multiwalled nanobtubes were obtained from CNTs (Republic of Korea). *N*-[3-(trimethoxy silyl) propyl] aniline (TMSPA), PVDF, gold(III) chloride trihydrate ($HAuCl_4$) and Cyt C (horse heart) were purchased from Sigma-Aldrich (USA) and used as received. Indium doped tin oxide (ITO) coated glass plates (specific surface resistance ~ 30 Ω, Corning, USA) were cleaned with acetone and distilled water, prior to use.

2.2. Characterization

The morphology of electrospun NF membranes was examined by FESEM (Hitachi S-4200) combined with EDAX measurements. Electrospun fibres or composite fibres were characterized by XRD analysis (D8 Advanced Bruker AXS diffractometer using Cu αK radiation) and thermogravimetric analysis (TMA120, Seiko, Japan). Electrochemical experiments were performed using an IviumStat and a CompactStat (IVIUM, Netherlands) in a conventional three electrode electrochemical cell using twisted platinum wire as the auxiliary electrode and Ag/AgCl as the reference electrode. An ITO/PVDF-Si@Au NP NW modified electrode was employed as the working electrode.

2.3. Preparation of PVDF@silica/Au NP NW by γ radiation

γ radiation was used for postmodification of the PVDF NF into PVDF@silica/Au NP NW. Figure 1 shows the steps involved in the formation of PVDF@silica/Au NP NW. The detailed experimental procedure is as follows.

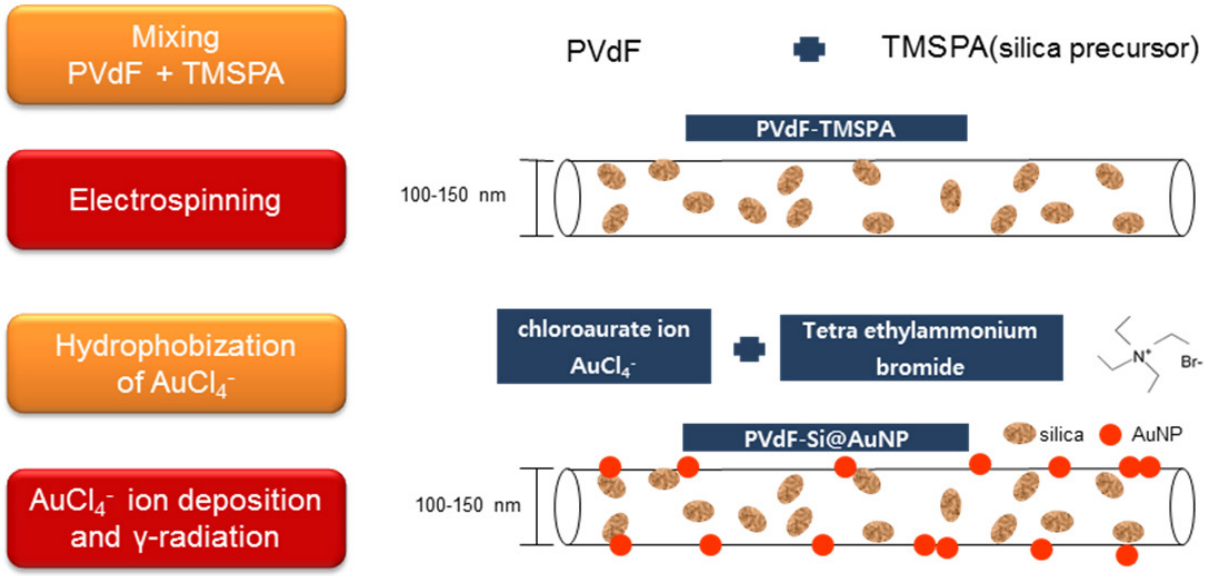

FIG. 1. Preparation of electrospun PVDF@silica/Au NP NW.

2.3.1. Preparation of PVDF@silica/Au NP NW

PVDF (0.1 g) was dissolved in 10 mL of dimethylformamide under stirring at 60°C. To the PVDF solution, TMSPA (silica source, 50mM) (7/3 v/v) was added and stirred for 4 h to obtain a homogeneous solution. Electrospinning of the resultant solution was performed at a flow rate of 0.5 mL/h with a potential difference of 25 kV between the syringe tip (NanoNC, NNC-PN-25 GA (diameter 0.25 mm, model 25 G 1/4″)) and the collector. The PVDF NW containing TMSPA was accumulated on the collector (drum) over the aluminium foil and dried at 60°C in an oven for 24 h. An aqueous solution of $HAuCl_4$ (10 mL, 0.5 mmol/L) was mixed with a solution of tetraoctylammonium bromide in toluene (80 mL, 50 mmol/L). The two phase mixture was stirred until $AuCl_4^-$ was transferred into the organic layer. The colour of the organic layer changed to yellow [4]. The organic layer containing $AuCl_4^-$ was separated from the aqueous layer and gun sprayed onto silica loaded PVDF NW to obtain TMSPA and Au loaded PVDF NW. TMSPA and $HAuCl_4$ loaded PVDF NF was irradiated with γ radiation (^{60}Co source) for a total dose of 30 kGy (dose rate = 6.48×10^5 Gy/h) to obtain silica and Au NPs incorporated into the NW (PVDF@silica/Au NP NW). For comparison, TMSPA loaded PVDF NW was also irradiated to obtain PVDF@silica NW.

2.3.2. Preparation of PVDF@silica/Au NP/Cyt C biocatalytic NW for detection of nitrite ions

A volume of 20 mL of Cyt C solution (10 mg in 0.1M PBS, pH7.0) was dropped onto the surface of the NWs and dried at room temperature. The resultant Cyt C immobilized PVDF@silica/Au NP NW (designated as PVDF@silica/Au NP/Cyt C NW) was tested for electrocatalytic detection of nitrite ions.

3. RESULTS AND DISCUSSION

3.1. Preparation of PVDF@silica/Au NP NW

PVDF electrospun fibres were loaded with silica and Au NPs by γ irradiation. Upon γ irradiation, the silica (TMSPA) and gold sources loaded onto the PVDF electrospun fibre were converted into silica and Au NPs to result in PVDF@silica/Au NP NW via sequential reactions induced by γ irradiation. TMSPA undergoes hydrolysis and condensation to result in silica within the PVDF matrix. $HAuCl_4$ undergoes γ irradiation induced reduction to generate Au NPs. The silica and Au NP loaded PVDF fibres impart hydrophilic biocompatible and catalytic properties to the PVDF matrix.

The optical micrographs of pristine PVDF (Fig. 2(a)), silica loaded PVDF (Fig. 2(b)) and PVDF@silica/Au NP NW (Fig. 2(c)) are presented in Fig. 2. PVDF (pristine) NF and PVDF@silica NW are white in colour (Figs 2(a) and 2(b)). The colour of PVDF@silica/Au NP NW produced by γ irradiation is pink (Fig. 2(c)).

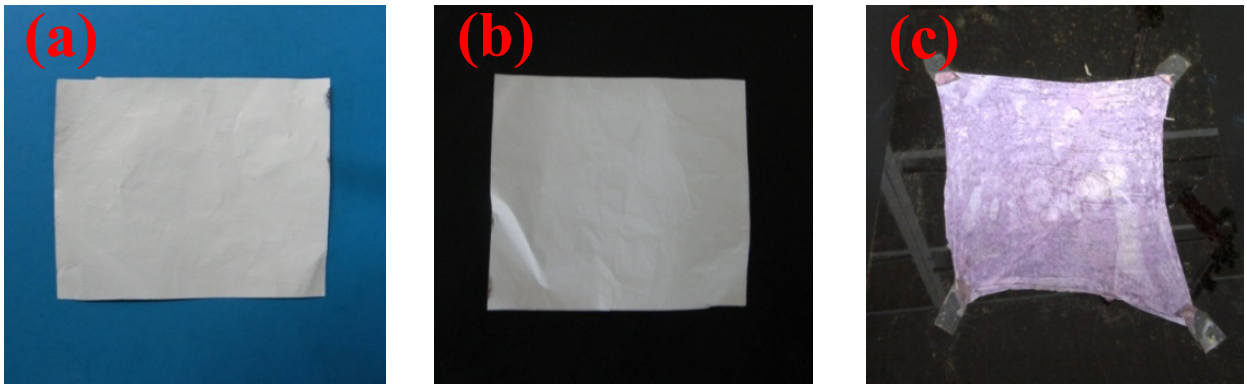

FIG. 2. Photographs of (a) PVDF NF, (b) PVDF@silica NW and (c) PVDF@silica/Au NP NW.

3.2. Morphology and microstructure

The morphology and elemental composition of NWs were examined by FESEM and EDAX measurements. FESEM micrographs of PVDF NF (Fig. 3(a)), PVDF@silica NW (Fig. 3(b)) and PVDF@silica/Au NP NW (Fig. 3(c)) were compared to examine the morphological variations between the NWs. The average diameter of pristine PVDF NF was 150 nm (n = 10) (Fig. 3(a)). The fibres in PVDF NF were smooth without beads. After incorporation of silica, the average diameter of PVDF NF increased to 210 nm (n = 10) (Fig. 3(b)). The average diameter of fibres in PVDF@silica/Au NP NW was 240 nm (n = 10). The distribution of spherical Au NPs and silica can be seen (Fig. 3(c)). Furthermore, a higher magnification image (Fig. 3(c), inset) clearly depicts the distribution of Au particles onto PVDF@silica NW. The selected area Au particle size distribution chart is presented in Fig. 3(d).

It is inferred that most of the Au particles have sizes between 60 nm and 70 nm. The EDAX spectrum of PVDF@silica/Au NP NW confirms the presence of silica and Au NPs in the NW (Fig. 4). The atomic percentages of silica in PVDF@silica NW (Fig. 4(a)) and PVDF@silica/Au NP NW (Fig. 4(b)) are 1.8 at.% and 0.58 at.%, respectively. The atomic percentage of Au is 0.26 at.% (Fig. 4(b)).

FTIR spectroscopy was used for the identification of functional groups in the NWs. FTIR spectra of (a) PVDF NF, (b) PVDF@silica NW and (c) PVDF@silica/Au NP NW are shown in Fig. 5. In the spectra of PVDF NW, PVDF@silica NW and PVDF@silica/Au NP NW, the bands of $–CF_2$ wagging (470 cm^{-1}), $–CF_2$ stretching (1400 cm^{-1}) and $–CF_2$ bending (1400 cm^{-1}) vibration are assigned. The presence of a peak around 1130 cm^{-1} in PVDF@silica NW confirms the presence of Si–O–Si linkages (Fig. 5, curve b). In addition, the peak around 3400 cm^{-1} corresponds to –NH stretching. The strong peaks around 1510 cm^{-1} and 1600 cm^{-1} in the spectra of PVDF@silica NW (Fig. 5, curves b and c) are assigned to benzenoid amine and quinoid imine units [5], respectively. The bands corresponding to quinoid and benzenoid stretching in the FTIR spectrum of PVDF@silica NW indicate that PVDF@silica NW contains polyamide type structures.

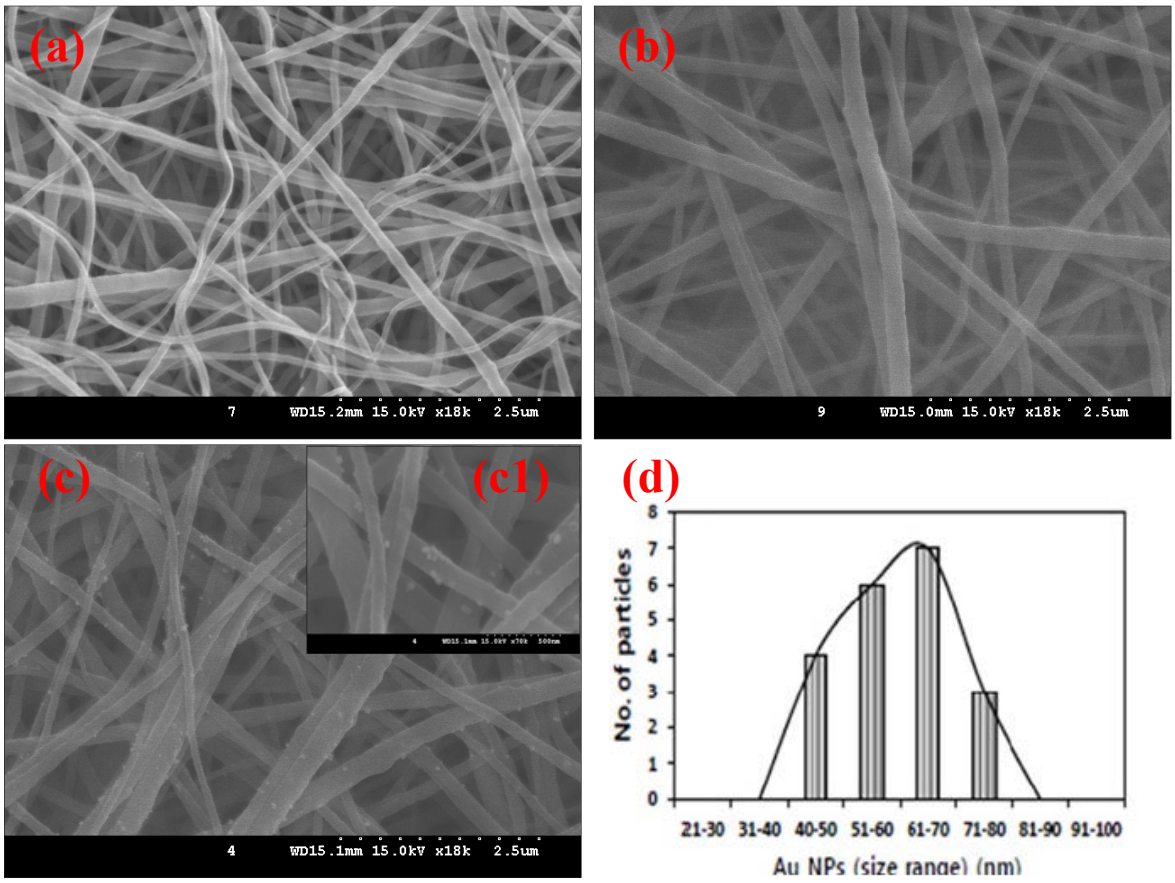

FIG. 3. FESEM images of (a) PVDF NF, (b) PVDF@silica NW and (c) PVDF@silica/Au NP NW. (c1) Higher magnification FESEM image of (c). (d) Selected area Au particle size distribution chart.

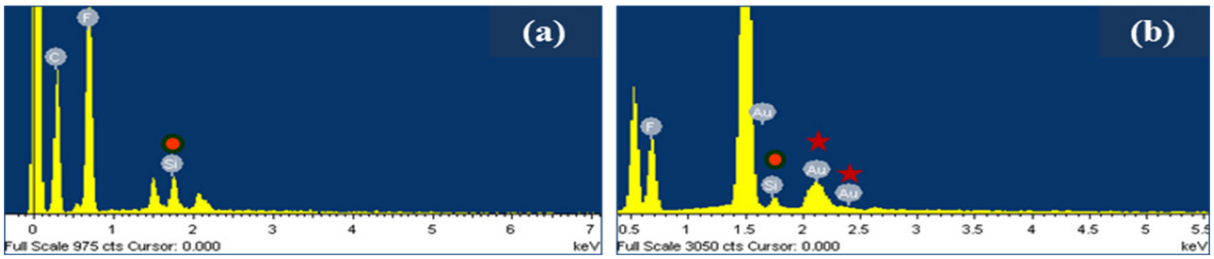

FIG. 4. EDAX images of (a) PVDF@silica NW and (b) PVDF@silica/Au NP NW.

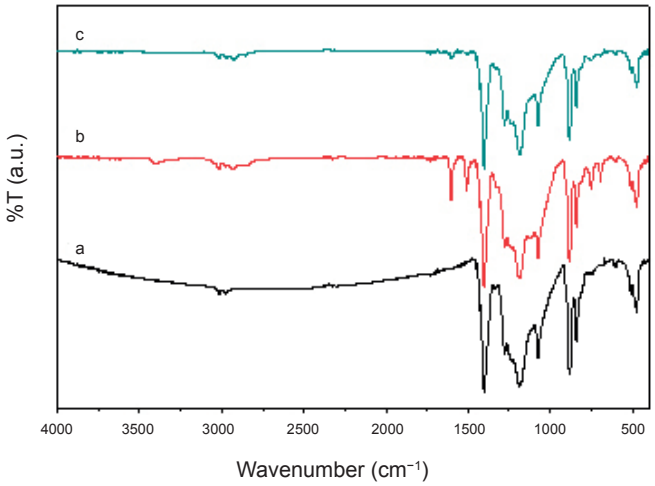

FIG. 5. FTIR spectra of electrospun: (a) PVDF NF, (b) PVDF@silica NW and (c) PVDF@silica/Au NP NW.

XRD patterns of PVDF NF (Fig. 6, curve a), PVDF@silica NW (Fig. 6, curve b) and PVDF@silica/Au NP NW (Fig. 6, curve c) were compared. The XRD pattern of pristine PVDF showed diffraction peaks at $2\theta = 20.61°$, 30.31° and 35.31°, which correspond to (110) and (021) hkl reflection planes of a crystallographic phase [6]. The XRD pattern of PVDF@silica NW exhibited an additional peak at 18.31°, which corresponds to the β crystallographic phase of PVDF (Fig. 6, curve b). This suggests that inclusion of silica into PVDF NF and PVDF@silica/Au NP NW causes phase transitions from α to β forms [7]. Furthermore, the crystal structure of silica in PVDF@silica NW is evident from the low angle XRD measurements. The existence of peaks at $2\theta = 2.71°$, 5.91° and 6.71° (Fig. 6, inset) are attributed to the (100), (200) and (210) hkl lattice planes of silica. The crystalline phase transformation (α to β) in PVDF (Fig. 6, curve b) suggests that there can be molecular level interactions between silica and PVDF groups in PVDF@silica NW [8]. While the α form of PVDF is non-polar, the β form of PVDF may exhibit polar properties [9]. Thus, inclusion of silica into PVDF NF induces hydrophilic properties to PVDF [10]. The XRD pattern of PVDF@silica/Au NP NW (Fig. 6, curve c) exhibits three major Bragg diffraction peaks around 38.31°, 45.41° and 64.81°, which are assigned to the (111), (200) and (220) hkl planes of face centred cubic lattices of Au, respectively [11]. However, the peak intensity at $2\theta = 38.31°$ (111) is much higher compared to the other lattice plane reflection peaks (Fig. 6, curve c). This suggests that Au NPs retain predominant (111) orientation in PVDF@silica/Au NP NW [12].

Figure 7 displays the thermograms of PVDF NF (curve a), PVDF@silica NW (curve b) and PVDF@silica/Au NP NW (curve c) owing to the incorporation of silica and Au NPs. The major weight losses observed between 400°C and 500°C are attributed to the decomposition of PVDF NF backbone structures. Importantly, the thermogram of pristine PVDF exhibits higher weight loss (~67%) (curve a) compared to PVDF@silica NW (~60%) (curve b) and PVDF@silica/Au NP NW (~50%) (curve c) NWs. Thus, incorporation of silica into PVDF NF improves the thermal stability of PVDF NF [13]. The weight losses beyond 500°C (~5%–10%) may correspond to carbonization of PVDF NF. The residual mass at 600°C is ~28% for PVDF@silica/Au NP NW (curve c), which is much higher than PVDF@silica NW (curve b) (26%) and PVDF NF (curve a) (19%).

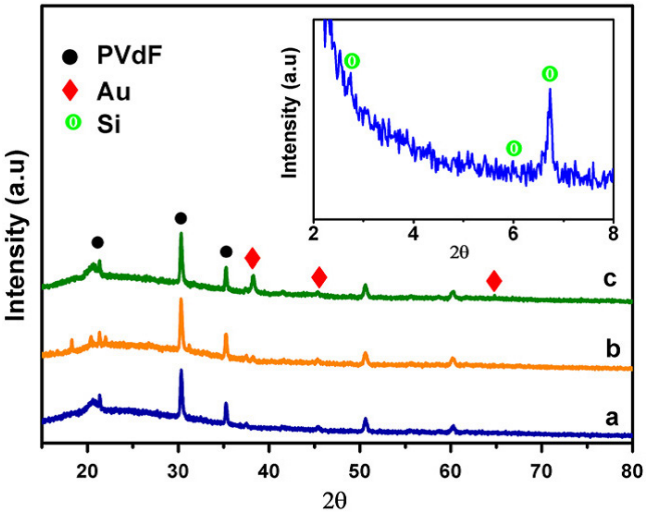

FIG. 6. XRD patterns of (a) PVDF NF, (b) PVDF@silica NW and (c) PVDF@silica/Au NP NW.

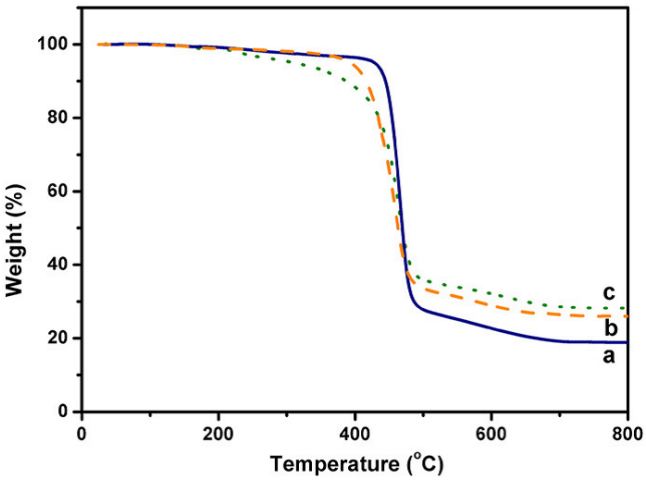

FIG. 7. Thermogravimetric analysis curves of (a) PVDF NF, (b) PVDF@silica NW and (c) PVDF@silica/Au NP NW.

3.3. Electrochemical properties

Firstly, electrochemical properties of PVDF NF (Fig. 8, curve a), PVDF@silica NW (Fig. 8, curve b) and PVDF@silica/Au NP/Cyt C NW (Fig. 8, curve c) were investigated by cyclic voltammetry using $Fe(CN)_6^{3-/4-}$ as the redox marker at a scan rate (ν) of 20 mV/s in 0.1M KCl. Well defined peaks for Fe^{2+}/Fe^{3+} redox transitions are observed with a peak potential separation of ~0.2 V at the ITO/PVDF@silica/Au NP/Cyt C NW electrode. However, the ITO/PVDF/Cyt C and ITO/PVDF@silica/Cyt C NW electrodes show much lower peak currents. Cyclic voltammograms of the PVDF@silica/Au NP modified electrodes exhibit symmetrical anodic and cathodic peaks that are associated with the Fe^{2+}/Fe^{3+} redox transitions. The ratio of anodic to cathodic peak current is nearly unity, which indicates a quasi-reversible reaction at the electrodes. For the PVDF@silica/Au NP/Cyt C electrode, the peaks corresponding to the redox processes are observed at 0.29 V (anodic) and 0.06 V (cathodic). The comparison of peak current at the $Fe(CN)_6^{3-}/Fe(CN)_6^{4-}$ redox transition reveals the effectiveness of surface modifications. The PVDF@silica/Au NP/Cyt C electrode exhibits a peak current nearly 1.7 times that of the PVDF/Cyt C and nearly 3.2 times that of the PVDF@silica/Cyt C electrodes.

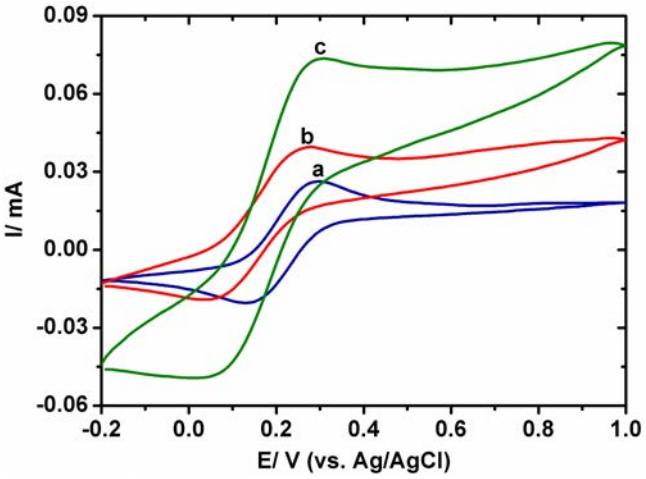

FIG. 8. Cyclic voltammogram of: (a) PVDF NF/Cyt C, (b) PVDF@silica NW/Cyt C and (c) PVDF@silica/Au NP NW/Cyt C biosensors in $Fe(CN)_6^{3-/4-}$ (0.1M KCl). Scan rate = 20 mV/s.

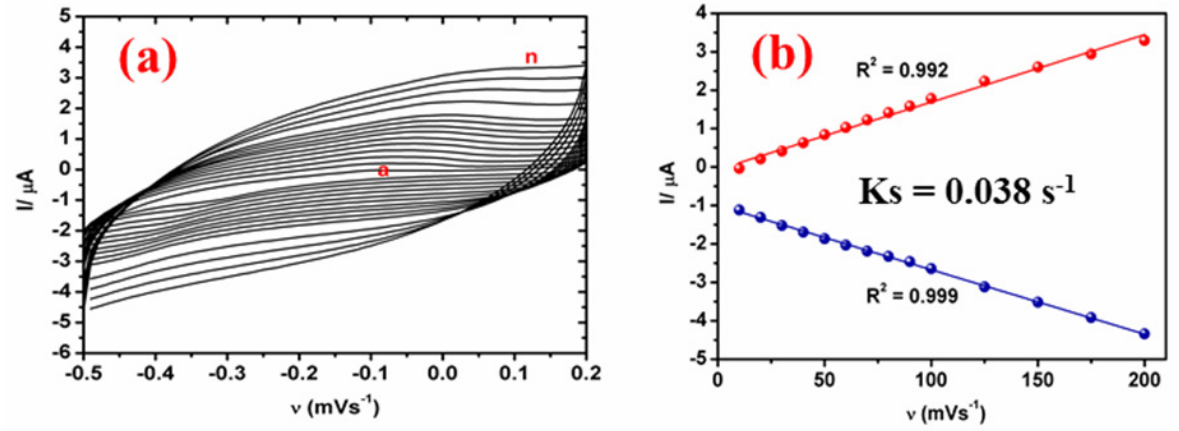

FIG. 9. Cyclic voltammograms of: (a) PVDF-Si@Au NP/Cyt C in phosphate buffer (0.1M) (pH7.0) at different scan rates: (a–n) 10 mV/s, 20 mV/s, 30 mV/s, 40 mV/s, 50 mV/s, 60 mV/s, 70 mV/s, 80 mV/s, 90 mV/s, 100 mV/s, 125 mV/s, 150 mV/s, 175 mV/s and 200 mV/s. (b) Linear calibration plot.

Cyclic voltammograms recorded for the PVDF@silica/Au NP/Cyt C electrode in 0.1M PBS (pH7.0) at different scan rates (ν) (10–200 mV/s) to the electrode are presented in Fig. 9. The cyclic voltammograms reveal that the cathodic and anodic peak currents which correspond to direct electron transfer of Cyt C increase linearly with the square root of ν. This observation signifies that the electrode process is diffusion controlled. The electron transfer rate constant (K_s) for direct electron transfer of Cyt C at the PVDF-Si@Au NP/Cyt C electrode is 0.038 s^{-1}. The much higher rate constant at the PVDF@silica/Au NP/Cyt C electrode demonstrates that the electron transfer between Cyt C and the electrode surface is faster than at the other electrodes.

3.4. Bioelectrocatalysis and nitrite ion detection

The bioelectrocatalytic property of the PVDF@silica/Au NP/Cyt C NW electrode was evaluated by oxidation of nitrite ion (0.1mM) in 0.1M PBS (pH7.0) at a scan rate of 50 mV/s (Fig. 10). The ITO/PVDF@silica/Au NP/Cyt C NW electrode exhibited a peak for biocatalytic oxidation of the nitrite ion at around +0.6 V, with a higher current value (~1.75 mA) compared to ITO/PVDF@silica/Cyt C (~1.1 mA) and ITO/PVDF/Cyt C (~0.15 mA) electrodes. The nitrite ion oxidation current at the ITO/PVDF/Cyt C electrode was 1.7 and 11.6 times higher than at the ITO/PVDF@silica/Cyt C and ITO/PVDF/Cyt C electrodes, respectively. A higher bioelectrocatalytic peak current for the oxidation of nitrite ions was noticed at the ITO/PVDF@silica/Au NP/Cyt C electrode,

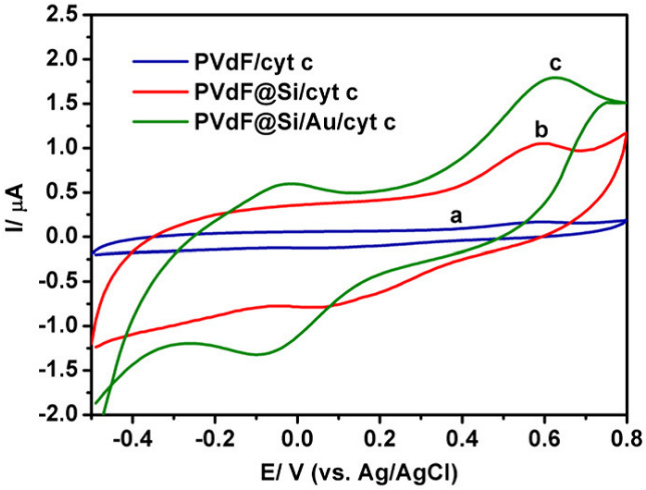

FIG. 10. Cyclic voltammograms of: (a) PVDF@Cyt C, (b) PVDF@silica/Cyt C and (c) PVDF@silica/Au NP/Cyt C NW in 0.1mM nitrite ion (0.1M PBS, pH7.0) at a scan rate of 50 mV/s.

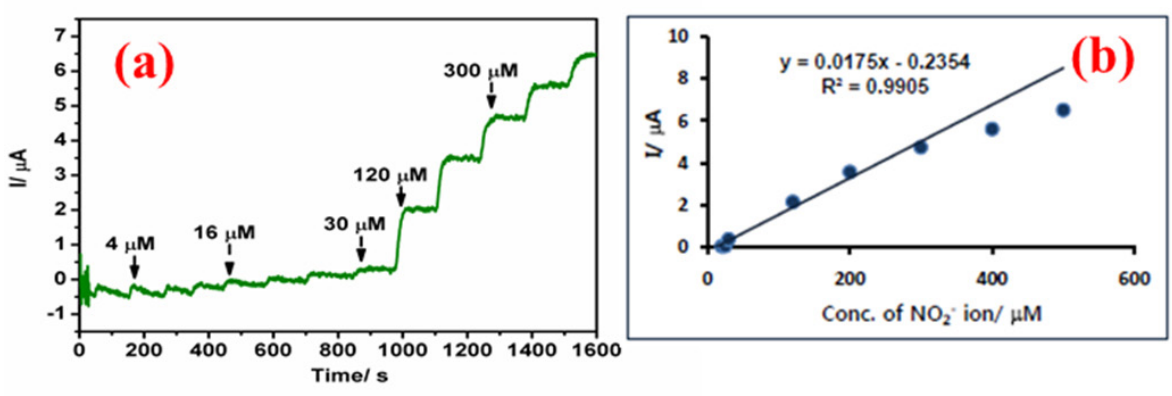

FIG. 11. (a) Current time plot of PVDF@silica/Au NP/Cyt C electrode for successive addition of nitrite ion in phosphate buffer (0.1M) (pH7.0) at +0.6 V. (b) Calibration plot.

which originates from the presence of silica and Au NPs in PVDF@silica/Au NP NW. The presence of silica in the PVDF@silica/Au NP/Cyt C NW electrode improves immobilization of Cyt C. In addition, Au NPs provide electrical connectivity for the transfer of electrons from Cyt C to the electrode surface. As a result, the PVDF@silica/Au NP electrode exhibited a good bioelectrocatalytic performance.

The current time plot recorded at the PVDF@silica/Au NP/Cyt C electrode for successive addition of nitrite ion with a working potential of +0.6 V is shown in Fig. 11. The PVDF@silica/Au NP/Cyt C electrode exhibited a rapid and sensitive current response to the changes in nitrite ion concentration. Figure 11(b) shows that the current varies linearly in a calibration plot of response current versus concentration of nitrite ions. The regression equation reveals a concentration range for nitrite ion detection from 2μM to 300μM, with a correlation coefficient of 0.9905 (n = 10). The sensitivity of nitrite at the PVDF@silica/Au NP electrode is 0.0175 μA/μM.

4. CONCLUSION

The functional conductive NW, PVDF@silica/Au NP/Cyt C NW, was successfully prepared by sequential steps: electrospinning, γ radiation induced reduction of gold ions and immobilization of the enzyme Cyt C. FESEM images, EDAX and XRD of the PVDF-Si@Au NP NW revealed the morphology and microstructure. The PVDF@silica/Au NP modified electrode was fabricated and used for bioelectrocatalytic determination of nitrite ion. The PVDF-Si@Au NP/Cyt C NW modified electrode exhibited a high electroactivity and direct electron transfer

between Cyt C and the electrode. Amperometric responses of the nitrite ion modified electrode were recorded for PVDF-Si@Au NP/Cyt C NW. Multifunctional electrospun membranes are expected to find applications in sensors and electrocatalysis.

REFERENCES

[1] LEE, K.P., PARK, J.W., GOPALAN, A.I., RAGHUPATHY, D., MANESH, K.M., Fabrication and properties of poly(vinylidenefluoride)/PdS/Au heterogeneous nanostructures, J. Nanosci. Nanotechnol. **9** (2008) 15.

[2] DU, C.H., ZHU, B.K., XU, Y.Y., A study on the relationship between the crystal structure and hard elasticity of PVDF fibres, Macromol. Mater. Eng. **290** (2005) 786.

[3] DEMIR, M.M., GULGUN, M.A., MENCELOGLU, Y.Z., Palladium nanoparticles by electrospinning from poly(acrylonitrile-co-acrylic acids)-$PdCl_2$ solutions: Relations between preparation conditions, particle size, and catalytic activity, Macromol. **37** (2004) 1787.

[4] BRUST, M., WALKER, M., BETHELL, D., SCHIFFRIN, D.J., WHYMAN, R., Synthesis of thiol-derivatised gold nanoparticles in a two-phase liquid-liquid system, J. Chem. Soc. Chem. Commun. (1994) 801.

[5] KOMATHI, S., GOPALAN, A.I., LEE, K.P., Covalently linked silica-multiwall carbon nanotube-polyaniline network: An electroactive matrix for ultrasensitive biosensor, Biosensor. Bioelectron. **25** (2009) 944.

[6] TONELLI, A.E., Nanostructuring and functionalizing polymers with cyclodextrins, Polym. **49** (2008) 1725.

[7] BUCKLEY, J., et al., Nanocomposites of poly(vinylidene fluoride) with organically modified silicate, Polym. **47** (2006) 2411.

[8] PRIYA, L., JOG, J.P., Intercalated poly(vinylidene fluoride)/clay nanocomposites: structure and properties, Polym. Sci. Part B: Polym. Phys. **41** (2003) 31.

[9] LINARES, A., ACOSTA, J.L., Pyro-piezoelectrics polymers materials—I. Effect of addition of PVA and/or PMMA on overall crystallization kinetics of PVDF from isothermal and non-isothermal data, Eur. Polym. J. **31** (1995) 615.

[10] SHAH, D., et al., Dramatic enhancements in toughness of polyvinylidene fluoride nanocomposites via nanoclay-directed crystal structure and morphology, Adv. Mater. **16** (2004) 1173.

[11] EL-DEAB, M.S., On the preferential crystallographics orientation of Au nanoparticles: Effect of electrodeposition time, Electrochim. Acta. **54** (2009) 3720.

[12] HOU, Z.N., ABBOTT, L., STROEVE, P., Electroless gold as a substrate for self-assembled monolayers, Langmuir **14** (1998) 3287.

[13] KIM, Y.J., AHN, C.H., CHOI, M.O., Effect of thermal treatment on the characteristics of electrospun PVDF-silica composite nanofibrous membrane, Eur. Polym. J. **46** (2010) 1957.

RADIATION SYNTHESIS OF PEGDA AND APO NANOSIZED GELS FOR BIOACTIVE IMMOBILIZATION

M.Y. HAMZAH, R. TAJAU, M. ZAH SALLEH, N. MAT ISA, K. HASHIM
Malaysian Nuclear Agency
43000 Kajang, Selangor
Malaysia

Abstract

The use of microemulsions in the development of nanosized gels based on PEGDA and APO is demonstrated. PEGDA was solubilized in n-heptane using AOT at 0.15M concentration to form reverse micelles, while APO was solubilized with SDS in water to form direct micelles. Both of these systems were depicted by means of ternary phase diagrams. These micelles were then irradiated at 1 kGy, 3 kGy, 5 kGy, 10 kGy, 15 kGy and 30 kGy using γ irradiation or EB radiation to cross-link the entrapped polymer in the micelles. Ionizing radiation was imparted to the emulsions to generate cross-linking reactions in the micelles that were formed. The nanosized gel was evaluated in terms of particle diameter using DLS, and the images of the nanosized gel were studied using TEM. Results showed that the size, charge and shape of the particles were influenced by the concentration of surfactants and the radiation dose. The current study has shown that this method can be utilized to produce nanosized gels.

1. METHOD A: SYNTHESIS OF PEGDA NANOGEL USING IRRADIATION OF INVERSE MICELLES

Application of nanogels in biomedical fields have been a subject of interest in recent years owing to the extensive development of bioactive materials. While nanogels are used for targeting specific cell types, they are also known to act as a protection layer to the bioactive macromolecules contained from enzymatic degradation [1]. There are various possible ways to synthesize nanogels, including classical chemistry [2, 3] and radiation [4]. The latter has been proven to be advantageous in terms of safety of use in biomedical applications owing to the non-involvement of hazardous chemical additives. This work is aimed at synthesizing nanogels from irradiation of water in oil micelles from PEGDA in n-heptane.

Inverse or reverse micelles are microemulsions of three or more components. The external part of inverse micelles is formed of the more hydrophobic portion of a surfactant (hydrocarbon), while the more hydrophilic (polar or charged) fragment forms the internal part of the aggregate. The system can be applied to impregnate hydrophilic polymers, which is useful for synthesis of nanopolymeric gel. The final size of the inverse micelles can be adjusted by varying the molar ratio of water to surfactant. The more surfactant that is used, the smaller the micelles will be, owing to suppression of the hydrophobic part of the surfactant inside the aggregates.

1.1. Preparation of inverse microemulsions

Emulsions were prepared by dissolution of PEGDA in ultrapure water, stirred and filtered with 0.45 μm filters (Minisart, Sartorius). To 100 mL of n-heptane containing 0.05M–0.25M of AOT, 10 mL of PEGDA was added. The size of the micelles in the emulsion was measured using DLS and TEM. In this work, the emulsion with the smallest micelles was used (Fig. 1).

1.2. Irradiation of inverse micelles containing PEGDA

The mixture mentioned above was then irradiated at 1 kGy, 3 kGy, 5 kGy, 10 kGy, 15 kGy, 20 kGy and 25 kGy with 3 MeV of voltage and 5 mA of beam current (Fig. 2). All the mixtures were saturated with argon gas prior to irradiation. The nanosized gel formed during the irradiation process was then recovered by evaporation of n-heptane using a rotary evaporator and precipitation of the dry mass with a mixture of acetone and methanol (9/1). The precipitate was washed five times with the acetone/alcohol mixture to remove excess AOT. The nanosized gel was than measured using DLS (Fig. 3).

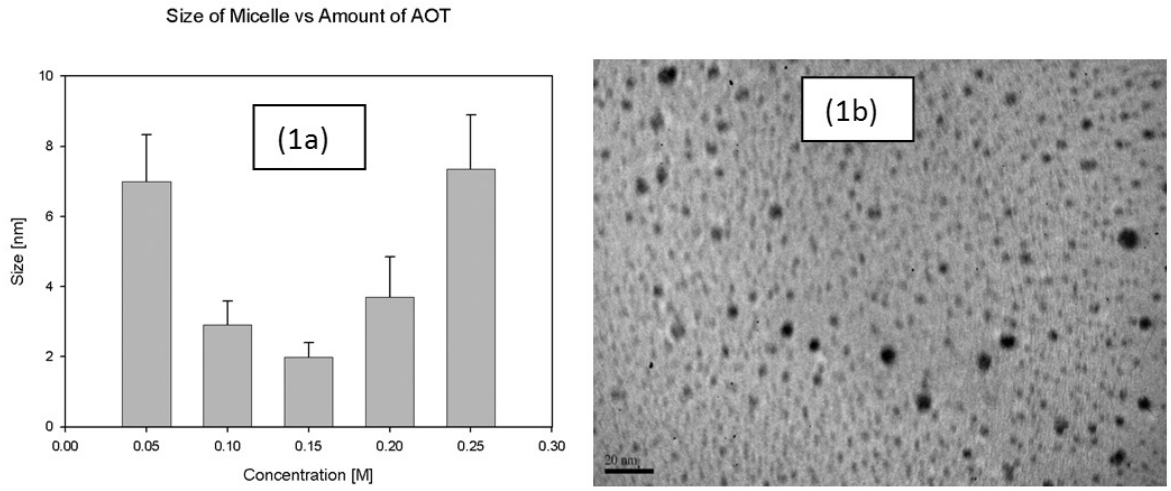

FIG. 1. (a) Effect of AOT concentration on micelle size. (b) TEM image of micelles at 0.15M surfactant.

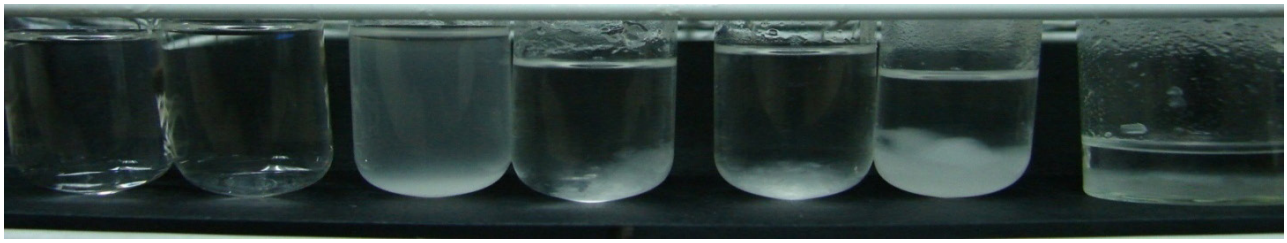

FIG. 2. Products of 10% PEGDA in 0.15 M of AOT in n-heptane microemulsion irradiated with an EB at 1 kGy, 3 kGy, 5 kGy, 10 kGy, 15 kGy, 20 kGy and 25 kGy (from left to right).

There was no physical change observed when the microemulsions were irradiated with an EB at 1 kGy and 3 kGy. DLS measurement for these samples showed no gel was formed because the particle count rate was too low. When the sample was irradiated at 5 kGy, a cloudy liquid was formed. However, as the irradiation power was increased to 10 kGy, 15 kGy, 20 kGy and 25 kGy, precipitations were observed at the bottom of the vessels (Fig. 2).

Figures 4 and 5 show TEM images of the nanosized gel obtained from irradiation of the inversed micelle of PEGDA.

1.3. Static light scattering study

Average MW data from a static light scattering study indicates that the micrometre sized gels' average MWs increased from 775 g/mol to 5.87×10^5 g/mol as the irradiation dose was increased from 0 kGy to 25 kGy (Fig. 6).

Increases in MW as irradiation dose increased were also observed by Akira et al. [5, 6], where the increase in MW was attributed to particle nucleation from the propagation of monomer swollen micelles. The same was also observed by Thomas et al. [7] and Wang et al. [8], where intermolecular cross-linking was found to be predominant. Ming et al. [9] reported that an increase in the MW of the resulting microgels was caused by interparticle agglomeration.

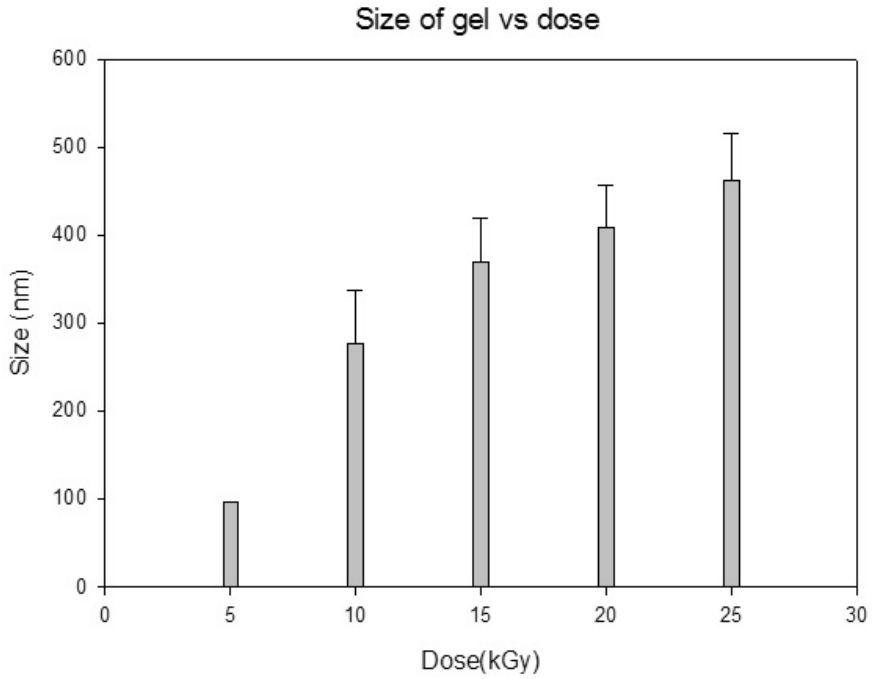

FIG. 3. Gels were formed at 5 kGy and above; size increases were observed at higher doses.

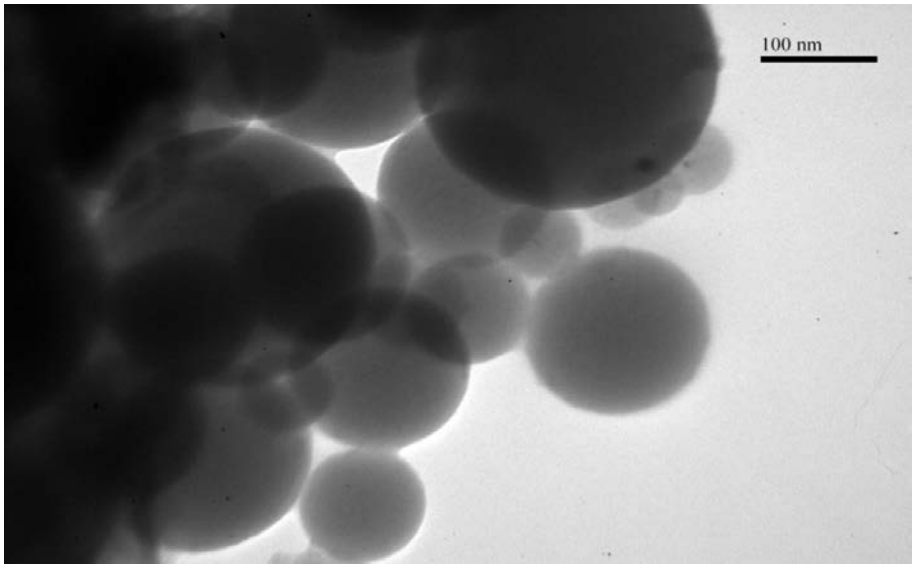

FIG. 4. TEM image of nanosized gel at 5 kGy (30 000×).

1.4. Curcumin loading and release study

Curcumin was added to PEGDA nanogel and later lyophilized. A mass of 100 mg of the lyophilized sample was then resuspended in a PBS solution at pH7.4 in several centrifuge tubes and later centrifuged at predetermined intervals of time. The release amount of curcumin was determined spectrophometrically, and its release profile is shown in Fig. 7. It was observed that within 1 h, more than 80% of the drug had been released.

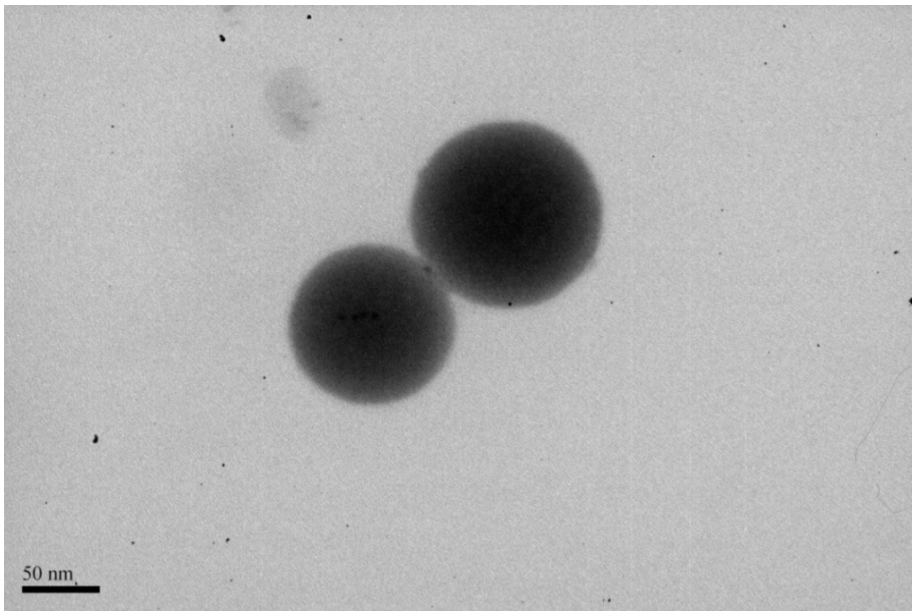

FIG. 5. TEM image of nanosized gel at 5 kGy (40 000×).

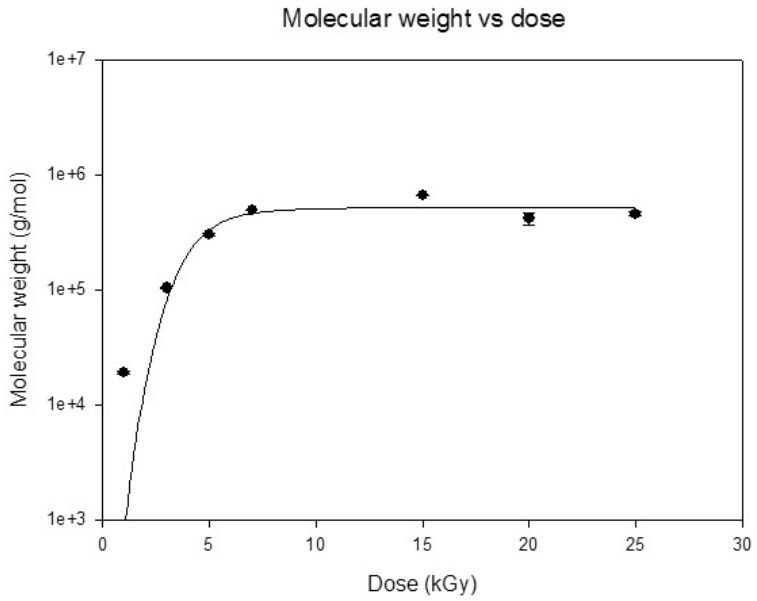

FIG. 6. Relationship between average MW of PEGDA microgels and dose.

2. METHOD B: SYNTHESIS OF NANOSIZED GEL FROM APO MICROEMULSION USING RADIATION

Various nanostructure polymers have been devised in drug delivery research. Over the past few decades and with advances in nanoscience and nanotechnology, researchers have shown an interest in developing biodegradable NPs as drug delivery devices. In this case, natural polymers, such as vegetable oils (palm oil and soybean oil), are potential materials and have been used to synthesize NPs. The NPs in the form of micellar solutions consisting of small particles of 10–400 nm diameter, called polymeric micelles, have shown great promise as potent vehicles for controlled drug delivery [10].

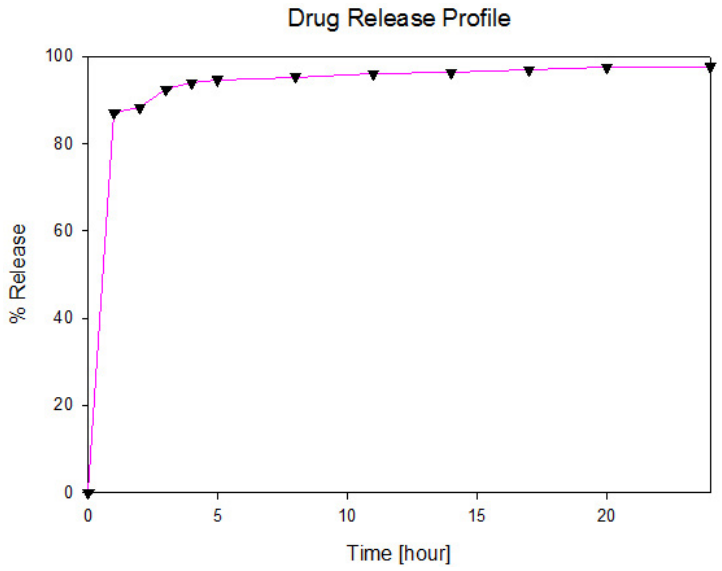

FIG. 7. Curcumin release profile from PEGDA nanogel.

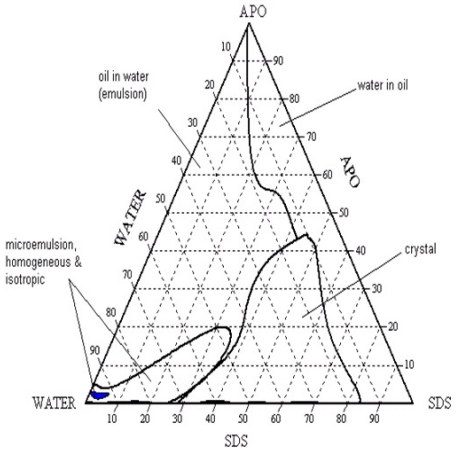

FIG. 8. Ternary phase diagram of water/SDS/APO.

2.1. Preparation of the microemulsion

The micellar system was prepared based on oil in water and was created using a ternary phase and solubilization diagrams. The solubilizations of these three basic components, i.e. oil (APO), water and surfactant, were observed to determine the microemulsion/nanoemulsion regions illustrated in Fig. 8.

Different concentrations of APO (~2% and ~0.2%) with different concentrations of the surfactant (above and below the SDS critical micelle concentration region) in an aqueous solution were prepared. These samples were used for size and stability measurements.

Two main properties of APO in water systems (water/SDS/APO) have been found. The first property is known as an emulsion, shown in Fig. 9(a). Emulsions can be described as unstable solutions and have been visualized as two layer phases. In this system, the emulsions undergo coalescence and creaming. When the APO concentration is lower, the system forms microemulsions (Fig. 9(b)). Its appearance can be determined as the solution that has a lower amount of polymer content. These microemulsions were then used for further analysis.

(a)

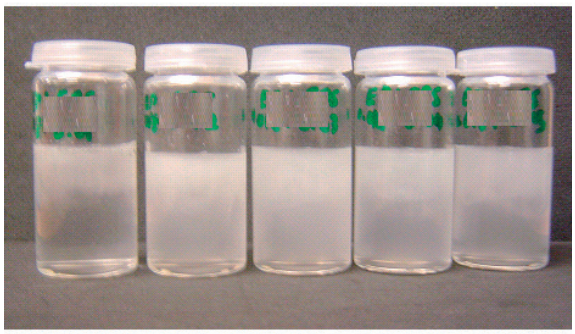

(b)

FIG. 9. Solubilization images of the water/SDS/APO systems: (a) emulsion systems and (b) microemulsion systems.

2.2. Particle sizing

The samples were filtered using a disposable polytetrafluorethylene Teflon filter for removing suspended materials and impurities. The sizes of the micelles were determined by photon cross-correlation spectroscopy using a dynamic light scatterer (Sympatec Nanophox) at a wavelength of 632 nm.

2.3. Radiation synthesis of NPs

Subsequently, the micelles, which were in the form of microemulsions, were irradiated at different doses using γ radiation at 1 kGy, 5 kGy, 10 kGy, 15 kGy and 25 kGy. After irradiation, the irradiated micelles were subjected to size determination.

2.4. TEM

TEM was performed using a Zeiss microscope (JEOL, Japan) at 120 keV, with a magnification of 30 000× for the measurement of emulsion sizes (before irradiation) and gel sizes (after irradiation). Figure 10 shows the effect of surfactant concentration. In this case, 0.008M SDS is simply not enough to separate the APO, while addition of 0.01M SDS is adequate for forming good micelles.

Figure 11 shows the effect of irradiation at 25 kGy of the APO emulsion at 0.008M and 0.01M of SDS. The use of the surfactant gives better results in the formation of the nanosized gel, where a more defined gel was obtained with a higher amount of surfactant.

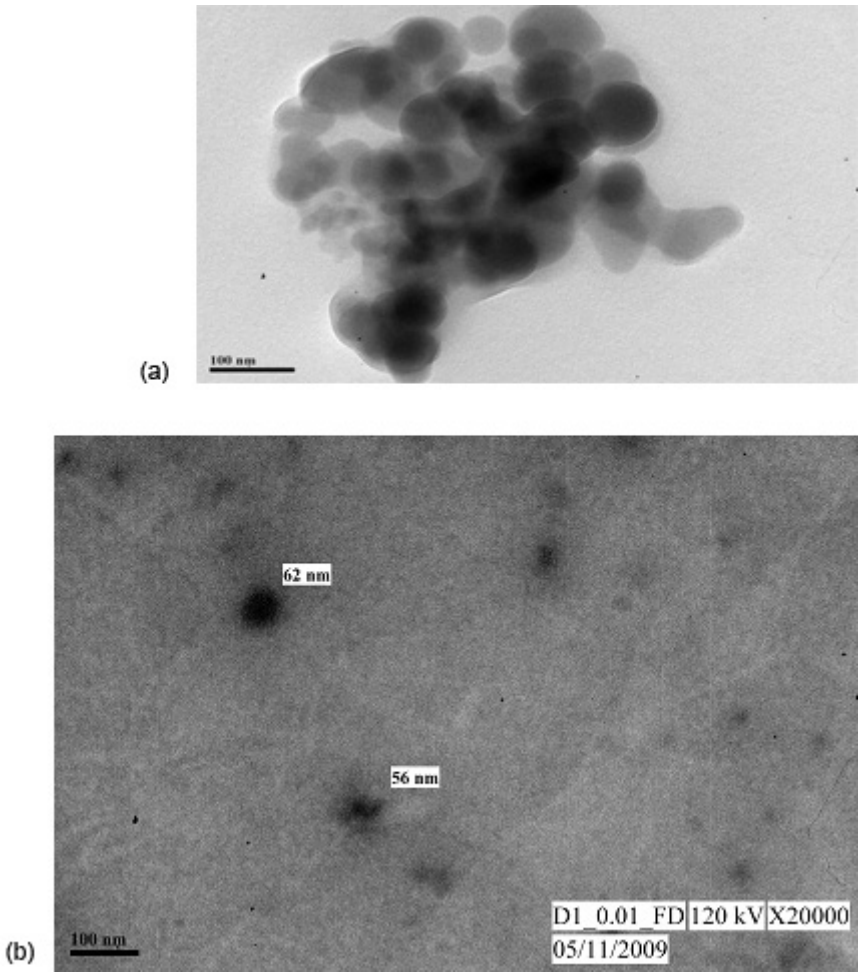

FIG. 10. (a) Water/SDS 0.008M/1.8% APO emulsion image. (b) Water/SDS 0.01M/1.8% APO emulsion image. Both at 120 keV, 30 000×.

2.5. Release profile of a drug, thymoquinone, from thymoquinone loaded APO NPs

Approximately 1 L of 0.2 mol of the PBS solution was prepared at pH7.4 as a medium for a thymoquinone release study. The calibration plot of thymoquinone in the PBS solution was analysed using a UV spectrophotometer (Shimadzu, Japan) at a wavelength of 258 nm. Approximately 0.01 g of the dried samples from the thymoquinone/SDS/APO matrices was poured into 1 L flasks, followed by 500 mL of 0.2 mol PBS solution. Then, the flasks were put into the water bath and stirred with the temperature set at 37°C. The water bath was equipped with stirrers, and the speed was set at 100 rev./min. Then, about 10 mL of the sample was taken from the solution at times of 1 min, 3 min, 5 min, 30 min, 45 min, 60 min, 120 min, 240 min, 360 min and 1440 min. Every 10 mL of the sample taken was refilled by 10 mL of 0.2 mol PBS solution. Then, the samples were analysed using the UV spectrophotometer at a wavelength of 258 nm to obtain the absorbance maximum peak value. The amount of thymoquinone release from the thymoquinone loaded APO NP was calculated based on the calibration plot. The percentage of thymoquinone release was calculated in accordance with the following equation:

$$\text{drug release (mg)} = (m_t/m_\infty) \times 100 \quad (1)$$

where m_t is the amount of drug release in time t and m_∞ is the maximum release.

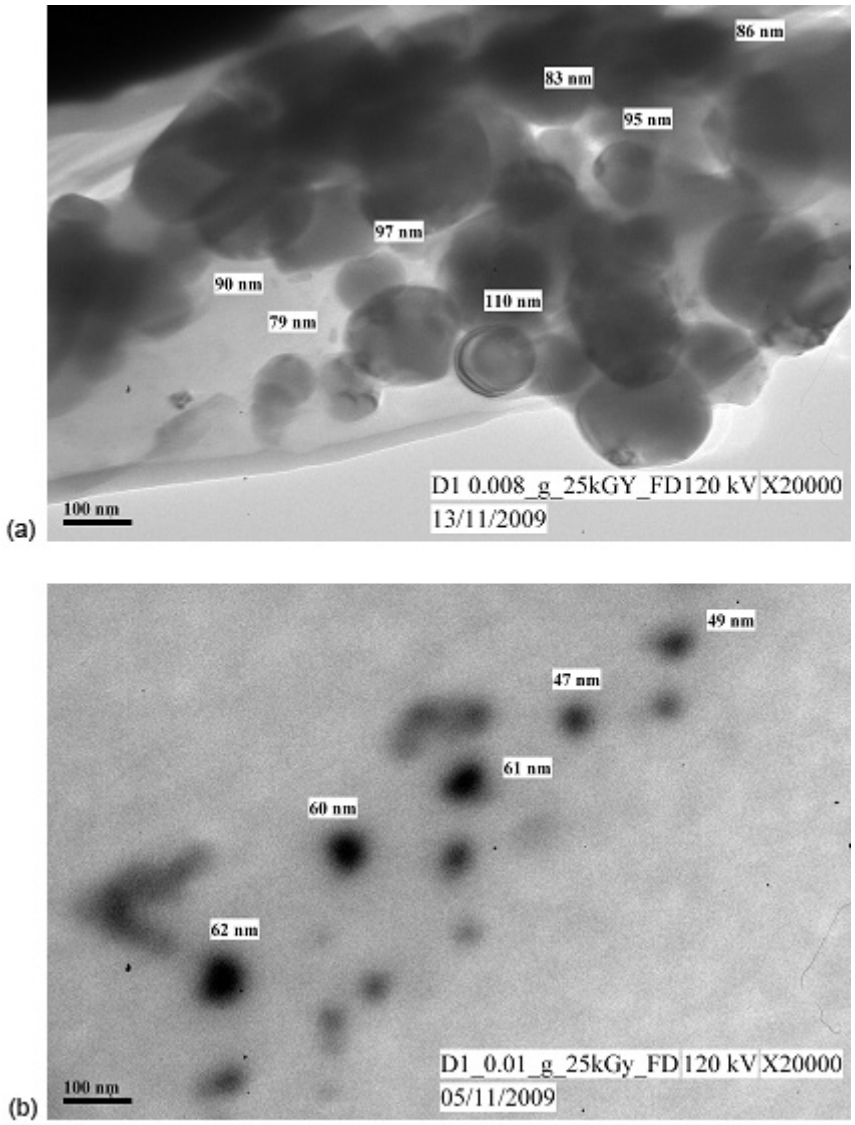

FIG. 11. (a) Water/SDS 0.008M/1.8% APO emulsion image and (b) water/SDS 0.01M/1.8% APO gel image (after irradiation at 25 kGy). Both at 120 keV, 20 000×.

2.6. Thymoquinone release profile from thymoquinone loaded APO NPs

Figure 12 shows the release profile of the thymoquinone. The thymoquinone release rate was found to be directly proportional to the size of the thymoquinone loaded APO NPs (Fig. 12). In this study, the two different sizes of the thymoquinone loaded APO NPs were irradiated at different doses of γ irradiation, i.e. the particle size of 117 nm was irradiated at 25 kGy, whereas the particle size of 198 nm was irradiated at 5 kGy. It is believed that the size of the APO NPs and the absorbed dose (5 kGy and 25 kGy) played a major role in controlling the release rate of the thymoquinone from the SDS/APO NP. A larger particle size of 198 nm showed a faster release of thymoquinone compared to that of smaller particles (see Fig 12). Therefore, the study also revealed that smaller particles (117 nm) retained and showed slow release of the active substance compared to the larger particles (198 nm) (see Fig. 12). Thus, the smaller particles (irradiated at 25 kGy) showed the compactness and tight cross-linking of a molecular structure network that allowed the structure to hold the thymoquinone compared to the larger particles (irradiated at 5 kGy), which showed a loose networking structure that prevented them from effectively holding the bioactive material. In addition, smaller particles give rise to larger surface areas, which allows the structure to increase the molecular payload.

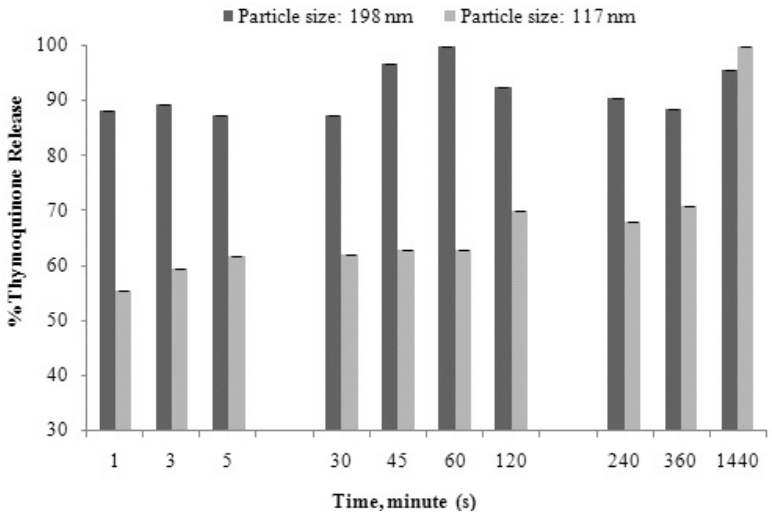

FIG. 12. Release profile of thymoquinone from thymoquinone loaded APO/SDS NPs.

3. CONCLUSION

PEGDA and APO nanogels can be produced via irradiation of micelles containing the respective polymers, and the size and MW of the gels can be controlled by varying the irradiation dose. Curcumin can be loaded into the PEGDA nanogel, but 80% of the drug was released within 1 h. Thymoquinone can be absorbed and released by the APO nanogel. The nanogel with smaller particle sizes gave a sustained release, while the nanogel with larger particle sizes released most of the drug during the initial time period (burst effect).

REFERENCES

[1] DODANE, V., KHAN, M., MERWIN, J.R., Effect of chitosan on epithelial permeability and structure, Int. J. Pharm. **182** (1999) 21.

[2] MONA, G., AJAY, K.G., In vitro cytotoxicity studies of hydrogel pullulan nanoparticles prepared by AOT/n-hexane micellar system, J. Pharm. Pharm. Sci. **7** (2004) 38.

[3] McALLISTER, K., et al., Polymeric nanogels produced via inverse microemulsion polymerization as potential gene and anti sense delivery agent, J. Am. Chem. Soc. **124** (2002) 15 198.

[4] ULANSKI, P., ROSIAK, J.M., The use of radiation technique in the synthesis of polymeric nanogels, Nucl. Instrum. Methods Phys. Res., Sect. B **151** (1999) 356.

[5] AKIRA, M., KUNIHIRO, K., YASUYOSHI, M., HIROYUKI, A., Emulsion crosslinking polymerization of allyl methacrylate, J. Macromol. Sci., Part A: Pure Appl. Chem. **35** (1998) 1459.

[6] AKIRA, M., KUNIHIRO, K., HIROYUKI, A., IGNAC, C., Kinetics of emulsion crosslinking polymerization and copolymerization of allyl methacrylate, Eur. Polym. J. **35** (1999) 1509.

[7] THOMAS, S., et al., Pulsed electron beam irradiation of dilute aqueous poly(vinyl methyl ether) solutions, Polym. **46** (2005) 9908.

[8] WANG, B., HONG, Y., FENG, J., GONG, Y., GAO, C., Rings of hydrogel fabricated by a micro-transfer technique, Macromol. Rapid. Commun. **28** (2007) 567.

[9] MING, W., JONES, F.N., FU, S.K., Synthesis of nanosize poly (methyl methacrylate) micro latexes with high polymer content by a modified micro emulsion polymerization, Polym. Bull. **40** (1998) 749.

[10] KAPARISSIDES, C., ALEXANDRIDOU, S., KOTTI, K., CHAITIDOU, S., Recent advances in novel drug delivery systems, J. Nanotechnol. Online **2** (2006) 1.

POLYMERIC NANOGELS AND NANOLAYERS OBTAINED BY RADIATION TECHNIQUES

P. ULANSKI, S. KADŁUBOWSKI, A. HENKE, A.K. OLEJNIK, B. ROKITA, R. WACH, J.M. ROSIAK
Institute of Applied Radiation Chemistry
Technical University of Lodz
Wroblewskiego 15, 93590 Lodz
Poland

Abstract

Ionizing radiation is a valuable tool to synthesize nanomaterials for biomedical applications. The report concerns two kinds of nanomaterials: polymer nanogels and thermosensitive nanolayers. The radiation method of nanogel synthesis by intramolecular cross-linking, invented by our team in the late 1990s and described in previous patents and papers, is subject to further optimization and development. Here, two approaches are described which make it possible to obtain nanogels of predefined size and, independently, predefined weight. The first procedure consists of two steps. In the first step, where intermolecular cross-linking prevails, the desired molecular weight is reached, while in the second step, consisting of intramolecular cross-linking, the size is adjusted. The second procedure makes it possible to achieve control over cross-link density by adjusting the way in which dose is delivered to the system (simultaneous or step-wise free radical generation). In these two ways the coil density of nanogels can be controlled. In addition to nanogels, radiation technique can be used to synthesize thin thermosensitive surfaces that allow cultivation of cell sheets (e.g. fibroblast layers used in burn wound treatments) and subsequent spontaneous detachment of the cell layer triggered by a mild temperature change. While the idea of synthesizing such surfaces by radiation grafting of N-isopropylacrylamide was postulated in early 1990s, no fully functional product has been achieved so far. The ongoing attempts described in this work, using the original concept but a different class of polymers and a different grafting procedure, have led to promising results (i.e. surfaces characterized by relatively fast temperature triggered detachment of fibroblast sheets).

1. INTRODUCTION

Nanogels, consisting of cross-linked particles of less than 100 nm size made of hydrophilic polymers, are considered in addition to linear, branched, comb like, dendritic, etc., polymers as a distinct topological class of macromolecules [1, 2]. Such structures, along with their bigger analogues — microgels — are tested for a number of practical applications, starting from fillers in a coating industry to 'smart' drug delivery systems [3] and vectors for gene therapy [4].

First reports regarding microgels date from the 1930s when Staudinger et al. [5] described the formation of styrene divinylbenzene microgel. Since then, hundreds of reports (e.g. [6]) have been published on this topic, and a multitude of techniques for the synthesis of microgels and nanogels have been developed to obtain microgels of different chemical structures, architectures and properties. These methods can be divided into two groups: the first one comprises techniques based on simultaneous polymerization and cross-linking, where the substrates are monomers or their mixtures, and the second one comprises methods based on intramolecular cross-linking of macromolecules where the starting material is not a monomer but a polymer [7].

One example of the latter group is radiation induced intramolecular cross-linking, also called preparative pulse radiolysis. In this approach, a pure aqueous solution of a polymer is subjected to a short (few microseconds), intense, pulse of ionizing radiation. In this way, many radicals are generated simultaneously along each polymer chain, and their intramolecular recombination leads to the formation of nanogels. This approach was first tested on the neutral water soluble polymer PVA [8]. A slight increase in MW (owing to a small contribution of intermolecular cross-linking) was accompanied by a decrease in the dimensions of the polymer coils (i.e. R_g) and the solution viscosity. These coil shrinkage effects, analogous to those reported by Brasch and Burchard [7], are interpreted to be as a result of intramolecular cross-linking. Recently, the same method has been applied to obtain nanogels of PVP [9], poly(vinyl methyl ether) [10] and PAAc [11, 12]. A drawback of this method is that it does not allow easy synthesis of nanogels of independently chosen MWs and dimensions.

One of the main goals of the work in this CRP was to find a way to overcome this limitation. A method of radiation induced synthesis of nanogels to obtain tailored internally cross-linked macromolecules of independently

chosen MWs and dimensions [13] (or, in other words, nanogels of a preselected coil density) is presented. This goal was attained by employing a two stage process involving γ radiation and subsequent EB irradiation.

2. SYNTHESIS OF TAILORED NANOGELS BY MEANS OF TWO STAGE IRRADIATION

Irradiation of a cross-linkable polymer (such as PVP) in an oxygen free solution at high or moderate concentrations at a low dose rate leads, in most cases, to intermolecular cross-linking. This is evidenced by increases in average MW and the size of macromolecules and, above the gelation dose, by formation of permanent, macroscopic gel. When irradiation is stopped before the gelation dose, the only polymeric structures present in solution are branched macromolecules of higher MW and size than the parent linear chains. This situation is schematically represented in Fig. 1. If, subsequently, this solution is diluted below the chain overlapping concentration, and irradiated in the pulsed mode by EB, the number of radicals generated by each pulse on every macromolecule is now much higher than one. This allows for intramolecular recombination, leading to a significant reduction in molecular dimensions because of additional bonds formed between the chain segments, while the MW does not change significantly [9–12]. This results in the formation of nanogels (Fig. 1(d)).

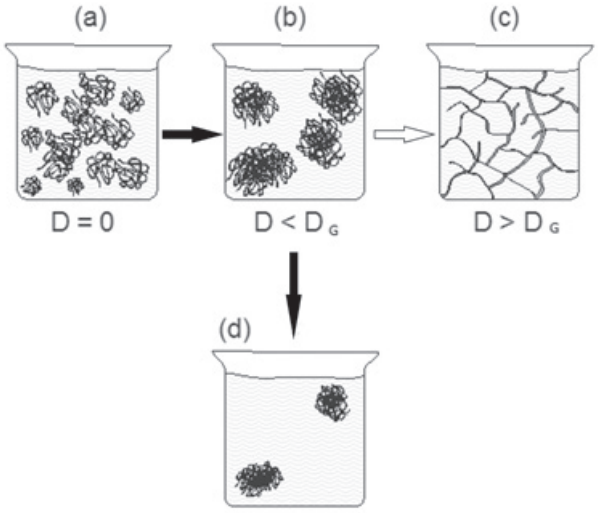

FIG. 1. Schematic representation of two stage synthesis of nanogels: (a) polymer solution with concentration higher than the critical one (chains do overlap), (b) polymer solution as in (a) after γ irradiation below the gelation dose, (c) polymer solution as in (a) irradiated with a dose higher than the gelation dose (formation of a gel), (d) polymer solution as in (b), irradiated by electron pulses: formation of nanogels [13].

Changes in weight averaged MW and R_g during the above described two step synthesis are shown in Figs 2 and 3, respectively.

During γ irradiation (i.e. the first step of the synthesis), increases in MW and R_g can be observed as a result of intermolecular recombination. Based on viscosity measurements, the overlapping concentration for the parent PVP is equal to 0.036 mol/L. The concentration of the polymer used for γ irradiation (0.4 mol/L) was thus 11 times higher than the critical one. Under these conditions (low dose rate of 1.5 kGy/h), the average number of radicals present simultaneously on each chain was lower than 0.001. This is why radicals recombine with the formation of intermolecular bonds (Fig. 1(b)).

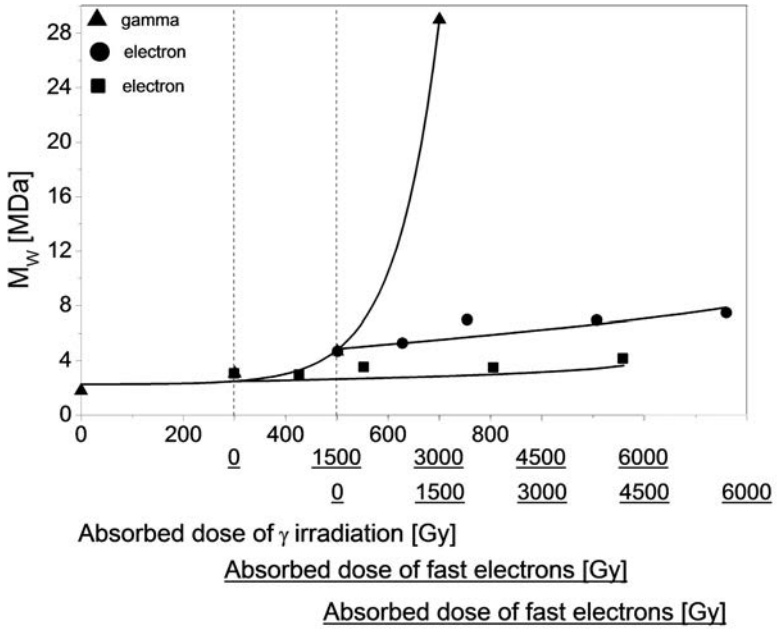

FIG. 2. Changes in weight averaged MW of PVP as a function of absorbed dose.▲: γ irradiation at a dose rate of 1.5 kGy/h, [PVP] = 0.4 mol/L, solution saturated with N_2O; ●, ■: irradiation with pulses of electrons (dose per pulse = 950 Gy, pulse duration = 2 μs), [PVP] = 15 mmol/L, solution saturated with N_2O; ■: sample initially γ irradiated with a dose of 300 Gy; ●: sample initially γ irradiated with a dose of 500 Gy [13].

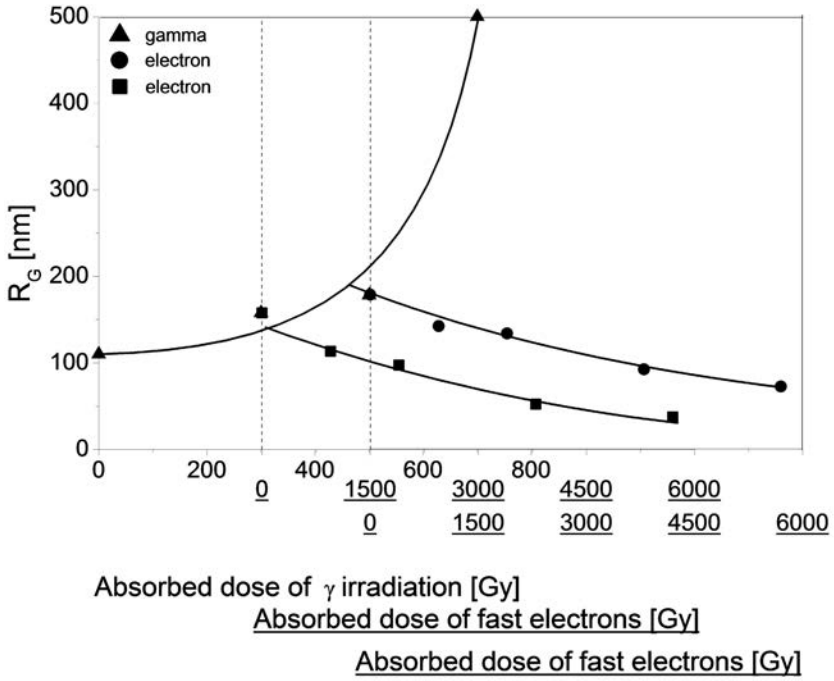

FIG. 3. Changes in z-averaged Rg of PVP as a function of absorbed dose. ▲: γ irradiation at a dose rate of 1.5 kGy/h, [PVP] = 0.4 mol/L, solution saturated with N_2O; ●, ■: irradiation with pulses of electrons (dose per pulse = 950 Gy, pulse duration = 2 μs), [PVP] = 15 mmol/L, solution saturated with N2O; ■: sample initially γ irradiated with a dose of 300 Gy; ●: sample initially γ irradiated with a dose of 500 Gy.

To test the two step procedure, in two series of experiments, it was decided to run γ irradiation (first step) up to doses of 300 Gy and 500 Gy. The sample that was γ irradiated at a dose of 300 Gy contained PVP of MW = 3.00 MDa and R_g = 158 nm, while the sample irradiated with a dose of 500 Gy led to PVP of MW = 4.68 MDa and R_g = 178 nm.

After 26-fold dilution (down to [PVP] = 15 mmol/L), each of these samples was irradiated with pulses of fast electrons from the accelerator (dose per pulse = 950 Gy). At these conditions, more than 100 radicals were generated at each PVP chain by each pulse. In the second step of irradiation, for a solution initially γ irradiated with 300 Gy, almost no change in MW could be observed upon pulse irradiation: the MW change was less than 0.2 kDa/kGy. At the same conditions but for the sample initially γ irradiated with 500 Gy, the increase in MW during pulse irradiation was somewhat more pronounced, but also very moderate when compared with an identical sample irradiated by γ rays beyond the initial dose of 500 Gy.

On the other hand, as expected, pulse irradiation of both samples (γ irradiated at 300 Gy and 500 Gy) caused pronounced decreases in R_g. For the polymer initially γ irradiated with a dose of 300 Gy, the value of R_g decreased by more than four times (for the highest applied dose, i.e. 5.7 kGy). One should note that the final molecular dimensions of the product nanogel (38 nm) were much smaller than the size of the initial coil (158 nm), while the final MW was approximately twice as high as the initial one. This indicates that, as expected, the nanogels formed had much higher coil densities than the starting non-cross-linked coils of the parent PVP.

Concluding, the proposed two step synthesis procedure, consisting of low dose rate irradiation of a semiconcentrated polymer solution followed by pulse irradiation of its diluted solution, allowed polymeric nanogels of controlled properties to be obtained. The average MW and dimensions of the products may be independently controlled by proper choice of dose and polymer concentration in both stages. The method allows synthesis of nanogels of desired properties in a pure polymer/water system, eliminating the use of monomers, cross-linking agents or other auxiliary substances. A more detailed discussion can be found in Ref. [13].

3. SYNTHESIS OF PVP/PAAc NANOGELS BY RADIATION INDUCED CROSS-LINKING OF THEIR HYDROGEN BONDED COMPLEXES IN DILUTE AQUEOUS SOLUTION

Another group of nanometric polymeric systems investigated during the project were hydrogen bonded IPCs, which represent a class of pH sensitive materials with broad potential applications in the field of pharmaceuticals [14]. Extensive studies on the biomedical applications of IPCs were reported, for example, by Peppas and co-workers [15].

For the preparation of hydrogen bonded IPCs, PVP (Kollidon, BASF) of weight averaged MW = 650 kDa and two PAAcs of MW = 5 kDa (Polyscience Inc.) and 50 kDa (Aldrich), denoted further as PAA5 and PAA50, respectively, were used.

IPC solutions prepared according to the procedure described by Henke et al. [16] were irradiated at pH2.8, pH3.0 or pH3.4, depending on the polyacid used and the aggregation characteristics of the complexes. The N_2O saturated PVP/PAAc solutions in a glass reactor were irradiated with doses of 2 kGy, 5 kGy, 8 kGy, 10 kGy, 12 kGy and 15 kGy. Covalent stabilization of PVP/PAAc complexes was followed by analysis of the irradiation products by laser light scattering at pH10, as at these conditions, no stable hydrogen bonds are formed between both polymers. Thus, if intracomplex cross-linking did not take place in the system, the MW and the size should remain at the level typical for non-irradiated samples (dose = 0). To limit the influence of the aggregation process, irradiation experiments were performed 24 h after preparation of PVP/PAAc solutions. Changes of MW as a function of absorbed dose for PVP, PAA50 and PVP/PAAc solutions are presented in Fig. 4.

For absorbed dose = 0, aggregates of PVP/PAAc IPCs were unstable at pH10 and disintegrated in individual components, giving values of molar masses in the range 600–800 kDa (single PVP chains). Thus, a considerable increase of MW in PVP/PAAc solutions up to 7.5 kGy was ascribed to intermolecular cross-linking between PVP and PAAc chains within IPC aggregates, which led to the formation of permanent particles with molar masses between 5 MDa (PVP/PAA5) and 15 MDa (PVP/PAA50). Starting from 10 kGy, the MW did not change significantly, indicating that covalent stabilization of IPC particles reached a certain maximum level.

More information concerning stabilization of PVP/PAAc aggregates was provided by the analysis of R_g and R_h changes, both at irradiation conditions (low pH) and at basic pH.

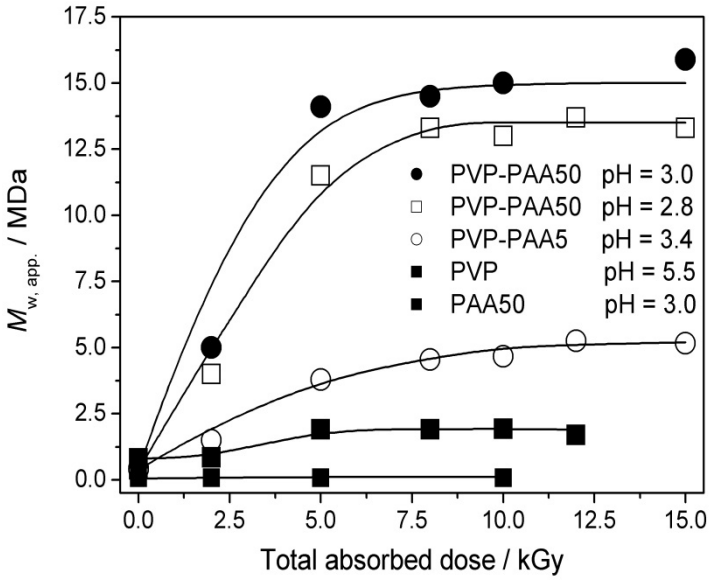

FIG. 4. Changes of the apparent weight averaged MW at pH10 as a function of total absorbed dose by N_2O saturated PVP, PAA50 and PVP/PAAc solutions. pH values in the legend correspond to the irradiation conditions.

As presented in Fig. 5(A), R_g and R_h measured in PVP/PAA50 solutions at pH2.8 remained almost unchanged, regardless of the irradiation dose. This effect resulted from the compact structure of formed particles that limited their further contraction upon intracomplex cross-linking. On the other hand, for the PVP/PAA5 system at pH3.4, R_g and R_h underwent pronounced changes. At the initial stage of the irradiation, i.e. up to 5 kGy, R_h and R_g decreased almost by half and reached values that were typical for single IPC particles. This could be because of two effects. PVP/PAA5 aggregates may have disintegrated partially, probably owing to vigorous solution mixing in the preparative pulse radiolysis experiments. One can also assume that the observed size decrease could be induced by pronounced intracomplex cross-linking. For instance, a twofold decrease of PAAc size upon irradiation of macromolecules in earlier studies [11] was observed. However, as compact particles contain less water in their interior (~50%–60% when compared to 90%–95% in the case of the polymeric coil) [17], it is difficult to predict such a strong contraction of a complex structure upon irradiation. Further irradiation of PVP/PAA5 solutions caused an increase in R_g and an R_g/R_h ratio close to a uniform sphere model (the latter parameter changed from ~0.58 at 0 kGy to ~0.69 at 15 kGy), indicating that cross-linking was taking place in the whole particle volume.

More detailed information on IPC formation can be found in Ref. [16].

4. INFLUENCE OF NUMBER OF RADICALS GENERATED ON MACROMOLECULE SIZE

In addition to characterization of intermolecular cross-linking products, some attempts to discuss mechanisms of nanogel formation have also been carried out. The kinetics of intramolecular recombination was followed. It was found that the decay of radicals in these processes does not follow classical, homogeneous second order kinetics that is typical of intermolecular recombination of radical pairs. When analysed in these classical terms, the rate constant of intrachain recombination, k, decreases during the course of the reaction. This indicates that there is a dispersion of reactivity, and that the dispersion changes in time. Therefore, it was found more appropriate to describe the intramolecular recombination by dispersive kinetics models such as, for example, the model developed by Plonka [18].

During this work, it was found interesting to determine the influence of irradiation conditions on the structure of the products described as distance between meres (mass points) and centre of mass, i.e. R_g.

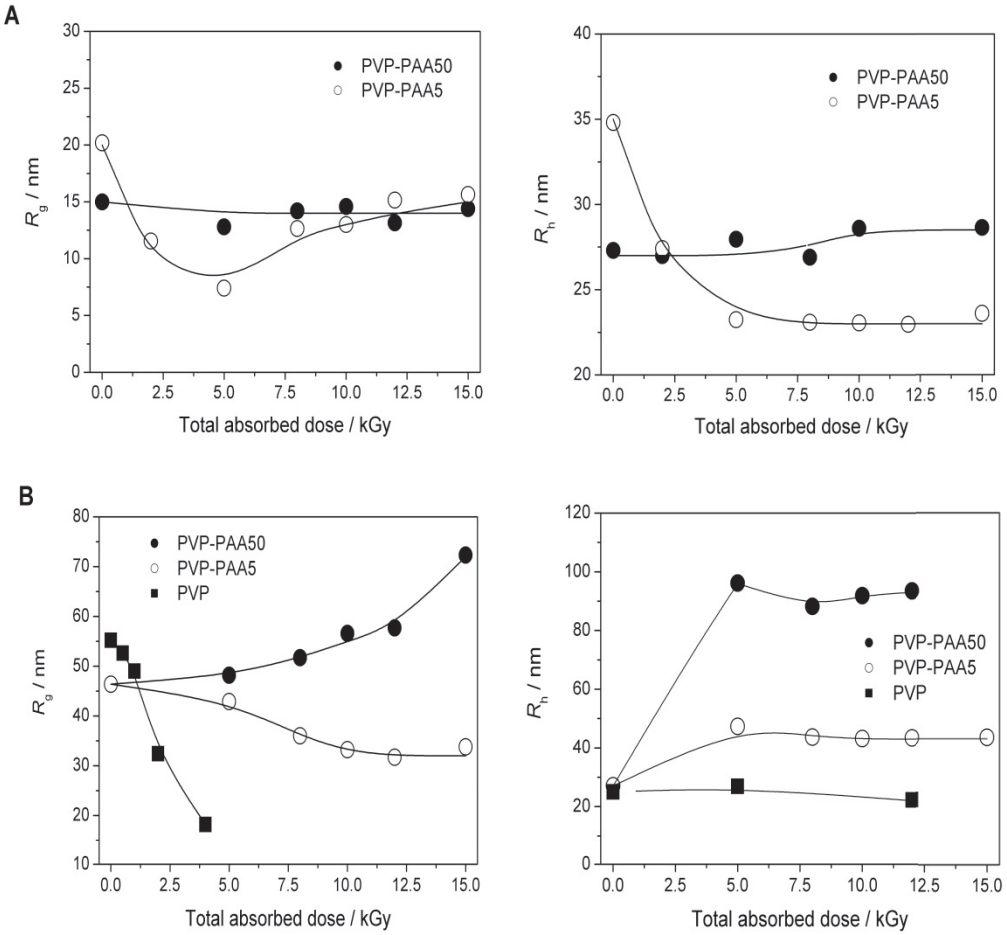

FIG. 5. Changes of R_g (left) and R_h (right) as a function of total absorbed dose, measured at (A) pH2.8 and pH3.4 in N_2O saturated PVP/PAA50 and PVP/PAA5 solutions, respectively, and (B) pH10.

Particularly remarkable is the question of whether single generation of *n* radicals per chain leads to the same product structure as double generation of *n*/2 radicals, or generally *i*-fold generation of *n*/*i* radicals. Computer simulation of this process indicates that there is a dependence of a number of radicals, generated per chain, on the structure of the nanogel, as well as on the number of irradiation cycles *i*. An aim of this part of the work was to experimentally demonstrate the influence of irradiation conditions, mainly dose delivery to the irradiated system, on the structure of the nanogels obtained by radiation induced intramolecular cross-linking.

Changes in weight averaged MW are presented in Fig. 6. Series of data represent doses cumulated from electron pulses of 0.108 kGy, 0.256 kGy, 0.433 kGy and 0.9 kGy. It can be seen that regardless of the dose assembly (single versus multiple pulses) and number of irradiation cycles, the MW remains almost constant among all doses.

At the same time, a tremendous change is visible for the R_g of irradiated polymer solutions. Similar to the other polymers such as PVA [8], irradiated under the same conditions, R_g significantly decreases (Fig. 7) because of intramolecular cross-linking. The degree of this decrease is dependent on dose delivery to the irradiated system, mainly on the number of PVP macroradicals generated within a single pulse of electrons. The same dose delivered in the form of a few electron pulses (lower number of PVP macroradicals) caused stronger R_g decreases (Figs 7(b)–(d)). The lowest size (highest cross-link density) has been obtained for samples irradiated with a dose cumulated from electron pulses with the lowest energy (in this work, it was 0.112 kGy), i.e. when the number of radicals generated per chain was the lowest.

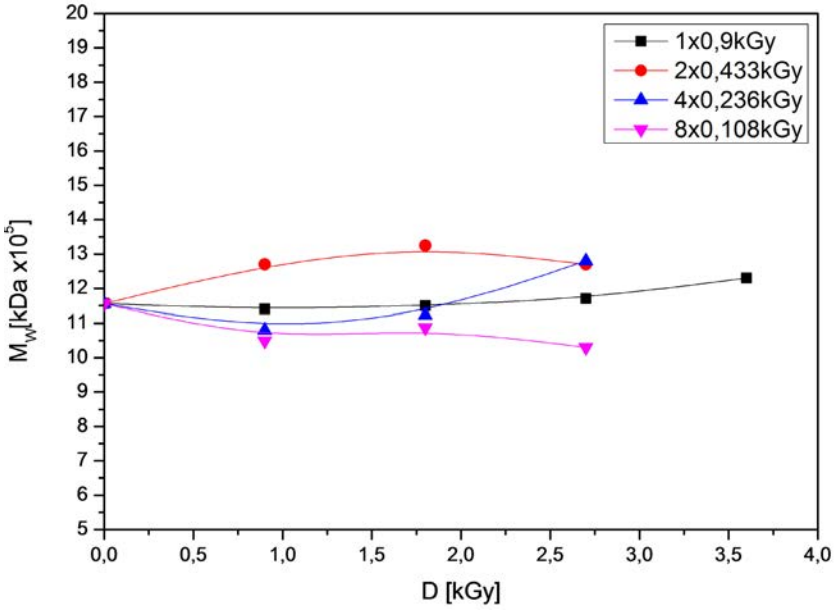

FIG. 6. Changes in weight averaged MW as a function of dose absorbed by aqueous solution of PVP, [PVP]=10 mmol/L, saturated with N_2O, irradiated with pulses of fast electrons from the LAE. Pulse duration = 2 μs, frequency = 2 Hz. Series of data represent doses cumulated from electron pulses of 0.108 kGy, 0.256 kGy, 0.433 kGy and 0.9 kGy.

Figure 7(a) shows a series of data representing doses cumulated from electron pulses of 0.108 kGy, 0.236 kGy, 0.433 kGy and 0.9 kGy. Figure 7(b) shows changes of R_g for a total absorbed dose of 0.9 kGy (dose cumulated from electron pulses of 0.112 kGy, 0.236 kGy, 0.430 kGy and 0.903 kGy). Figure 7(c) shows changes of R_g for a total absorbed dose of 1.8 kGy (dose cumulated from electron pulses of 0.112 kGy, 0.430 kGy and 0.903 kGy). Figure 7(d) shows changes of R_g for a totally absorbed dose of 2.7 kGy (dose cumulated from electron pulses of 0.112 kGy, 0.430 kGy and 0.903 kGy).

Knowing the values of R_h and R_g, ρ, which describes the architecture of the macromolecules in solution, can be calculated as:

$$\rho = \frac{R_g}{R_h} \tag{1}$$

Regardless of dose assembly, ρ decreases for all totally absorbed doses. For a non-irradiated solution of PVP, $R_g/R_h = 1.6$, which means that there is a polydisperse sample of a polymer with a linear structure. With irradiation, the value of ρ decreases to 1.2–0.7 (depending on the absorbed dose), which indicates the existence of branched and/or internally cross-linked structures [19]. Comparing values of ρ obtained for irradiated samples, it can be seen that in the case of the generation of a smaller number of radicals in a single pulse of electrons (eight times 0.108 kGy), R_g/R_h reaches smaller values (0.7) than for a higher number of radicals per chain (higher dose in pulse, e.g. 0.9 kGy). In fact, this reflects stronger changes of the coil structure.

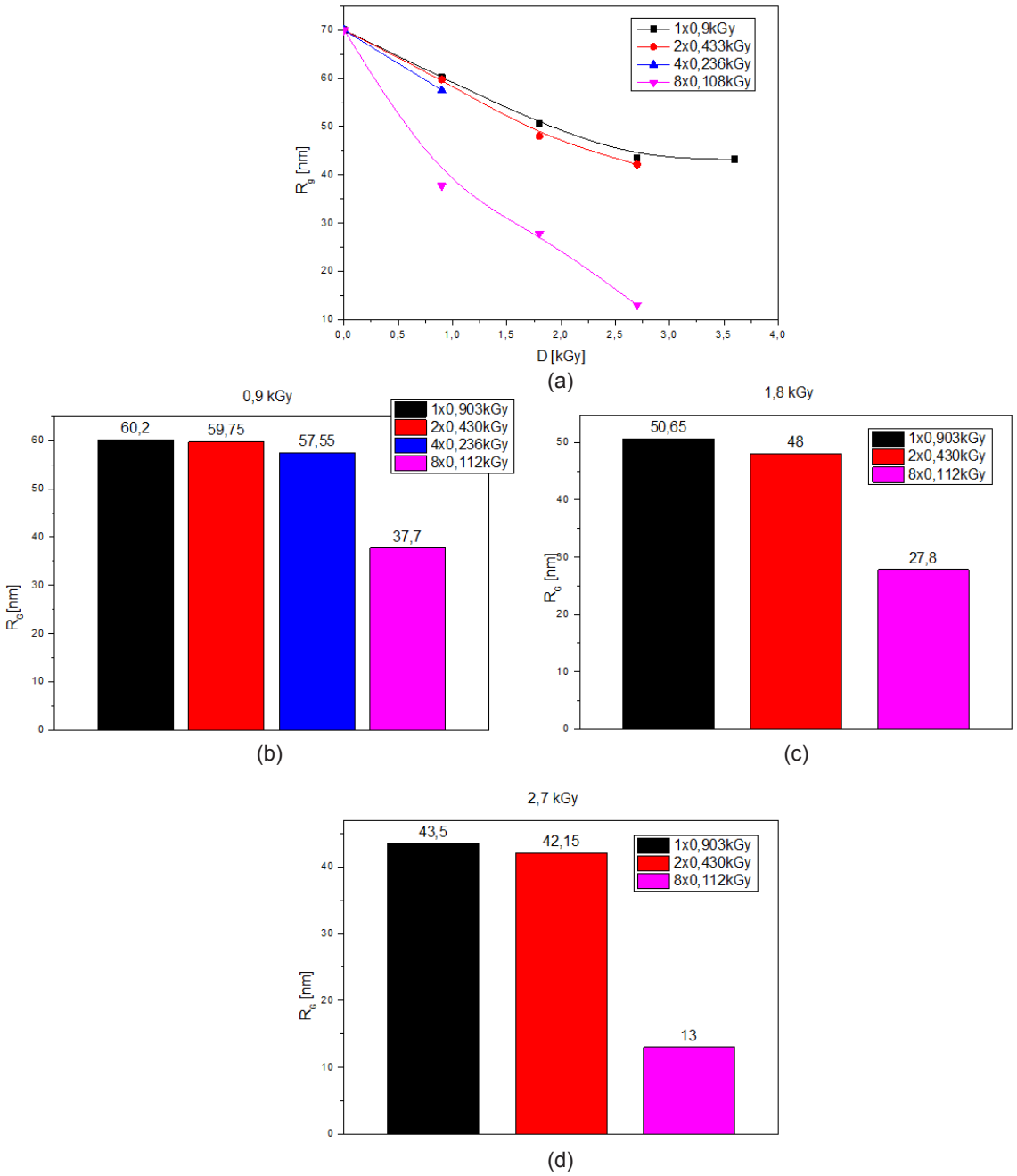

FIG. 7. Changes in R_g *as a function of dose absorbed by aqueous solution of PVP, [PVP] = 10 mmol/L, saturated with* N_2O*, irradiated with pulses of fast electrons from the LAE. Pulse duration = 2 μs, frequency = 2 Hz.*

The structure of an irradiated macromolecule can also be described by calculation of its volume and density. Both parameters change with an increase of absorbed dose as a result of intramolecular recombination. According to changes observed for R_g and ρ, irradiation with a high number of low dose electron pulses leads to formation of structures of lower volume than irradiation with the same dose but with pulses of higher energy, i.e. generating higher number of radicals per chain. This dependency was also confirmed by changes in coil density: because the dimensions (radius, volume) decrease and the number of segments (MW) does not change, the density increases.

5. APPLICATION OF RADIATION TECHNIQUES FOR SYNTHESIZING NANOLAYERS AND MICROLAYERS OF THERMORESPONSIVE POLYMERS AND GELS

Burn wounds are one of the most frequently occurring injuries. This kind of wound is a serious problem, not only because of its high incidence, but also because of the complications arising during healing. Many conventional treatments of burn wounds are costly, slow and ineffective. Skin grafts are considered to be one of the best solutions; however, cell culture procedures used to obtain large surface grafts have still to be optimized. A persisting problem is how to detach the grown skin sheet from the substrate without causing excessive damage to the product. One possible solution is to use substrates with thermosensitive surfaces. The latter are currently recognized as valuable new materials for biomedical research fields such as artificial organs, biofunctional materials, drug delivery systems, separations of biomolecules and regenerative medicine.

Thermoresponsive polymers are commonly used as surface modifiers. One of the well known temperature responsive polymers, PNIPA, has a lower critical solution temperature (LCST) of 32°C in water. Below the LCST, the polymer is fully hydrated and soluble in water, but collapses and becomes insoluble above the LCST. When PNIPA is grafted onto the surface of a cell culture substrate, at 37°C, the cells can adhere and grow easily on the surface, while lowering the temperature to 25°C makes the surface hydrophilic, which should facilitate cell layer detachment without cell damage [20–23]. A scheme depicting the action of such a material is shown in Fig. 8. Another temperature responsive polymer, TMA (thermoresponsive methacrylate), has an LCST of 22°C in water.

The aim of this part of the project was to obtain new thermocontrolled scaffolds intended for skin cell sheet cultures by grafting nanolayers and microlayers of PNIPA and TMA onto PP surfaces, using radiation techniques.

Grafting of the polymers was performed by preirradiation of PP layers with 6 MeV electrons from an LAE and the subsequent reaction of these substrates with the monomer in deoxygenated solutions at 70°C. This procedure, adjusted and optimized for the present syntheses, is based on a well known mechanism of radiation grafting by the peroxide method (Fig. 9).

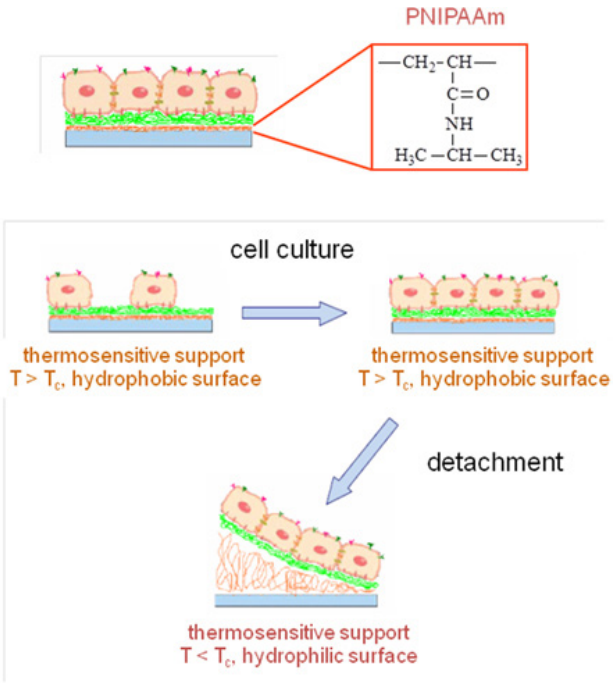

FIG. 8. Schematic representation of thermosensitive nanolayer or microlayer polymer support for culture and easy detachment of skin cell layers.

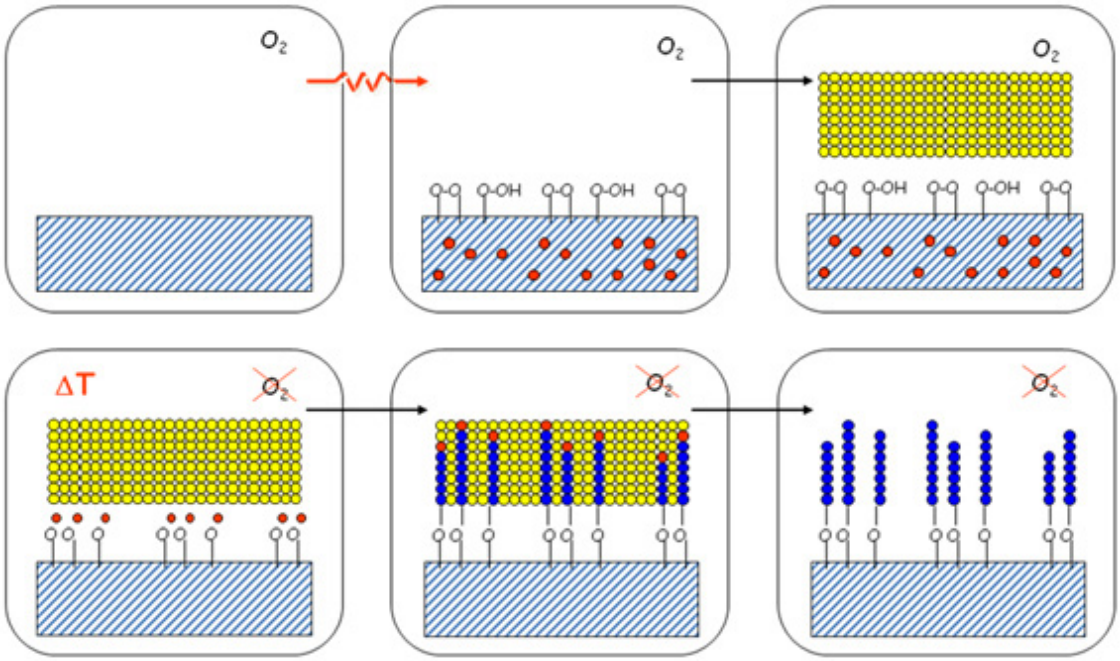

FIG. 9. General scheme of radiation grafting by the peroxide method, as used in the current synthetic procedure. Red dots denote radicals, yellow dots denote monomer molecules and blue dots denote monomer units of a grafted polymer chain.

The influence of monomer concentration and reaction time on grafting percentage was studied (Fig. 10). Obtained products were analysed by FTIR (Fig. 11) and gravimetric and CA measurements (Fig. 12). Results indicate that radiation grafted PNIPA and TMA form thermoresponsive layers on PP films and Petri dishes. Products have been subjected to biological tests in fibroblast cultures. Efficient fibroblast growth on the thermosensitive surfaces was observed, and fully confluent cell sheets have been obtained. Subsequently lowering the temperature below LCST resulted in detachment of cell sheets (Fig. 13). The synthetic technique and the product properties do still require optimization, but the obtained preliminary results, including cell cultivation and temperature triggered detachment, appear to be promising.

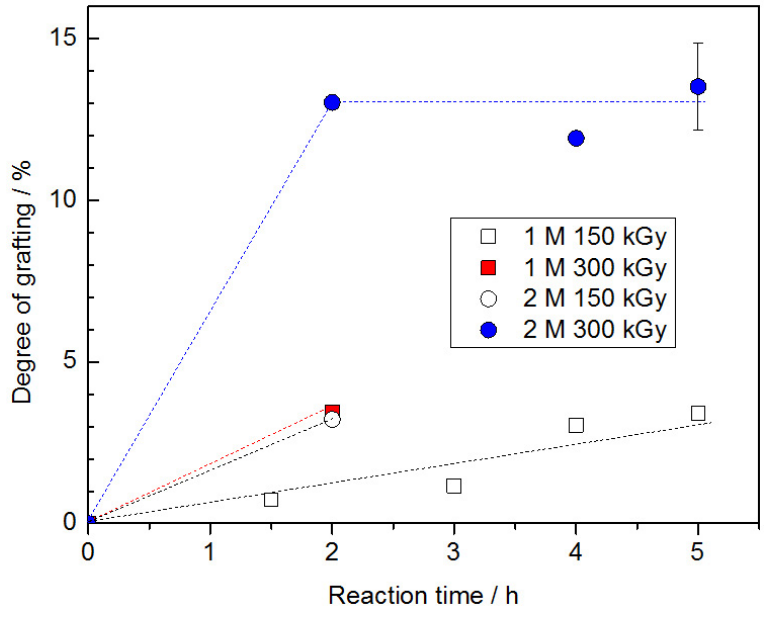

FIG. 10. Influence of reaction parameters (irradiation dose, monomer concentration and reaction time) on the GD of TMA on PP foil.

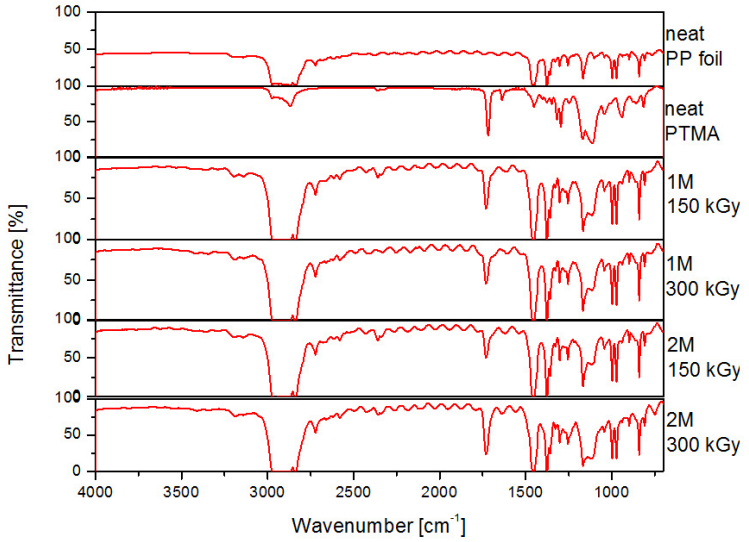

FIG. 11. FTIR spectra confirming the grafting of TMA on PP foil. Spectra of neat PP, neat polyTMA (PTMA) and products obtained at various conditions. A carbonyl peak at c. 1720 cm^{-1} is clearly seen in the grafted products.

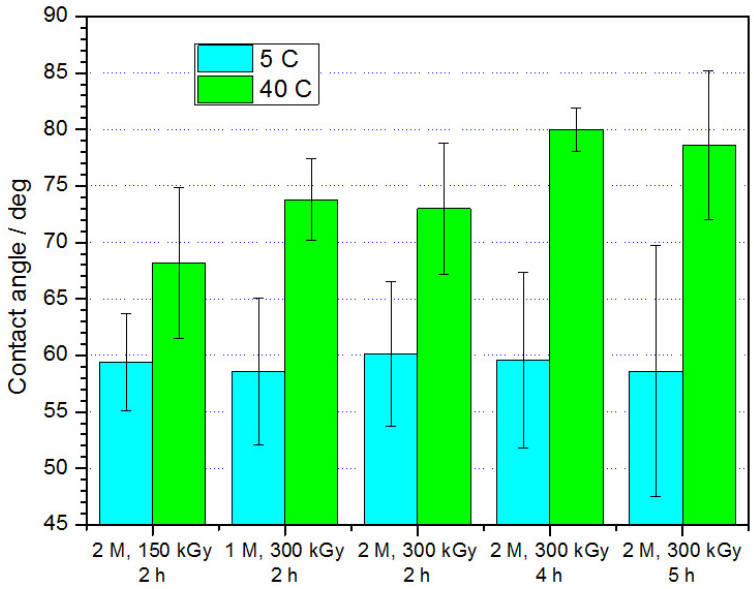

FIG. 12. CA values determined at 5°C and 40°C for PP-g-TMA surfaces obtained at various synthetic conditions.

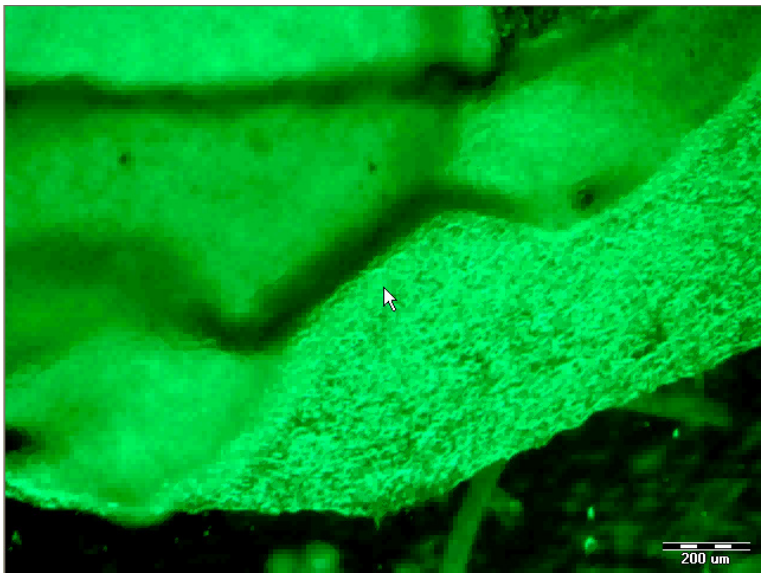

FIG. 13. A snapshot microscope photograph illustrating temperature triggered detachment of a fibroblast cell layer from the radiation synthesized PP-g-TMA surface.

REFERENCES

[1] ALEMÁN, J., et al., Definitions of terms relating to the structure and processing of sols, gels, networks, and inorganic-organic hybrid materials (IUPAC Recommendations 2007), Pure Appl. Chem. **79** (2007) 1801–1829.

[2] FUNKE, W., OKAY, O., JOOS-MULLER, B., Microgels-intramolecularly crosslinked macromolecules with a globular structure, Adv. Polym. Sci. **136** (1998) 139–234.

[3] PEPPAS, N.A. (Ed.), Hydrogels in Medicine and Pharmacy, Vol. I, Fundamentals 1, CRC Press Inc., Boca Raton, FL, Vol. 1 (1986), Vols 2 and 3 (1987).

[4] KIM, C., et al., Self-crosslinked polyethylenimine nanogels for enhanced intracellular delivery of siRNA, Macromol. Res. **19** (2011) 166–171.

[5] STAUDINGER, H., HEUER, W., HUSEMANN, E., RABINOVITCH, I.J., The insoluble polystyrene, Trans. Faraday Soc. **32** (1936) 323–335.

[6] ULANSKI, P., ROSIAK, J.M., "Polymeric nano/microgels," Encyclopedia of Nanoscience and Nanotechnology, Vol. 8 (NALWA, H.S., Ed.), American Scientific Publishers, Stevenson Ranch, CA (2004) 845–872.

[7] BRASCH, U., BURCHARD, W., Preparation and solution properties of microhydrogels from poly(vinyl alcohol), Macromol. Chem. Phys. **197** (1996) 223–235.

[8] ULANSKI, P., JANIK, I., ROSIAK, J.M., Radiation formation of polymeric nanogels, Radiat. Phys. Chem. **52** (1998) 289–294.

[9] ULANSKI, P., ROSIAK, J.M., The use of radiation technique in the synthesis of polymeric nanogels, Nucl. Instrum. Methods B **151** (1999) 356–360.

[10] SCHMIDT, T., et al., Pulsed electron beam irradiation of dilute aqueous poly(vinyl methyl ether) solutions, Polym. **46** (2005) 9908–9918.

[11] KADLUBOWSKI, S., GROBELNY, J., OLEJNICZAK, W., CICHOMSKI, M., ULANSKI, P., Pulses of fast electrons as a tool to synthesize poly(acrylic acid) nanogels. Intramolecular cross-linking of linear polymer chains in additive-free aqueous solution, Macromol. **36** (2003) 2484–2492.

[12] ULANSKI, P., KADLUBOWSKI, S., ROSIAK, J.M., Synthesis of poly(acrylic acid) nanogels by preparative pulse radiolysis, Radiat. Phys. Chem. **63** (2002) 533–537.

[13] KADLUBOWSKI, S., ULANSKI, P., ROSIAK, J.M., Synthesis of tailored nanogels by means of two-stage irradiation, Polym. **53** (2012) 1985–1991.

[14] KHUTORYANSKIY, V.V., Hydrogen-bonded interpolymer complexes as materials for pharmaceutical applications, Int. J. Pharm. **334** (2007) 15–26.

[15] PEPPAS, N.A., BURES, P., LEOBANDUNG, W., ICHIKAWA, H., Hydrogels in pharmaceutical formulations, Eur. J. Pharm. Biopharm. **50** (2000) 27–46.

[16] HENKE, A., et al., The structure and aggregation of hydrogen-bonded interpolymer complexes of poly(acrylic acid) with poly(*N*-vinylpyrrolidone) in dilute aqueous solution, Macromol. Chem. Phys. **212** (2011) 2529−2540.

[17] ZHANG, G., WU, C., Folding and formation of mesoglobules in dilute copolymer solutions, Adv. Polym. Sci. **195** (2006) 101–176.
[18] PLONKA, A., Dispersive Kinetics, Kluwer Academic Publishers, Dordrecht (2001).
[19] BURCHARD, W., Solution properties of branched molecules, Adv. Polym. Sci. **143** (1999) 113–194.
[20] YAMADA, N., et al., Thermo-responsive polymeric surfaces; control of attachment and detachment of cultured cells, Makromol. Chem., Rapid Commun. **11** (1990) 571–576.
[21] MIZUTANI, A., KIKUCHI, A., YAMATO, M., KANA, H., OKANO, T., Preparation of thermoresponsive polymer brush surfaces and their interaction with cells, Biomater. **29** (2008) 2073–2081.
[22] FUKUMORI, K., et al., Temperature-responsive glass coverslips with an ultrathin poly(N-isopropylacrylamide) layer, Acta Biomater. **5** (2009) 470–476.
[23] CHUMAKOV, M.K., et al., Electron beam induced grafting of N-isopropylacrylamide to a poly(ethylene-terephthalate) membrane for rapid cell sheet detachment, Radiat. Phys. Chem. **80** (2011) 182–189.

RADIOLYTICALLY SYNTHESIZED HYBRID NANOSYSTEMS FOR BIONANOTECHNOLOGIES

Z. KACAREVIC-POPOVIC, A. RADOSAVLJEVIC (KRKLJES), J. KRSTIC, J. SPASOJEVIC
Laboratory for Radiation Chemistry and Physics — GAMMA
Vinča Institute of Nuclear Sciences
University of Belgrade
P.O. Box 522, 11001 Belgrade
Serbia

Abstract

In this report, a review of the main results and the studies carried out under the scope of the project Radiolytically Synthesized Hybrid Nanosystems for Bionanotechnologies, as part of the IAEA CRP Nanoscale Radiation Engineering of Advanced Materials for Potential Biomedical Applications, is presented. In particular, two topics are discussed: (i) achievements in radiation synthesis of Ag NPs in previously radiolytically polymerized and/or cross-linked hydrogels, which are chosen for potential biomedical applications as dressing materials and tissue expanders, and (ii) the ability of γ irradiation for decoration of CNTs with Ag nanoclusters, to obtain a potential optical teranostic probe. In addition, the influence of the structure of the capping agent on the optical properties of resulting Ag NPs during synthesis by γ irradiation is investigated.

1. SYNTHESIZING Ag/HYDROGEL NANOCOMPOSITES BY γ IRRADIATION FOR POTENTIAL BIOMEDICAL APPLICATIONS

1.1. Background

Hydrogels are hydrophilic bicomponent or multicomponent systems consisting of a three dimensional network of polymer chains and liquid, which fills the space between the macromolecules. They have both the cohesive properties of solids and the diffusive transport properties of liquids. Hydrogels possess the ability to absorb large amounts of water or biological liquids and consequently swell, i.e. increase their mass and volume, but they do not dissolve. Because of this property, they are biocompatible, which is the main reason for their wide use in medical and pharmaceutical applications. Hydrogels are considered as being promising biomaterials for contact lenses, wound dressings, artificial corneas, soft tissue substances, etc. Hydrogels are applied in medical devices ranging from tissue expanders to coatings for penile and testicular implants, urology devices and materials, as well as for wound dressing. In some cases, even in diabetic foot wound therapy, a tissue expander can be used for resolving an open wound.

On the other hand, nearly synchronous with the advent of prosthetic medical devices, strategies have been developed to attempt to minimize the risks of infections. In recent years, nanoscale antibacterial materials as novel antimicrobial species have been seen as promising candidates for application because of their high surface to volume ratio and their novel physical and chemical properties on the nanoscale level. Many kinds of nanometre sized antibacterial materials such as TiO_2, ZnO, MgO, CS, calamine, copper and silver have been reported on in this area. Among them, nanocrystalline silver (Ag) has been proved to be the most effective antimicrobial agent because silver and its compounds have powerful antimicrobial capabilities and broad inhibitory biocidal spectra for microbes, including bacteria, viruses and eukaryotic microorganisms [1]. Silver is especially important for the treatment of diabetic wounds, which are usually polymicrobial.

Enhanced antibacterial properties of nanocrystalline silver have been demonstrated, both in vitro and in vivo. In addition, MNPs such as silver, provide interesting research areas because they have close lying conduction and valence bands, in which electrons can move freely. Because of their ability to absorb and scatter light and their biocompatible nature, they are therefore well suited for NP optical and biological applications. In 2005, investigators first reported that Ag NPs prevented human immunodeficiency virus type 1 infection. Findings suggested that the particles interacted with the viral particles in a size dependent manner. The interaction of Ag NPs and gp120 glycoprotein present in the viral envelope prevented viral fusion with cells, thus preventing infection.

However, in general, a high avidity of silver for protein, and the presence of a protein conditioning film, or any extraneous plasma protein, has been assumed to inactivate any Ag^+ ions released from silver coated medical devices and decrease the antimicrobial potential, with obvious clinical implications. The surfaces of medical devices rapidly become coated with glycoprotein from tissue and plasma, and this has been cited as one of the main reasons for clinical failure of silver coated devices. However, in the case of impregnation with nanoAg, there is both a depot effect and a diffusion pressure available to 'push' the Ag^+ ions through the conditioning film. To do this, there must be enough Ag^+ ions available over a sufficient period to exceed those lost to protein binding. Another clinically important advantage of impregnation is the protection of inner and outer surfaces of medical devices and dressings [ag]ainst bacterial colonization. This has been shown to be crucial in clinical trials of efficacy. These two advantages of impregnation, i.e. the continued release of Ag^+ ions in antimicrobial concentrations, even in the presence of a conditioning film, and the ability to protect both inner and outer surfaces of devices, could be expected from the use of novel radiolytic methods to impregnate polymeric biomaterials—hydrogels with Ag NPs.

Recent research efforts are heading for exploitation of the in situ synthesis of noble metal NPs within polymeric network architectures. Three dimensional hydrogels are appropriate templates for producing noble metal NPs and have advantages over conventional non-aqueous and polymeric systems for biomedical applications in view of their exceptional compatibility with biological molecules, cells and tissues [2, 3]. In this way, the carrier systems act as nanoreactors that immobilize NPs and provide easy handling.

A radiolytic method is the method of choice in the synthesis of hydrogels, and it is very suitable for generating noble metal NPs within the polymer network of hydrogels. Even though the chemical methods for synthesis of NPs involve a very simple procedure, they employ chemical reducing agents, such as citrate, borohydride or other organic compounds, which are toxic to living organisms and hence render them unsuitable for medical use. Solvated electrons and secondary radicals, formed by radiolysis of water, have significant reduction power and ability to convert silver ions (Ag^+) to their atomic state as precursors for formation of NPs [4, 5].

1.2. Research objectives

The aims of the work were to systematically develop synthetic strategies for incorporation of nanoAg into hydrogel networks by γ irradiation, using liquid filled cavities in hydrogels as nanoreactors (template synthesis) in order to design a hydrogel controlled release system of Ag^+ ions, to explore the favourable characteristics of radiation technology for nanoscale engineering of materials specifically for biomedical applications with easy process control, and to investigate the possibility of combining synthesis and sterilization in one technological step. The radiation technique does not require any extra substances, and does not need any further purification. The incorporation of template technologies with synthesis techniques, such as γ ray irradiation methods, is expected to produce more elaborate Ag NPs that are suitable for biomedical applications.

The chosen hydrogels, which have been previously synthesized or cross-linked by γ irradiation, are suitable for various applications in reconstructive surgery, including wound dressings, tissue expanders, etc. [6–8]. PVP, as well as PVA, has been used successfully in many biomedical applications as a basic material for the manufacturing of hydrogel wound dressings. In addition, research activities in this project were focused on the development of temperature and pH stimuli hydrogel matrices, based on PNIPA and poly(2-HEMA), respectively. The use of IA provides polymer chains with carboxylic acid groups that are highly hydrophilic and which are able to form hydrogen bonds with corresponding groups.

1.3. Synthesis of nanocomposites

Reactants used in the syntheses of the investigated systems in this project, and their general chemical structures are shown in Fig. 1.

The gels were polymerized and/or cross-linked by γ irradiation radical copolymerization and/or cross-linking. The reaction mixture was degassed prior to polymerization and placed between two glass plates, which were sealed with a spacer. The solutions were irradiated using a ^{60}Co radiation source, under ambient conditions, to an absorbed dose of 25 kGy. To remove any unreacted chemicals, the hydrogels were immersed in deionized water, which was changed every day, for at least 1 week.

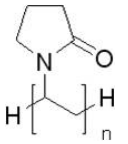

poly(*N*-vinyl-2-pyrrolidone)

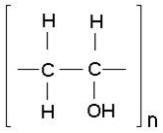

poly(vinyl alcohol)

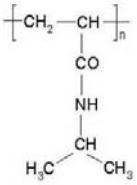

poly(*N*-isopropylacrylamide)

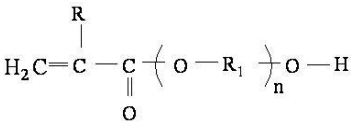

bisomers (R=H or CH_3; R_1=ethylene or propylene groups)

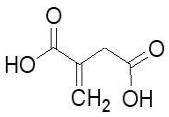

itaconic acid

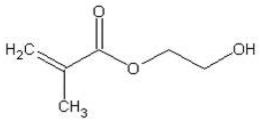

2-hydroxyethylmethacrylate

FIG. 1. Reactants used in the syntheses of the investigated systems.

The Ag/hydrogel nanocomposites were prepared by swelling the cross-linked polymer samples with water solutions of $AgNO_3$ and 2-propanol. Swelling of Ar saturated gels was carried out in tightly closed containers for 48 h at room temperature in the dark; using longer swelling periods had no effect. In the second step, Ag^+ ions were reduced in hydrogel using electron transfer reactions from radical species formed in water radiolysis. γ irradiation was performed using the ^{60}Co radiation facility, at room temperature until complete reduction of Ag^+ ions was achieved.

The primary products of water radiolysis are shown in Eq. (1):

$$H_2O \rightarrow e_{aq}^-(2.7),\ OH^{\bullet}(2.7),\ H^{\bullet}(0.6),\ H_2(0.45),\ H_2O_2(0.7) \quad (1)$$

The numbers in parentheses represents the respective *G* values. The *G* value for a given irradiated system is the absolute chemical yield expressed as the number of individual chemical events occurring per 100 eV of absorbed energy. Thus, the *G* (e_{aq}^-), *G* ($OH^{\bullet}$), etc., are the numbers of solvated electrons, hydroxyl radicals, etc., formed per 100 eV of absorbed energy. In the presence of alcohol, the $OH^{\bullet}$ and $H^{\bullet}$ radicals abstract hydrogen from the alcohol to produce an alcohol radical. It is well known that the radiation cross-linking of polymer (POLYM) molecules is mainly induced by $OH^{\bullet}$ radicals in aqueous medium (with the *G* value of irradiation induced intermolecular cross-linking = 0.48):

$$2\ \text{POLYM (H)} + 2OH^{\bullet} \rightarrow \text{POLYM} - \text{POLYM (cross-linked polymer)} + 2H_2O \quad (2)$$

Under the given experimental conditions, the Ag^+ ions are reduced by strongly reducing hydrated electrons, the 2-propanol radical and the polymeric radicals formed by H atom abstraction from the polymer chains by hydroxyl radicals:

$$nAg^+ + ne_{aq}^-/(CH_3)_2\ C^{\bullet}OH/POLYM^{\bullet} \rightarrow (Ag)_n \quad (3)$$

After γ irradiation, yellow coloured Ag/polymer hydrogel nanocomposites were obtained. The yellow colour is characteristic of silver NPs, as shown for the Ag/PVP hydrogel nanocomposite in Fig. 2.

FIG. 2. Photograph of PVP hydrogel (left) and Ag/PVP hydrogel nanocomposite (right).

1.4. Characterization of Ag/hydrogel nanocomposites

1.4.1. Optical and structural properties

UV/VIS absorption spectra of Ag/hydrogel nanocomposites were recorded in the wavelength range 300–800 nm using an Evolution 600 (Thermo Scientific) spectrophotometer. TEM measurements were performed using an EM400 (Philips) microscope operated at an accelerating voltage of 120 kV. The XRD measurements of the Ag/hydrogel nanocomposites was carried out on a D8 ADVANCE (Bruker) diffractometer (Cu $K_{\alpha 1}$ radiation, $\lambda = 0.1541$ nm).

1.4.2. Swelling properties

For the swelling studies, xerogel discs were immersed in an excess of water or Kokubo's SBF solution [9], with a pH value of 7.1, to obtain equilibrium swelling at 25°C and 37°C. Kokubo's SBF is an acellular SBF that has inorganic ion concentrations similar to those of human extracellular fluid. From the swelling characteristics, a diffusion model was obtained.

1.4.3. Mechanical properties

The influence of Ag NPs on the mechanical properties of the hydrogel was obtained under bioreactor conditions. The bioreactor mimics conditions in articular cartilage and combines dynamic compression and medium flow through the cultivated tissue in the dark. The bioreactor was configured as a unit of six cultivation cartridges placed in a holder, secured on a metal base. The base could be moved vertically by a stepper motor mounted underneath, while average loads imposed on all six cartridges were measured by a load cell (Scaime AL3C3SH5e). Movements of the bioreactor base and data acquisition were computer controlled.

1.4.4. Release of silver

The release of Ag^+ ions from Ag/hydrogel nanocomposites was determined by atomic absorption spectroscopy using a Pye Unicam SP9 (Philips) atomic absorption spectrophotometer. A drug delivery paradigm was developed for this system to improve the potential of nanoAg technologies through controlled release formulations. The results of the study of Ag release kinetics, obtained by the atomic absorption spectrophotometer method were correlated to the solubility of Ag NPs calculated using the Ostwald–Freundlich equation.

1.4.5. Antimicrobial properties

An investigation of antimicrobial activity of *E. coli* and *S. aureus* was conducted under in vitro conditions and compared to the release of Ag^+ ions. The in vitro method of investigation has advantages because complex conditions, which are needed for in vivo investigation, can be avoided.

1.5. Results and discussion

1.5.1. Optical and structural properties

Reduction of Ag^+ ions in the hydrogel matrix yielded a typical SPR band of Ag NPs for all investigated systems, with no broad absorptions at wavelengths longer than the particle plasmon band, as shown in Fig. 3.

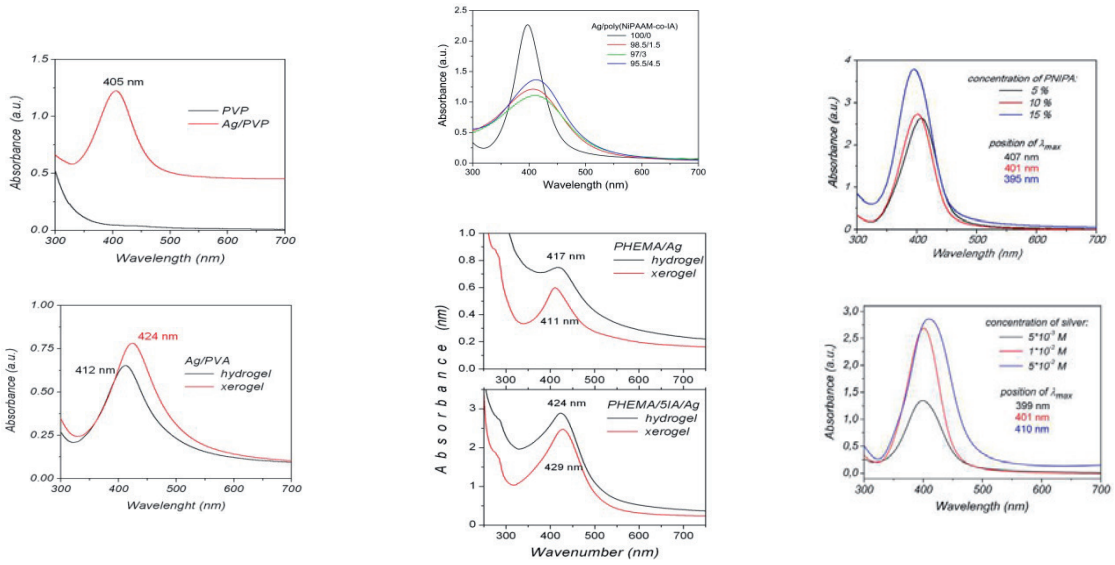

FIG. 3. Characteristic SPR bands of Ag NPs in UV/VIS spectra of nanocomposite systems. PHEMA: polyHEMA.

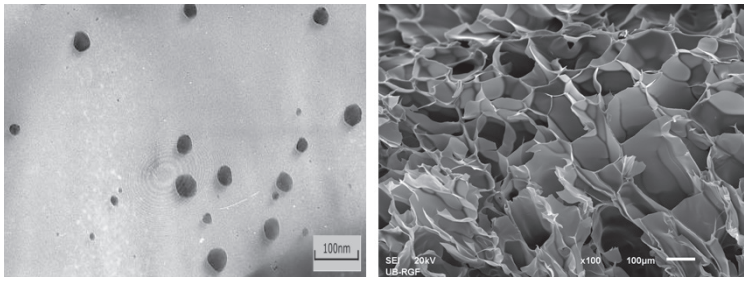

FIG. 4. (Left) TEM image of Ag NPs formed in PVP hydrogel and (right) SEM image of PNIPA network (right).

Figure 3 depicts the appearance of the crystallite surface plasmon bands in the different types of Ag/hydrogel nanocomposite systems investigated. Irradiation of $AgNO_3$ loaded hydrogels resulted in a strong, sharp absorption centred in the range 400–430 nm. No significant change in the UV/VIS characteristics of the Ag NPs formed in these hydrogels was observed, as shown in Fig. 3. The sharp absorption pattern indicates that the particle size distribution is quite narrow.

To investigate the morphology and size of Ag NPs, a TEM micrograph of Ag NPs is shown in Fig. 4 (left). It is obvious that these Ag NPs, like in all the investigated systems, assume sphere like morphologies at nanoscale levels.

The XRD patterns presented in Fig. 5, as in all investigated systems, matched exactly the (111) (200) and (220) crystal planes of Ag with face centred cubic crystal structures. Scherrer's diffraction formula was used to estimate the crystalline domain size (D):

$$D = k\lambda/\beta \cos\theta \tag{4}$$

where $k = 0.9$ is constant for a cubic structure, $\lambda = 0.1541$ nm is the X ray wavelength, β is the peak angular width and θ is the diffraction angle. The crystalline domain size for all systems was found to be less than 20 nm, which means that the obtained particles are in an intrinsic size regime.

Accurate determination of size and concentration of NPs is essential for biomedical applications. Because of the discrete size domains of synthesized Ag NPs in the intrinsic regime, a quasi-static approximation of Mie theory and the Hayakawa equation were used to determine the particle sizes from UV/VIS measurements [10]. The relation $r = \nu_f/\Delta\omega_{1/2}$ was used to calculate the particle radius, where ν_f is the Fermi velocity of the metal and $\Delta\omega_{1/2}$ is the full width at half-maximum for the SPR band (in units of angular frequency). Assuming that the silver bulk density is 5.86×10^{22} atoms/cm^3, it is possible to determine the average number of atoms (N_{av}) belonging to spherical NPs

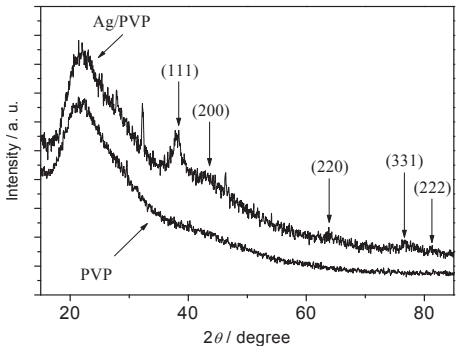

FIG. 5. XRD patterns of PVP and Ag/PVP nanocomposite.

in the metallic phase. The average number of atoms in Ag NPs was calculated using the equation $N_{av} = \rho(Ag)V_{sf}$, where ρ(Ag) is the theoretical density of silver and V_{sf} is the volume of the nanosphere. The molar concentration of the Ag NPs in colloids was calculated using $C = N_{tot}/(N_{av}VN_A)$, where V is the volume of the reaction solution, N_A is Avogadro's constant and N_{tot} is the total amount of silver. The theoretical effective surface area (SA) of NPs was also calculated using $SA = 6/D_{sf}\rho$, where D_{sf} is the diameter of Ag NPs and ρ is the theoretical density of silver (10.5 g/cm^3) [11]. The obtained values for the parameters of Ag NPs in Ag/PVA hydrogel nanocomposites are listed in Table 1.

TABLE 1. VALUES FOR PARAMETERS OF Ag NPs IN Ag/PVA HYDROGEL NANOCOMPOSITES: CONCENTRATION OF SILVER (c_{Ag}), RADIUS (r), AVERAGE NUMBER OF ATOMS PER NP (N_{AV}), MOLAR CONCENTRATION IN SYSTEM (C), THEORETICAL EFFECTIVE SURFACE AREA (SA) AND SOLUBILITY OF NPs (S_r)

c_{Ag} (mM)	r (nm)	N_{av} (atoms/NP)	C (mol/L)	SA (m^2/g)	S_r (mg/L)
4	4.12	17 211	2.32×10^{-7}	69.28	0.067
8	3.30	8 782	9.10×10^{-7}	86.69	0.111
16	4.00	15 731	1.02×10^{-6}	71.38	0.071

1.5.2. Swelling properties

Swelling of the cross-linked polymers in the chosen solvent is their most important property. Moreover, preliminary studies in a buffered solution of pH similar to that of biological fluids are very important for the application of hydrogels as biomaterials. The intake of xerogels, and Ag/xerogel nanocomposites, were followed for a long period of time in SBF solution at 37°C. Examples of swelling curves are plotted in Fig. 6.

As can be seen from Fig. 6, the swelling capabilities of PVA hydrogel (xerogel) and Ag/PVA hydrogel (xerogel) nanocomposites increase with time, reaching a constant swelling (equilibrium swelling) after a certain period of time. Another observation is that the swelling of the gels is slightly greater for the hydrogel containing Ag NPs; this was the case in all the investigated systems. Examples of the swelling parameters obtained from the swelling measurements are shown in Table 2.

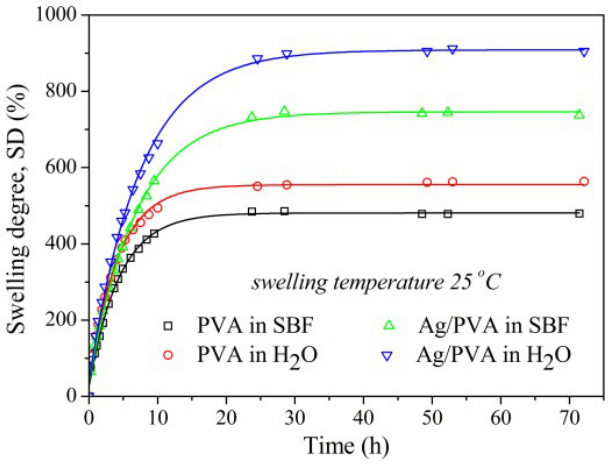

FIG. 6. Swelling curves of PVA and Ag/PVA nanocomposites in water and SBF solution.

TABLE 2. VALUES OF THE CONCENTRATION OF SILVER (c_{Ag}), EQUILIBRIUM SWELLING DEGREE (SD_{eq}), DIFFUSION EXPONENT (n), KINETIC CONSTANT (k), DIFFUSION COEFFICIENT (D) AND INITIAL SWELLING RATE (υ_0) FOR PVA AND Ag/PVA HYDROGELS, IN SBF SOLUTION AT 25°C AND 37°C

Temperature (°C)	c_{Ag} (mM)	SD_{eq} (%)	n	k (s^{-1})	D (cm^2/s)	υ_0 (%/min)
25	0	480	0.58	0.267	1.16×10^{-7}	3.46
	4	709	0.60	0.206	0.87×10^{-7}	3.01
	8	738	0.62	0.183	0.78×10^{-7}	3.02
	16	796	0.63	0.177	0.78×10^{-7}	2.88
37	0	576	0.64	0.295	1.68×10^{-7}	4.97
	4	737	0.66	0.278	1.74×10^{-7}	5.74
	8	811	0.65	0.221	1.19×10^{-7}	5.42
	16	867	0.64	0.247	1.36×10^{-7}	6.37

The values of swelling parameters obtained (shown in Table 2) are dependent on the particle radius (Table 1).

1.5.3. Mechanical properties

Studies of mechanical properties in bioreactor conditions have shown that hydrogels and nanocomposite systems exhibit highly elastic behaviour. Values of Young's modulus obtained for nanocomposites were higher than those of the blank hydrogel (see Table 3). Results suggest that the presence of Ag NPs influences the network structure, making it slightly firmer and more suitable for biomedical applications, in terms of mechanical strength.

TABLE 3. REPRESENTATIVE VALUES OF YOUNG'S MODULUS (E) AND THE SHEAR MODULUS (G), EFFECTIVE CROSS-LINK DENSITY (ν_e) AND MOLAR MASS BETWEEN CROSS-LINKS (M_c) FOR CROSS-LINKED PVP AND Ag/PVP NANOCOMPOSITES

Sample		E [a] (kPa)	G [b] (kPa)	ν_e (mol/m)	M_c (kg/mol)
PVP	Minimum range value	26.5	8.83	52.8	15.9
	Maximum range value	27.1	9.03	54.0	15.5
Ag/PVP	Minimum range value	30.7	10.2	71.3	13.9
	Maximum range value	55.5	18.5	129	7.65

[a] Average values from three measurements.
[b] $E = 3G$ was used for determination of shear modulus G.

1.5.4. Release of silver

A sustained, steady supply of active silver is an important property of materials for biomedical applications. Investigations indicated that the release of Ag^+ ions from nanocomposite systems is continuous over a long period of time for all synthesized Ag/hydrogel nanocomposite systems, so all investigated hydrogel nanosystems meet those criteria.

The elements of the drug delivery paradigm were applied to Ag/PVA hydrogel nanocomposites for the study of silver release kinetics. To investigate the mechanism of in vitro silver release from hydrogels, obtained data were analysed using various kinetic models. Modelling was performed using the parameters that provide the closest fit between experimental observations and the non-linear function. The model that best fits the release data was selected based on the correlation coefficient (R^2); this model was Kopcha's model (Fig. 7).

Faster release for an initial silver concentration of 8mM was correlated with the particle size and increasing effective SA of the Ag NPs, as well as their increased solubility. It was shown that dissolution of Ag NPs is size controlled. The modified form of the Kelvin equation (Ostwald–Freundlich relation) [12] is used to relate particle solubility to its radius, and the results are shown in Tables 1 and 2.

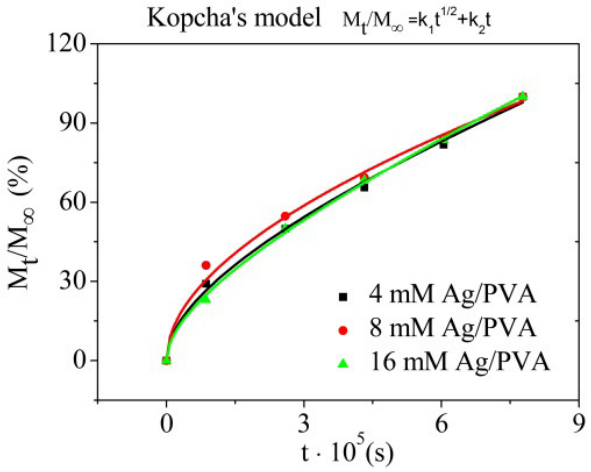

FIG. 7. Release of silver from Ag/PVA hydrogel nanocomposites.

1.5.5. Antimicrobial properties

The antibacterial activity of Ag/hydrogel nanosystems was assayed against two common bacterial species: *E. coli* (Gram negative) and *S. aureus* (Gram positive). It is noteworthy here that in the case of *S. aureus*, the Ag NPs are more effective as antibacterial agents compared with *E. coli* (Fig. 8).

Moreover, this result clearly indicates that NPs of smaller size are more potent, probably owing to their greater solubility. Therefore, the antibacterial potential of the investigated systems is not directly related to the initial concentration of Ag ions loaded in the hydrogels.

In addition, the in vitro study of neat hydrogel biocompatibility showed neither evidence of cell toxicity nor any considerable haemolytic activity. Moreover, incorporation of IA increased the cytocompatibility of neat hydrogels. Furthermore, a microbe penetration test showed that neither *S. aureus* nor *E. coli* passed through the neat hydrogel dressing.

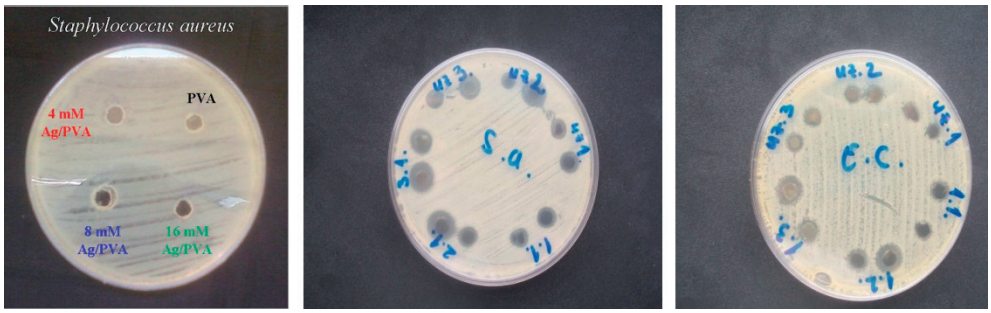

FIG. 8. Serial plate transfer test for S. aureus *(centre) and* E. coli *(right), clearly showing a zone of growth inhibition surrounding the disc with Ag NPs, compared with the control (left).*

1.6. Conclusion

The results obtained indicated that γ irradiation is suitable for in situ generation of Ag NPs in the investigated hydrogel matrix using the radiolytic products of water. XRD analysis confirms the face centred cubic crystal structure of Ag NPs. The swelling properties of synthesized hydrogels, neat and Ag/hydrogel nanocomposites, investigated in the SBF solution at 37°C, showed that Ag/hydrogel nanocomposite systems have higher equilibrium swelling compared with neat hydrogel. The release of silver Ag^+ from nanocomposite systems was continuous over long periods of time, which means that the investigated hydrogel nanosystems meet the criteria of a sustained, steady supply of active silver. The results thus obtained clearly indicate that the Ag/hydrogel nanosystems with smaller NPs are more potent, probably owing to their greater solubility.

2. FUNCTIONALIZATION OF CNTs WITH SILVER CLUSTERS BY γ IRRADIATION[1]

2.1. Background

The major areas of CNT research are polymer composites and biomedical materials and devices including biosensors and drug and vaccine delivery vehicles. For the purpose of application of CNTs and also for establishing their genotoxicity, functionalization of CNTs is important.

Considerable research efforts have been devoted to the fabrication of Ag NPs supported on CNTs. For the development of new functional materials, irradiation has been proven to be a powerful tool. As previously shown, Ag NPs can be easily prepared by the reduction of metal ions with irradiation. Generally, irradiation induced

[1] Section 2 authored by J. Cveticanin, A. Radosavljevic (Krkljes), O. Neskovic and Z. Kacarevic-Popovic, Laboratory for Radiation Chemistry and Physics — GAMMA, Vinča Institute of Nuclear Sciences, University of Belgrade, Serbia.

reactions exhibit the following advantages: the products are free of residual initiators or catalysts, and reactions can be conducted at low temperatures and in gaseous, liquid or even solid state phases. Moreover, irradiation grafting is an efficient and easy method for producing an inorganic/organic material interface and modifying the surface to form functional composites. The usage of irradiation has proven to be an efficient method to functionalize CNTs with Ag.

2.2. Results and discussion

The functionalization of CNTs with Ag NPs was achieved via anchoring of the polymer to the surface of CNTs and simultaneous reduction of Ag^+ ions under irradiation [13]. The polymer used in this work was the commercially available polymer PVA. A simple and efficient one step method of producing a hybrid of uniformly dispersed Ag NPs supported on CNTs without acid purification or using any surfactant or polyelectrolyte to functionalize CNTs was developed.

In addition, the structure and stability in the gas phase of Ag_n silver clusters formed by γ irradiation using MALDI TOF and MALDI TOFTOF techniques and theoretical ab initio calculations were investigated [14]. The stability of Ag clusters was studied with the aid of the MALDI TOFTOF technique, which is a tandem mass spectrometry method. In the MALDI TOFTOF technique, the collision induced dissociation technique is coupled with TOF, which enables tandem mass spectrometry analysis. Both the theoretical and experimental results showed that the most stable clusters were small clusters with an odd number of atoms.

2.3. Structural and optical characteristics of Ag/PVP nanosystems synthesized by γ irradiation

Results have shown that rod shaped Ag NP agglomerates were obtained from the solution of lower PVP concentration and lower MW, while spherical Ag NPs with a narrow size distribution and diameter of 6 nm were obtained from the solution of higher PVP concentration and higher MW, as well as in hydrogel networks [15]. The very small interparticle distances in rod shaped agglomerates allow plasmon coupling between them, which gives rise to a low energy UV/VIS absorption band and green colour, as opposed to all other yellow Ag/PVP nanosystems. On C coated Cu grids, some Ag NPs stabilized by higher concentrations of longer chains formed dendritic Ag nanostructures after deposition. The optical properties of the investigated Ag/PVP nanosystems, as measured by the values of optical band gap energy E_g, obtained by employing Tauc's expression, were the result of the simultaneous effects of several parameters: the interparticle distance, the concentration, the structure of surrounding PVP macromolecules and finally the surface effect on the Ag NP lattice.

ACKNOWLEDGEMENTS

Collaborators Z. Jovanovic, V. Miskovic-Stankovic and S. Tomic, as well as consultants S. Popovic, M. Colic and M. Dragasevic contributed to this report.

REFERENCES

[1] FURNO, F., MORLEY, K.S., WONG, B., SHARP, B.L., Silver nanoparticles and polymeric medical devices: A new approach to prevention of infection, J. Antimicrob. Chemother. **54** (2004) 1019–1024.

[2] MOHAN, Y.M., LEE, K., PREMKUMAR, T., GECKELER, K.E., Hydrogel networks as nanoreactors: A novel approach to silver nanoparticles for antibacterial applications, Polym. **48** (2007) 158–164.

[3] SATURKAR, N.S., HILT, J.Z., Hydrogels nanocomposites as remote controlled biomaterials, Acta Biomater. **4** (2008) 11–16.

[4] KACAREVIC-POPOVIC, Z., TOMIC, S., KRKLJES, A., MICIC, M., SULJOVRUJIC, E., Radiolytic synthesis of Ag-poly(BIS-co-HEMA-ci-IA) nanocomposites, Rad. Phys. Chem. **76** (2007) 2661–2665.

[5] KRKLJES, A., NEDELJKOVIC, J., KACAREVIC-POPOVIC, Z., Fabrication of Ag-PVA hydrogel nanocomposite by gamma irradiation, Polym. Bull. **58** (2007) 271–279.

[6] JOVANOVIC, Z., et al., "Properties of Ag/PVP hydrogel nanocomposite synthesized in situ by gamma irradiation", Trends in Nanophysics: Theory, Experiment and Technology (ALDEA, A., BÂRSAN, V., Eds), Springer-Verlag, Berlin, Heidelberg (2010) 315–328.

[7] KACAREVIC-POPOVIC, Z., et al., On the use of radiation technology for nanoscale engineering of silver/hydrogel based nanocomposites for potential biomedical application, Open Conf. Proc. J. **1** (2010) 200–206.
[8] JOVANOVIC, Z., et al., Synthesis and characterization of Ag/PVP hydrogel nanocomposite obtained by in situ radiolytic method, Rad. Phys. Chem. **80** (2011) 1208–1215.
[9] KOKUBO, T., KUSHITANI, H., SAKKA, S., KITSUGI, T., YAMAMURO, T., Solutions able to reproduce in vivo surface-structure changes in bioactive glass-ceramic A-W, J. Biomed. Mater. Res. **24** (1990) 721–734.
[10] VEENAS, C.L., NISSAMUDEN, K.M., SMITHA, S.L., BIJU, V., GOPCHANDRAN, K.G., Off-axis PLD: A novel technique for plasmonic engineering of silver nanoparticles, J. Optoelectr. Adv. Mater. **11** (2009) 114–122.
[11] IRSHAD, A.W., APARNA, G., JAHANGEER, A., TOKEER, A., Silver nanoparticles: Ultrasonic wave assisted synthesis, optical characterization and surface area studies, Mater. Lett. **65** (2011) 520–522.
[12] MA, R., et al., Size-controlled dissolution of organic-coated silver nanoparticles, Environ. Sci. Technol. **46** (2012) 752–759.
[13] CVETICANIN, J., et al., Functionalization of carbon nanotubes with silver clusters, Appl. Surf. Sci. **256** (2010) 7048–7055.
[14] CVETICANIN, J., et al., MALDI TOF and theoretical investigation of silver clusters obtained by gamma irradiation, Vacuum **89** (2012) 47–52.
[15] JOVANOVIC, Z., et al., Structural and optical characteristics of silver/poly(N-vinyl-2-pyrrolidone) nanosystems synthesized by γ-irradiation, Radiat. Phys. Chem. **81** (2012) 1720–1728.

MODIFICATION OF CS NPs BY RADIOLYTIC METHODS: APPROACH TO DRUG CONTROLLED RELEASE SYSTEMS

W. PASANPHAN[1,2], T. RATTANAWONGWIBOON[2], S. CHOOFONG[1], P. RIMDUSIT[1]
[1] Department of Applied Radiation and Isotopes
Faculty of Science
Kasetsart University
Bangkok
[2] Nanomaterials Science
Faculty of Science
Kasetsart University
Bangkok

Thailand

Abstract

Investigation of the radiolytic protocol for preparation of non-modified CS NPs and hydrophobic/hydrophilic modified CS NPs is proposed. The CS NPs are aimed at drug controlled release systems. γ radiation from a ^{60}Co source was used for nanomaterialization by controlling the MW, molecular structure, morphology and particle size of CS NPs. In the present work, the role of ionizing radiation is in induced chain scission and grafting. Radiolysis serves as an environmentally friendly method and simple procedure for preparation of nanoscale sized CS NPs. Amphiphilic core shell CS NPs with a size of 80 nm are obtained, and the shell thickness can be controlled via the irradiation dose. Water insoluble drug encapsulation efficiency and in vitro release behaviour confirm the efficacy of CS NPs for drug controlled release systems. A bioactivity study using a paper disc diffusion method supports not only the inherent antibiotic property of the drug, but also the controlled release aspect of CS NPs. Cytotoxicity tests confirm that the synthesized CS NPs obtained by radiolysis are of benefit for reducing the toxicity of drugs.

1. INTRODUCTION

Naturally occurring polymers, especially polysaccharides such as CS and alginate, have been extensively researched in recent years as a primary material for forming carriers. CS is a biodegradable polysaccharide derived by partial deacetylation of chitin, which is a copolymer of glucosamine and *N*-acetyl-d-glucosamine linked together by β glycosidic bonds [1]. CS can be degraded into *N*-acetyl glucosamine by general Lys in the body, which is subsequently excreted as carbon dioxide via the glycoprotein synthetic pathway [2]. CS has been widely used in pharmaceutical and medical applications, owing to favourable biological characteristics such as biodegradability, biocompatibility, low toxicity and haemostatic, bacteriostatic, fungistatic, anticancerogen and anticholesteremic properties [3].

It is well known that polymer micelles have a unique core shell architecture composed of hydrophobic segments as the internal core and hydrophilic segments as the surrounding corona in the aqueous medium. The hydrophobic core provides a loading space for water insoluble drugs, whereas the modification of the hydrophilic shell affects pharmacokinetic behaviour [4]. Additionally, the nanoscaled polymer micelles exhibit many advantages for the use of drug delivery carriers, such as prolonged circulation, tumour localization by the enhanced permeability and retention effect [5] and controlled drug release by using stimuli sensitive copolymers [6].

Self-assembly through chemical modification is one of the most widely used processes for CS NP fabrication. This aggregation process, caused by incorporation [7] of hydrophobic organic substances into micelles, can play very important roles in the adsorption, transfer and slow release of drugs when treating humans. Various hydrophobilized polymers have been synthesized by modifying an organic group on a hydrophilic polymer [8]. Phthaloyl CS methoxy PEG as a hydrophobic/hydrophilic microsphere with an average size of 1500 nm has been developed [9]. Deoxycholate modified chitosan (DCCS) particles have been widely proposed as solid capsules for lipid drug carriers. Pang et al. [10] reported DCCS with particle sizes in the range 200–600 nm, and that they had the ability to encapsulate tocopherol acetate and stearic methyl ester. Kim et al. [11] carried out a study to control

the particle size and size distribution of self-aggregates of deoxycholic acid (DC) modified CS as a gene delivery carrier within the range 130–300 nm. PEG is one of the biocompatible monomers.

Based on previous reports, chemical modification is the most widely used protocol in preparing hydrophobic/hydrophilic self-assembly CS NPs. In this method, a conjugating agent and a purification step are required. In addition, the nanoscale material has been defined to be less than 100 nm [12]. Therefore, the systematic protocol in reducing and controlling the particle size of CS still requires further studies to achieve not only a simple and effective preparation protocol but also a superior potential product. To the best of our knowledge, there have not been reports on the preparation and modification of non-modified CS NPs and hydrophobic/hydrophilic modified CS NPs using ionizing radiation.

In the present work, radiolytic methodologies to modify CS NPs are studied. The modified CS NPs are mainly proposed for biomedical application purposes, i.e. as drug carriers for drug controlled release. Therefore, the systematic examination of the fabrication conditions of non-modified CS NPs and core shell modified CS NPs using a radiolytic methodology is investigated. γ radiation from a ^{60}Co source was used as the high energy radiation to produce radiolysis products and subsequently induce radical reactions. This mild process is expected to be a novel, nontoxic, simple and effective protocol to prepare CS NPs as drug carrier devices for controlled release systems.

2. EXPERIMENTAL SECTION

2.1. Fabrication of non-modified CS NPs by γ irradiation

CS was prepared in three forms: (i) flake (CS flake), (ii) colloidal (CS colloid) and (iii) acidic aqueous solution (CS acid) [13]. For (i), CS in the form of solid flake was originally used. In the case of (ii), 0.5% w/v CS was predissolved with 1% v/v acetic acid and then precipitated in 1% w/v sodium hydroxide to obtain white colloidal particles. The reprecipitate product was washed with water several times and the 0.5% w/v colloidal product was kept in distilled water. For (iii), 0.5% w/v CS was dissolved in 1% v/v acetic acid. The samples were γ ray irradiated with doses of 5 kGy, 10 kGy, 20 kGy, 40 kGy and 100 kGy (dose rate of 10 kGy/h) at ambient temperature. The irradiated samples were characterized using a calibrated Ubbelohde viscometer, FTIR, TEM and AFM.

2.2. Deoxycholate modified γ irradiated CS NPs

CS colloid and CS flake, irradiated with varying doses of 0 kGy, 5 kGy, 10 kGy, 20 kGy, 40 kGy and 100 kGy, were used as the starting CS for chemical modification. The starting irradiated CS for chemical conjugation was in colloidal form, which was prepared according to Pasanphan et al. [13, 14]. For the heterogeneous system, DC in methanolic solution was added to colloidal CS. EDC was then added to the mixture of CS and DC. Heterogeneous reactions were carried out at ambient temperature for 1–24 h. The sample was rigorously washed with methanol and then dried to obtain DCCS NPs. In the case of the homogeneous reaction, colloidal CS was predissolved in *N*-hydroxysuccinimide with distilled water and stirred for 0.5 h. Then, DC and EDC in methanol solution were added to *N*-hydroxysuccinimide dissolved CS to obtain intermediates, followed by the product DCCS.

2.3. Polyethylene glycol monomethacrylate DCCS NPs by γ irradiation

The DCCS colloidal NPs were dispersed in water. Polyethylene glycol monomethacrylate (PEGMA) was dissolved in water and then mixed with aqueous colloidal DCCS solution. The mixtures were γ ray irradiated with absorbed doses of 2 kGy under ambient temperature in air. The reaction solution was transferred into a dialysis membrane, which was enclosed in 2 L of deionized water and dialysed with renewed water for 72 h. After dialysis, the dialysis solution was freeze-dried at −40°C. The resulting PEGMA grafted DCCS (PEGMA-g-DCCS) NPs were obtained. The degree of grafting (% grafting) was determined by the percentage increase in weight according to the relationship $[(W_g - W_0)/W_0] \times 100$, where W_0 and W_g represent the initial weight of DCCS and the grafted weight of PEGMA-g-DCCS, respectively [15].

2.4. Drug encapsulation efficiency of CS NPs fabricated from radiolytic methods

The effect of PEGMA-g-DCCS NPs and drug concentrations on drug loading efficiency was studied. For the effect of NP concentration, PEGMA-g-DCCS NPs with concentrations varying from 0.1 mg/mL to 5.0 mg/mL were used to load berberine (BBR) with a concentration of 0.0125 mg/mL [15]. For studying the effects of drug concentration, BBR with various concentrations of 0.05–1.0 mg/mL were used under dispersion of 3 mg/mL PEGMA-g-DCCS NPs. Supernatant from centrifugation was carefully decanted, and the drug content in the supernatant was analysed with a UV/VIS spectrometer. The drug encapsulation efficiency of PEGMA-g-DCCS NPs was determined from $[(A - A_0)/A_0] \times 100$, where A and A_0 are the absorbances at the maximum wavelength of the initial amount of drug and the free amount of drug in the supernatant, respectively.

2.5. Drug controlled release behaviour of CS NPs fabricated from radiolytic methods

The release studies were performed in water at 37°C. Drug encapsulated NPs (556 mg) were suspended in 3 mL of release medium and transferred into the dialysis membrane (MWCO = 6000–8000 Da). The sample in the dialysis membrane was immersed in release medium (25 mL) and stirred in a horizontal laboratory shaker and maintained at 37°C in a water bath. Samples (1 mL) were periodically removed, filtered and assayed. The same volume of fresh medium replaced the volume of each sample withdrawn. The amount of released drug was analysed with a spectrophotometer. The drug release studies were performed in triplicate for each of the samples.

2.6. Assay of in vitro cytotoxicity

The relative cytotoxicity of PEGMA-g-DCCS NPs was estimated by MTT viability assay against a normal human skin fibroblast cell line (CRL 2522). The cells were grown in DMEM with 10% foetal bovine serum in a 25 cm^2 culture flask cultured in a humidified incubator with 5% CO_2 at 37°C. After cells grew to the desired concentration, they were centrifuged at 2000 rev./min for 5 min. The cells were washed with PBS and resuspended in DMEM to reach a final cell concentration of 100 000 cells/mL. After treating the cells with PEGMA-g-DCCS NP solution at different concentrations of 0.1–3000 μg/mL, the cell viability was determined using the MTT assay. Viable cells are capable of metabolizing MTT. After treatment, the medium was removed and the culture wells were washed in PBS. The MTT solution was added to each well and incubated for 2 h. The absorbance at 570 nm was recorded using a SpectraMax M2 reader [16].

3. RESULTS AND DISCUSSION

3.1. Fabrication of non-modified CS NPs by γ irradiation

Although several researchers have reported MW reduction of CS by ionizing radiation, most of the CS was irradiated in the conditions of flake, CS in acidic aqueous solution, CS flake dispersed in water or in $K_2S_2O_8$ and H_2O_2 [13, 17–20]. It is suspected that the key factors of lowering the MW were not just the radiation absorbed dose but also the irradiation condition in terms of the physical forms of CS. Therefore, a novel irradiation condition — aqueous colloidal CS (CS colloid)—was studied compared to the most widely used irradiation conditions, such as solid flake and aqueous acetic acid solution. To elucidate the effect of irradiation conditions on MW reduction and chemical structure, CS was irradiated in three different physical forms: CS flake, CS colloid and CS acid. Figure 1 shows that the viscosity averaged MW of CS decreased continuously as the γ ray dose increased. The significant reduction of the MW implies chain scission. It was found that the MW of CS decreased in the order of CS acid, CS colloid and CS flake. In comparison, the MW of CS flake, CS colloid and CS acid decreased by 3, 10 and 1000 times compared to the original MW, respectively.

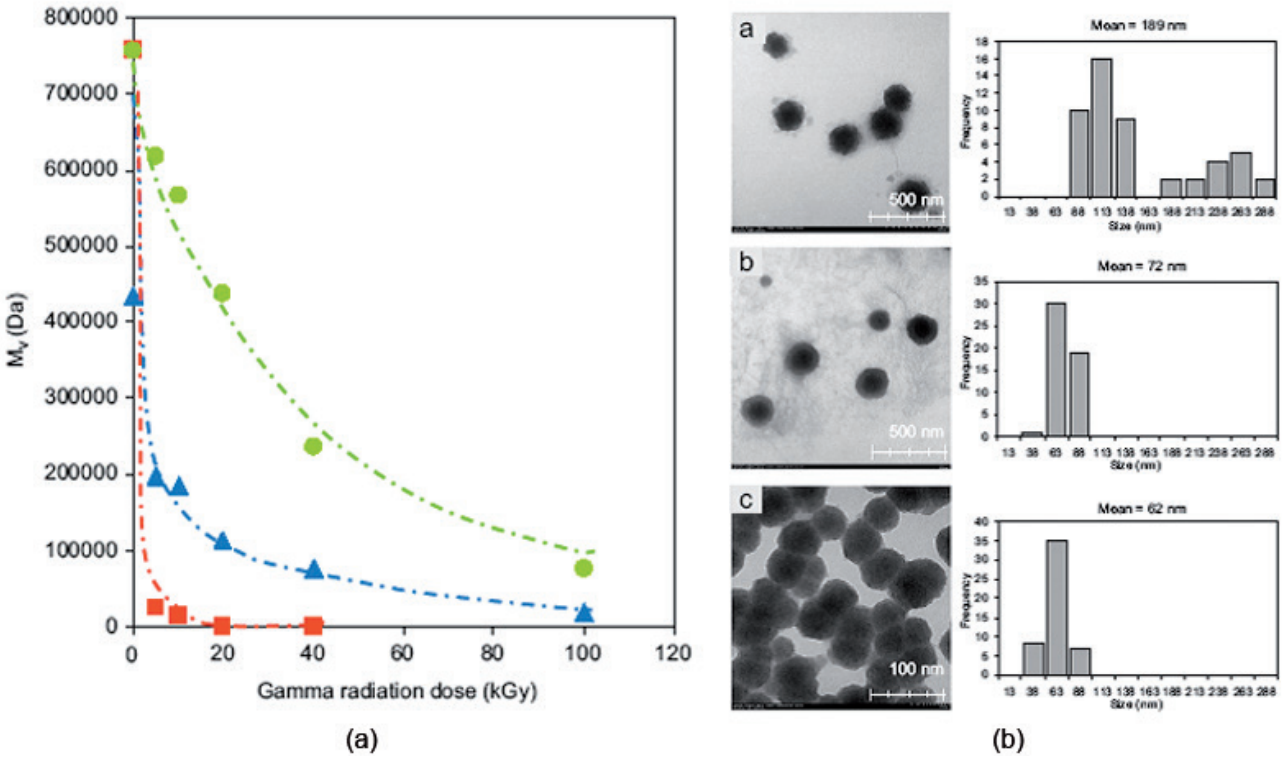

FIG. 1. (A) Viscosity averaged MW of irradiated condition of CS flake (●), CS colloid (▲) and CS acid (■). (B) Representative TEM images and size distribution of non-modified CS NPs from CS colloid irradiated with doses of: (a) 0 kGy, (b) 5 kGy and (c) 10 kGy.

This can be confirmed by the fact that the amount that chain scission lowered the MW was also based on the physical formulation of CS during irradiation. The MW of CS flake decreased significantly — by 70% for the first 50 kGy, whereas it decreased by as much as 90% in the case of CS colloid. The level of MW reduction in CS flake was consistent with a previous report [15]. However, CS colloid showed the most efficient irradiation condition compared to that of CS flake, which was dispersed in water. From prior observations, CS flake resulted in about the same MW reduction as CS flake dispersed in water, which was a 70% reduction when compared to the original MW. In this work, irradiation of CS colloid gave MWs that were three to four times lower than those of CS flake when irradiated with a dose of 5–100 kGy.

As the study was mainly focused on the systematic preparation of CS NPs by γ ray irradiation, the particle size was essentially investigated. The observations from TEM provided information on the particle shape and size. The irradiations of the CS flake (data not shown) and CS colloid (Fig. 1(B)) gave the individual spherical shapes. On the other hand, it was difficult to identify the irradiated CS acid as a spherical shape (data not shown). CS particles from CS acid were found in variable shapes: spherical, whisker, spiral, etc.

The relationship between radiation dose and particle size as shown in Fig. 2(a) confirmed that the higher the radiation dose, the smaller the particle size. Additionally, the irradiation of CS in CS colloid seemed to bring the particle sizes down to lower than those in CS flake. The particle sizes were less than 100 nm, i.e. 72 nm, when using a γ ray dose as low as 5 kGy. The particle size decreased by 70% when CS colloid was exposed to a γ ray dose of 10 kGy—the particle size achieved was around 50 nm—whereas the particle size decreased by only 30% when CS flake was exposed to an equal radiation dose. To reduce the particle size to 50 nm in the case of CS flake, the γ ray dose must be increased to 40–100 kGy. The number of particles of spherical shape was more easily observed in the case of CS colloid than in CS flake. In the case of CS acid, the particle size exhibited a noticeable variation with radiation doses (Fig. 2(b)). Based on the present investigation, it is suspected that CS colloid would serve as a proper route under mild irradiation conditions for preparing CS NPs via γ ray irradiation.

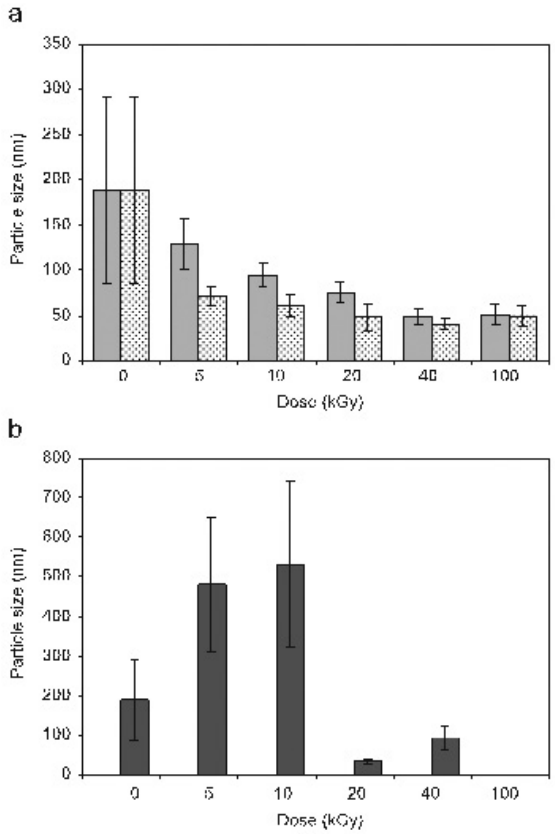

FIG. 2. Relationship between particle size and γ radiation dose of: (a) CS flake (solid bars) and CS colloid (hatched bars) and (b) CS acid [13, 14].

3.2. Preparation of DCCS NPs: Chemical conjugation of DC onto γ irradiated CS NPs

To formulate the hydrophobic core of CS, DC was chemically conjugated onto both non-irradiated and irradiated CS flake and CS colloid (Fig. 3(A)). The preparation was carried out in heterogeneous and in homogeneous systems [14, 21]. The possible chemical structures of DCCS achieved from heterogeneous and homogeneous reactions are as in compounds (a) and (b), respectively (Fig. 3(B)).

The morphologies of DCCS were also observed using AFM. Figure 3(C) shows AFM images of non-modified CS colloid (Fig. 3(C), part a) and DCCS from the heterogeneous (Fig. 3(C), part b) and homogeneous (Fig. 3(C), part c) reactions. The morphologies of DCCS were confirmed as having a spherical shape, as seen in TEM images (data not shown). Compared with the non-modified CS colloid, the particle sizes of DCCS from the heterogeneous and homogeneous systems were reduced by 25% and 10%, respectively. It is suspected that the amount of conjugated DC moieties and the CS chain length may play important roles in determining particle size. The appropriate amount of conjugated molecules, as well as the CS chain length, may lead to desirable particle shapes and sizes. CS NPs obtained in the preparation described in Section 3.1 were in the colloidal form. It is suspected that the DC could be conjugated onto the surface of the colloidal CS particle. In an aqueous hydrophilic system, the self-assembly formulation occurred when the DC side group turned into the interior particle to serve as a hydrophobic core.

Figure 4(A) indicates that the preirradiation dose, the physical formulation of CS and the DC conjugation all influence the particle size of DCCS. The average particle size of DCCS was as small as 46 nm for CS colloid (Fig. 4(A), part d) and 72 nm for CS flake (Fig. 4(A), part b) when DC was conjugated onto 10 kGy γ preirradiated CS in Fig. 4(A), parts c and a. Figure 4(B), part b, shows that the 10 kGy preirradiation could reduce the particle size of DCCS when the conjugation system was carried out under a simple heterogeneous reaction. In this way, only the EDC conjugating agent was used. For homogeneous reactions, DCCS exhibited a preirradiated dose that was completely independent. Therefore, preirradiation with a dose of only 10 kGy of CS before heterogeneous

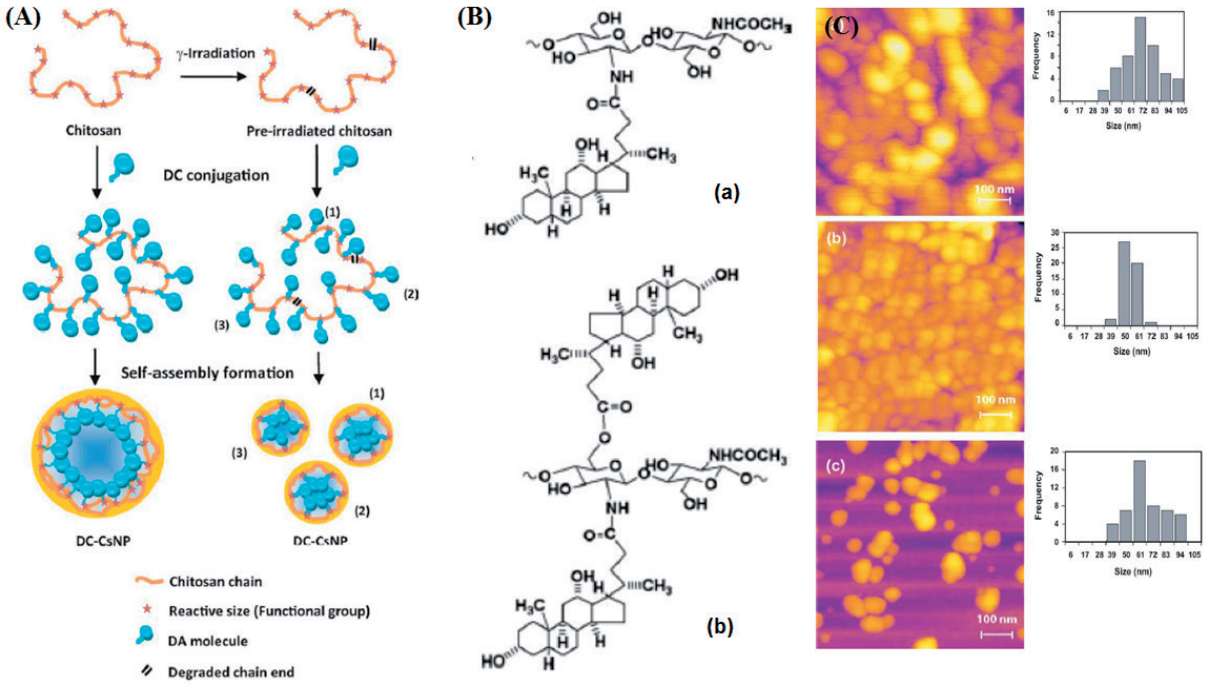

FIG. 3. (A) Possible formation of DCCS NPs from non-irradiated CS and preirradiated CS. (B) Possible chemical structures of DCCS NPs from (a) heterogeneous and (b) homogeneous reactions. (C) AFM images and size distribution plots of: (a) 10 kGy preirradiated CS colloid, (b) DCCS NPs from conjugation of DC onto (a) in the heterogeneous system and (c) DCCS NPs from conjugation of DC onto (a) in the homogeneous system [14].

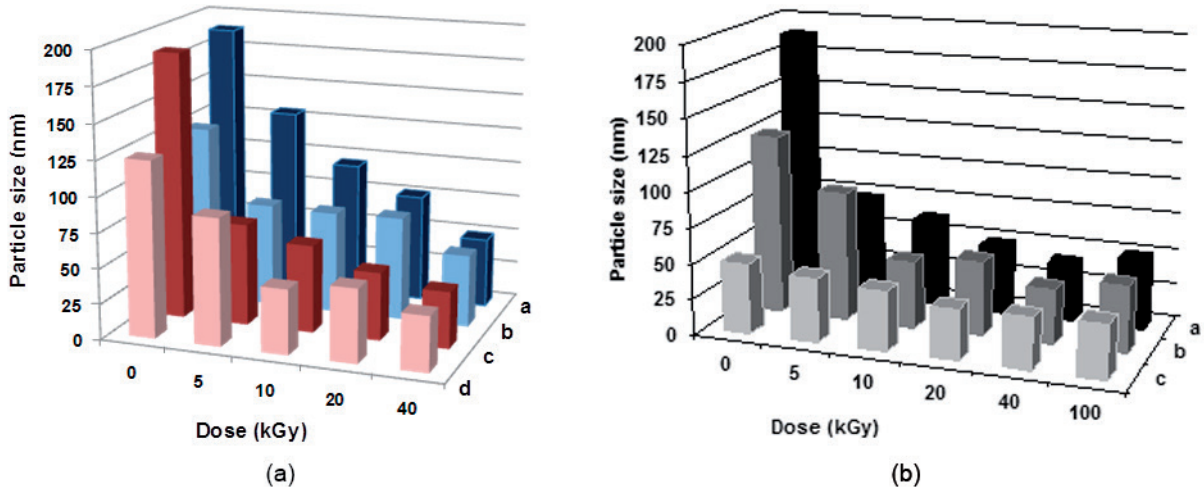

FIG. 4. (A) Particle size of: (a) irradiated CS flake, (b) irradiated CS flake after conjugation with DC, (c) irradiated CS colloid and (d) irradiated CS colloid after conjugation with DC. (B) Particle size of: (a) CS colloid, (b) DCCS from heterogeneous reactions and (c) DCCS from homogeneous reactions.

conjugating DC onto CS would be a potential method for achieving nanoscale particles instead of using many types of conjugating agents with many steps of preparation and purification, as in homogenous reactions.

3.3. PEGMA-g-DCCS by γ radiation synthesis

The representative TEM image in Fig. 5 shows that PEGMA-g-DCCS formed spherical shapes with core shell structures. The particle morphology was interpreted as two distinct layers of PEGMA shell and DC core. The average particle size was calculated to be ~80 nm.

3.4. Drug encapsulation efficiency

The encapsulation efficiency of BBR into PEGMA-g-DCCS NPs was substantially affected by the initial amount of PEGMA-g-DCCS and drug concentration (Fig. 6). For the effect of NP concentration and by controlling the BBR concentration at 0.0125 mg/mL, the maximum encapsulation efficiency of PEGMA-g-DCCS with a particle size of 80 nm was 9% when the initial amount of PEGMA-g-DCCS was 0.1 mg/mL (Fig. 6(A)). A remarkable decrease in the encapsulation efficiency to less than 1% was observed when the initial amount was 5 mg/mL. The increase in solution viscosity with higher PEG-g-DCCS NP concentrations could be a major contributor to the decrease of encapsulation efficiency. It has been reported that the high viscosity associated with increased CS concentrations hinders encapsulation of the drug [2].

For the drug concentration effect (Fig. 6(B)), it was found, in 80 nm particles, that the encapsulation efficiency increased from 7% to 29% when the BBR concentration was increased from 0.05 mg/mL to 0.7 mg/mL, whereas a remarkable decrease in the encapsulation efficiency to 21% was found when the BBR concentration increased to 1 mg/mL. By using 3 mg/mL NP concentrations with a particle size of 80 nm, the optimum concentration of BBR was 0.7 mg/mL.

3.5. Drug controlled release studies

To evaluate the potential of PEGMA-g-DCCS NPs as drug carriers of BBR, the release behaviour of BBR from PEGMA-g-DCCS NPs was assessed at 37°C in water. During these experiments, the sink conditions were maintained by regularly replacing the dialysis medium with the same amount removed. The in vitro release profile of BBR-PEGMA-g-DCCS NPs in water is shown in Fig. 7. This shows that almost 90% of BBR was released after 1 h, followed by fluctuated, reduced and sustained release for 550 h. However, the BBR encapsulated NPs provided an almost constant 10% BBR release in water for about 1 month.

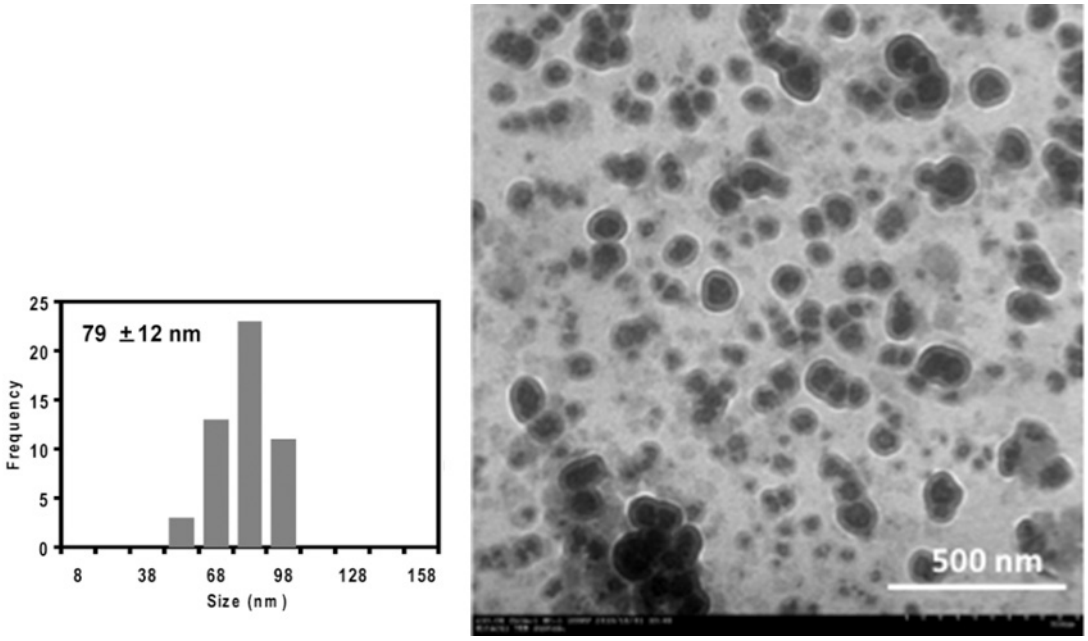

FIG. 5. (Left) Size distribution plot and (right) TEM image of PEGMA-g-DCCS prepared from radiation synthesis with a dose of 2 kGy [15].

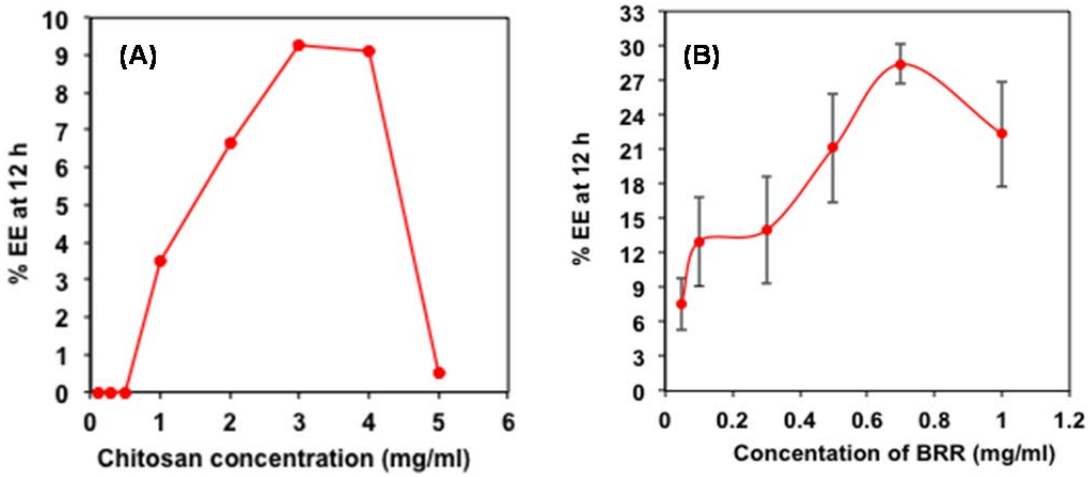

FIG. 6. Effect of (A) CS NP concentration and (B) drug concentration on drug loading efficiency [15]. %EE: percentage encapsulation efficiency.

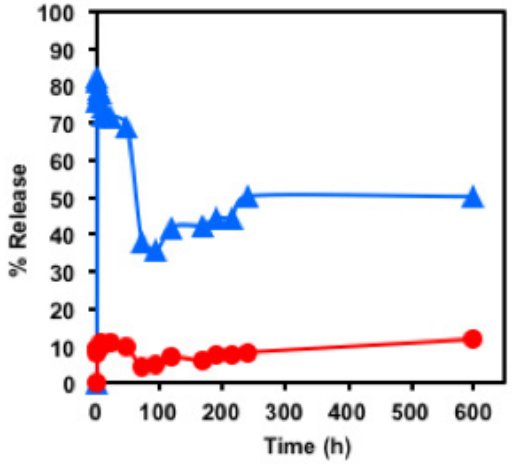

FIG. 7. Kinetic release profile of unloaded BBR (▲) and BBR loaded PEGMA-g-DCCS NPs (●) in water.

3.6. Cytotoxicity tests

The cytotoxicity of PEGMA-g-DCCS NPs was evaluated to ensure its capacity for use in biomedical applications. The cell viability of the human skin fibroblast cell profile is shown in Fig. 8. The inhibition concentration at 50% of empty PEGMA-g-DCCS was observed to be 2616 μg/mL. The PEGMA-g-DCCS NPs are non-toxic to human skin fibroblast cells.

4. CONCLUSIONS

The present experiments have proved that an alternative radiolytic methodology is a simple and effective procedure to fabricate both non-modified CS and hydrophobic/hydrophilic modified CS NPs. γ radiation is not only useful for degradation of CS but also for controlling the particle size in the nanoscale range (1–100 nm). It can also be used to graft the hydrophilic molecule, i.e. PEGMA, onto CS NPs without any conjugating agent. This modification under mild conditions in the presence of water could be carried out also as the final step of modification. The PEGMA-g-DCCS NPs exhibit mostly spherical shapes as small as 80 nm. The BBR drugs are successfully encapsulated into PEGMA-g-DCCS NPs. The encapsulated drugs were slowly and constantly released (10% per day) from the particles for 20 d. MTT cytotoxic tests indicated that the PEGMA-g-DCCS

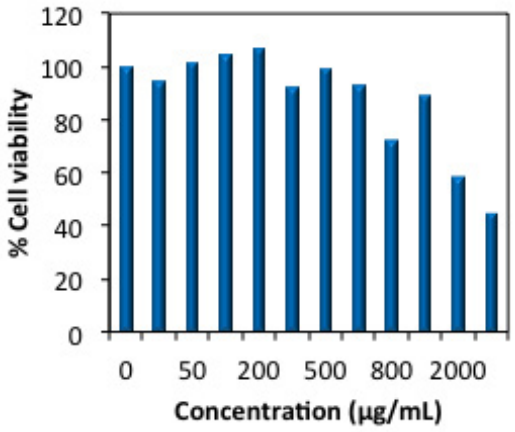

FIG. 8. In vitro cytotoxicity of PEGMA-g-DCCS NPs against human breast cancer cells (normal human skin fibroblast) cell line CRL 2522 by MTT assay.

NPs are non-toxic to human skin cells. Based on observations, the radiolytic method can be used as a potential environmentally friendly, non-toxic, energy efficient process to develop biomedical materials and health products.

ACKNOWLEDGEMENTS

The authors of this report gratefully acknowledge the IAEA for financial support and the Faculty of Science, Kasetsart University, Thailand, for the Science Research Fund matching grant. The Office of Atoms for Peace and Thailand Institution of Nuclear Technology, Thailand, are appreciated for providing some facilities. Thanks to S. Chirachanchai for providing the transmission electron microscope (Hitachi H-7650).

REFERENCES

[1] DOUGLAS, K.L., PICCIRILLO, C.A., TABRIZIAN, M., Effects of alginate inclusion on the vector properties of chitosan-based nanoparticles, J. Controll. Release **115** (2006) 354–361.
[2] GAN, Q., WANG, T., Chitosan nanoparticle as protein delivery carrier — systematic examination of fabrication conditions for efficient loading and release, Coll. Surf. B: Biointerfaces **59** (2007) 24–34.
[3] HEJAZI, R., AMIJI, M., Chitosan-based gastrointestinal delivery systems, J. Controll. Release **89** (2003) 1–165.
[4] HUH, K.M., et al., Hydrotropic polymer micelle system for delivery of paclitaxel, J. Controll. Release **101** (2005) 59–68.
[5] MAEDA, H., The enhanced permeability and retention (EPR) effect in tumour vasculature: The key role of tumour-selective macromolecular drug targeting, Adv. Enzyme Regul. **41** (2001) 189–207.
[6] YOO, H.S., PARK, T.G., Folate receptor targeted biodegradable polymeric doxorubicin micelles, J. Controll. Release **96** (2004) 273–283.
[7] LEE, K.Y., KWON, I.C., KIM, Y.H., JO, W.H., JEONG, S.Y., Preparation of chitosan self-aggregates as a gene delivery system, J. Controll. Release **51** (1998) 213–220.
[8] DESBRIES, J., MARTINES, C., RINAUDO, M., Hydrophobic derivatives of chitosan: Characterization and rheological behaviour, Int. J. Biol. Macromol. **19** (1996) 21–28.
[9] YOKSAN, R., AKASHI, M., HIKATARI, K., CHIRACHANCHAI, S., Controlled hydrophobic/hydrophilicity of chitosan for spheres without specific processing technique, Biopolym. **69** (2003) 386–390.
[10] PANG, H.T., CHEN, X.G., PARK, H.J., CHA, D.S., KENNEDY, J.F., Preparation and rheological properties of deoxycholate-chitosan and carboxymethyl-chitosan in aqueous systems, Carbohydr. Polym. **69** (2007) 419–425.
[11] KIM, Y.H., GIHM, S.H., PARK, C.R., Structural characteristics of size-controlled self-aggregates of deoxycholic acid-modified chitosan and their application as a DNA delivery carrier, Bioconj. Chem. **12** (2001) 932–938.
[12] RATNER, M., RATNER, D., Nanotechnology: A Gentle Introduction to the Next Big Idea, Prentice Hall, New Jersey (2001) 7.
[13] PASANPHAN, W., RIMDUSIT, P., CHOOFONG, S., PIROONPAN, T., NILSUWANKOSIT, S., Systematic fabrication of chitosan nanoparticle by gamma irradiation, Radiat. Phys. Chem. **79** (2010) 1095–1102.

[14] PASANPHAN, W., CHOOFONG, S., RIMDUSIT, P., Deoxycholate-chitosan nanosphere fabricated by γ-irradiation and chemical modification: nanoscale synthesis and controlling studies, J. Appl. Polym. Sci. **123** (2012) 3309–3320.
[15] PASANPHAN, W., RATTANAWONGWIBOON, T., RIMDUSIT, P., "A green radiolytic synthesis of PEGMA-*grafted*-deoxycholate chitosan as a drug carrier", Proc. 10th Mtg Ionizing Radiation and Polymers (IRaP2012), Krakow, Poland, 14–19 October 2012.
[16] WANG, S., et al., Challenge in understanding size and shape dependent toxicity of gold nanomaterials in human skin keratinocytes, Chem. Phys. Lett. **463** (2008) 145–149.
[17] RIMDUSIT, P., PASANPHAN, W., "Gamma-ray generated chitosan nanoparticle: systematic preparation study", Proc. 7th Eco-Energy and Materials Science and Engineering Symp., Chiang Mai, Thailand, 17–22 November 2009.
[18] YOKSAN, R., AKASHI, M., MIYATA, M., CHIRACHANCHAI, S., Optimum γ-ray dose and irradiation conditions for producing low-molecular-weight chitosan that retain its chemical structure, Radiat. Res. **161** (2004) 84–93.
[19] HUANG, Q.Z., WANG, S.M., HUANG, J.F., ZHUO, L.H., GUA, Y.C., Study on the heterogeneous degradation of chitosan with hydrogen peroxide under the catalysis of phosphotungstic acid, Carbohydr. Polym. **68** (2007) 761–765.
[20] QIN, C.Q., DU, Y.M., XIAO, L., Effect of hydrogen peroxide treatment on the molecular weight and structure of chitosan, Polym. Degrad. Stab. **76** (2002) 211–218.
[21] CHOOFONG, S., PASANPHAN, W., "Particle size lowering of chitosan nanosphere by gamma irradiation and chemical modification", Proc. 7th Eco-Energy and Materials Science and Engineering Symp., Chiang Mai, Thailand, 17–22 November 2009.

SURFACE AND BULK NANOSTRUCTURING OF POLYMERS BY RADIATION ENGINEERING FOR BIOMEDICAL APPLICATIONS

O. GÜVEN, M. BARSBAY, M. AKBULUT, S. DUYGU SÜTEKİN
Department of Chemistry
Hacettepe University
Beytepe, 06800, Ankara
Turkey

Abstract

This report compiles the results of work on using radiation for nanoscale grafting of responsive polymers onto the surface of cellulose, AAc and *N*-isopropylacrylamide (NIPAAm), which are the two monomers that show pH and temperature responsiveness. The second part of the report is related to the synthesis of molecularly imprinted polymeric matrices with the ultimate aim of using them as recognitive systems—drug delivery systems. The nanoscale cavities produced during radiation induced cross-linking of functional polymers around the template molecule D-glucose have been shown to be the key factor in controlling the performance of these systems in molecular imprinting. The third part of the report is related to the preparation of nanogels. Although radiation preparation is straightforward, control of the particle sizes of nanogels has been a challenging issue. The results of recent work on using radiation for the synthesis of PVP nanogels in the range 40–200 nm by making use of the principles of solution thermodynamics of aqueous polymer solutions are reported. The use of radiation as a constant source of radical generation and RAFT agents for the control of free radical polymerization provided full control over the MW and distribution of homopolymers and copolymers that were synthesized in this project.

1. INTRODUCTION

The scope of this research contract on radiation formation of nanostructures can be split into three parts, which are all related to the final application of developed systems for biomedical use.

The first part concerns the preparation of well defined nanoscale polymeric brushes on cell culture devices that would allow easy detachment of cell sheets grown on these surfaces [1]. The monomer used for grafting, namely NIPAAm, has temperature responsive behaviour, which causes the graft chains to undergo large volume changes upon small temperature differences for the non-invasive, non-destructive release of surface grown cell sheets.

The second part of the project is related to the synthesis of molecularly imprinted polymeric matrices with the ultimate aim of using them as recognitive systems—drug delivery systems [2, 3]. The nanoscale cavities produced during radiation induced cross-linking of functional polymers around the template will be the key factor in controlling the performance of these systems in molecular imprinting.

The third part deals with developing a methodology for the radiation synthesis of PVP nanogels with controlled sizes.

In the first part of this work, γ radiation and RAFT polymerization were combined for the preparation of graft copolymers with well defined and smart surface properties. Renewable and natural based intelligent cellulosic surfaces that respond to several stimuli (i.e. temperature and pH) and clean themselves have been prepared via this facile and powerful combination. In this study, novel thermoresponsive cellulose surfaces of PNIPA and pH responsive cellulose surfaces of PAAc were prepared using the γ initiated RAFT graft polymerization technique. The responses of these surfaces to changing temperature and pH values were investigated by following the changes in the CA of water.

Radiation induced molecular imprinting of D-glucose onto a poly(2-HEMA) matrix was achieved to create three dimensional cavities to recognize and bind D-glucose. The optimization of imprinting capability of matrices was achieved by investigating the effects of various parameters such as the type and amount of cross-linking agent, type of solvent, template to monomer ratio and total absorbed dose. Cross-linking agents with increasing chain lengths and different flexibilities were used in an attempt to elucidate the impact of relevant imprint parameters on the effectiveness of the imprinting technique. The absorbed doses varied from 1 kGy to 15 kGy. Cavity sizes of molecular imprinted polymers (MIPs) were measured by positron annihilation lifetime spectroscopy experiments [4]. Control matrices were synthesized with exactly the same composition in the absence of D-glucose.

Separation of D-glucose has been shown to be successfully achieved in high performance liquid chromatography (HPLC) columns filled with MIPs, whereas no separation was observed for non-imprint matrices [5].

Preparation of hydrogels on the nanoscale has become of great importance because of their potential applications, especially in the delivery of water insoluble drugs. To control their sizes for better bioavailability and longer circulation times in the body, a methodology based on the solution thermodynamics of aqueous solutions of PVP has been developed. PVP nanogels within the size range 40–200 nm were thus prepared from water/acetone mixtures close to theta conditions.

2. EXPERIMENTAL METHOD

2.1. Synthesis of PNIPA and PAAc brushes

2.1.1. Polymerization

The monomers, NIPAAm (Aldrich) and AAc (BDH), after purification, were dissolved separately with the RAFT agent 3-benzylsulphanylthiocarbonylsulphanyl propionic acid (BPATT) in a deionized water/ethanol mixture (9/1 v/v). The monomer concentrations and the monomer/chain transfer agent ratios are given in Table 1. After complete dissolution of the reactants, the stock solution was divided into 10 mL aliquots and transferred to glass sample vials. BPATT immobilized cellulose, i.e. the macrochain transfer agent (~0.01 g), was also added to vials as the substrate to be grafted (the synthesis of BPATT immobilized cellulose and the reason for using a RAFT agent immobilized substrate instead of a pristine surface are explained elsewhere [6]). The vials were capped with rubber septa and deoxygenated by purging with nitrogen gas for 20 min each. The samples were γ irradiated with a ^{60}Co source at ambient temperature, and then removed periodically to determine the conversion and relevant properties of the synthesized polymers. Monomer to polymer conversions were evaluated using ^{1}H NMR spectroscopy. Synthesized cellulosic copolymers were purified with sufficient rinsing. Details of this purification and calculation method for graft ratio (GR, wt%) and graft frequency (GF) have been described elsewhere [6].

TABLE 1. RAFT GRAFT POLYMERIZATION OF NIPAAm AND AAc BY γ INITIATION (0.02 kGy/H) WITH BPATT AS THE RAFT AGENT[a]

Entry	Monomer	$\frac{[M]_0}{[CTA]_{0\ b}}$	Time (min)	Conversion[c] (%)	GR[d] wt%	GF[d]	$M_{n,theor}$[d] (g/mol)	$M_{n,SEC}$[e] (g/mol)	PDI[e]
1	NIPAAm	311	200	14	~3	1.48	5 200	9 900	1.14
2	NIPAAm	311	390	37	7	2.22	13 280	17 900	1.16
3	NIPAAm	311	750	61	13	2.36	21 720	30 500	1.14
4	NIPAAm	311	1 440	96	19	2.55	34 020	41 800	1.15
Blank[f]	NIPAAm	—	390	>98	12	0.12	—	492 300	3.06
5	AAc	285	390	21	<2	1.14	4 590	8 800	1.24
6	AAc	285	630	47	5	1.97	9 920	13 300	1.12
7	AAc	285	750	51	6	2.14	10 740	14 100	1.26
8	AAc	285	990	73	9	3.04	15 260	19 500	1.17

TABLE 1. RAFT GRAFT POLYMERIZATION OF NIPAAm AND AAc BY γ INITIATION (0.02 kGy/H) WITH BPATT AS THE RAFT AGENT[a] (cont.)

Entry	Monomer	$\frac{[M]_0}{[CTA]_{0\ b}}$	Time (min)	Conversion[c] (%)	GR[d] wt%	GF[d]	$M_{n,theor}$[d] (g/mol)	$M_{n,SEC}$[e] (g/mol)	PDI[e]
9	AAc	285	1 440	93	14	3.45	19 360	23 100	1.19
Blank[f]	AAc	—	630	>98	8	0.11	—	397 200	2.62

[a] RAFT graft polymerization of $[NIPAAm]_0$ = 1.5 mol/L and $[AAc]_0$ = 2 mol/L from BPATT functionalized cellulose (~0.01 g) initiated via γ irradiation (0.02 kGy/h) in water/ethanol (9/1 v/v) at room temperature.

[b] Ratio of the concentration of monomer to that of the RAFT agent.

[c] Monomer conversion was determined from NMR analysis.

[d] See Ref. [6] for the details of GR, GF and theoretical number averaged MW, $M_{n,theor}$, calculations.

[e] Number averaged MW, M_n and PDI values, determined via SEC, using dimethylacetamide as the eluent with polystyrene standards for the non-grafted polymers formed during grafting.

[f] The filter paper was not modified with BPATT, but subjected to polymerization conditions, and no free BPATT was added to the medium.

Note: — = conventional graft polymerizations.

2.1.2. Characterization

GPC was performed in dimethylacetamide (0.03% w/v LiBr, 0.05% butylated hydroxyl toluene) at 40°C (flow rate = 1 mL/min). CA measurements were achieved using a DSA100 CA goniometer (Krüss). Drop volumes were 10 µL and average CA values were obtained by measuring the same sample in four different positions. XPS measurements were carried out on an ESCALAB220i-XL (VG) surface analysis instrument with a monochromatized Al Kα X ray source.

2.2. Synthesis of D(+)glucose imprinted polymers

D(+)glucose imprinted polymers were synthesized in the presence of dimethyl sulphoxide/isopropyl alcohol (3/1, v/v) mixture as porogen, at room temperature, in air by the radical polymerization method where γ rays were used as the initiator. The irradiation dose was 15 kGy, the mole ratio of functional monomer to target molecule was 3/1 and the amounts of cross-linking agents were 20% and 30%, by mole. In a typical synthesis, first, a template molecule was dissolved in dimethyl sulphoxide, and then HEMA was added to provide formation of a prepolymerization complex between the template and the functional monomer. The cross-linking agent was dissolved in isopropyl alcohol, and then added to the mixture of HEMA and D(+)glucose. After that, the solution was purged with nitrogen for 5 min. Free radical polymerization was initiated and carried out in air at room temperature in a Gamma cell 220, ^{60}Co γ irradiator (Nordion, Canada). After the polymerization, polymer monoliths were crushed and ground to sizes between 100 µm and 150 µm. In addition to the monoliths, some of the imprinted polymers were synthesized between the clamped glass slides (60 mm × 60 mm × 2 mm), which were separated from each other with a natural rubber ring to obtain a disc to be used in positron annihilation lifetime experiments. Both types of imprinted polymers were washed in water to remove the template molecule and unpolymerized material. The swilling solution was changed at 12 h, and checked using a UV/VIS spectrophotometer (Varian, Cary100) and HPLC (Waters). After washing was completed, the discs were dried at 40°C in an oven. The non-imprinted polymers that do not include D(+)glucose were synthesized with the same procedure.

2.3. Synthesis of PVP nanogels

PVP (BASF, MW = (1.278 ± 0.023) × 10^6 g/mol, determined by static light scattering) was used as received without further purification. Acetone (Sigma-Aldrich, Chromasolve for HPLC, 99.9%) was used without further purification, and all the solutions were prepared with deionized water with a maximum conductivity of 0.01 μS and filtered through 0.2 μm pore size Durapore filters (Millipore) prior to the experiments.

PVP nanogels were synthesized via the radiation induced cross-linking method in the presence and absence of acetone in aqueous solutions of PVP. All solutions were prepared freshly and placed in glass vials sealed with rubber septa and saturated with N_2O for 10 min prior to irradiation. Deionized water and HPLC grade solvents were used for sample preparation and analysis.

γ irradiation was carried out at Sarayköy Nuclear Research and Training Center, Turkey, by placing the samples inside the irradiation chamber of a Gamma cell (Tenex Issledovatel) at ambient temperature. A ^{60}Co source with an average dose rate of 1.34 kGy/h was used for irradiation. Samples were taken from the chamber at different time intervals to adjust the total absorbed doses to 5 kGy, 10 kGy and 15 kGy.

The nanogels were characterized using nanosizer, AFM and SEM techniques.

3. RESULTS AND DISCUSSION

3.1. Synthesis of PNIPA brushes

Table 1 and Figs 1 and 2 summarize the results of homopolymers formed during the graft polymerization of NIPAAm and AAc from a cellulose substrate under γ irradiation at room temperature in aqueous media.

As can be seen from Table 1, the apparent number averaged MW, M_n, values obtained using polystyrene standards are almost comparable to the theoretical M_n values $M_{n,theor}$, of both PNIPA and PAAc. The PDI values of the resulting polymers are narrow, i.e. PDI ≤ 1.26, indicating that a well controlled polymerization occurred via the RAFT process. The difference between the theoretical and the experimental MWs can be attributed to the calibration of the GPC on the basis of polystyrene equivalents, universal calibration. In addition to the RAFT mediated graft polymerizations, conventional graft polymerizations were also achieved (denoted as '—' in Table 1), and comparison of the results clearly confirms the controlled fashion and success of the grafting mediated via RAFT (compare the M_n, PDI and GF values). As can be seen from Figs. 1(a) and 2(a), the GPC traces were unimodal and narrow at all conversions.

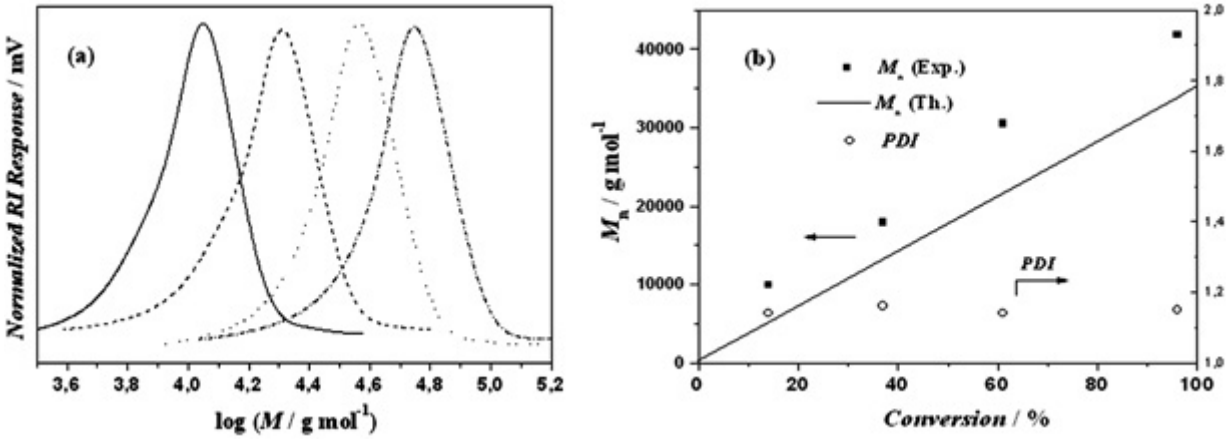

FIG. 1. (a) Evolution of MW distribution and (b) evolution of Mn and PDI versus monomer conversion: free PNIPA formed during γ initiated graft polymerization from cellulose mediated via BPATT. [NIPAAm] = 1.5 mol/L, dose rate = 0.02 kGy/h, in water/ethanol (9/1 v/v) and [NIPAAm]/[BPATT] = 310/1, at room temperature.

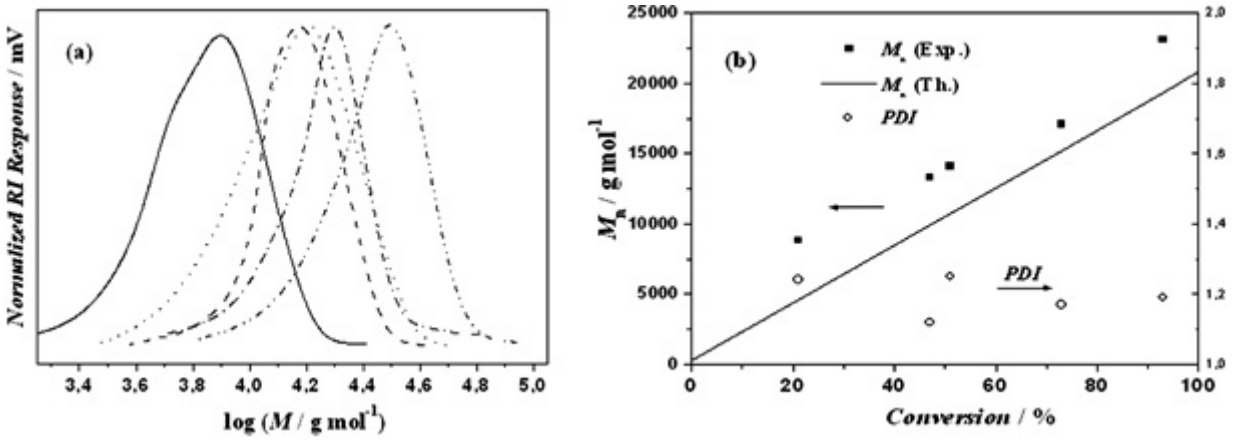

FIG. 2. (a) Evolution of MW distribution and (b) evolution of Mn and PDI versus monomer conversion. [AAc] = 2 mol/L, dose rate = 0.02 kGy/h, in water ethanol (9/1 v/v) and [AAc]/[BPATT] = 285/1, at room temperature.

Moreover, it is obvious that the MW increases linearly with conversion (see Figs 1(b) and 2(b), where M_n and the PDI evolutions with the conversion are depicted), which again demonstrates the well defined behaviour of the grafting for both monomers under the mentioned reaction conditions (homopolymers formed during grafting are direct indicators for the characterization of grafted chains, see Ref. [7] for more details).

XPS was used to confirm the grafting of both monomers from cellulose. The surface chemical compositions calculated using the peak areas of the XPS survey wide scans indicate significant changes following the grafting: the C atom amount increases from 62.8% to 78.3% and 69.0%, whereas the O atom amount decreases from 34.1% to 11.2% and 30.7% for the copolymers of NIPAAm and PAAc, respectively (see the quantification results inserted in the C 1s XPS spectra in Figs 3(A)–(C)). The C 1s XPS spectra show a considerable change in carbon atom amounts in different functional groups: the C 1s spectrum of BPATT immobilized cellulose (Fig. 3(A)) consists of a main peak with a binding energy of 286.5 eV, which is attributed to C–O bonds. However, after the grafting of NIPAAm and AAc, the main peaks appear at 285 eV, which are attributed to non-oxygenated C, i.e. C–C and C–H bonds. Moreover, the C 1s spectrum of cellulose-g-PNIPA presents a new band at 286.1 eV, which corresponds to C–N bonds. These results confirm the successful grafting of both polymers from cellulose.

3.1.1. Responsive behaviour of graft polymers

PNIPA is one of the most widely studied synthetic responsive polymers, and it undergoes a sharp coil to globule transition in water around its LCST of 32°C, changing from a hydrophilic state below this temperature to a hydrophobic state above it [8]. PAAc responds to changes in pH and ionic strength by changing the coil dimensions and solubility. In general, PAAc displays a broad pKa value of 4–5 and thus a proportion of its side chain carboxyls are ionized around pH5–pH6. Below this pH value, a PAAc grafted surface is hydrophobic with collapsed polymer brushes, whereas it becomes hydrophilic in neutral and alkaline aqueous media [9].

The effect of temperature on the wettability of the 19% PNIPA grafted cellulose surfaces was characterized by static CA measurements. At temperatures below the LCST (i.e. 25°C), a water droplet applied to the surface had a CA of 101.4° ± 2.8°; however, it was gradually adsorbed into the surface and disappeared within 60 s. When the temperature increased to 35°C (i.e. above the LCST), the CA was 111.0° ± 3.1°, with an increased stability; it was around 38° and 22° after 60 s and 90 s, respectively, and became totally absent at the end of the second minute (see Fig. 4). The increased durability of CA above the LCST is attributed to the hydrophobicity of the surface induced by PNIPA grafts. However, results also indicate that the surface of cellulose was not totally covered with PNIPA, and the exposed areas led to the adsorption of water because of their hydrophilicity.

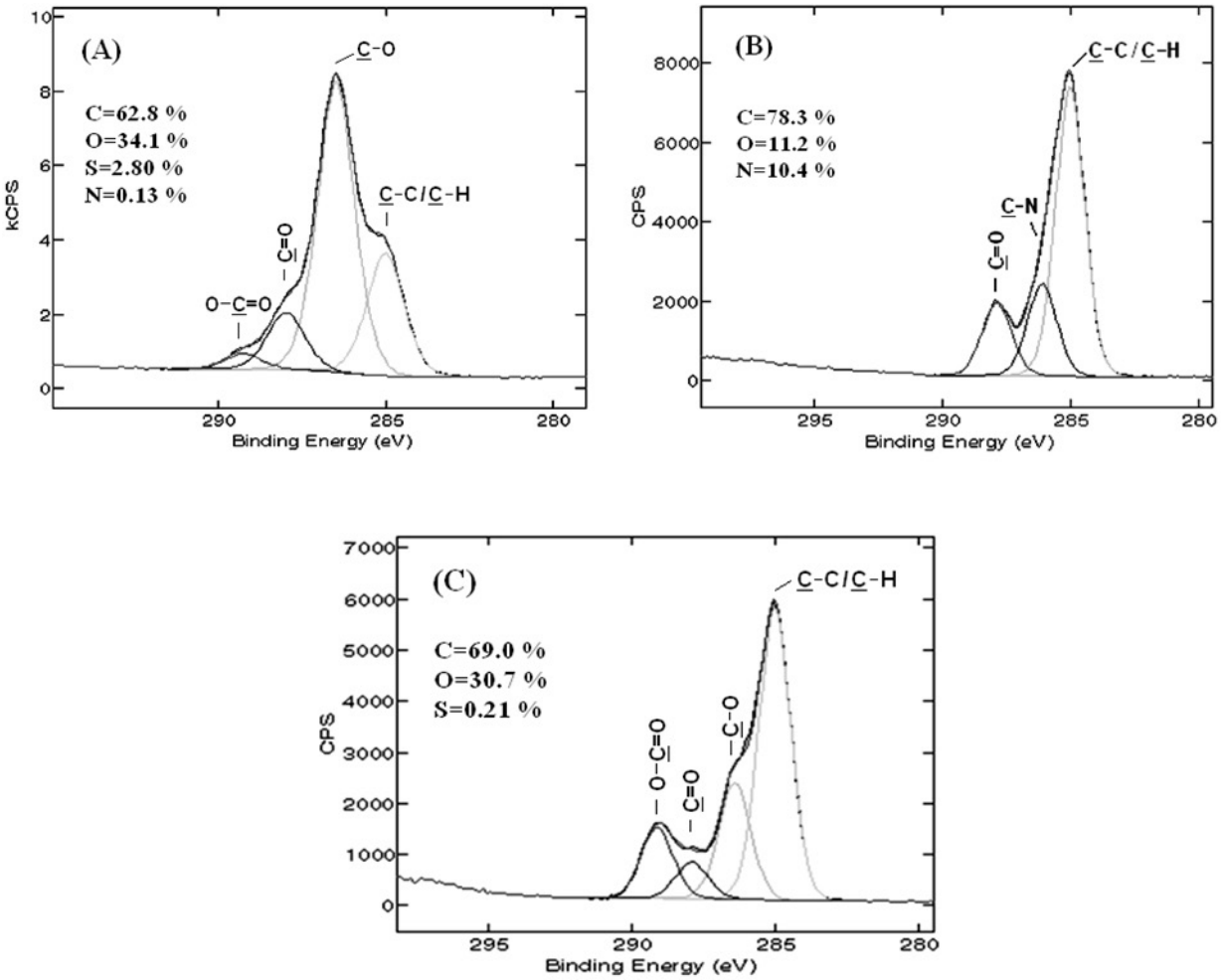

FIG. 3. C 1s XPS spectra of (A) BPATT immobilized cellulose, (B) cellulose-g-PNIPA copolymer with 19% GR and (C) cellulose-g-PAAc copolymer with 14% GR. The percentages inserted to C 1s spectra show the surface chemical compositions calculated using the peak areas of the XPS survey wide scans.

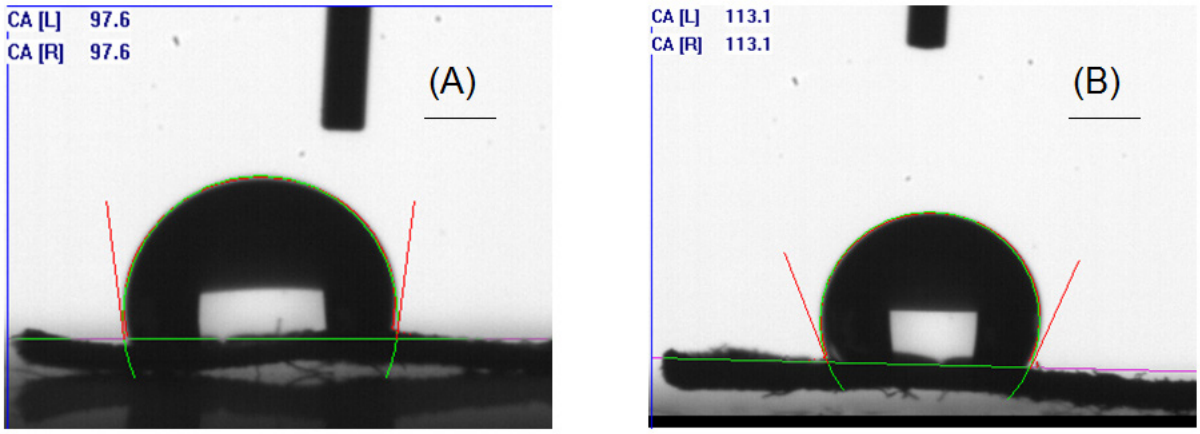

FIG. 4. CAs of PNIPA grafted cellulose surface at: (A) T = 25°C and (B) T = 35°C.

The response of 14% PAAc grafted cellulosic copolymer to change in pH was characterized by static CA measurements at pH3 and pH11. The collapse of the brushes in acid media (i.e. pH3) was reflected by changes in the wettability of the surface. At pH11, the ionized PAAc modified cellulose surface was hydrophilic, and the applied water droplet was rapidly adsorbed into the surface within a couple of seconds (the CA measured at the third second was 28.6° ± 2.4°). At pH3, which is well below the pKa for PAAc, the cellulose surface presented an increased hydrophobic character with a CA of 68.7° ± 4.5° because of the collapse of the polymer brushes. Representative diagrams for this phenomenon are shown in Fig. 5.

In addition to thermal and pH responsivity, a polystyrene grafted cellulosic copolymer prepared in a previous study promises a self-cleaning ability because of its roughness and high hydrophobicity (CA = 138°). Along with further investigations of the novel pH and temperature responsive cellulosic surfaces, this will constitute a part of future work.

3.2. Synthesis of D(+)glucose imprinted polymers

3.2.1. Positron annihilation lifetime experiments and data analysis

The pick-off annihilation lifetime of the ortho-positronium (o-Ps) can be directly correlated to the size of the free volume holes by a semiempirical equation proposed by Nakanishi and Jean [10] according to the quantum mechanical model of Tao [11], which was later developed by Eldrup et al. [12]:

$$\tau_{o-Ps} = 0.5\left[1 - \frac{R}{R+\Delta R} + \frac{1}{2\pi}\sin\left(\frac{2\pi R}{R+\Delta R}\right)\right]^{-1} \quad (1)$$

In this equation τ_{o-Ps} is the lifetime of the *o*-Ps in ns, R is the radius of free volume holes in nm, and ΔR is a constant whose value is 0.1656 nm.

The radius of free volume holes (Table 2) was calculated using Eq. (1). According to the results, there was a 0.025 nm difference between the *R* values of MIPs that were swollen in water and the water/acetonitrile mixture. This is consistent with the results of swelling experiments, which were undertaken with samples prepared by using different type of crosslinking agents such as diethylene glycol diacrylate (DEGDA) and polyethylene glycol(200) diacrylate (PEG(200)DA).

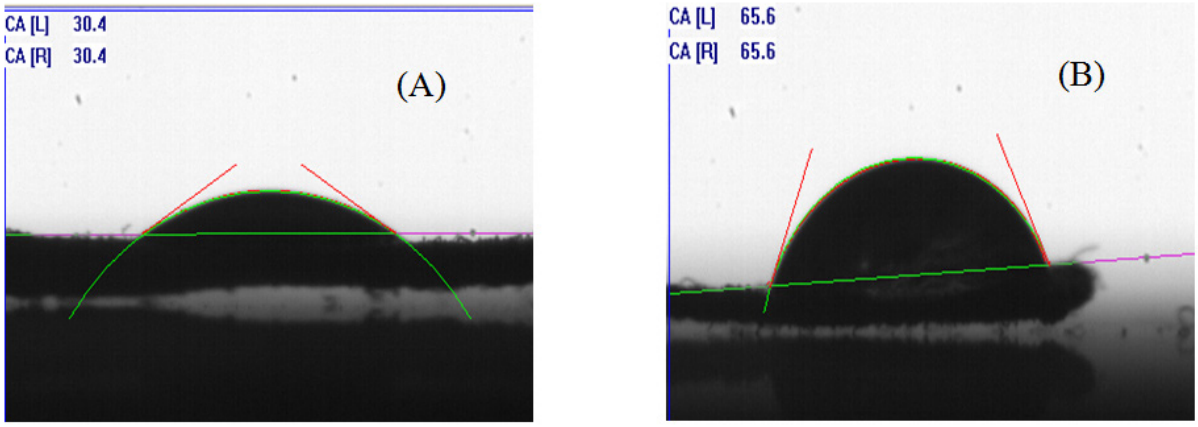

FIG. 5. CAs of PAAc grafted cellulose surface at: (A) pH11 and (B) pH3.

TABLE 2. ANNIHILATION LIFETIMES (τ_3) OF o-Ps, AVERAGE RADIUS OF HOLES (R) AND INTENSITIES (I_3) OF o-Ps OF SELECTED SAMPLES

Amount and type of cross-linking agent	Swelling property	τ_3 ± standard deviation (ns)	R ± standard deviation (nm)	I_3 ± standard deviation (%)
20% PEG(200)DA	Imprinted (swollen in water)	1.6903 ± 0.0100	0.254 ± 0.001	26.57 ± 0.13
20% PEG(200)DA	Non-imprinted (swollen in water)	1.6776 ± 0.0100	0.253 ± 0.001	26.91 ± 0.13
20% PEG(200)DA	Imprinted (swollen in acetonitrile/water)	1.9398 ± 0.0100	0.279 ± 0.001	22.29 ± 0.13
30% PEG(200)DA	Imprinted (swollen in water)	1.6898 ± 0.0100	0.254 ± 0.001	26.64 ± 0.13
30% PEG(200)DA	Non-imprinted (swollen in water)	1.6797 ± 0.0100	0.253 ± 0.001	26.77 ± 0.13
20% DEGDA	Imprinted (swollen in water)	1.7329 ± 0.0100	0.259 ± 0.001	25.14 ± 0.13

3.2.2. HPLC experiments using MIPs

To evaluate the recognition property of MIPs according to some variables such as the mobile phase and the type and amount of cross-linking monomer, HPLC experiments were carried out. In these experiments, β(−)lactose and glycerol were used as the analyte in addition to D(+)glucose.

All analyses were performed using an HPLC (Waters) system with a binary pump system and a refractive index detector. Two commercial stainless steel HPLC columns (4.0 mm inner diameter and 150 mm length) (Tosoh, Japan) were filled with MIPs or non-imprinted polymers (polymers prepared using the same procedure as for MIPs but in the absence of glucose) and attached together through an adaptor and mounted serially. All samples were eluted at a flow rate of 0.3 mL/min. Substrate solutions were prepared at a concentration of 500 mg/L, and 200 μL of solution was injected for analysis. Each injection was repeated three times. All chromatographic analyses were carried out at 30°C.

The most effective separation for glycerol, glucose and lactose whose hydrated diameters were 2.75 Å, 4.25 Å and 5.25 Å, respectively, was obtained with the MIPs that included PEG(200)DA as the cross-linking agent. In this system, an acetonitrile/water (1/5, v/v) mixture and water were used as the mobile phases (Figs 6 and 7).

3.3. Synthesis of PVP nanogels

3.3.1. DLS analysis

Figures 8 and 9 show the peak mean diameters of PVP nanogels that were synthesized from 1 mg/mL and 2 mg/mL aqueous PVP solutions using γ radiation. It can be clearly seen that the 2 mg/mL concentration is rather high because there is a large increase in particle size owing to the formation of intermolecular cross-links. Diameters as high as 248 nm support this idea where the size broadening may be a result of the combination of two processes: intramolecular and intermolecular cross-linking, which occur concomitantly. Additionally, the results were found to be very striking in that 1 mg/mL γ irradiated samples showed no sensitivity to total absorbed dose; this was also the case for the samples prepared in acetone/water mixtures.

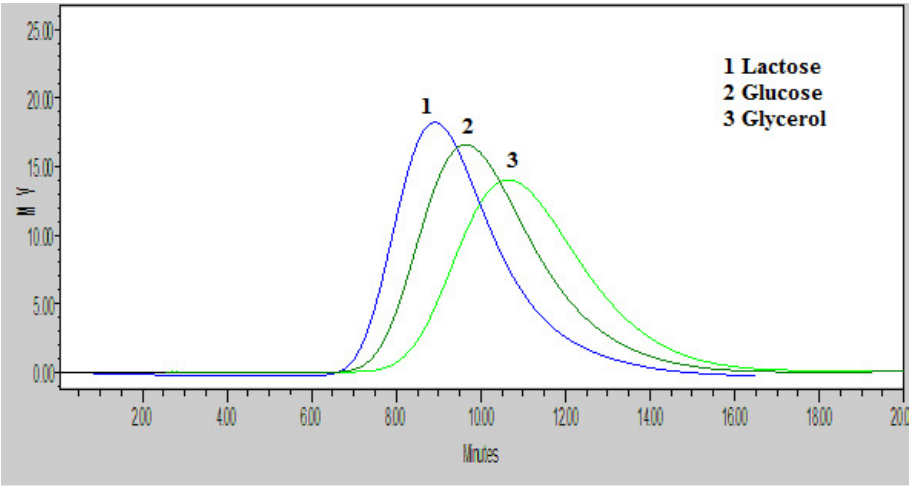

FIG. 6. Chromatograms of D-glucose, β-lactose and glycerol with column packing material consisting of MIPs cross-linked with 20% PEG(200)DA, containing 3/1 HEMA/glucose mole ratio, irradiated to 15 kGy. (The mobile phase was water.)

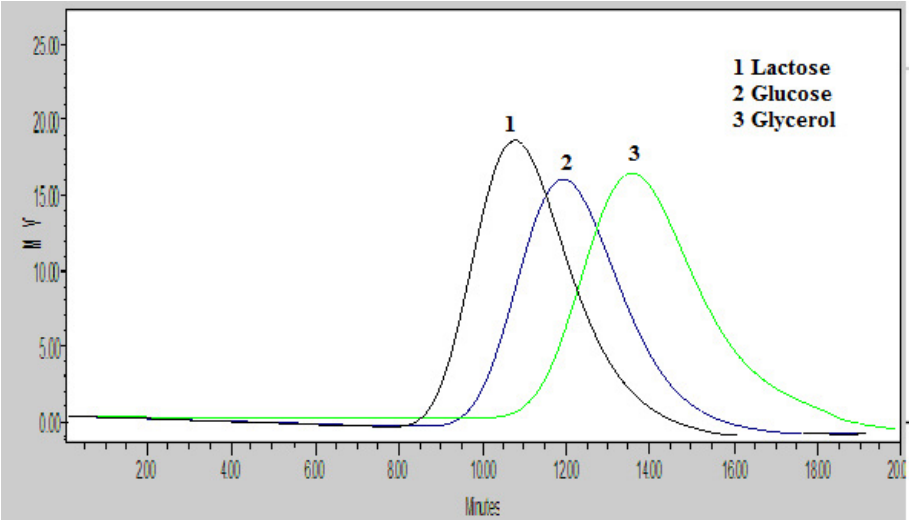

FIG. 7. Chromatograms of D-glucose, β-lactose and glycerol with column packing material consisting of MIPs cross-linked with 20% PEG(200)DA, containing 3/1 HEMA/glucose mole ratio, irradiated to 15 kGy. (The mobile phase was acetonitrile/water mixture with a 1/5 ratio by volume.)

Size distributions of non-irradiated PVP coils and PVP nanogels obtained from irradiated acetone/water solutions are shown in Fig. 10. The broad distribution observed for the pristine PVP is seen to develop in the presence of acetone owing to its non-solvent effect by bringing the solution to theta conditions. The resulting PVP nanogels thus become narrower in size distribution, with an increasing extent of intermolecular cross-linking upon formation, owing to contracted coils.

4. CONCLUSIONS

The unique advantages of ionizing radiation have been utilized for development of nanostructured polymers for potential biomedical applications. In addition to the proposals at the beginning of this project, such as preparation of nanoscale grafted surfaces and molecularly imprinted matrices and nanogels, a new direction of research was implemented to prepare polymer drug conjugates via radiation induced RAFT mediated synthesis of some copolymers.

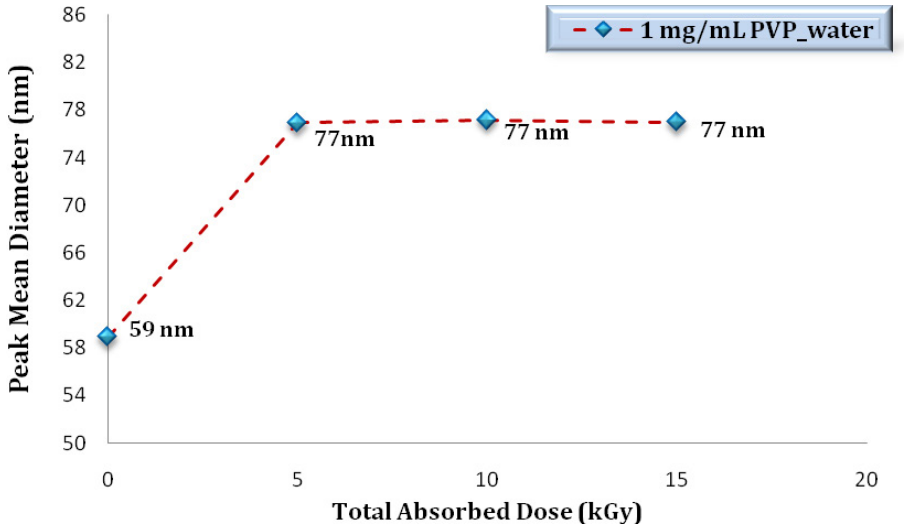

FIG. 8. Effect of total absorbed dose on the peak mean diameter of PVP nanogels that were synthesized from 1 mg/mL aqueous PVP solutions by γ radiation.

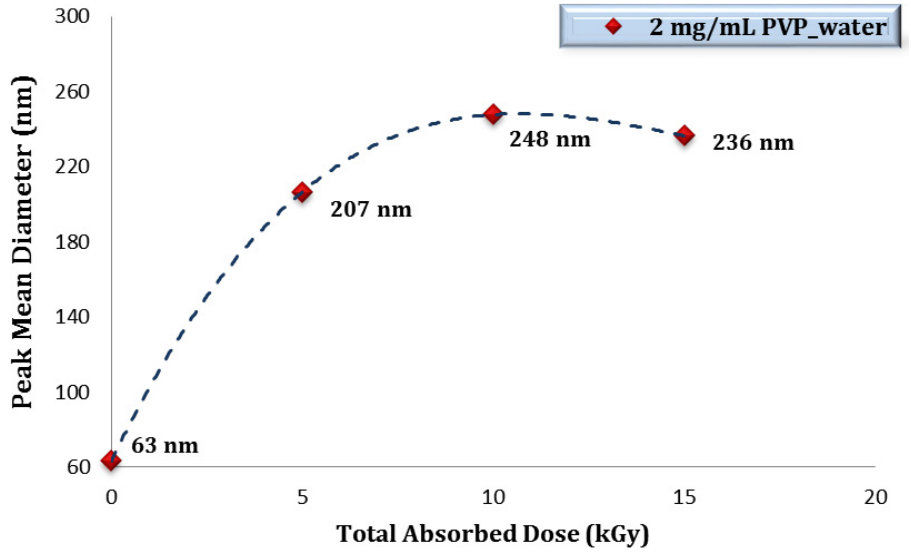

FIG. 9. Effect of total absorbed dose on the peak mean diameter of PVP nanogels that were synthesized from 2 mg/mL aqueous PVP solutions by γ radiation.

γ radiation and RAFT polymerization have been combined for the preparation of graft copolymers with well defined and responsive surface properties. Renewable and natural based intelligent cellulosic surfaces that respond to several stimuli (i.e. temperature and pH) have been prepared via this facile and powerful combination.

Radiation synthesis of densely cross-linked HEMA matrices were prepared with controlled nanoscale porosity, with the aim of using the fine powders of these polymers as column packing materials for separation of target compound D(+)glucose in the presence of similar substances.

PVP nanogels with narrow and well defined sizes have been prepared by considering the solution thermodynamics of acetone/water solutions under close to theta conditions.

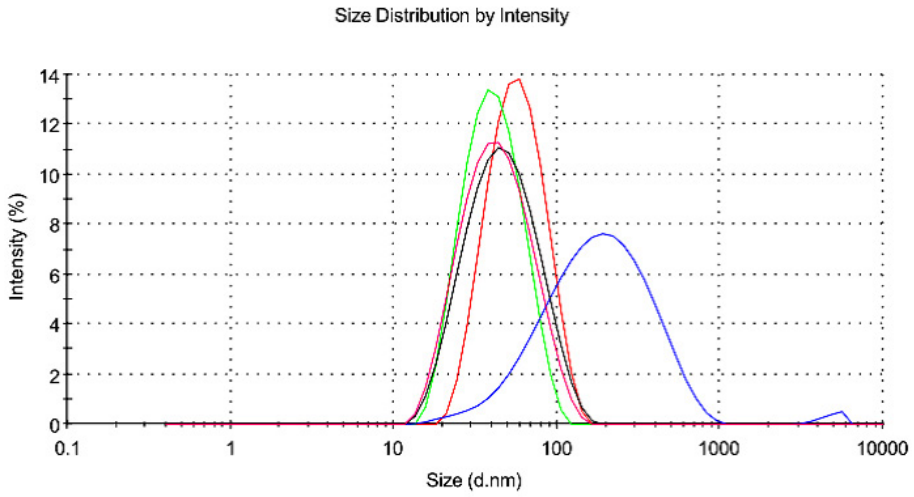

FIG. 10. Size distribution graph based on scattered light intensities of non-irradiated PVP (blue) and PVP nanogels prepared in acetone/water mixtures with acetone ratios of: 0.60 (red), 0.62 (black), 0.64 (pink) and 0.66 (green) from 2 mg/mL PVP solutions using γ rays with a total absorbed dose of 15 kGy.

REFERENCES

[1] YAMATO, M., OKANO, T., Cell sheet engineering, Mater. Today (May 2004) 42–47.
[2] BEILER, B., SAFRANY, A., Polymer monoliths synthesized by radiation copolymerization in solution, Rad. Phys. Chem. **76** (2007)1351–1354.
[3] ZSEBI, Z., HORVATH, V., SAFRANY, A., HORVAI, G., Analytical follow up of the gamma initiated synthesis of a molecularly imprinted polymer, Anal. Chim. Acta **608** (2008)197–203.
[4] DJOURELOV, N., ATES, Z., GÜVEN, O., MISHEVA, M., SUZUKI, T., Positron annihilation lifetime spectroscopy of molecularly imprinted hydroxyethyl methacrylate based polymers, Polym. **48** (2007) 2692–2699.
[5] ATES, Z., GÜVEN, O., Radiation-induced molecular Imprinting of D-glucose onto poly(2-hydroxyethyl methacrylate) matrices using various crosslinking agents, Rad. Phys. Chem. **79** (2010) 219–222.
[6] BARSBAY, M., GÜVEN, O., DAVIS, T.P., BARNER-KOWOLLIK, C., BARNER, L., RAFT-mediated polymerization and grafting of sodium 4-styrenesulfonate from cellulose initiated via γ-radiation, Polym. **50** (2009) 973–980.
[7] BARSBAY, M., et al., Verification of Controlled Grafting of Styrene from Cellulose via Radiation-Induced RAFT Polymerization, Macromol. **40** (2007) 7140–7147.
[8] GUPTA, K.C., KHANDEKAR, K., Temperature-responsive cellulose by ceric(IV) ion-initiated graft copolymerization of N-isopropylacrylamide, Biomacromol. **4** (2003) 758–765.
[9] IWATA, H., HIRATA, I., IKADA, Y., Atomic force microscopic images of solvated polymer brushes, Langmuir **13** (1997) 3063–3066.
[10] NAKANISHI, H., JEAN, Y.C., "Positrons and positronium in liquids", Positron and Positronium Chemistry, Elsevier Science, Amsterdam (1988) 159–192.
[11] TAO, S.J., Positronium annihilation in molecular substances, J. Chem. Phys. **56** (1972) 5499.
[12] ELDRUP, M., PEDERSEN, N.J., SHERWOOD, J.N., Positron annihilation study of defects in succinonitrile, Phys. Rev. Lett. **43** (1979) 1407.

PUBLICATIONS RESULTING FROM THE COORDINATED RESEARCH PROJECT

Journals, Book Chapters and Conference Proceedings

ABD EL-REHIM, H.A., HEGAZY, E.-S.A., HAMED, A.A., SWILEM, A.E., Controlling the size and swellability of stimuli responsive poly(vinylpyrrolidone)/poly(acrylic acid) (PVP/PAAc) nanogels synthesized by gamma radiation-induced template polymerization, Eur. Polym. J. **49** (2013) 601–612.

ABD EL-REHIM, H.A., KLINGNER, A., HEGAZY, E.-S.A., HAMED, A.A., SWILEM, A.E., Developing the potential ophthalmic applications of pilocarpine entrapped into polyvinylpyrrolidone-poly(acrylic acid) nanogel dispersions prepared by γ radiation, Biomacromol. **14** (2013) 688–698.

AKBULUT, M., et al., Microplates with adaptive surfaces, ACS Comb. Sci. **13** (2011) 646–652.

ALCÂNTARA, M.T.S., et al., Influence of dissolution processing of PVA blends on the characteristics of their hydrogels synthesized by radiation—part I: Gel fraction, swelling, and mechanical properties, Radiat. Phys. Chem. **81** (2012) 1465–1470.

ATES, Z., GÜVEN, O., Radiation-induced molecular ımprinting of D-glucose onto poly(2-hydroxyethyl methacrylate) matrices using various crosslinking agents, Radiat. Phys. Chem. **79** (2010) 219–222.

BARSBAY, M., GÜVEN, O., A short review of radiation-induced RAFT-mediated graft copolymerization, Radiat. Phys. Chem. **78** (2009) 1054–1059.

BARSBAY, M., GÜVEN, O., BESSBOUSSE, H., WADE, T.L., CLOCHARD, M.-C., Nanopore size tuning of polymeric membranes using the RAFT-mediated radical polymerization, J. Membr. Sci. **445** (2013) 135–145.

BARSBAY, M., GÜVEN, O., DAVIS, T.P., BARNER-KOWOLLIK, C., BARNER, L., RAFT-mediated polymerization and grafting of 4-styrenesulfonate from cellulose initiated via gamma-radiation, Polym. **50** (2009**)** 973–982.

BEHNOODFAR, D., DADBIN, S., FROUNCHI, M., PLA microspheres-embedded PVA hydrogels prepared by gamma-irradiation and freeze-thaw methods as drug release carriers, Int. J. Polymer. Mater. **62 (2013)** 28–33.

BISWAL, J., RAMNANI, S.P., SHIROLIKAR, S., SABHARWAL, S., Seedless synthesis of gold nanorods employing isopropyl radical generated using gamma radiolysis technique, Int. J. Nanotechnol. **7** (2010) 907–918.

BISWAL, J., RAMNANI, S.P., SHIROLIKAR, S., SABHARWAL, S., Synthesis of rectangular plate like gold nanoparticles by in situ generation of seeds by combining both radiation and chemical methods, Radiat. Phys. Chem. **80** (2011) 44–49.

BISWAL, J., RAMNANI, S.P., TEWARI, R., DEY, G.K., SABHARWAL, S., Short aspect ratio gold nanorods prepared using gamma radiation in the presence of cetyltrimethyl ammonium bromide (CTAB) as a directing agent, Radiat. Phys. Chem. **79** (2010) 441–445.

BISWAL, J., SINGH, S., RATH, M.C., RAMNANI, S.P., SABHARWAL, S., Synthesis of CdSe quantum dots in PVA matrix by radiolytic methods, Int. J. Nanotechnol. **7** (2010) 1013–1026.

CHEN, J., LI, D., KOSHIKAWA, H., ASANO, M., MAEKAWA, Y., Crosslinking and grafting of polyetheretherketone film by radiation techniques for application in fuel cells, J. Membr. Sci. **362** (2010) 488–494.

CHEN, Q.D., SHEN, X.H., Formation of mesoporous $BaSO_4$ microspheres with a larger pore size via Ostwald ripening at room temperature, Cryst. Growth Des. **10** (2010) 3838–3842.

CHEN, Q.D., SHEN, X.H., GAO, H.C., Radiolytic syntheses of nanoparticles in supramolecular assemblies, Adv. Colloid Interface Sci. **159** (2010) 32–44.

CHOOFONG, S., PASANPHAN, W., "Particle size lowering of chitosan nanosphere by gamma irradiation and chemical modification", Proc. 7th Eco-Energy and Materials Science and Engineering Symp., Chiang Mai, Thailand (2009) 125–130.

CVETICANIN, J., et al., Functionalization of carbon nanotubes with silver clusters, Appl. Surf. Sci. **256** (2010) 7048–7055.

CVETICANIN, J., et al., MALDI TOF and theoretical investigation of silver clusters obtained by gamma irradiation, Vacuum **89** (2012) 47–52.

CVETICANIN, J., et al., "Mass spectrometric investigation of silver clusters", Proc. 10th Int. Conf. Fundamental and Applied Aspects of Physical Chemistry, Physical Chemistry, Belgrade, Serbia (2010) 60–62.

DADBIN, S., "Structural changes in poly (lactic acid)/hydroxyapatite nanocomposites by gamma irradiation", 4th Int. Biennial Conf. Ultrafine Grained and Nanostructured Materials (UFGNSM2013), Tehran, Islamic Republic of Iran, 5–6 November 2013.

DADBIN, S., KHEIRKHAH, Y., Gamma irradiation of melt processed of biomedical PDLLA/HAP nanocomposites, Radiat. Phys. Chem. **97** (2014) 270–274.

DADBIN, S., NAIMIAN, F., Gamma radiation induced property modification of poly(lactic acid)/hydroxyapatite bio-nanocomposites, Polym. Int. **63** (2014) 1063–1069.

DADBIN, S., NAIMIAN, F., Poly (lactic acid)/hydroxyapatite bio-nanocomposites: Effects of gamma irradiation and composition on crystallinity, mechanical properties and morphology, Polym. Int. (in preparation).

DADBIN, S., NAIMIAN, F., AKHAVAN, A., Poly(lactic acid) layered silicate nanocomposite films: Morphology, mechanical properties and effects of gamma radiation, J. Appl. Polym. Sci. **122** (2011) 142–149.

DADBIN, S., NAIMIAN, F., HASANPOUR, S., Structural changes in poly (lactic acid)/hydroxyapatite nanocomposites by gamma irradiation, Adv. Mater. Res. **18** (2014) 258–262.

DISPENZA, C., et al., "Biocompatible polyaniline nanocomposites build a soft interface between biology and opto-electronics", Proc. Polymerfest, Palermo, Italy (2009) 223–224.

DISPENZA, C., et al., E-beam irradiation and UV photocrosslinking of microemulsion-laden poly(*N*-vinyl-2-pyrrolidone) hydrogels for "*in situ*" encapsulation of volatile hydrophobic compounds, Poly. Chem. **2** (2011) 192–202.

DISPENZA, C., et al., "Macromolecular engineering of hydrogels: From macro to nano scalar materials for different levels of biointeraction", Proc. Polymerfest, Palermo, Italy (2009) 237–238.

ENOMOTO, K., MAEKAWA, Y., TAKANO, S., IWASAKI, M., NARITA, T., Electron-beam-induced chromism combined with photo-or thermal reverse reaction for colour imaging, J. Photopolym. Sci. Technol. **23** (2010) 217–224.

ENOMOTO, K., TAKAHASHI, S., MAEKAWA, Y., Novel characterization method for graft polymer structures chemically attached on thermally stable polymer films, Macromol. Chem. Phys. **213** (2012) 72–78.

ENOMOTO, K., TAKAHASHI, S., ROHANI, R., MAEKAWA, Y., Synthesis of copolymer grafts containing sulfoalkyl and hydrophilic groups in polymer electrolyte membranes, J. Membr. Sci. **415–416** (2012) 36–41.

ENOMOTO, K., TAKAHASHI, S., YAMASHITA, T., MAEKAWA, Y., Degradation manner of polymer grafts chemically attached on thermally stable polymer films: Swelling-induced detachment of hydrophilic grafts from hydrophobic polymer substrates in aqueous media, J. Mater. Chem. **21** (2011) 9343–9349.

GOPALAN, A., et al., Radiation induced preparation of new multifunctional nanobiowebs, Radiat. Phys. Chem. **81** (2012) 1407–1410.

JOVANOVIĆ, Ž., et al., Bioreactor validation and biocompatibility of Ag/poly(*N*-vinyl-2-pyrrolidone) hydrogel nanocomposites, Coll. Surf. B: Biointerfaces **105** (2013) 230–235.

JOVANOVIĆ, Ž., et al., "Properties of Ag/PVP hydrogel nanocomposite synthesized in situ by gamma irradiation", Trends in Nanophysics: Theory, Experiment and Technology (ALDEA, A., BÂRSAN, V., Eds) Springer-Verlag, Berlin, Heidelberg (2010) 315–328.

JOVANOVIĆ, Ž., et al., Structural and optical characteristics of silver/poly(*N*-vinyl-2-pyrrolidone) nanosystems synthesized by gamma irradiation, Radiat. Phys. Chem. **81** (2012) 1720–1728.

JOVANOVIĆ, Ž., et al., Synthesis and characterization of Ag/PVP hydrogel nanocomposite obtained by in situ radiolytic method, Radiat. Phys. Chem. **80** (2011) 1208–1215.

JOVANOVIĆ, Ž., RADOSAVLJEVIĆ, A., KAČAREVIĆ-POPOVIĆ, Z., MIŠKOVIĆ-STANKOVIĆ, V., Silver/poly(N-vinyl pyrrolidone) nanocomposites obtained by electrochemical synthesis, Chem. Ind. **65** (2011) 687–696 (in Serbian).

HAMZAH, Y., YUNUS, W., ISA, N.M., Synthesis of polymeric nanogel via irradiation of inverse micelles technique, Pertanika J. Sci. Technol. **20** (2012) 401–407.

HAMZAH, Y., YUNUS, W., ISA, N.M., TAJAU, R., HASHIM, K., Synthesis of polyethylene glycol diacrylate nanogel using irradiation of inverse micelles technique, e-Polym. **12** (2012) 533–538.

HASEGAWA, S., et al., Radiation-induced graft polymerization of functional monomer into poly(ether ether ketone)film and structure-property analysis of the grafted membrane, Polym. **52** (2011) 98–106.

HENKE, A., et al., The structure and aggregation of hydrogen-bonded interpolymer complexes of poly(acrylic acid) with poly(*N*-vinylpyrrolidone) in dilute aqueous solution, Macromol. Chem. Phys. **212** (2011) 2529−2540.

IWASE, H., SAWADA, S., YAMAKI, T., MAEKAWA, Y., KOIZUMI, S., Preirradiation graft polymerization of styrene in a poly(tetrafluoroethylene) film, investigated by time-resolved small-angle neutron scattering, Int. J. Polym. Sci. **2011** (2011) 301807.

KAČAREVIĆ-POPOVIĆ, Z., et al., On the use of radiation technology for nanoscale engineering of silver/hydrogel based nanocomposites for potential biomedical application, Open Conf. Proc. J. **1** (2010) 200–206.

KADLUBOWSKI, S., ULANSKI, P., ROSIAK, J.M., Synthesis of tailored nanogels by means of two-stage irradiation, Polym. **53** (2012) 1985–1991.

KRSTIĆ, J., KRKLJEŠ, A., KAČAREVIĆ-POPOVIĆ, Z., "Swelling behaviour of Ag/PVA hydrogel nanocomposite synthesized by γ-irradiation", Proc. 10th Int. Conf. Fundamental and Applied Aspects of Physical Chemistry, Physical Chemistry 2010, Belgrade, Serbia (2010) 110–112.

KRSTIĆ, J., SPASOJEVIĆ, J., RADOSAVLJEVIĆ, A., KAČAREVIĆ-POPOVIĆ, Z., "Non-isothermal kinetics of dehydration of Ag/PVA hydrogel nanocomposite synthesized by gamma irradiation", Proc. 11th Int. Conf. Fundamental and Applied Aspects of Physical Chemistry, Physical Chemistry 2012, Belgrade, Serbia (2012) 212–214.

LEE, K.-P., LEE, S.-H., KOMATHI, S., GOPALAN, A., Preparation of Co/Pd alloy particles dispersed multiwalled carbon nanotube supported nanocatalysts via gamma irradiation, Radiat. Phys. Chem. **81** (2012) 1422–1425.

MISRA, N., BISWAL, J., GUPTA, A., SAINIS J.K., SABHARWAL, S., Gamma radiation induced synthesis of gold nanoparticles in aqueous polyvinyl pyrrolidone solution and its application for hydrogen peroxide estimation, Radiat. Phys. Chem. **81** (2012) 195–200.

MISRA, N., KUMAR, V., BORDE, L., VARSHNEY, L., Localized surface plasmon resonance-optical sensors based on radiolytically synthesized silver nanoparticles for estimation of uric acid, Sens. Actuators B: Chem. **178** (2013) 371–378.

MOMESSO, R.G.R.A., MORENO, C.S., ROGERO, S.O., ROGERO, J.R., SPENCER, P.J., LUGAO, A.B., Radiation stability of resveratrol in immobilization on poly vinyl pyrrolidone hydrogel dressing for dermatological use, Radiat. Phys. Chem. **79** (2010) 283–285.

NUNUNG, N., et al., Poly(vinylidene fluoride)-based ion track membranes with different pore diameters and shapes: SEM observations and conductometric analysis, Electrochem. **78** (2010) 146–149.

OLIANI, W.L, PARRA, D.F., RIELLA, H.G., LIMA, L.F.C.P., LUGAO, A.B., Polypropylene nanogel: "myth or reality", Radiat. Phys. Chem. **81** (2012) 1460–1464.

OLIVEIRA, M.J.A., AMATO, V.S., LUGAO, A.B., PARRA, D.F., Hybrid hydrogels produced by ionizing radiation technique, Radiat. Phys. Chem. **81** (2012) 1471–1474.

OLIVEIRA, M.J.A., PARRA, D.F., AMATO, V.S., LUGAO, A.B., Hydrogel membranes of PVAl/clay by gamma radiation, Radiat. Phys. Chem. **84** (2013) 111–114.

PASANPHAN, W., CHOOFONG, S., RIMDUSIT, P., Deoxycholate-chitosan nanosphere fabricated by γ-irradiation and chemical modification: Nanoscale synthesis and controlling studies, J. Appl. Polym. Sci. **123** (2012) 3309–3320.

PASANPHAN, W., RATTANAWONGWIBOON, T., RIMDUSIT, P., A green radiolytic synthesis of PEGMA-grafted-deoxycholate chitosan as a drug carrier, Radiat. Phys. Chem. (in preparation).

PASANPHAN, W., RIMDUSIT, P., CHOOFONG, S., PIROONPAN, T., NILSUWANKOSIT, S., Systematic fabrication of chitosan nanoparticle by gamma irradiation, Radiat. Phys. Chem. **79** (2010) 1095–1102.

RICCA, V., FODERÀ, GIACOMAZZA, D., LEONE, M., SPADARO, G., DISPENZA, C., Probing the internal environment of PVP networks generated by irradiation with different sources, Colloid. Polym. Sci. **288** (2010) 969–980.

RIMDUSIT, P., PASANPHAN, W., "Gamma-ray generated chitosan nanoparticle: systematic preparation study", Proc. 7th Eco-Energy and Materials Science and Engineering Symp., Chiang Mai, Thailand (2009) 131–135.

SAWADA, S., et al., Structural analysis of radiation-grafted polymer electrolyte membranes by dissipative particle dynamics simulation, Kobunshi Ronbunshu **67** (2010) 224–227 (in Japanese).

SAWADA, S., MAEKAWA, Y., Proton conduction characteristics in radiation-grafted polymer electrolyte membranes based on perfluorinated and aromatic hydrocarbon polymers, ECS Trans. **41** (2011) 2125–2133.

SAWADA, S., SUZUKI, A., TERAI, T., MAEKAWA, Y., TEMPO addition into pre-irradiated fluoropolymers and living-radical graft polymerization of styrene for preparation of polymer electrolyte membranes, Radiat. Phys. Chem. **79** (2010) 471–478.

SOTO ESPINOZA, S.L., ARBEITMAN, C.R., CLOCHARD, M.-C., GRASSELLI M., Functionalization of nanochannels by radiation-induced grafting polymerization on PET track-etched membranes, Radiat. Phys. Chem. **94** (2014) 72–75.

SOTO ESPINOZA, S.L., SÁNCHEZ, M.L., RISSO, V., SMOLKO, E., GRASSELLI, M., Radiation synthesis of seroalbumin nanoparticles, Radiat. Phys. Chem. **81** (2012) 1417–1421.

SPASOJEVIĆ, J., KRSTIĆ, J., RADOSAVLJEVIĆ, A., KALAGASIDIS-KRUŠIĆ, M., KAČAREVIĆ-POPOVIĆ, Z., "Poly(NiPAAm-co-IA) hydrogels synthesized by gamma-irradiation: Swelling behaviour in water", Proc. 11th Int. Conf. Fundamental and Applied Aspects of Physical Chemistry, Physical Chemistry 2012, Belgrade, Serbia (2012) 550–552.

SPASOJEVIĆ, J.P., KRSTIĆ, J.I., RADOSAVLJEVIĆ, A.N., KALAGASIDIS-KRUŠIĆ, M.T., KAČAREVIĆ-POPOVIĆ, Z.M., "Radiation-chemical synthesis of thermosensitive silver/poly(*N*-isopropylacrilamide) hydrogel nanocomposites", Proc. Golden Jubilee Mtg Serbian Chemical Society, Belgrade, Serbia (2012) 86–89 (in Serbian) CD-ROM.

SWILEM, A.E., Radiation Synthesis of Nano-Scale Materials for Biomedical Applications, Masters Thesis, Faculty of Science, Ain Shams University, Egypt (2012).

TAJAU, R., et al., Development of palm oil based nano drug carrier using radiation technique, J. Nucl. Related Technol. (in preparation).

TAJAU, R., et al., Preparation of nanoparticles from acrylated palm oil microemulsion using radiation technique, J. Nucl. Related Technol. **8** (2011) 6–12.

TAJAU, R., et al., Preparation of nanoparticles from acrylated palm oil microemulsion using radiation technique, Pertanika J. Sci. Technol. **8** (2012) 6.

TAJAU, R., ZAMAN, D.K.M, MAHMOOD, M.H., YUNUS W.M.Z.W., KAMARUDDIN, H., Radiation induced formation of acrylated palm oil (APO) nanoparticles using cetyltrimethylammonium bromide microemulsion system, Adv. Mat. Res. **364** (2012) 278–282.

VERES, M., et al., Surface functionalization of nanocrystalline diamond using free radical polymerization, Diam. Relat. Mater. (in preparation).

WALO, M., PRYZBYTNIAK, G., KAVAKLI, A.P., GÜVEN, O., Radiation-induced graft polymerization of *N*-vinyl pyrrolidone onto segmented polyurethane based on isophorone diisocyanate, Radiat. Phys. Chem. (in preparation).

YAMAKI, T., et al., Conductometric analysis for the formation of poly(vinylidene fluoride)-based ion track membranes, ECS Trans. **35** (2011) 1–12.

YANG, S.G., CHEN, Q.D., SHI, J.F., SHEN, X.H., Controllable radiolytic reduction of Cu^{2+} in aqueous solution by β-cyclodextrin, Acta Phys. Chim. Sin. **26** (2010) 805–810 (in Chinese).

Patents

BARSBAY, M., GÜVEN, O., BESSBOUSSE, H., CLOCHARD, M.-C., WADE, T., Method for Preparing a Functionalized Nanoporous Track-etched PVDF Membrane with RAFT Polymerization, EP11306648.4, deposited 13 November 2011.

BESBOUSSE, H., WADE, T., CLOCHARD, M.-C., BARSBAY, M., GÜVEN, O., RAFT-Mediated Radiation-induced Grafting of Acrylic Acid from Track-etched PVDF Membranes to Develop Polymer Film Electrodes, European Patent 2011DI0057.

Scientific Conferences, Abstracts

BARTOSZEK, N., ULANSKI, P., ROSIAK, J.M., "Free-radical reactions involving macromolecules as studied by pulse radiolysis – factors influencing reaction rate constants", Proc. 4th European Young Investigators Conf., Slubice, Poland (2009).

BARTOSZEK, N., ULANSKI, P., ROSIAK, J.M., "Pulse radiolysis as a method for determination of rate constants in radical polymerization", Proc. 52nd Mtg Polish Chemical Society, Lodz, Poland (2009) (abstract).

BEILER, B., VERES, M., HIMICS, L., KOÓS, M., SÁFRÁNY, Á., "Raman spectroscopic study on porous polymer monoliths prepared by radiation initiated polymerization", Proc. 12th Tihany Symp. Radiation Chemistry, Zalakaros, Hungary (2011).

CASAJÚS, G., SOTO ESPINOZA, S.L., SMOLKO, E.E., GRASSELLI, M., "Síntesis de nanopartículas de proteína mediante radiación ionizante de ^{60}Co", Proc. XII Encuentro Superficie y Materiales Nanoestructurados, La Falda, Argentina (2012).

CHOOFONG, S., SUWANMALA, P., PASANPHAN, W., "Water-soluble chitosan-gold composite nanoparticle: preparation by radiolysis method", Proc. 18th Int. Conf. Composite Materials, Jeju, Republic of Korea (2011).

DADBIN, S., AHMADIAN, V., "Crystallinity of PLA/HAP nanocomposites: effect of gamma irradiation", Proc. Iranian Sem. Polymer Science and Technology (ISPST2012), Tehran, Islamic Republic of Iran, 21–25 October 2012.

DADBIN, S, AKHAVAN, A., "In vitro enzymatic degradation of PLA/layered silicate nanocomposites", Proc. Iranian Sem. Polymer Science and Technology (ISPST2012), Tehran, Islamic Republic of Iran, 21–25 October 2012.

DADBIN, S., NAIMIAN, F., KHEIRKHAH, Y., "PLA/clay nanocomposites: effects of preparation method on morphology and mechanical properties", Proc. Iranian Sem. Polymer Science and Technology (ISPST2012), Tehran, Islamic Republic of Iran, 21–25 October 2012.

DISPENZA, C., LOPRESTI, M.R., SPADARO, G., BLANAZS, A., BATTAGLIA, G., "Biocompatible nanostructured hydrogels incorporating polyaniline nanoparticles", Proc. Frontiers in Polymer Science, Mainz, Germany (2009).

DISPENZA, C., SPADARO, G., "Nuovi materiali nanocompositi a base di idrogeli e polimeri conduttori per l'elettronica molecolare", Proc. III Workshop Nazionale AICING, Genova, Italy (2009).

FRANCIS, S., et al., "Gamma radiolytic synthesis of gold nanoplates in presence of polydiallyldimethylammoniumchloride as the capping agent", Proc. NSRP, Meghalaya, India (2013).

FRANCIS, S., TEWARI, R., MITRA, D., VARSHNEY, L., "Gold nanoplate synthesis by hydrogen peroxide reduction of gold chloride", Proc. ISMC, Mumbai, India (2012).

GOPALAN, A., et al., "Radiation induced preparation of new multifunctional nanobiowebs", Proc. 12th Tihany Symp. Radiation Chemistry, Zalakaros, Hungary (2011).

GRASSELLI, M., et al., "Radiation-induced grafting of porous polymers for biological applications", Proc. V Argentine-Chilean Polymer Symp., VIII Argentine Polymer Symp., IX Chilean Symp. Polymer Chemistry and Physical Chemistry, Los Cocos, Córdoba, Argentina (2009).

HAMZAH, Y., ISA, N.M., YUNUS, W., HASHIM, K., "Synthesis of polyethylene glycol diacrylate nanogel using irradiation of inverse micelles technique", Proc. Int. Conf. Nanotechnology (INSC), Serdang, Malaysia (2011).

HAMZAH, T.R., YUNUS, W.M.Z.W., HASHIM, K., DAHLAN, K.Z.M., "Radiation syntheses of nanogel", Proc. Fundamental Science Congress, Serdang, Malaysia (2010).

HOFFMAN, A.S., "Evolution of biomaterials into the nano-era", Proc. 10th Mtg Ionizing Radiation and Polymers Symp. (IRaP2012), Krakow, Poland (2012) 16.

JEVREMOVIĆ, I., et al., "Silver/poly(*N*-vinyl-2-pyrrolidone) biomaterial nanocomposite: comparison of electrochemical and radiation-chemical synthesis", Proc. Int. Workshop on Processing of Nanostructured Ceramics, Polymers, and Composites, Belgrade, Serbia (2010) 94–95 (in Serbian).

JOVANOVIĆ, Ž., et al., "Properties of Ag/PVP hydrogel nanocomposite synthesized in situ by gamma irradiation", Proc. Workshop Trends in nanoscience: theory, experiment, technology, Sibiu, Romania (2009).

KAČAREVIĆ-POPOVIĆ, Z., et al., "On the use of radiation technology for nanoscale engineering of silver/hydrogel based nanocomposites for potential biomedical application", Proc. 2nd Int. Conf. Drug Discovery and Therapy, Dubai, United Arab Emirates (2010) 117 (abstract).

KAČAREVIĆ-POPOVIĆ, Z., RADOSAVLJEVIĆ, A., KRSTIĆ, J., SPASOJEVIĆ, J., "On the use of gamma irradiation for the nanoengineering of the Ag and Au/hydrogel based nanosystems for the potential biomedical applications", Proc. 28th Miller Conf. Radiation Chemistry, Dead Sea, Israel (2013) 25 (abstract).

KADLUBOWSKI, S., CZECHOWSKA-BISKUP, R., ULANSKI, P., ROSIAK, J.M., "Radiation-initiated synthesis of polymer nanogels", Proc. 3rd Ntl Nanotechnology Conf. (NANO 2009), Warsaw, Poland (2009).

KADLUBOWSKI, S., WACH, R., DESSY, C., BURES, K., ULANSKI, P., ROSIAK, J.M., "System for time-resolved pulse radiolysis with multi angle light scattering detection", Proc. 10th Mtg Ionizing Radiation and Polymers (IRaP2012), Krakow, Poland (2012).

KRKLJEŠ, A., KAČAREVIĆ-POPOVIĆ, Z., NEDELJKOVIC, J., "Radiolytic synthesis and characterization of thermoresponsive Ag/PNIPA hydrogel nanocomposites", Proc. 2nd Int. Conf. Physics of Optical Materials and Devices (ICOM 2009), Herceg Novi, Montenegro (2009) 177 (abstract).

KRKLJEŠ, A., KAČAREVIĆ-POPOVIĆ, Z., NEDELJKOVIC, J., "The influence of network parameters on the properties of thermoresponsive Ag/PNIPA hydrogel nanocomposite synthesized by gamma irradiation", Proc. 11th Annual Conf. YUCOMAT 2009, Herceg Novi, Montenegro (2009) 176 (abstract).

KRSTIĆ, J., KRKLJEŠ, A., MITRIC, M., KAČAREVIĆ-POPOVIĆ, Z., "Characterization and swelling kinetics of Ag/PVA hydrogel nanocomposites synthesized by γ-irradiation", Proc. Int. Workshop on Processing of Nanostructured Ceramics, Polymers, and Composites, Belgrade, Serbia (2010) 48 (abstract).

KRSTIĆ, J., KRKLJEŠ, A., PERIC-GRUJIC, A., MITRIC, M., KAČAREVIĆ-POPOVIĆ, Z., "Hybrid Ag/PVA hydrogel nanocomposites for potential biomedical application synthesized by gamma irradiation", Proc. X Int. Conf. Nanostructured Materials (NANO 2010), Rome, Italy (2010) 191 (abstract).

KRSTIĆ, J., SPASOJEVIĆ, J., KRKLJEŠ, A., KAČAREVIĆ-POPOVIĆ, Z., "Swelling kinetics and antimicrobial activity of radiolytically synthesized nano-Ag/PVA hydrogels", Proc. 12th Tihany Symp. Radiation Chemistry, Zalakaros, Hungary (2011) 110 (abstract).

KRSTIĆ, J., SPASOJEVIĆ, J., RADOSAVLJEVIĆ, A., KAČAREVIĆ-POPOVIĆ, Z., "Drug delivery paradigm of silver ions released from Ag/PVA hydrogel nanocomposites obtained by radiation chemistry nanoreactor method", Proc. 11th Young Researchers' Conf. Materials Science and Engineering 2012 and 1st European Early Stage Researchers' Conf. Hydrogen Storage, Belgrade, Serbia (2012) 107 (abstract).

KRSTIĆ, J., SPASOJEVIĆ, J., RADOSAVLJEVIĆ, A., KAČAREVIĆ-POPOVIĆ, Z.M., "Gamma irradiation technique for plasmonic nanoengineering of Ag/hydrogels nanocomposites", Proc. 3rd Int. Conf. Physics of Optical Materials and Devices (ICOM 2012), Belgrade, Serbia (2012) 240 (abstract).

KUMAR, V., GOEL, N.K., FRANCIS, S. BHARDWAJ, Y.K., VARSHNEY, L., "Hybrid organic/inorganic nanocomposite coating by electron beam curing process", Proc. Thermans, Mumbai, India (2012).

LEE, K.-P., LEE, S.-H., KOMATHI, S., GOPALAN, A., "Preparation of Co/Pd alloy particles dispersed multiwalled carbon nanotube supported nanocatalysts via gamma irradiation", 12th Tihany Symp. Radiation Chemistry, Zalakaros, Hungary (2011).

MISRA, N., BISWAL, J., DHAMGAYE, V., LODHA, G.S., SABHARWAL, S.M., "Synthesis of silver nanoparticles by using synchrotron radiation", Proc. INDUS II, ETALAN, TSH, Mumbai, India (2011).

MISRA, N., BISWAL, J., SABHARWAL, S., "Synthesis of polyvinylpyrrolidone stabilized gold nanoparticles by gamma irradiation", Proc. NSRP, Rajasthan, India (2011).

MISRA, N., BISWAL, J., SABHARWAL, S., VARSHNEY, L., "Colorimetric estimation of trace levels of hydrogen peroxide using radiolytically synthesized gold nanoparticles", Proc. ICWNCN, New Delhi, India (2012).

MISRA, N., KUMAR, V., VARSHNEY, L., "Silver nanoparticles based optical biosensors for estimation of uric acid", Proc. ISMC, TSH, Mumbai, India (2012).

NAGORNIWWICZ, B., KADLUBOWSKI, S., ULANSKI, P., ROSIAK, J.M., "Radiation synthesis of nanogels in microemulsion", Proc. 10th Mtg Ionizing Radiation and Polymers (IRaP2012), Krakow, Poland (2012).

PASANPHAN, W., CHUNKOH, L., CHOOFONG, S., "Magnetic gadolinium-chitosan composite nanoparticle created by radiolytic synthesis", Proc. 18th Int. Conf. Composite Materials, Jeju, Republic of Korea (2011).

PASANPHAN, W., RIMDUSIT, P., CHOOFONG, S., CHIRACHANCHAI, S., "Chitosan nanoparticle formation: systematic condition based on gamma irradiation and chemical modification studies", Proc. 6th European Conf. Marine Natural Products, Porto, Portugal (2009) 163 (abstract)

QUIROGA, F.Y., GRASSELLI, M., "Modificación superficial de HDPE con injertos catiónicos para la adsorción de microorganismos. Aplicaciones en el área de biocatálisis", Proc. Iº Simposio Argentino de los Procesos Biotecnológicos, Rosario, Argentina (2010).

QUIROGA, F.Y., GRASSELLI, M., "Analysis of surface cationic microhydrogel structures by in situ fluorescence detection", Proc. 3rd South American Workshop; Int. Gregorio Weber Conf. and Workshop on Advance Fluorescence Techniques, Buenos Aires, Argentina (2011).

QUIROGA, F.Y., GRASSELLI, M., "Síntesis y caracterización de una red catiónica injertada en HDPE para promover la adsorción de microrganismos", Proc. XII Encuentro Superficie y Materiales Nanoestructurados, La Falda, Argentina (2012).

QUIROGA, F.Y., LELES DA SOUZA, A., LAMEIRAS, F.S., GRASSELLI, M., "Microhidrogeles catiónicos injertados sobre HDPE: síntesis, caracterización fisicoquímica y estudios funcionales en la adsorción de Escherichia coli", Proc. XL Reunión Anual de la Sociedad Argentina de Biofísica, Buenos Aires, Argentina (2011).

RATTANAWONGWIBOON, T., PASANPHAN, W., "Gamma-rays induced stearyl-grafted-chitosan as a novel nanofiller for PLA blends", Proc. 18th Int. Conf. Composite Materials, Jeju, Republic of Korea (2011).

RIDA, T., et al., "Radiation synthesis of micro-nano particle of acrylated palm oil", Proc. Fundamental Science Congress, Serdang, Malaysia (2010).

RIMDUSIT, P., SUWANMALA, P., PASANPHAN, W., "Radiation synthesis of poly(ethylene glycol)-chitosan nanoparticle: a modified biodegradable polymer for PLA blends", Proc. 18th Int. Conf. Composite Materials, Jeju, Republic of Korea (2011).

ROKITA, B., KOMOROWSKI, P., ULANSKI, P., WALKOWIAK, B., ROSIAK, J.M., "Sonolysis of DNA from calf thymus in aqueous solution", Proc. 4th European Young Investigators Conf., Slubice, Poland (2009).

ROKITA, B., KOMOROWSKI, P., ULAŃSKI, P., WALKOWIAK, B., ROSIAK, J.M., 'Wpływ ultradźwięków na kwas deoksyrybonukleinowy — DNA", Proc. 52nd Zjazd Polskiego Towarzystwa Chemicznego oraz Stowarzyszenia Inżynierów i Techników Przemysłu Chemicznego, Lodz, Poland (2009).

SANCHEZ, M.L., SOTO ESPINOZA, S.L., QUIROGA, F.Y., CARBAJAL, M.L., GRASSELLI, M., "Procesos de modificación superficial de polímeros mediante radiación gamma", Proc. II Workshop de Transferencia de Tecnología en el Área de Materiales, Mar del Plata, Argentina (2011).

SMOLKO, E.E., et al., "Radiation-induced grafting of porous polymers for biological applications", Proc. Latin American Section of the American Nuclear Society (LAS/ANS), Symp. Integration of Nuclear Technologies in Latin America, Argentina (2009) (abstract).

SOTO ESPINOZA, S.L., GRASSELLI, M., "Análisis fluorométrico de nanoinjertos en membranas de poros perfectos", Proc. Encuentro Superficie y Materiales Nanoestructurados, La Falda, Argentina (2012).

SOTO ESPINOZA, S.L., GRASSELLI, M., "Synthesis and modification of cylindrical and conical nanopores on track-etched membranes", Proc. VIII Congreso Iberoamericano en Ciencia y Tecnología de membranas, Salta, Argentina (2012).

SPASOJEVIĆ, J., KRSTIĆ, J., RADOSAVLJEVIĆ, A., KALAGASIDIS-KRUŠIĆ, M., KAČAREVIĆ-POPOVIĆ, Z., "Thermoresponsive silver/poly(*N*-isopropylacrylamide) hydrogel nanocomposites synthesized by gamma irradiation", Proc. 10th Young Researchers' Conf., Materials Science and Engineering, Belgrade, Serbia (2011) 44 (abstract).

SPASOJEVIĆ, J., KRSTIĆ, J., RADOSAVLJEVIĆ, A., KALAGASIDIS-KRUŠIĆ, M., KAČAREVIĆ-POPOVIĆ, Z., "Swelling studies of thermo- and pH-sensitive Ag-poly(NiPAAm/IA) hydrogel nanocomposites synthesized by gamma irradiation" , Proc. 11th Young Researchers' Conf., Materials Science and Engineering 2012 and 1st European Early Stage Researchers' Conf. Hydrogen Storage, Belgrade, Serbia (2012) 108 (abstract).

SPASOJEVIĆ, J., RADOSAVLJEVIĆ, A., KRSTIĆ, J., KALAGASIDIS-KRUŠIĆ, M., KAČAREVIĆ-POPOVIĆ, Z., "Thermosensitive Ag/poly(NiPAAM-co-IA) hydrogel nanocomposites synthesized by gamma irradiation", Proc. 10th Mtg Ionizing Radiation and Polymers Symp. (IRaP2012), Krakow, Poland (2012) 157 (abstract).

TAJAU, R., et al., "Acrylated vegetable oil nanoparticle as a carrier and controlled release of the anticancer drug-thymoquinone", Proc. Int. Conf. Enabling Science and Nanotechnology, Johor Bharu, Malaysia (2012).

TAJAU, R., et al., "Development and characterization of acrylated palm oil nanoparticles using ionizing radiation", Proc. Int. Conf. Nanomaterials Synthesis and Characterization (ICONT), Sabah, Malaysia (2011).

TAJAU, R., et al., "Preparation of nanoparticles from acrylated palm oil microemulsion using radiation technique", Proc. Nuclear Science, Technology and Engineering Conf., Kuala Lumpur, Malaysia (2010).

TAJAU, R., YUNUS, W., DAHLAN, K.Z.M., MAHMOOD, M.H., HASHIM, K., "Radiation induced formation of acrylated palm oil (APO) nanoparticles using CTAB microemulsion system", Proc. Int. Conf. Nanotechnology (INSC), Serdang, Malaysia (2011).

ULANSKI, P., "Radiation chemistry of polymers – some opportunities and trends", Proc. Radiation Chemistry in the 21st Century – A Visionary Mtg, South Bend, IN (2009).

ULAŃSKI, P., KADŁUBOWSKI, S., JESZKA, J.K., ROSIAK, J.M., "Synthesis of nanogels by radiation-induced intramolecular crosslinking of single polymer chains", Proc. Workshop Progress in Bio- and Nanotechnology, Lodz, Poland (2009).

VARCA, G.H.C., "Advances in the use of radiation technology and nanotechnology in tissue engineering", Proc. Nanotecnología aplicada a la salud, IAEA-ARCAL CVIII Mtg, São Paulo, Brazil (2012).

VARCA, G.H.C., "Computational tools applied to the development of protein-based drug carriers", Proc. Sistemas Avanzados de Administración de Medicamentos, Mexico City, Mexico (2012).

VARCA, G.H.C., "Radio-induced protein reticulation for biomedical purposes", Proc. Latin American Congress on Biomaterials, Natal, Brazil (2012).

VARCA, G.H.C., et al., "Gamma irradiation effects over papain activity in different media", Proc. 9th Ionizing Radiation and Polymer Symp. (IRaP2010), College Park, MD (2010).

VARCA, G.H.C., et al., "Stabilization of papain by cyclic oligosaccharides: influence of B-CD and B-derivatives over the biological properties of papain", Proc. Int. Conf. Protein Stabilization (PROSTAB 2012), Lisbon, Portugal (2012).

VARCA, G.H.C., FERRAZ, C.C., LOPES, P.S., GRASSELLI, M., LUGÃO, A.B., "Radio-synthesized papain nanoparticles for biomedical purposes", Proc. 10th Ionizing Radiation and Polymer Symp. (IRaP2012), Krakow, Poland (2012).

VERES, M., et al., "Nanodiamond-polymer composites prepared by gamma radiation initiated free radical polymerization", Proc. Int. Conf. Diamond and Carbon Materials, Granada, Spain (2012).

VERES, M., et al., "Surface functionalization of nanocrystalline diamond using free radical polymerization", Proc. 22nd European Conf. Diamond, Diamond-like Materials Carbon Nanotubes and Nitrides, Garmisch-Paterkirchen, Germany (2011).

ABBREVIATIONS

AAc	acrylic acid
a-C:H	amorphous hydrogenated carbon
AFM	atomic force microscopy
AOT	dioctyl sodium sulphosuccinate
APMAM	(N-3-aminopropyl) methacrylamide hydrochloride
APO	acrylated palm oil
ASA	accessible surface area
BBR	berberine
BPATT	3-benzylsulphanylthiocarbonylsulphanyl propionic acid
BSA	bovine serum albumin
CA	contact angle
CD	circular dichroism
CEA	Atomic Energy and Alternative Energies Commission
CNT	carbon nanotube
cPTFE	cross-linked polytetrafluoroethylene
CRP	coordinated research project
CS	chitosan
CTAB	cetyltrimethyl ammonium bromide
Cyt	cytochrome
DC	deoxycholic acid
DCCS	deoxycholate modified chitosan
DEGDMA	diethylene glycol dimethacrylate
DLS	dynamic light scattering
DMEM	Dulbecco's modified Eagle's medium
DMFC	direct methanol fuel cell
DSC	differential scanning calorimetry
EB	electron beam
EDAX	energy dispersive X ray analysis
EDC	1-ethyl-3-(3′-dimethylaminopropyl) carbodiimide
ETFE	ethylene tetrafluoroethylene
FDA	Food and Drug Administration
FESEM	field emission scanning electron microscopy
FITC	fluorescein isothiocyanate
FTIR	Fourier transform infrared
GD	grafting degree
GF	graft frequency
GMA	glycidyl methacrylate
GPC	gel permeation chromatography
GR	graft ratio
HAP	hydroxyapatite
HEMA	hydroxyethylmethacrylate
HGNP	hollow gold nanoparticle
HPLC	high performance liquid chromatography
IA	itaconic acid
IPC	interpolymer complex
ITO	indium doped tin oxide
LAE	linear accelerator
LCST	lower critical solution temperature
LET	linear energy transfer
Lys	lysozyme

MALDI TOF	matrix assisted laser desorption/ionization, time of flight
MIP	molecularly imprinted polymer
MNP	metal nanoparticle
MTT	3-(4,5-dimethylthiazol-2-yl)-2,5diphenyltetrazolium bromide
MW	molecular weight
MWCO	molecular weight cut-off
ND	nanodiamond
NF	nanofibre
NIPAAm	N-isopropylacrylamide
NIR	near infrared
NMR	nuclear magnetic resonance
NP	nanoparticle
NW	nanoweb
PAAc	poly(acrylic acid)
PB	Prussian blue
PBS	phosphate buffered saline
PDI	polydispersity index
PEG	polyethylene glycol
PEGDA	polyethylene glycol diacrylate
PEGMA	polyethylene glycol monomethacrylate
PEM	polymer electrolyte membrane
PET	poly(ethylene terephthalate)
PLA	polylactic acid
PLLA	poly L lactic acid
PNIPA	poly(N-isopropylacrylamide)
PP	polypropylene
PVA	polyvinyl alcohol
PVDF	polyvinylidene fluoride
PVP	polyvinylpyrrolidone
RAFT	reversible addition fragmentation chain transfer
RCM	research coordination meeting
RFU	relative fluorescent unit
SANS	small angle neutron scattering
SAXS	small angle X ray scattering
SBF	simulated body fluid
SDS	sodium dodecyl sulphate
SEC	size exclusion chromatography
SEM	scanning electron microscopy
SMA	styrene maleic anhydride
SPR	surface plasmon resonance
STF	simulated tear fluid
TAIC	triallyl isocyanurate
TBUT	tear break-up time
TEM	transmission electron microscopy
TMA	thermoresponsive methacrylate
TMSPA	N-[3-(trimethoxy silyl) propyl]aniline
TRITC	tetramethyl rhodamine isothiocyanate
UV	ultraviolet
UV/VIS	ultraviolet/visible
v/v	volume per volume
w/v	weight per volume
XPS	X ray photoelectron spectroscopy
XRD	X ray diffraction

LIST OF PARTICIPANTS

Chen, Q.	Institute of Applied Chemistry, Peking University, 1 Loudouqiao, Hai Dian, Beijing 100871, China Email: qdchen@pku.edu.cn
Dadbin, S.	Atomic Energy Organization of Islamic Republic of Iran, Nuclear Science and Technology Research Institute, P.O. Box 14155-1339, Tehran, North Kargar, Islamic Republic of Iran Email: sdadbin@yahoo.comt
Dispenza, C.	Dipartimento di Ingegneria Chimica dei Processi e dei Materiali, Universita degli Studi di Palermo, Viale delle Scienze (Parco d'Orleans), 90128 Palermo, Italy Email: clelia.dispenza@unipa.it
Francis, S.	Radiation Technology Development Division, Bhabha Atomic Research Centre, Trombay, Mumbai, Maharashtra 400 085, India Email: sanju@barc.gov.in
Grasselli, M.	Universidad de Quilmes, Quesada 2422, piso 11, dpto. C, C1429BNP Buenos Aires, Argentina Email: mgrasse@unq.edu.ar
Güven, O.	Department of Chemistry, Hacettepe University, Beytepe, 06800, Ankara, Turkey Email: guven@hacettepe.edu.tr
Hamzah, M.Y.	Ministry of Science, Technology and Innovation, Malaysian Nuclear Agency, Bangi, 43000 Kajang, Selangor, Malaysia Email: m_yusof@nuclearmalaysia.gov.my
Hegazy, E.	National Center for Radiation Research and Technology, 3-Ahmed Al-Zomoor St, P.O. Box 29, Nasr City, Cairo, Egypt Email: hegazy_ea@hotmail.com
Hoffman, A.S.	Department of Bioengineering and Chemical Engineering, University of Washington, P.O. Box 355061, Seattle, WA 98195-5061, United States of America Email: hoffman@u.washington.edu
Lee, K.-P.	Advanced Analytical Science & Nanomaterials Laboratory, Kyungpook National University, 1370 Sankyuk-dong, Puk-gu, Daegu 702-701, Republic of Korea Email: kplee@knu.ac.kr
Lugão, A.B.	Instituto de Pesquisas Energeticas e Nucleares, Comissão Nacional de Energia Nuclear, Av. Prof. Lineu Prestes, 2242 Cidade Universitária, 05508-000 São Paulo, Brazil Email: ablugao@ipen.br
Maekawa, Y.	Department of Material Development, Takasaki Radiation Chemistry Research Establishment, Japan Atomic Energy Agency, 1233 Watanuki-Machi, Takasaki, Gunma-ken 370-1292, Japan Email: maekawa.yasunari@jaea.go.jp
Pasanphan, W.	Department of Applied Radiation and Isotopes, Faculty of Science, Kasetsart University, 50 Phahonyothin Road, Chatuchak, Bangkok 10900, Thailand Email: wanvimol.p@ku.ac.th

Radosavljevic (Krkljes), A. — Laboratory of Radiation Chemistry and Physics (Laboratory 030), Vinča Institute of Nuclear Sciences, St. Mike Petrovica Alasa 12-14, P.O. Box 522, 11001 Belgrade, Serbia
Email: krkljes@vin.bg.ac.rs

Rizza, G. — Saclay Institute of Matter and Radiation B.P. 591191 Gif sur Yvette CEDEX, France
giancarlo.rizza@polytechnique.edu

Ulanski, P. — Institute of Applied Radiation Chemistry, Technical University of Lodz, ul. Wroblewskiego 15, 93-590 Lodz, Poland
Email: ulanskip@mitr.p.lodz.pl

Veres, M. — Department of Laser Applications, Institute for Solid State Physics and Optics, Wigner Research Centre for Physics, Hungarian Academy of Sciences, Konkoly Thege Miklós ut 29-33, 1525 Budapest, Hungary
Email: vm@szfki.hu

Observers

Rattanawongwiboon, T. — Department of Applied Radiation and Isotopes, Faculty of Science, Kasetsart University, Bangkok 10900, Thailand

Varca, G. — Instituto de Pesquisas Energéticas e Nucleares, Centro de Química e Meio Ambiente, Av. Professor Lineu Prestes, Cidade Universitária, 05508000, São Paulo, Brazil
Email: gustavovarca@hotmail.com

Research Coordination Meetings

Vienna, Austria: 30 March–3 April 2009
Paris, France: 15–19 November 2010
Krakow, Poland: 8–12 October 2012

IAEA
International Atomic Energy Agency

No. 24

ORDERING LOCALLY

In the following countries, IAEA priced publications may be purchased from the sources listed below or from major local booksellers.
Orders for unpriced publications should be made directly to the IAEA. The contact details are given at the end of this list.

BELGIUM

Jean de Lannoy
Avenue du Roi 202, 1190 Brussels, BELGIUM
Telephone: +32 2 5384 308 • Fax: +32 2 5380 841
Email: jean.de.lannoy@euronet.be • Web site: http://www.jean-de-lannoy.be

CANADA

Renouf Publishing Co. Ltd.
22-1010 Polytek Street, Ottawa, ON K1J 9J1, CANADA
Telephone: +1 613 745 2665 • Fax: +1 643 745 7660
Email: order@renoufbooks.com • Web site: http://www.renoufbooks.com

Bernan Associates
4501 Forbes Blvd., Suite 200, Lanham, MD 20706-4391, USA
Telephone: +1 800 865 3457 • Fax: +1 800 865 3450
Email: orders@bernan.com • Web site: http://www.bernan.com

CZECH REPUBLIC

Suweco CZ, s.r.o.
SESTUPNÁ 153/11, 162 00 Prague 6, CZECH REPUBLIC
Telephone: +420 242 459 205 • Fax: +420 284 821 646
Email: nakup@suweco.cz • Web site: http://www.suweco.cz

FRANCE

Form-Edit
5 rue Janssen, PO Box 25, 75921 Paris CEDEX, FRANCE
Telephone: +33 1 42 01 49 49 • Fax: +33 1 42 01 90 90
Email: fabien.boucard@formedit.fr • Web site: http://www.formedit.fr

Lavoisier SAS
14 rue de Provigny, 94236 Cachan CEDEX, FRANCE
Telephone: +33 1 47 40 67 00 • Fax: +33 1 47 40 67 02
Email: livres@lavoisier.fr • Web site: http://www.lavoisier.fr

L'Appel du livre
99 rue de Charonne, 75011 Paris, FRANCE
Telephone: +33 1 43 07 43 43 • Fax: +33 1 43 07 50 80
Email: livres@appeldulivre.fr • Web site: http://www.appeldulivre.fr

GERMANY

Goethe Buchhandlung Teubig GmbH
Schweitzer Fachinformationen
Willstätterstrasse 15, 40549 Düsseldorf, GERMANY
Telephone: +49 (0) 211 49 874 015 • Fax: +49 (0) 211 49 874 28
Email: s.dehaan@schweitzer-online.de • Web site: http://www.goethebuch.de

HUNGARY

Librotrade Ltd., Book Import

Pesti ut 237. 1173 Budapest, HUNGARY
Telephone: +36 1 254-0-269 • Fax: +36 1 254-0-274
Email: books@librotrade.hu • Web site: http://www.librotrade.hu

INDIA

Allied Publishers

1st Floor, Dubash House, 15, J.N. Heredi Marg, Ballard Estate, Mumbai 400001, INDIA
Telephone: +91 22 4212 6930/31/69 • Fax: +91 22 2261 7928
Email: alliedpl@vsnl.com • Web site: http://www.alliedpublishers.com

Bookwell

3/79 Nirankari, Delhi 110009, INDIA
Telephone: +91 11 2760 1283/4536
Email: bkwell@nde.vsnl.net.in • Web site: http://www.bookwellindia.com

ITALY

Libreria Scientifica "AEIOU"

Via Vincenzo Maria Coronelli 6, 20146 Milan, ITALY
Telephone: +39 02 48 95 45 52 • Fax: +39 02 48 95 45 48
Email: info@libreriaaeiou.eu • Web site: http://www.libreriaaeiou.eu

JAPAN

Maruzen Co., Ltd.

1-9-18 Kaigan, Minato-ku, Tokyo 105-0022, JAPAN
Telephone: +81 3 6367 6047 • Fax: +81 3 6367 6160
Email: journal@maruzen.co.jp • Web site: http://maruzen.co.jp

RUSSIAN FEDERATION

Scientific and Engineering Centre for Nuclear and Radiation Safety

107140, Moscow, Malaya Krasnoselskaya st. 2/8, bld. 5, RUSSIAN FEDERATION
Telephone: +7 499 264 00 03 • Fax: +7 499 264 28 59
Email: secnrs@secnrs.ru • Web site: http://www.secnrs.ru

UNITED KINGDOM

The Stationery Office Ltd. (TSO)

St. Crispins House, Duke Street, Norwich, NR3 1PD, UNITED KINGDOM
Telephone: +44 (0) 333 202 5070
Email: customer.services@tso.co.uk • Web site: http://www.tso.co.uk

UNITED STATES OF AMERICA

Bernan Associates

4501 Forbes Blvd., Suite 200, Lanham, MD 20706-4391, USA
Telephone: +1 800 865 3457 • Fax: +1 800 865 3450
Email: orders@bernan.com • Web site: http://www.bernan.com

Renouf Publishing Co. Ltd.

812 Proctor Avenue, Ogdensburg, NY 13669-2205, USA
Telephone: +1 888 551 7470 • Fax: +1 888 551 7471
Email: orders@renoufbooks.com • Web site: http://www.renoufbooks.com

Orders for both priced and unpriced publications may be addressed directly to:

IAEA Publishing Section, Marketing and Sales Unit
International Atomic Energy Agency
Vienna International Centre, PO Box 100, 1400 Vienna, Austria
Telephone: +43 1 2600 22529 or 22530 • Fax: +43 1 2600 29302
Email: sales.publications@iaea.org • Web site: http://www.iaea.org/books

15-16581

The availability of a variety of chemical structures and functionality together with precise control of molecular architecture and morphology has enabled new uses of advanced materials. This has brought about a recent explosion of developments in the field of materials science. However, despite their widespread use in health care, many biomaterials lack the desired properties to interface with biological systems. There are thus unmet needs to create biomaterials with enhanced specific functionalities, improved biocompatibility and minimal natural rejection. This can be achieved by introduction of proper functionalities at the nanoscale dimension, a task for which radiation techniques are uniquely suited. Under the coordinated research project entitled Nanoscale Radiation Engineering of Advanced Materials for Potential Biomedical Applications, 18 Member State institutions collaborated and developed methodologies for radiation induced synthesis that enables precise control of the product structure, size and functionality at the nanoscale. This publication showcases these achievements.

INTERNATIONAL ATOMIC ENERGY AGENCY
VIENNA
ISBN 978–92–0–101815–1
ISSN 2225–8833